

# Tectonic-mechanical properties of the Alborz region, Iran



seit 1558

## Dissertation

zur Erlangung des akademischen Doktorgrades doctor rerum naturalium

(Dr. rer. nat.)

Vorgelegt dem Rat der Chemisch-Geowissenschaftlichen Fakultät der Friedrich-

Schiller-Universität- Jena

von Azadeh Abdollahi

geboren am 07.01.1979 im Iran/Tehran

**Gutachter:**

**1.** Prof. Dr. Nina Kukowski  
Lehrstuhl für Allgemeine Geophysik  
Institut für Geowissenschaften  
Friedrich-Schiller-Universität Jena

**2.** Prof. Dr. Martin Meschede  
Lehrstuhl für Regionale und Strukturgeologie  
Institut für Geographie und Geologie  
Ernst-Moritz-Arndt-Universität Greifswald

**Tag der Verteidigung:** 09.03.2016

## Summary

This study to analyse geo-hazard focused mainly on two parameters: geodynamics and mechanical property of the orogen. The Alborz region in northern Iran was selected as the study area. The Alborz mountain range in Iran is an ideal object to investigate the potential influence of past tectonic regimes on the future evolution of this long-lived convergence. For this purpose, previous geodynamic results were reviewed and compiled with data on present day tectonic activity at crustal and upper mantle scale. Previously published models indicate that the Iran Plate was subjected to a series of extensional and compressional tectonic regimes, ultimately linked with the opening and closure of the Tethys Ocean and related basins. Two subduction-collision cycles are recognized: one cycle occurred as a result of the subduction of the Iran Plate beneath the Turan Plate and in this cycle the subduction phase ceased in the Cenozoic and since the Cenozoic it is in a collision phase. The other cycle took place as a result of the subduction of the Arabian Plate beneath the Iran Plate, and in this cycle the subduction phase began in the Mesozoic and is ending now. Thus, the current tectonic situation in the Alborz is a direct consequence from the ongoing Cenozoic subduction-collision cycle.

GPS and earthquake data indicate that the Alborz region, resulting from the collision of the Iran Plate with the Turan Plate, is still an area of recently active compression. Moho and tomographic data show that there is no connection between slab remnants of the oceanic crust and the Iran Plate. Furthermore, the Moho beneath the central Alborz is about 20 km deeper than in surrounding areas, indicating further advancement of collision there. However, the collision is continuing and the shortened area between the Iran Plate and the Turan Plate may increase. During the crustal thickening, a deep Moho area can also develop. This evolution can be expected in the tectonic cycle between the Arabian Plate and the Iran Plate, and also other places of the Alpine-Himalayan Belt (AHB), such as the Caucasus region.

I investigated also the mechanical properties of the Alborz orogen to analyse geo-hazard in this region. For this purpose, the critical taper theory has been applied. This theory can show the equilibrium of an orogenic wedge. Stability or instability of an orogenic wedge can affect the initiation of earthquakes and landslides. An unstable orogen can generate new geo-hazards (e.g. earthquakes and landslide) and reactivate old geo-hazards more than a stable orogen.

Four main parameters of the critical taper theory, i.e. surface slope ( $\alpha$ ), basal dip ( $\beta$ ), coefficient of friction ( $\mu$ ) and pore pressure ratio ( $\lambda$ ), which affect the geometry and mechanical wedge situation of an orogenic wedge, have been surveyed for the study area. Surface slope from topographic profile and basal dip from geological cross-sections have been obtained to calculate the F-value ( $F = \alpha + (\alpha + \beta)$ ). First, the value of these parameters and consequently the wedge state have been estimated for the Alborz and the Caucasus region (as neighboring orogen). Then, a similar analysis was concluded for other orogens of the AHB from the Apennines to the Himalayas.

In order to better analyse the mechanical state of a wedge, several parameters, such as lithology, climate and tectonic setting were compared with the results of taper analysis. Three classes were distinguished to identify the mechanical state of the AHB orogens: **a)** Situation of pro- and retro-wedge based on alpha-

beta values (the critical taper theory), **b)** Situation of pro- and retro-wedge based on lithology and climate, **c)** Situation of pro- and retro-wedge based on faults and local slopes. This classification indicates that all of the AHB orogens are in a critical to stable situation.



## Zusammenfassung

Diese Studie zum besseren Verständnis von Georisiken konzentriert sich auf zwei Parameter: ein geodynamisches Modell und die mechanischen Eigenschaften des Orogens. Als Forschungsgebiet ist die Alborz Region in Nord Iran ausgewählt worden.

Die Alborz Region im Iran ist ein ideales Gebiet, um potenzielle Auswirkung der vergangenen tektonischen Regimes auf die zukünftige Entwicklung dieser Konvergenz zu untersuchen. Zu diesem Ziel sind die vorherigen geodynamischen Entwicklungen zusammengestellt und mit gegenwärtigen tektonischen Aktivitäten, sowohl auf der Oberfläche als auch in der Tiefe, kombiniert worden.

Bisher veröffentlichte Modelle zeigen, dass die iranische Platte verschiedenen Extensions- und Kompressionsregimes unterworfen war, die letztendlich in einer Verbindung mit der Öffnung und dem Schließen des Tethys-Ozeans und verbundener Becken standen.

Zwei Subduktion-Kollision-Zyklen werden daraus abgeleitet: ein Zyklus entstand als Folge der Subduktion der Arabischen Platte unter die Turan-Platte. In diesem Zyklus endete die Subduktionsphase im Känozoikum, seitdem befindet sich die Region in einer Kollisionsphase.

Der andere Zyklus ereignete sich als Folge der Subduktion der Arabischen Platte unter die Iranische Platte; in diesem Zyklus begann die Subduktionsphase im Mesozoikum und endet nun. Deshalb ist die momentane tektonische Situation in Alborz eine Konsequenz des laufenden Subduktion-Kollision-Zyklus.

GPS- und Erdbebendaten zeigen, dass die Alborz Region, die sich aus der Kollision der Iran-Platte und der Turan-Platte ergibt, immer noch ein Gebiet rezent aktiver Kompression ist. Moho- und tomographische Daten zeigen, dass es keine Verbindung zwischen den Slab-Resten der ozeanischen Kruste und der Iran-Platte gibt. Außerdem ist die Moho unter Zentral Alborz etwa 20 km tiefer als in der Umgebung, was auf weiteres Fortschreiten der Kollision dort hindeutet. Allerdings entwickelt sich die Kollision und deshalb könnte der verkürzte Bereich zwischen der Iran-Platte und der Turan-Platte größer werden.

Während der Verdickung kann sich eine tiefe Moho Region entwickeln. Diese Entwicklung kann man im tektonischen Zyklus zwischen der Arabischen Platte und Iran-Platte und auch in anderen Regionen des Alpen-Himalaya-Gürtels (AHB) wie der Kaukasus-Region erwarten.

In dieser Studie wurden die mechanischen Eigenschaften des Alborz-Gebirges untersucht, um die Georisiken in dieser Region besser zu verstehen. Zu diesem Zweck wurde die Critical Taper Theorie angewendet. Die Theorie kann das Gleichgewicht eines Orogens darstellen. Stabilität oder Instabilität eines Orogens kann die Initiation von Erdbeben oder Hangrutschen beeinflussen. Beispielsweise kann ein instabiles Orogen mehr als ein stabiles Orogen neue Geo-Risiken generieren oder alte Geo-Risiken reaktivieren.

Vier Haupt-Parameter: Oberflächenneigung ( $\alpha$ ), basale Neigung ( $\beta$ ), Koeffizient der Reibung ( $\mu$ ) und Porenwasserdruck ( $\lambda$ ), die die Keilgeometrie und die mechanische Situation des Orogens beeinflussen können, wurden untersucht. Die Oberflächenneigung wurde aus topographischen Profilen, die basale Neigung aus geologischen Profilen entnommen, um den sogenannten F-Wert oder die Störungsfestigkeit ( $F = \alpha + (\alpha + \beta)$ ) zu berechnen. Diese Werte sind erstmalig für die Alborz- und

Kaukasus-Region (als Nachbar-Orogen) abgeschätzt worden. Außerdem wurden die Ergebnisse für Alborz mit der Situation in anderen Orogenen des Alpen-Himalaya-Gürtels vom Apennin bis zum Himalaya verglichen.

Um den mechanischen Zustand der Orogene besser zu analysieren wurden einige Parameter wie Lithologie, Klima und tektonische Eigenschaften mit den Ergebnissen der Taperanalyse korreliert. Deshalb wurden drei Klassifizierungen unterschieden, um den mechanischen Zustand der Alpen-Himalaya Orogene zu identifizieren. Klassifizierung **a)** Zustand des Orogens basierend auf Alpha- und Beta-Werten (Critical Taper Theorie). Klassifizierung **b)** Zustand des Orogens basierend auf Lithologie und Klima. Klassifizierung **c)** Zustand des Orogens basierend auf Störungen und lokalen Hangneigungen. Alle diese Klassifizierungen zeigen, dass alle Orogene des AHB in einem fast kritischen-stabilen Zustand sind.

# CONTENTS

<b>1 INTRODUCTION.....</b>	<b>1</b>
1.1 Tectonic setting of the Alpine-Himalayan Belt.....	1
1.2 Iran as a part of the Alpine-Himalayan Belt.....	2
1.3 Alborz as a part of the Alpine-Himalayan Belt.....	4
1.3.1 Tectonic setting of the Alborz region.....	4
1.3.2 Geo-hazard of the Alborz region.....	6
1.4 Mechanics of the Alborz orogen.....	7
1.5 Research questions.....	8
1.5.1 Tectonic evolution.....	8
1.5.2 Mechanical state of orogen.....	9
1.6 Structur of the thesis.....	10
<b>2 A SUBDUCTION-COLLISION CYCLE EVOLUTIONARY MODEL FOR THE ALBORZ, IRAN.....</b>	<b>12</b>
2.1 Introduction.....	12
2.2 Data.....	15
2.3 Review of the geodynamic evolution of the Alborz region.....	16
2.3.1 Paleozoic.....	16
2.3.2 Mesozoic.....	17
2.3.2.1 Lower Triassic (Late Ladinian-Carnian/c. 230-216 Ma).....	17
2.3.2.2 Lower-Upper Triassic (Norian-Rhaetian /216-200 Ma).....	18
2.3.2.3 Main Cimmerian event (c. 200 Ma) to early Lias (ca. 200-183 Ma).....	18
2.3.2.4 Lower Jurassic-Middle Jurassic (Toarcian-early Bajocian /183-170 Ma).....	20
2.3.2.5 Middle Jurrasic (Late Bajocian-Late Jurrasic/170-150 Ma).....	20
2.3.3 Cenozoic.....	20
2.4 Recent situation.....	24
2.4.1 Near surface and crustal deformation.....	24
2.4.2 Seismicity.....	25
2.4.3 Moho and upper mantle.....	27
2.5 Discussion.....	30
2.5.1 Present day tectonic situation.....	30
2.5.2 Past tectonic situation.....	31
2.5.2.1 Subduction-collision cycle between Turan and Iran.....	32
2.5.2.2 Subduction-collision cycle between Arabian Plate and Iran.....	32
2.5.3 Caucasus.....	34
2.6 Conclusion.....	37
<b>3 CRITICAL TAPER ANALYSIS OF THE ALBORZ AND OTHER OROGENS OF THE ALPINE-HIMALAYAN BELT...38</b>	<b>38</b>
3.1 Introduction.....	38
3.2 Mechanical setting of a bivergent orogen.....	39
3.3 Method.....	42
3.3.1 Critical taper theory.....	42
3.3.2 Meassurements .....	43
3.3.2.1 Basal dip ( $\beta$ ).....	44
3.3.2.2 Slope ( $\alpha$ ).....	45

3.3.2.3	Fault strength (F).....	49
3.4	Alborz.....	50
3.4.1	Tectonic setting.....	50
3.4.2	Lithology.....	51
3.4.2.1	Pre-Tertiary.....	51
3.4.2.2	Paleocene-Eocene.....	51
3.4.2.3	Neogene-Quaternary.....	52
3.4.3	Climate.....	52
3.4.4	Parameters compiled for a critical taper analysis applied to the Alborz.....	54
3.4.4.1	Basal dip ( $\beta$ ) .....	54
3.4.4.2	Slope ( $\alpha$ ).....	57
3.5	Caucasus.....	60
3.5.1	Tectonic setting.....	60
3.5.2	Lithology.....	61
3.5.3	Climate.....	62
3.5.4	Parameters compiled for a critical taper analysis applied to the Caucasus.....	62
3.5.4.1	Basal dip ( $\beta$ ).....	62
3.5.4.2	Surface slope .....	64
3.6	Other orogens of the Alpine-Himalayan Belt.....	64
3.6.1	Zagros.....	64
3.6.1.1	Tectonics, Lithology and Climate.....	64
3.6.1.2	Parameters compiled for a critical taper analysis applied to the Zagros...7	67
3.6.2	Himalayas.....	68
3.6.2.1	Tectonics, Lithology and Climate.....	68
3.6.2.2	Parameters compiled for a critical taper analysis applied to the Himalayas.....70	70
3.6.3	Apennines.....	71
3.6.3.1	Tectonics, Lithology and Climate.....	71
3.6.3.2	Parameters compiled for a critical taper analysis applied to the Apennines.....73	73
3.7	Critical taper analysis.....	75
3.7.1	Alborz.....	75
3.7.2	Caucasus.....	81
3.7.3	Zagros.....	87
3.7.4	Himalayas.....	91
3.7.5	Apennines.....	95
3.8	Discussion.....	101
3.8.1	Mechanical state of orogens based on critical taper analysis .....	101
3.8.2	Wedge state of orogens based on F-value, lithology, slope and climate.....102	102
3.8.3	Comparison with analog experiments.....	106
3.9	Conclusion.....	108
<b>4</b>	<b>SYNTHESIS AND OUTLOOK.....</b>	<b>110</b>
4.1	Tectonic evolution of Alborz.....	110
4.2	Mechanical analysis of Alborz.....	112
4.3	Impact of mechanical state of orogen on geo-hazard.....	113
<b>5</b>	<b>REFERENCES.....</b>	<b>117</b>
<b>6</b>	<b>APPENDIX.....</b>	<b>132</b>

## List of abbreviations

AHB	Alpine-Himalayan Belt
CTT	Critical Taper Theory
PW	Pro-wedge
RW	Retro-wedge
NEIC	National Earthquake Information Center
WSM	Word Stress Map
CMT	Centroid Moment Tensor
USGS	United State Geological Survey
GPS	Global Positioning System
DEM	Digital Elevation Model
SRTM	Shuttle Radar Topography Mission
NOAA	National Oceanic and Atmospheric Administration
DTU	Technical University of Denmark
NW	North-West
SW	South-West
SE	South-East
NE	North-east
N-S	North-South
mm/yr	millimeter pro year
cm/yr	centimeter pro year
Ma	Million years ago
GC	Greater Caucasus
LC	Lesser Caucasus

## List of symbols

$M_s$	surface-wave magnitude
$\alpha$	surface slope
$\beta$	basal detachment
$F$	fault strength
$W$	wedge strength
$\lambda, \lambda_{int}$	pore water pressure
$\lambda_b, \lambda_{bas}$	basal Pore water pressure
$\mu, \mu_{int}$	friction
$\mu_b, \mu_{bas}$	basal friction coefficient
$\rho_f$	density of the fluid above the wedge (water or air)
$\rho_w$	density of seawater
$\rho$	mean density of rock
$S_b$	basal cohesion
$C$	compressive wedge strength
$\phi$	angle of internal friction
$\phi_b$	angle of basal friction
$H$	wedge thickness
$\sigma_1$	maximum principle stress
$\sigma_3$	minimum principle stress
$\Psi_0$	angle between $\sigma_1$ and surface slope
$\Psi_b$	angle between $\sigma_1$ and base of wedge

## List of figures

1-1. The Alpine Himalayan Belt.....	2
1-2. Tectonic map of the Iran region, after Sorkhabi and Macfarlane (1999).....	3
1-3. Seismicity of the Alborz region .....	5
1-4. Distribution of landslides in the Alborz region (a) and location of giant landslides (b),.....	6
1-5. An orogen as a wedge with main mechanical parameters.....	8
2-1. Introducing the Iran region and surroundings.....	13
2-2. Schematic structure of the study (chapter 2).....	15
2-3. Paleozoic evolution of Iran and surroundings .....	17
2-4. Mesozoic evolution of Iran and surroundings.....	19
2-5. Cenozoic evolution of Iran and surroundings .....	21
2-6. Map of stress regimes and shortening rates of Iran (a)/Alborz (b).....	23
2-7. Earthquakes and main faults in the Alborz region.....	27
2-8. Moho depth of the Alborz region.....	29
2-9. Map of stress regimes, Moho, and GPS velocities of the Alborz region.....	30
2-10. Sketch of Sketch of long-term geodynamic model as well as the subduction-collision cycles from the Paleozoic .....	33
2-11. Recent tectonic situation of the Caucasus region.....	35
3-1. Bivergent setting.....	41
3-2. Convergent wedge and its controlling parameters.....	42
3-3. Beta interpolation between two studied profiles (1 and 5).....	45
3-4. Surface slope estimation.....	47
3-5. Generalized geological-structural map of the Alborz, after Rezaeian (2008).....	50
3-6. Precipitation and erosion in the Alborz region (mm/yr).....	53
3-7. Measurement of basal dip in the Alborz, along the profile of Allen et al. (2003).....	55
3-8. Measurement of basal dip in the Alborz, along the profile of Alavi (1996).....	56
3-9. Measurement of basal dip in the Alborz, along the profile of Allen et al. (2004).....	57
3-10. Regional slope along the studied profile in the Alborz,.....	59
3-11. Geological and structural map of the Caucasus, after Mosar et al. (2010).....	61
3-12. Measurement of basal dip in the Caucasus along the profile of Mosar et al. (2010) and Egan et al. (2009).....	63
3-13. Geological map of the Zagros, after Molinaro et al. (2005).....	66
3-14. Measurement of basal dip in the Zagros region, along the profile of Molinaro et al. (2005).....	68
3-15. Geological map of the Himalayas, after Yin et al. (2010).....	69
3-16. Measurement of basal dip in the Himalayas, along the profile of Lavé and Avouac. (2000).....	71
3-17. Geological map of central Italy, after Rosenbaum et al. (2002).....	72
3-18. Measurement of basal dip in the Apennines, along the profile of Tozer et al. (2002).....	73
3-19. Regional slope along the main profiles.....	74-75
3-20. Elevation, local slope and earthquakes in the Alborz region.....	76-77
3-21. Map of F-values in the Alborz.....	79-80
3-22. Elevation and local slope in the Caucasus region.....	82
3-23. Map of earthquakes and tectonic regimes in the Caucasus.....	83
3-24. Landslide map of the Caucasus region,.....	83
3-25. Map of F-values in the Caucasus region.....	85-86
3-26. Local slope map of the zagros region.....	87
3-27. Map of F-values in the Zagros region.....	89-90
3-28. Local slope map of the Himalayan region.....	91
3-29. Map of F-values in the Himalayan Region.....	93-94
3-30. Local slope map of the Apennines region.....	95
3-31. Map of F-values in the Apennines region.....	97-98
3-32. Stability diagram.....	100
3-33. Local wedge state.....	104
3-34. Local wedge state based on final correlation.....	106
4-1. Cycle of wedge state in the collision phase of the Alborz region and the recent mechanical state of orogen.....	111
6-1. The Alborz, regional slope for the extra profiles .....	132

6-2. The Caucasus, regional slope for the extra profiles .....	133-134
6-3. The Zagros, regional slope for the extra profiles .....	135-136
6-4. The Himalayas, regional slope for the extra profiles .....	137
6-5. The Apennines, regional slope for the extra profiles .....	138-139
6-6. F-values of all of the orogens based on local slopes.....	139

## List of tables

2-1. Shortening rate in the Alborz region .....	25
3-1. Beta values of several orogens of the AHB.....	65
3-2. Comparison of AHB orogens .....	99

## List of Programs (in CD)

**ink2real\_file**: Program for transform Inkscape coordinates into real coordinates

**aintpol**: Interpolation of a piecewise constant function

**F**: F calculating for all 5 orogens

**intpol**: linear interpolation

**slopes**: slopes (2D)

**prof3**: slopes (3D)





# 1 INTRODUCTION

Geo-hazard is not evenly distributed around the Earth, but mainly occurs in regions of active tectonics, such as geologically young mountain belts. This suggests that tectonics and geo-hazard are related and that tectonic activity may be an important cause for geo-hazard. On the other hand, research during the last three decades has revealed that climate and tectonics are intimately linked to each other (e.g. Molnar and England, 1990; Willett et al., 1990; Willett 1993). Therefore, there may be links between tectonics, climate, and geo-hazard, which infers that relations between these processes may be complicated and multiform.

The mechanics of orogens may be a key factor to understand what parameters and processes control geo-hazard in actively converging tectonic settings (e.g. Hoth et al., 2007; von Hagke et al., 2014). To do so, the focus of recent research has been on e.g. active faults (e.g. Berberian, 1976; Nazari et al., 2009; Hesami and Jamali, 2006; Landgraf et al., 2009), seismicity (Nazari and Bozorgnia, 1992; Walker et al., 2005), landslides (e.g. Asadi and Zare, 2014; Hafezi and Ghafoori, 2007), or the mechanical state of an orogen, as described by the critical taper theory (e.g. Davis et al., 1983; Dahlen, 1990; von Hagke et al., 2014), just to name some important topics.

The Alpine-Himalaya Belt (AHB) of collision orogens, comprising of the Alps, Caucasus, Zagros, Alborz, Tibet, Tien Shan, and the Himalayas (Storetvedt, 1990; Fig. 1-1), is a prominent setting of plate convergence and a region of major geo-hazard. This is not only true for the entire region but also for its individual orogens, such as the Alborz in northern Iran, which is located close to Iran's capital Tehran and makes it one of those mega-cities, which are prone to geo-hazard (e.g. Berberian, 1976; Aghanabati, 2004).

The aim of this study is to better understand the geodynamic evolution of the Alborz and characterize its mechanical situation by performing a critical taper analysis. Since the Alborz is part of the AHB, its mechanical behaviour then is compared to that of other orogens of the AHB.

## 1.1 Tectonic setting of the Alpine-Himalayan Belt

According to Dewey and Bird (1970), Smith (1971), and Dewey et al. (1973), the AHB had formed through a continental collision of Africa and India with Eurasia, which closed the intervening Tethys Ocean. The AHB is one of the most seismic regions in the world and experienced ~17% of the world's largest earthquakes (Storetvedt, 1990).

Studies addressing the AHB are strongly linked to the evolution of the Tethys (Storetvedt, 1990). Thus, a review of the long-term tectonic evolution of the AHB orogens and an assessment of tectonic cycles would enable to better illustrate the origin and evolution of this mountain belt.

The AHB shows considerable shallow to intermediate-depth (50-300 km) seismicity. Earthquakes deeper than 300 km (deep-focus earthquakes) rarely occur throughout the belt (NEIC catalogue: National Earthquake Information Center). Most regions of the AHB experienced earthquakes with hypocenters of less than 100 km, e.g. Himalaya, Iran, Caucasus. These events are crustal, or of interplate origin (Storetvedt, 1990). On the other hand, in some regions, such as the Apennines, the Aegean, the Pamir, or Indo-China, seismicity nucleates at depths below 100 km (Koulakov et al., 2002). Stress drops of the intraplate earthquakes are significantly higher than those of interplate ones on average. Strain rates at plate boundaries are higher than those at intraplate faults, and recurrence intervals of interplate earthquakes are much shorter than those of intraplate earthquakes (Allmann and Shearer, 2009).

However, northern Iran is one of the most active parts of the AHB and experienced crustal and interplate earthquakes with magnitudes higher than seven and is a populous zone.

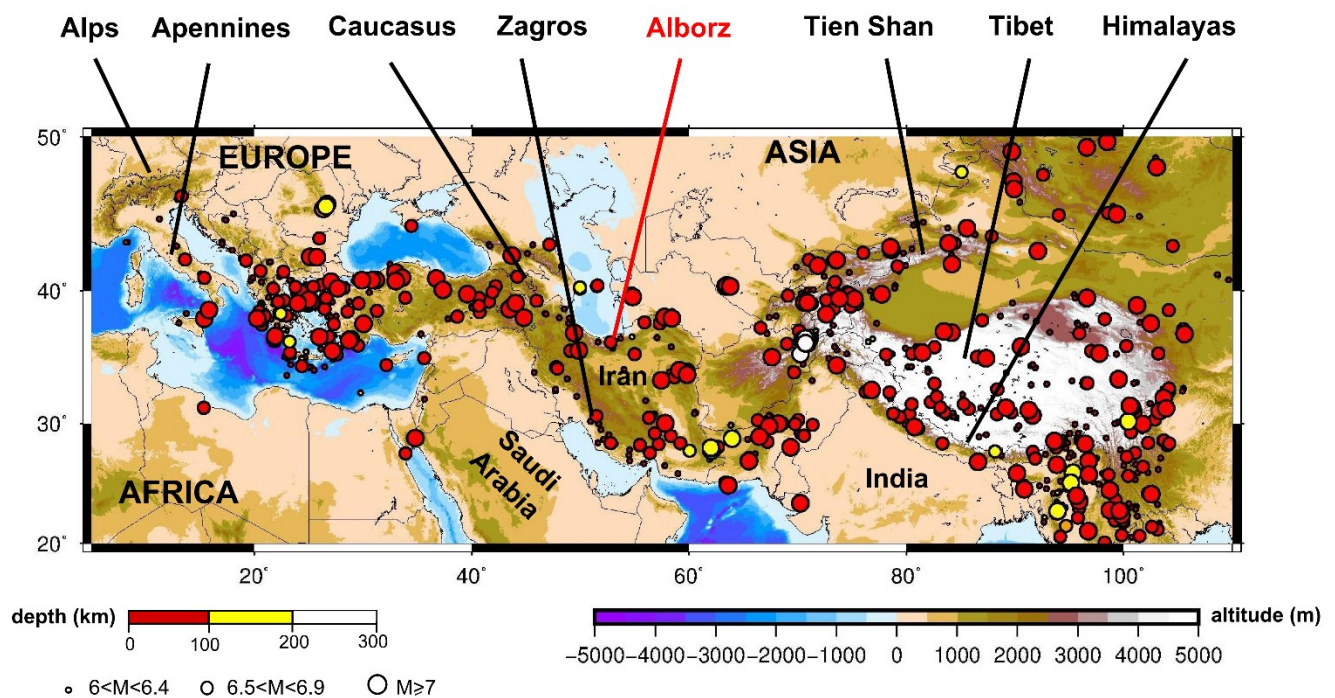


**Figure 1-1.** The Alpine Himalayan Belt. Topographic data (NOAA; Amante and Eaklins, 2009), earthquakes greater than magnitude 6 (USGS-NEIC Catalogue, 1900 - 2015).

## 1.2 Iran as a part of the Alpine-Himalayan Belt

The Iran Plate is a part of the AHB and is compressed between the Arabian Plate to the south and the Eurasian Plate to the north (Fig. 1-2). This compression is a cause for mountainous terrains in this region including Zagros and the Alborz mountains. Besides, tectonic studies indicate that the Iran Plate has a very high density of active faults, resulting in considerable shallow seismicity (e.g. Berberian, 1976; Aghanabati, 2004; Khodaverdian et al., 2015). Therefore, a contractional phase is present in this region.

may be a main cause for the formation of fault structures and consequently seismicity. To study the evolution of this region helps to understand the tectonic regimes, plate situation, and plate boundaries in northern Iran and adjacent regions. For example, for some orogens of the AHB, such as the Caucasus, there are different controversial suggestions for the plate tectonic situation (e.g. Mumladze et al., 2015; Forte et al., 2013) and it is still to debate, which one is the downgoing plate with the some of the AHB orogens.

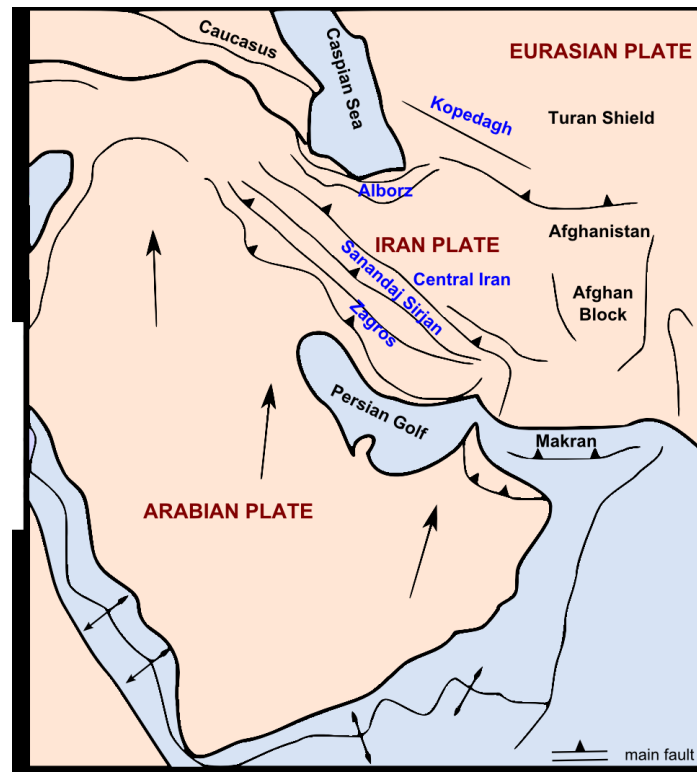


**Figure 1-2.** Tectonic map of the Iran region, after Sorkhabi and Macfarlane (1999).

Iran consists of different geological-seismological provinces. A province is defined as an area bounded by geological features, which marks a difference in seismic or geological characteristics of one province to its neighboring provinces (e.g. Tavakoli and Ghafoori-Ashtiani, 1999; Aghanabati, 2004). The boundaries of the provinces are established through analysis of seismic history, tectonic environments, active faults, regional geomorphology, and plate boundaries. Various opinions exist about the boundary of the provinces, and numerous authors (e.g. Stoklin, 1968; Takin 1972; Berberian, 1976; Tavakoli and Ghafoori-Ashtiani, 1999; Aghanabati, 2004) have differently divided Iran into geological-seismological provinces, but in all of the published studies, Alborz (North Unit), Zagros (South Unit) and Central Iran (Central Unit) have been suggested as main zones (Fig. 1-2). All of these zones have a different seismic potential, e.g. the ratio of strain to the number of earthquakes in the Alborz is generally higher than in the Kopedagh. Zagros is characterized by extensive seismicity and a high geodetically measurable strain. In contrast, Central Iran experiences low seismicity with close to no strain (Masson et al., 2006). The

Alborz region is one of the most active parts of northern Iran and has experienced several geo-hazards, such as destructive earthquakes  $M > 7$  (e.g. Ambraseys and Melville, 1982; Berberian and Yeats, 2001).

### **1.3 Alborz as a part of the Alpine-Himalayan Belt**

The Alborz mountains belong to the orogenic belt of Iran, which is the result of the convergence between the Arabian Plate and the Turan Shield as a part of the Eurasian Plate near the north-eastern border of Iran (Fig. 1-2) and has mainly developed in the Mesozoic-Cenozoic as a consequence of the closure of the Neotethys (e.g. Aghanabati, 2004). The Alborz region is a west-east striking mountain system south of the southern coast of the Caspian Sea. It has been affected by several successive tectonic events, from the Eo-Cimmerian orogeny to the Late Tertiary-Quaternary intracontinental transpression (Allen et al. 2003), and is still seismically strongly active (e.g. Ritz et al. 2006; Fig. 1-3).

#### **1.3.1 Tectonic setting of the Alborz region**

The Alborz region is a bivergent orogen and experiences active deformation resulting from forces accommodating the Iran-Turan collision (Fig. 1-2). Active deformation along the northeastern boundary of the Arabia-Eurasia collision zone is taken up by strike-slip faults, which may result from oblique convergence in this boundary zone (Vernant et al., 2004 b; Reilinger et al., 2006). Based on GPS data Masson et al. (2005) suggested that the Arabia-Eurasia convergence is distributed within several regions as mountains belts and large thrust and strike-slip faults. However, the seismotectonics of the Alborz range are largely controlled by major thrust faults (Jackson et al., 2002; Ashtari et al., 2005).

Alborz has experienced different tectonic regimes and is in a contractional phase now (e.g. Berberian and King 1981; Aghanabati, 2004; Wilmsen et al., 2009; Ballato et al., 2011). The capital of Iran, Tehran, is located near the foothills of the southern Central Alborz range and close to several active faults. As mentioned before, this region has experienced destructive earthquakes (e.g. Berberian and Yeats, 2001) and landslides (e.g. Ambraseys and Melville, 1982; Hafezi and Ghafouri, 2007; Asadi and zare, 2014).

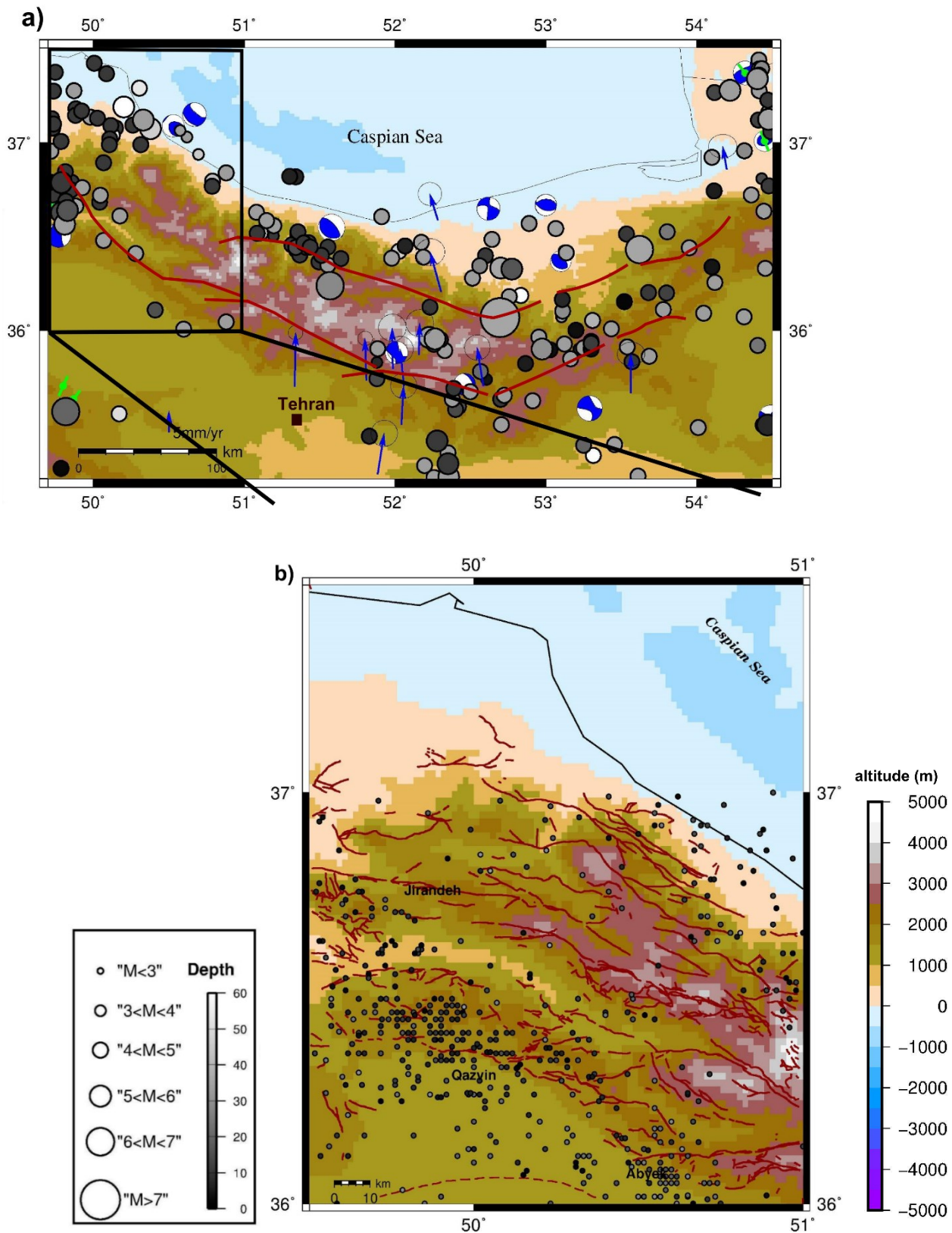


**Figure 1-3.** Seismicity of the Alborz region. Earthquakes and stress regimes of the Alborz region (a), and available local microseismicity with magnitude lower than 3 (b). Topographic data (DTU, Andersen and Knudsen, 2009), earthquakes (NEIC catalogue, 1900 to 2014), red lines: main thrust faults (Berberian et al., 1993; Hind et al, 2001; Allen et al., 2003), microseismic events (University of Tehran, 1900-2011), blue arrows: GPS velocity (Vernant et al., 2004 a, b), stress data (WSM Catalogue, Heidbach et al., 2008, green: thrust fault).



### 1.3.2 Geo-hazard of the Alborz region

As mentioned, the Alborz zone is a main tectonic and seismic province of Iran and forms a barrier between the south Caspian Sea and the Iran Plate. Stress data show a compressional regime in the Alborz region and according to the NEIC catalogue, the Alborz region is located in a high hazard region (Fig. 1-3 a). Several earthquakes also affected the Alborz region during historical times (Ambraseys and Melville, 1982). Some of the largest recent ones ( $M > 6$ ) occurred in the vicinity of Tehran (e.g. Ambraseys and Melville, 1982; Berberian and Yeats, 1999; Berberian and Yeats 2001).

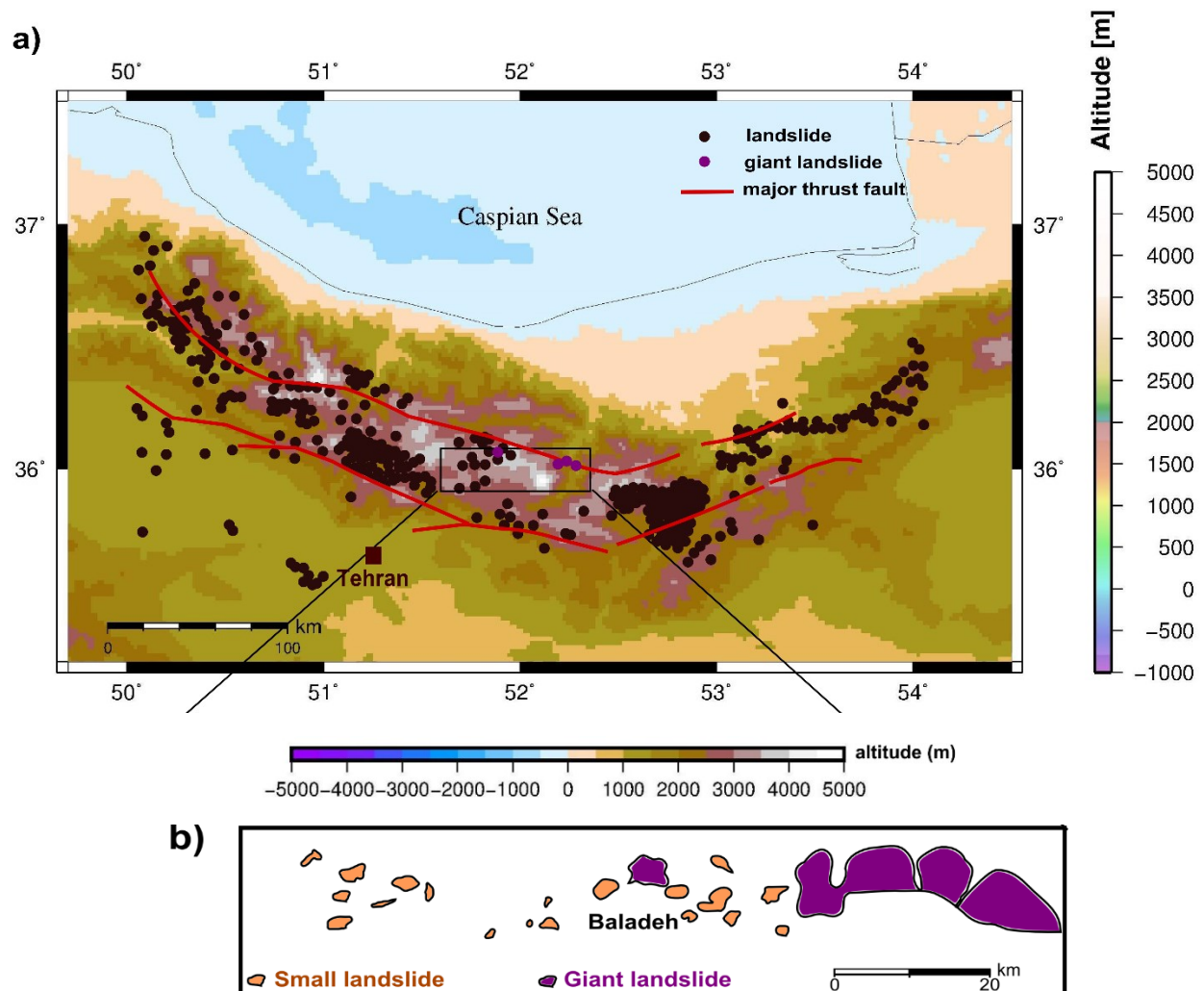


**Figure 1-4.** Distribution of landslides in the Alborz region (a) and location of giant landslides (b), after Hafezi and Ghafoori (2007), Asadi and Zare (2014); topographic data from DTU (Andersen and Knudsen, 2009).

An earthquake with a magnitude higher than seven occurred in central Alborz in Manjil (Fig. 1-3 a). For the entire Alborz, there is no local seismic network, but for a small area near Tehran (Qazvin) micro-seismic data are available from 1900 to 2011 (Fig. 1-3 b). From this data set, it seems that seismicity concentrates on the southern side of the Alborz. Generally, the depth of these micro seismic events is lower than 20 km.

Numerous landslides have been reported from the Alborz region (e.g. Hafezi and Ghafoori, 2007; Asadi and Zare, 2014; Fig. 1-4 a, b). In active mountain ranges, landslides in general and giant landslides in particular are important erosion processes (Pinto et al., 2008). A landslide is commonly named a “giant landslide” if its volume is as large as tens of  $\text{km}^3$  (Pinto et al. 2008). Such landslides have been reported from around the world, e.g. in southwest Iran, in Nepal or Mongolia. The volume of such landslides may be as large as  $100 \text{ km}^3$  and usually affects an area of  $10 - 10^3 \text{ km}^2$  (Asadi and Zare, 2014).

About 75 % of the giant landslides have occurred in tectonically active regions such as major orogenic belts (Korup et al. 2007; Asadi and Zare, 2014). In these regions, uplift along existing joints and faults can provide critical conditions for landslides to occur. On the other hand, earthquakes can also trigger landslides. Therefore, landslides can be used as an indicator of seismicity and tectonic activity of a region (Asadi and Zare, 2014).

The landslides of the Alborz region have been triggered probably by one or more earthquakes. These landslides are mostly located in the central Alborz with areas of  $\sim 16 - 160 \text{ km}^2$  and volumes of lower than  $10 \text{ km}^3$  (Asadi and Zare, 2014). There are also landslides, which are not related to fault activity (Hafezi and Ghafoori, 2007), but may relate to the steep slope of the orogen. Therefore, it is worthwhile to study the geometry of orogen.

Knowledge of critical taper (Davis et al., 1983) is a key to understand the geometry of orogen, which may affect geo-hazards, such as earthquakes or landslides, in an orogenic region (e.g. Hoth et al., 2007). In this regard, it is important to consider the effects of climate, such as erosion and precipitation, because these factors can change topography and geometry of an orogen, respectively (e.g. Hoth et al., 2007, 2008). Thus, the mechanics of an orogen and climate are two related topics (Willet et al., 1993; Willet, 1999; Molnar and England, 1990), which may influence the geo-hazards (Molnar et al., 2007). Besides, to have a better understanding of the mechanical setting of an orogen, a review of Earth history of the region is needed.

#### 1.4 Mechanics of the Alborz orogen

To better analyse geo-hazard (earthquakes and landslides), the geometry of an orogen or in other words, the mechanical state of orogen needs to be studied. If an orogen were considered as a wedge, the mechanical situation of the orogen can be estimated. For this analysis, the critical taper theory has been successfully applied (e.g. Davis et al., 1983; Dahlen, 1990). According to this theory, four main parameters characterize the geometry of an orogenic wedge: surface slope ( $\alpha$ ), basal dip ( $\beta$ ), and coefficients of internal and basal friction ( $\mu_{int}$ ,  $\mu_{bas}$ ) in case of “dry” wedges such as sand wedges. In case of “wet” wedges like orogenic wedges, additionally the internal and basal pore pressure ratio ( $\lambda_{int}$ ,  $\lambda_{bas}$ ) have to be considered (e.g. Davis et al., 1983; Dahlen, 1990; Fig. 1-5). In fact, the mechanical situation of a wedge describes potential equilibrium conditions of an orogen. Stability or instability of an orogen can relate to geo-hazards. For example, an unstable orogen can generate new hazard or

reactivate old hazard regions more than a stable orogen, but it depends on some factors, such as climate and lithology in nature.

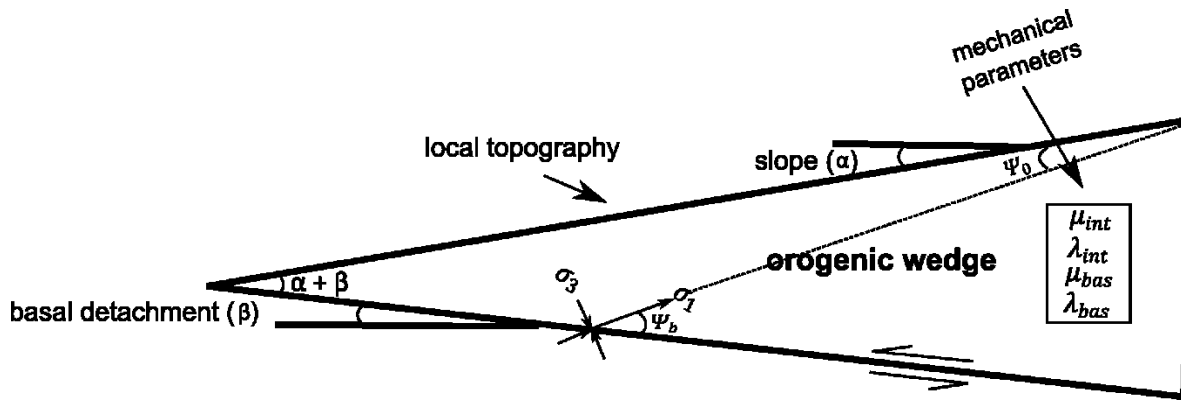


**Figure 1-5.** An orogen as a wedge with main mechanical parameters.  $\alpha$ -Surface slope;  $\beta$ -basal detachment;  $\mu_{int}$ -coefficient of internal friction;  $\mu_{bas}$ -coefficient of basal friction;  $\lambda_{int}$ -internal pore pressure ratio;  $\lambda_{bas}$ -basal pore pressure ratio;  $\sigma_1$ -maximum principle stress;  $\sigma_3$ -minimum principle stress;  $\Psi_0$ -angle between  $\sigma_1$  and surface slope;  $\Psi_b$ -angle between  $\sigma_1$  and wedge base), after Dahlen, 1990.

## 1.5 Research questions

As mentioned above, the Alborz region does not only experience earthquakes but also landslides, which have been considered as main geo-hazards for this region. This study focuses on two parameters to better analyse geo-hazards in the Alborz region: 1) its tectonic evolution 2) the mechanical state of an orogen.

### 1.5.1 Tectonic evolution

First of all, to better analyse geo-hazard it is important to know their source and origin. In the active region, such as the Alborz, this is mainly due to tectonic processes (e.g. Aghanabati, 2004; Berberian 1976). Thus, to study the tectonic evolution helps to understand the origin of orogens and tectonic reasons of geo-hazards. In addition, a study of the long-term tectonic evolution leads to not only interpret the recent tectonic situation of the Alborz, but also may help to detect if some tectonic events occur repeatedly (tectonic cycle).

Besides, the cycle of tectonic events helps to potentially identify a tectonic relationship, not only between past and recent events, but also between recent and probable future events, in some regions. For this aim, a long-term geodynamic model with its focus on the Alborz region is needed, a model, which indicates all of the related tectonic events from the Precambrian to the present time. The present tectonic situation, which is affected by past events, can explain the geo-hazard of the region.



Furthermore, a detection of the potential relationship between recent the tectonic situation and geo-hazards in an orogen, such as the Alborz can be extended to neighboring orogens (e.g. the Caucasus) to compare the mentioned relationship. Therefore, to study the tectonic evolution of the Alborz region, the following question and sub-questions are addressed:

- Which tectonic processes have occurred in the Alborz region, from the past to the recent time and which tectonic regime dominates today?
  - Is there any relationship between tectonic activities in the past and the recent time?
  - Is there any cycle of the tectonic evolution in this region?
  - Are the answers of the above questions the same for orogens near the Alborz (for example the Caucasus)?

Answers to the above questions will help us to better assess the recent tectonic situation of the Alborz region while considering the effects of past events. It can also assess the relation between recent tectonic events and the origin of geo-hazard in an orogen and its surrounding.

This part of the present study is based on a data compilation done in order to establish a new long-term geodynamic model, which summarises tectonic events and evolutionary cycles. For this purpose, three models as suggested by Berberian and King (1981), Wilmsen et al. (2009), and Ballato et al. (2011) will be integrated. To assess the present tectonic activities in the Alborz, I focus on the crust and upper mantle. Hence, I will compile the following two data sets:

The first data set consists of surface data, which will be obtained from GPS, seismic activity and stress regime data. The second data set consists of Moho and upper mantle data based on gravity, geoid and topography. These data define Moho depth and crustal thickness. It enables us to assess, if a tectonic phase, such as collision or subduction is over or is continuing.

Combining these data helps us to identify tectonic cycles, which can not only indicate a relation between the past and present tectonic events, but also enable to hypothesize a probable future tectonic situation. At the end, the Alborz region will be compared with the Caucasus as a neighboring orogen to determine, whether these active regions experienced a similar tectonic evolution and are in a same recent tectonic situation or not.

## 1.5.2 Mechanical state of an orogen

To better analyse geo-hazards, the recent mechanical orogenic state needs to be considered. In fact, tectonic events can be considered as the primary source of geo-hazards, and the mechanical state of an orogen can be considered as an important control on tectonic processes.

After determining the mechanical state of the Alborz and its relationship to geo-hazards of the region, I will compare my finding with a neighboring orogen, such as the Caucasus to determine, if they both have the same mechanical state and if these have a similar effect on the generation of geo-hazards.

Furthermore, since the Alborz and the Caucasus region are parts of the AHB, a comparison with other orogens of the AHB, such as the Zagros, the Himalayas, and the Apennines is useful. This provides a large-scale comparison of orogenic states along the AHB.

Therefore, by studying the recent mechanical orogenic state, I will address the below question and sub-questions:

- What is the mechanical orogenic state of the Alborz mountains?
- Which parameters affect the wedge state the most?
- Is the orogenic state of the Alborz region similar to that of a neighboring orogen (e.g. Caucasus)?
- Are the mechanical states of the Alborz and Caucasus region the same in all of the AHB orogens?

This part of my study is based on critical taper analysis. For this purpose, the critical taper theory will be applied. To obtain critical taper components, e.g. surface slope ( $\alpha$ ) and basal dip ( $\beta$ ), topographic profiles and geological cross-sections will be used, respectively. By using the resultant ( $\alpha$ ) and ( $\beta$ ) in the critical taper equations, the value of other critical taper components e.g. basal friction ( $\mu$ ) will be estimated.

## **1.6 Structure of the thesis**

After this introduction in the research questions addressed in this dissertation. Chapter 2 deals with the tectonic evolutionary model of the Alborz region. To present a tectonic evolutionary model showing all of the tectonic events from the Precambrian to the recent time focusing on the Alborz, three steps will be performed:

In a first step, the different models, which were established by other authors will be reviewed and combined. Consequently, a model of tectonic events from the Precambrian to the Cenozoic will be obtained. In a second step, this model will be joined with the present time tectonics. For the present time tectonic situation, the crust and upper mantle will be studied. Data, such as GPS velocities, earthquakes and stress regimes will be obtained from different catalogues, such as NEIC, CMT and WSM to study the surface. Tomographic and Moho data will be used to study the upper mantle of the region. In a third step, the Alborz region will be compared to the Caucasus as another orogen of the AHB. In this part, a tectonic evolutionary model of Caucasus and also its present tectonic situation will be briefly presented.

In chapter 3, a critical taper analysis will be performed, first for Alborz and then for other orogens of the AHB. To estimate “alpha” I will use topographic profiles derived from SRTM-90 m. The topographic profiles will be produced not only from a line, but also from a swath. A linear topographic profile can show the variation of elevation in two dimensions, whereas a swath profile can show it in three

dimensional views. The study of 2D and 3D topographic profiles provides a better estimation of “alpha”. To estimate “beta”, I will use geological cross-sections constructed by other authors. These cross-sections show basement and sedimentary layers. By means of lithological data, weak and strong layers can be identified. This helps to assess the detachment and consequently, to measure the basal dip or “beta”. Then, based on “alpha” and “beta” and by applying the critical taper equations, values of basal friction will be estimated. For the values of internal friction, the results of published studies (e.g. Dahlen, 1984) will be applied. Based on these parameters, I will try to suggest the mechanical state of the Alborz wedges. This state will be estimated in a first step by means of the critical taper equations. In a second step, the effect of some factors, such as lithology, tectonics, and climate on the estimated orogenic state will be considered.

In Chapter 4, the tectonic evolutionary model and the mechanical properties of the Alborz orogen are synthesized. This means that the effect of the tectonic and mechanical situation on geo-hazards is explained. For the first part (tectonics), I will try to explain a relationship between the detected tectonic cycles (refer to chapter 2) and the recent tectonic situation with geohazard. For the second part (mechanics), the relation between mechanical orogenic state and geohazard will be interpreted. In this regard, the effect of some natural factors, such as climate and lithology on mechanics of orogen will be considered. Lastly, I will outline topics of potential future studies.

## 2 A SUBDUCTION-COLLISION CYCLE EVOLUTIONARY MODEL FOR THE ALBORZ, IRAN

### Abstract

The Alborz mountain range in Iran is an ideal object to study the potential influence of past tectonic processes on the possible future evolution of this long-lived region of convergence. For this purpose, the outcome of earlier studies addressing the plate tectonics of the Alborz region has been reviewed and compiled with data on the present day tectonic activity at the crustal and upper mantle scale.

Previously published geodynamic concepts indicate that the Iran Plate was subjected to a series of extensional and compressional tectonic regimes, ultimately linked to the opening and closure of the Tethys Ocean and related basins. Two subduction-collision cycles are recognized. One of these occurred as a result of the subduction of the Iran Plate beneath the Turan Plate. In this cycle, the subduction phase ceased in the Cenozoic and since the Cenozoic it is in a collision phase. The other convergence cycle took place as a result of subduction of the Arabian Plate beneath the Iran Plate, and in this cycle the subduction phase began in the Mesozoic and is ending now. Thus, the current tectonic situation in the Alborz is a direct consequence of an ongoing Cenozoic subduction-collision cycle.

GPS and earthquake data indicate that the Alborz region is still an area of recently active compression. Moho and tomographic data show that there is no connection between slab remnants of the oceanic crust and the Iran Plate. In addition, the Moho beneath the central Alborz is about 20 km deeper than in surrounding areas, indicating further advancement of collision there. However, collision is continuing and the crustal area between the Iran Plate and the Turan Plate is increasingly shortening. This leads to thickening of the crust and deepening of the Moho from the center of the Alborz region towards its sides. Such an evolution can be also expected in other places of the Alpine-Himalayan Belt (AHB), such as the Caucasus region.

### 2.1 Introduction

Deformation resulting from the Arabia-Eurasia collision affects an area of ~3 Million km<sup>2</sup> of continental crust, making it one of the largest regions of convergent deformation on Earth (e.g. Allen et al., 2004). The Alborz range in northern Iran is a part of this Arabia-Eurasia collision zone (e.g. Allen et al., 2003) and builds the northern part of the Alpine-Himalayan orogen in western Asia (Fig. 2-1). It is located south of the Caspian Sea with about 3-5 km topography, a length of ~600 km in the east-west direction and a width of ~100 km in the north-south direction (Ritz et al., 2006).

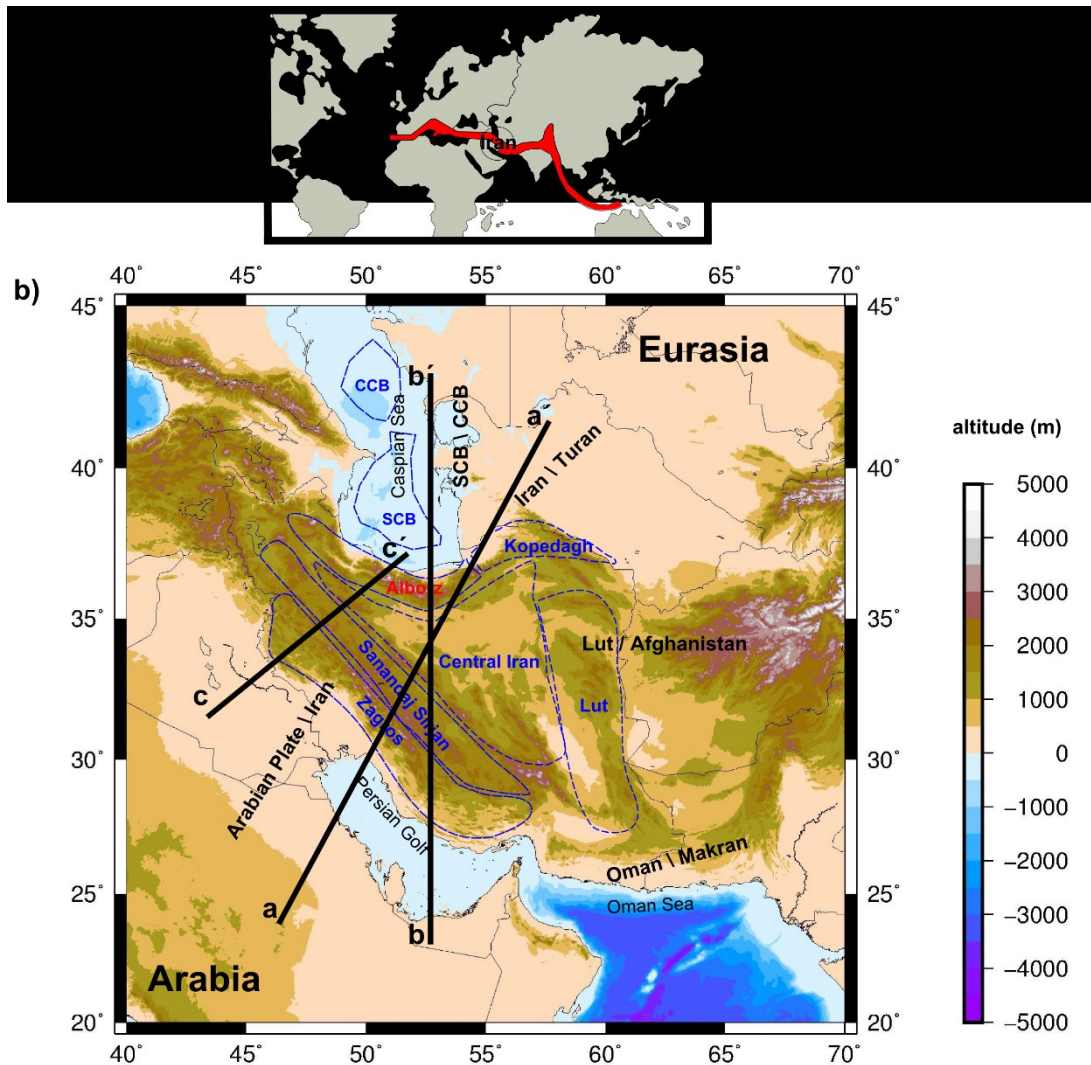


**Figure 2-1.** Introducing the Iran region and surroundings. **a)** Global view of Alpine-Himalayan Belt, **b)** Map of Iran/Alborz and surrounding area. Topography (DTU, Andersen and Knudsen, 2009). The studied profiles: **aa'** (Paleozoic evolution, cf. Berberian & King 1981; Fig. 2-3), **bb'** (Mesozoic evolution, cf. Wilmsen et al., 2009; Fig. 2-4), **cc'** (Cenozoic evolution, cf. Ballato et al., 2011; Fig. 2-5), geological-seismological zones (e.g. Aghanabati, 2004), **SCB\CCB**: subduction of the south Caspian Basin beneath Central Caspian Basin; **Iran\Turan**: subduction of Iran beneath Turan; **Lut\Afghanistan**: subduction of Afghanistan beneath Lut; **Arabian Plate\Iran**: subduction of the Arabian Plate beneath Iran.

GPS analysis reveals that shortening is varying across Iran. For example, in southern Iran shortening amounts to ~10 mm/yr, but in northern Iran (study area), within the central Alborz it is ~5 mm/yr over 100 km, i.e. 40% of the shortening between Central Iran and Eurasia (Vernant et al., 2004 a; Reilinger et al., 2006). Estimates for the crustal thickness of this collisional belt vary between 35 and 60 km in Iran (e.g. Tatar, 2001; Radjaee et al. 2007; Jiménez-Munt et al., 2012; Tunini et al., 2015). Dehghani and Makris (1984), Sodoudi et al. (2009), and Tatar (2001), suggested a crustal thickness of 35 to 36 km under the Alborz region. Abbassi et al. (2010) and Radjaee et al. (2007) proposed that the crustal thickness beneath the northern part of Central Iran and the Alborz mountains is about 58 km at maximum.

According to previously published geodynamic concepts, the Alborz region was subjected to a series of extensional and compressional tectonic processes, ultimately linked with the opening and closure of the Tethys Ocean and related basins (e.g. Ballato et al., 2011; Berberian and King, 1981; Wilmsen et al., 2009; Golonka, 2004). These evolutionary models resulted from a variety of different methodological approaches involving lithostratigraphy, sedimentology, petrology, and paleogeography focusing either on specific geological time intervals, e.g. only the Mesozoic (Wilmsen et al., 2009) or the Cenozoic (Ballato et al., 2011) or working at different spatial scales, e.g. Eurasia and the Arabian Plate, (e.g. Golonka, 2004) or only the Arabian Plate and the Iran Plate (e.g. Ballato et al., 2011). However, a long-term geodynamic evolutionary model for entire Iran, especially the Alborz region, involving recent tectonic activities on a plate tectonic scale, has not been provided to date. To achieve this goal, it is important to know, which tectonic regimes in which geological time dominated the Alborz region. Thus, focusing on the paleogeography, sedimentology, lithology, etc. is not the scope of this work.

Such a study will also illuminate a potential relationship between past and present tectonic events and also tectonic cycles. A long-term geodynamic model needs also to show the present time tectonic situation, comprehensively. For this purpose, I propose to combine studies of processes acting at the surface and close to the surface with those processes acting at depth. Knowledge of geodynamic processes having acted in the past and also the tectonic situation of the present time helps to develop a hypothesis about the tectonic situation of the region and also its future fate (Fig. 2-2).

The Alborz region, as an active area within the AHB, could have had tectonic evolutionary sequences similar and comparable to the other parts of this belt. The Caucasus region can be a suitable region for comparison, because it is not only a part of the AHB, but also near the Alborz region. A comparison between tectonic sequences of parts of the AHB, which helps to better understand the actual structure of the AHB orogens, has not been represented yet.

The intention of this study is two-fold. First, I review the tectonic evolution of Iran, especially the Alborz region. Second, I compile data to illustrate its present situation with regard to subduction/collision. From this, I develop a hypothesis for the ongoing collision of the present time and the future. The findings of the review of the geodynamic evolution of the Alborz region provide a consistent geodynamic framework from the Precambrian to the present and the future and enable to detect probable tectonic cycles and also to better understand the present-day mechanical situation of the orogen.

The main questions of the study are: (a) Which tectonic processes have shaped the Alborz region from the past to recent times? (b) Which regime is recently active? (c) Is there any relation between tectonic activities in the past and at present? (d) Is the tectonic evolution of this region a result of convergence cycles? (e) Are the answers to the above questions similar for an orogen neighboring the Alborz (for example the Caucasus)?

## 2.2 Data

This study has three steps (Fig. 2-2): To establish a geodynamic model from the Paleozoic to the recent time, three models suggested by other authors (Berberian and King, 1981; Wilmsen et al., 2009; Ballato et al., 2011) are compiled and integrated. To assess present tectonic activities in the Alborz, a study of the crust and upper mantle of the area is necessary. To do so, two datasets are used:

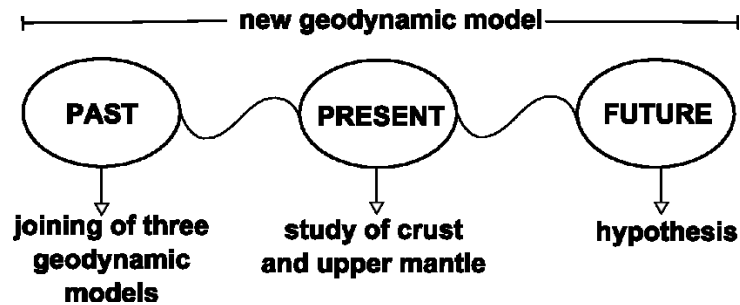


Figure 2-2. Schematic structure of the study (chapter 2).

The first data set consists of actual near surface and crustal deformation data, which have been obtained from GPS, seismic activity and stress regime data. With the help of GPS data, it is possible to study horizontal surface deformation. For this purpose, I use GPS data obtained by Vernant et al. (2004 a, b) and Reilinger et al. (2006). To understand seismic activity of the area, data from the NEIC catalogue (National Earthquake Information Center) from 1900 to 2014 have been used. This catalogue gives information, such as coordinates, depth, and magnitude of earthquakes in the studied region. To specify the stress regime, data from the Centroid Moment Tensor catalogue (CMT) from 1900 to 2014 and also the World Stress Map catalogue (WSM) have been used.

The second data set consists of Moho and upper mantle data based on gravity, geoid studies and topography. These data sets can illustrate the crustal depth of orogen. For this part, Moho data obtained by Motavalli-Anbaran et al. (2013) have been used. In addition, seismic tomographic data reveal the existence of subduction phases and potential connections between the slab and subducted plate. Eventually it can be identified, whether subduction is ongoing or if a new collision phase is already initiated. To do so, results from tomographic studies (e.g. Bijwaard et al., 1998; Alinaghi et al., 2007; Maggi and Priestley, 2005) have been used. To provide digital maps, the GMT software (Generic Mapping Tools, Wessel and Smith, 2010) has been used.

From the entire data set described here, I will not only get a good overview about present day tectonic activity, but also will be able to develop a hypothesis for the future development of the Alborz region. At the end, the Alborz region with the Caucasus as another orogen of the AHB is studied to understand, whether these active regions experienced the same tectonic sequence and are in a similar recent tectonic situation.

## 2.3 Review of the geodynamic evolution of the Alborz region

### 2.3.1 Paleozoic

In the Paleozoic, Iran experienced extensional and compressional regimes. From the Precambrian to the Mesozoic, strata in the Alborz ranges experienced shortening and uplift (e.g. Berberian and King, 1981; Aghanabati, 2004; Fig. 2-3).

An orogenic event, such as the Katangan orogeny, affected the Iran Plate in the Precambrian. After the Katangan orogenic event, from the Late Precambrian to the Middle Triassic, Iran as a stable platform has been covered by shallow sea, which occasionally was turned to land as a result of uplift and regression (Aghanabati, 2004). There are different geological reports about the effect of the Katangan orogeny on the Iran Plate. The majority of these reports, based on the age of Precambrian schists in north Iran (Gorgan), accepted that the Katangan event affected the region. In contrast, some reports based on eventual gradual changing to Neoproterozoic formations (e.g. Soltanieh Formation), denied that the Katangan orogeny had effect on the region (Aghanabati, 2004).

The oldest units exposed in the Alborz are Precambrian low-grade metasediments (Assereto, 1966). The following Paleozoic to Early Cenozoic sedimentary sequence is discontinuous, contains several angular unconformities, and consists of quartzites, sandstones, limestones, shales, dolomites, and a minor component of volcanic rocks, deposited in continental and shallow marine depositional environments. The Pre-Cambrian to the Early Cenozoic sedimentary sequence locally reaches ca. 10 km thickness (Assereto, 1966).

From the Upper Paleozoic (around the Carboniferous) there was the supercontinent Pangea. This supercontinent began to divide into two continents, Gondwana and Laurasia, in the Upper Paleozoic and Lower Mesozoic. Gondwana moved to the south, Laurasia moved to the north and in this time, the Paleotethys Ocean formed between these two continents (e.g. Berberian and King, 1981). The Alborz (Al.), Central Iran (C.I.), the Sanandaj Sirjan (S.S.), the High Zagros (H.Z.), and the Arabian plate (A.) belonged to Gondwana, whereas at that time, Kopedagh (K) belonged to Laurasia (e.g. Aghanabati, 2004; Berberian and King, 1981; Fig. 2-3 A, B).

From ~250 Ma, a contractional tectonic regime was present between Gondwana and Laurasia and the Paleotethys Ocean began to become smaller between the Alborz and Kopedagh (Aghanabati, 2004; Berberian and King 1981; Fig. 2-3 C, D). During the closure of the Paleotethys and related subduction, an extensional tectonic regime was present in the Main Thrust Fault Zagros (MTFZ) and also formed the Neotethys (the 'High-Zagros Alpine Ocean') between Zagros and Central Iran. As a result of these processes i.e. the closure of the Paleotethys and forming of the Neotethys, Zagros separated from the Arabian Plate and the Iran Plate moved to the north (e.g. Berberian and King, 1981; Fig. 2-3 D; Fig. 2-4 A).



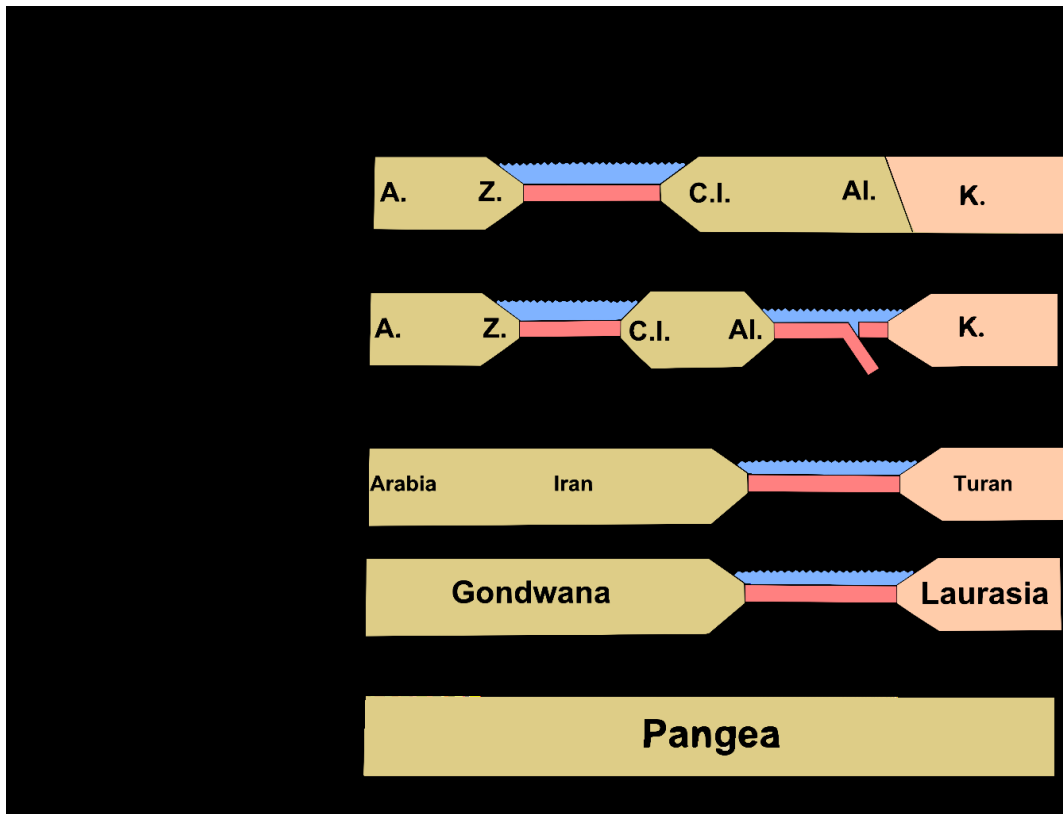


**Figure 2-3.** Paleozoic-Mesozoic evolution of Iran and surroundings. (A-B), Arabia and Iran belongs to Gondwana, but Turan belongs to Laurasia. (C), contractional regime between Iran and Turan, and closure of Tethys. (D), extensional regime in Iran and forming of the Neotethys. Arabian Plate (A), Zagros (Z.), Central Iran (C.I.), Alborz (Al.), Kopedagh (K.), after Berberian and King, 1981; Aghanabati, 2004. See also Fig. 2-1 for the position of profile aa'.

### 2.3.2 Mesozoic

In the Mesozoic, due to the subduction of the Iran Plate beneath the Turan Plate, and also the subduction of the Arabian Plate beneath the Iran Plate with NE-SW directions, a regional contractional regime dominated in entire Iran, but some local extensional regimes occurred in Central Iran and the Alborz region due to rifting processes (e.g. Berberian and King, 1981; Wilmsen et al., 2009; Fig. 2-4 C-F). According to Wilmsen et al. (2009), initial Cimmerian collision started in the Carnian with subsequent Late Triassic synorogenic peripheral foreland deposition (flysch, lower Shemshak Group). Subduction shifted south in the Norian (onset of Neotethys subduction below Iran) and slab break-off around the Triassic-Jurassic boundary caused rapid uplift of the Cimmerides followed by Liassic post orogenic molasse. During the Toarcian-Aalenian Neotethys backarc rifting, a deep-marine basin formed which developed into the oceanic South Caspian Basin during the Middle-Late Jurassic (Wilmsen et al., 2009; Fig. 2-4).

#### 2.3.2.1 Lower Triassic (Late Ladinian-Carnian/ ca. 230-216 Ma)

By the Late Ladinian, the residual Paleotethys had narrowed due to northward drift of the Iran Plate. Consequently, spreading rates decreased from ~20 cm/yr to ~6 cm/yr (Stampfli and Borel, 2002; Muttoni

et al., 2009). In the Early Carnian (c. 225 Ma), the northern margin of the Iran plate transformed into a peripheral foreland basin (Fig. 2-4 B). Flexural subsidence led to drown the Carnian platform in northern Alborz (e.g. Robertson, 1987, 1994, 2004; Galewsky, 1998; Garfunkel and Greiling, 2002). An “all-round erosional unconformity” occurred in the south and caused intensive weathering (deCelles and Giles, 1996). There was also local erosion due to forebulge uplift in the Paleozoic formations (deCelles and Giles, 1996 and references therein). Extensional faulting at the forebulge caused the subaerial eruption of basal alkaline volcanics in the central Alborz (Fig. 2-4 B). During rapid flexural subsidence, the northern Alborz was filled with red clays derived from erosion of lateritic soils of the Iran Plate, and dark fine-grained siliciclastics from the Turan margin. This suggests significant coupling between the Iran and the Turan Plate during the Carnian (Wilmsen et al., 2009).

### 2.3.2.2 Lower-Upper Triassic (Norian-Rhaetian / 216-200 Ma)

During the Norian–Rhaetian, the initiation of Neotethys subduction at the southern margin of the Iran Plate reduced compression of the Iran Plate with subsequent formation of extensional basins (Fürsich et al., 2005 b) and transgression of the sea onto the Iran Plate. During the remainder of the late Triassic, the flexural foreland basin in northern Iran was filled with syn-orogenic siliciclastic sediments (Wilmsen et al., 2009; Fig. 2-4 C). The Upper Triassic succession of the northern Alborz displays the classical parts of an underfilled peripheral foreland basin (Sinclair, 1997 a) with a drowned carbonate platform covered by deep marine fines and turbidites (flysch phase; Wilmsen et al., 2009).

### 2.3.2.3 Main Cimmerian event (c. 200 Ma) to Early Lias (c. 200-183 Ma)

Around the Triassic-Jurassic boundary, a significant deformation event associated with a distinct increase in sediment supply affected the Alborz foreland basin (Wilmsen et al., 2009; Fig. 2-4 D). In the north, this event was characterized by an angular unconformity at the base of the conglomeratic formation, while coarse sandstones were deposited in the south. In the lower Jurassic, during slab break-off, rapid uplift and exhumation, molasse-type sediments overlaid the flysch-type Upper Triassic strata (Zanchi et al., 2009). This caused also in other parts of the AHB, such as North Alpine foreland (von Blanckenburg and Davies, 1995; Sinclair, 1997 b; Regard et al., 2008). The events taking place in the Alborz are similar to the Cimmerides, in c. 20-25 Ma (Wilmsen et al., 2009; Fig. 2-4 D) and are comparable with the Alpine slab- break-off event happening 15-20 Ma after the end of subduction (Sinclair, 1997 b; Regard et al., 2008). A similar rapid deformation and uplift event occurred also in the Zagros foreland c. 15-20 Ma after initial plate coupling followed by deposition of coarse conglomerates (Agard et al., 2005; Mouthereau et al., 2006).

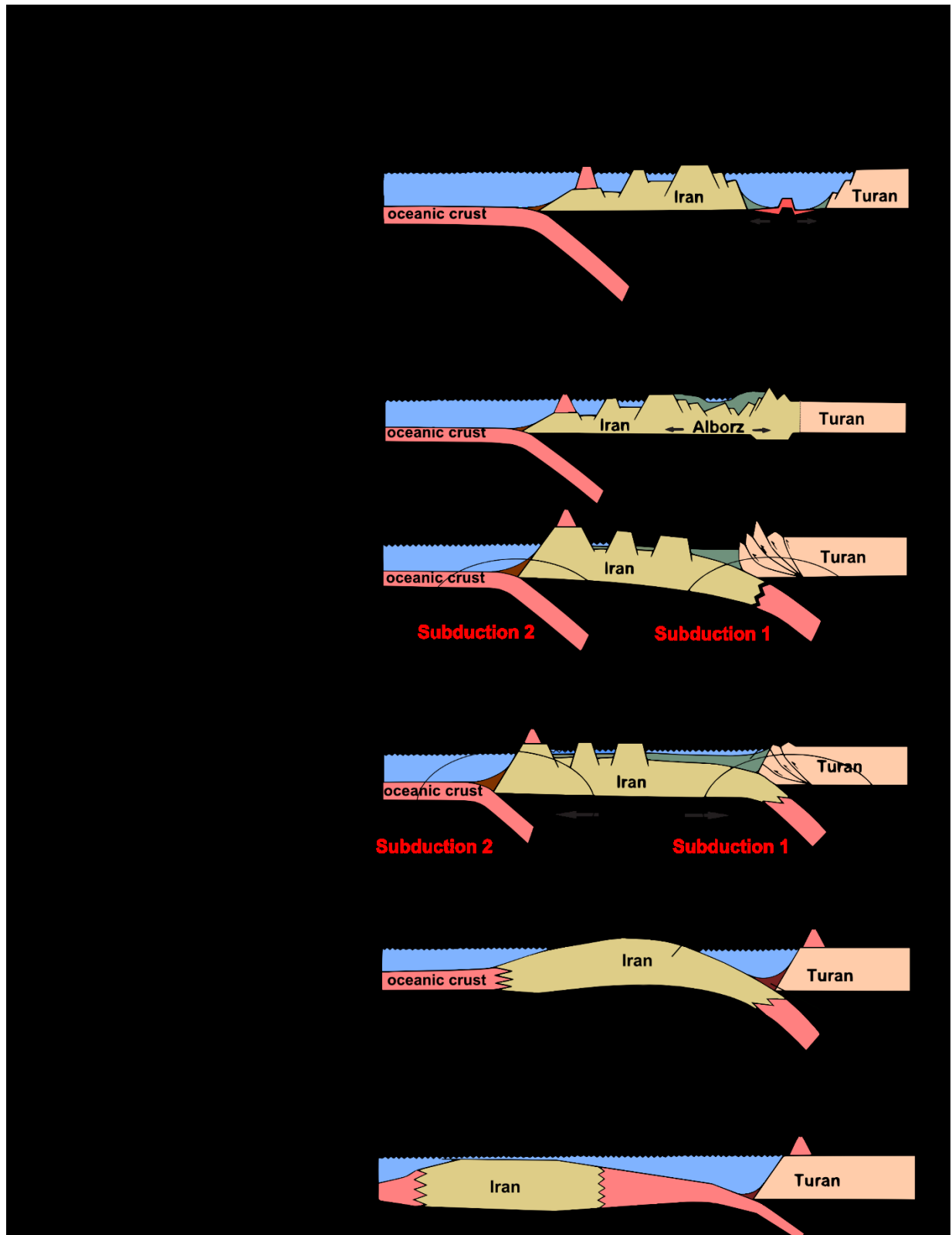


**Figure 2-4.** Mesozoic evolution of Iran and surroundings. This model focuses on geodynamic evolution between Iran and Turan, Arabian Plate is out of this profile but it is connected to the left of the oceanic crust. (A-B) the first subduction phase between Iran and Turan, (C) the second subduction phase between Iran and Arabia, (D) slab breakoff of Iran beneath Turan, (E) end of subduction phase between Iran and Turan, (F) birth of the South Caspian Basin with the Alborz mountains forming at its southern margin. Different time slices representing important phases of the, Zagros (Z.), Central Iran (C.I.), Alborz (Al.), Kopedagh (K), after Wilmsen et al., 2009. See also Fig. 2-1 for the position of profile bb'.

#### 2.3.2.4 Lower Jurassic-Middle Jurassic (Toarcian-early Bajocian /183-170 Ma)

During the Toarcian-Aalenian, high tectonic subsidence rates (60m/Ma) and rapid N-S thickness changes suggest a tectonic control by means of onset of extension in northern Iran (Fürsich et al., 2005 a, 2009 a). This Toarcian-Aalenian extension was related to the ongoing Neotethys subduction and the final opening of large back-arc-rift basins along the Eurasian margin (Zonenshain and Le Pichon, 1986; Stampfli, 1996, 2000; Stampfli and Borel, 2002; Brunet et al., 2003; Golonka, 2004). During the Early Bajocian, the Alborz basin filled rapidly with large deltaic sediments (Fürsich et al., 2005 a) through a short uplift phase of the basin margins (Mid Cimmerian Event; Fürsich et al., 2009 b).

#### 2.3.2.5 Middle Jurassic (Late Bajocian-Late Jurassic/170-150 Ma)

According to Wilmsen et al. (2009), after the Mid-Cimmerian event, as a result of crustal extension, a renewed phase of rapid subsidence occurred across the entire northern Iran from the Late Bajocian onwards. Due to crustal extension, considerable deepening and rotated fault blocks occurred (Fürsich et al., 2009 b). This event of increased back-arc-rifting represents the birth of the South Caspian Basin (Brunet et al., 2003), with the Alborz forming at its southern margin (Wilmsen et al., 2009; Fig. 2-4 E-F). The Late Bajocian-Late Jurassic extension also affected NE Iran and the South Caspian Basin (Taheri et al., 2009). The weakness of the Paleotethys suture facilitated the beginning of the rifting phase in the Toarcian. The brief mid-Bajocian uplift pulse of the Mid-Cimmerian tectonic event may indicate the break-up unconformity of the South Caspian Basin (Brunet et al., 2003; Fürsich et al., 2009 b), which developed into a back-arc ocean during the Middle-Late Jurassic (Stampfli, 2000; Stampfli and Borel, 2002).

### 2.3.3 Cenozoic

In the Cenozoic, the subduction of the Arabian Plate beneath the Iran Plate continued, therefore a contractional regime accompanied by an intense volcanic eruptive phase occurred in Iran (e.g. Ballato et al., 2011). Rapid sedimentation and erosion took place due to acceleration of shortening in Early Miocene (Axen et al., 2001). The time period between the initiation of continental collision (36 Ma) and the acceleration of regional deformation (20-17.5 Ma) reflects a two-stage collision process, involving the “soft” collision of stretched lithosphere at first and “hard” collision following the arrival of unstretched Arabian continental lithosphere in the subduction zone (Ballato et al., 2011). Crustal shortening in the present Alborz must have started shortly after the end of the arc-magmatic phase at ca. 36 Ma. All deformation processes, such as upper plate shortening, uplift, and basin formation recorded in the Alborz range were closely related to the convergence between Arabia and Eurasia (e.g. Ballato et al., 2008, 2011).

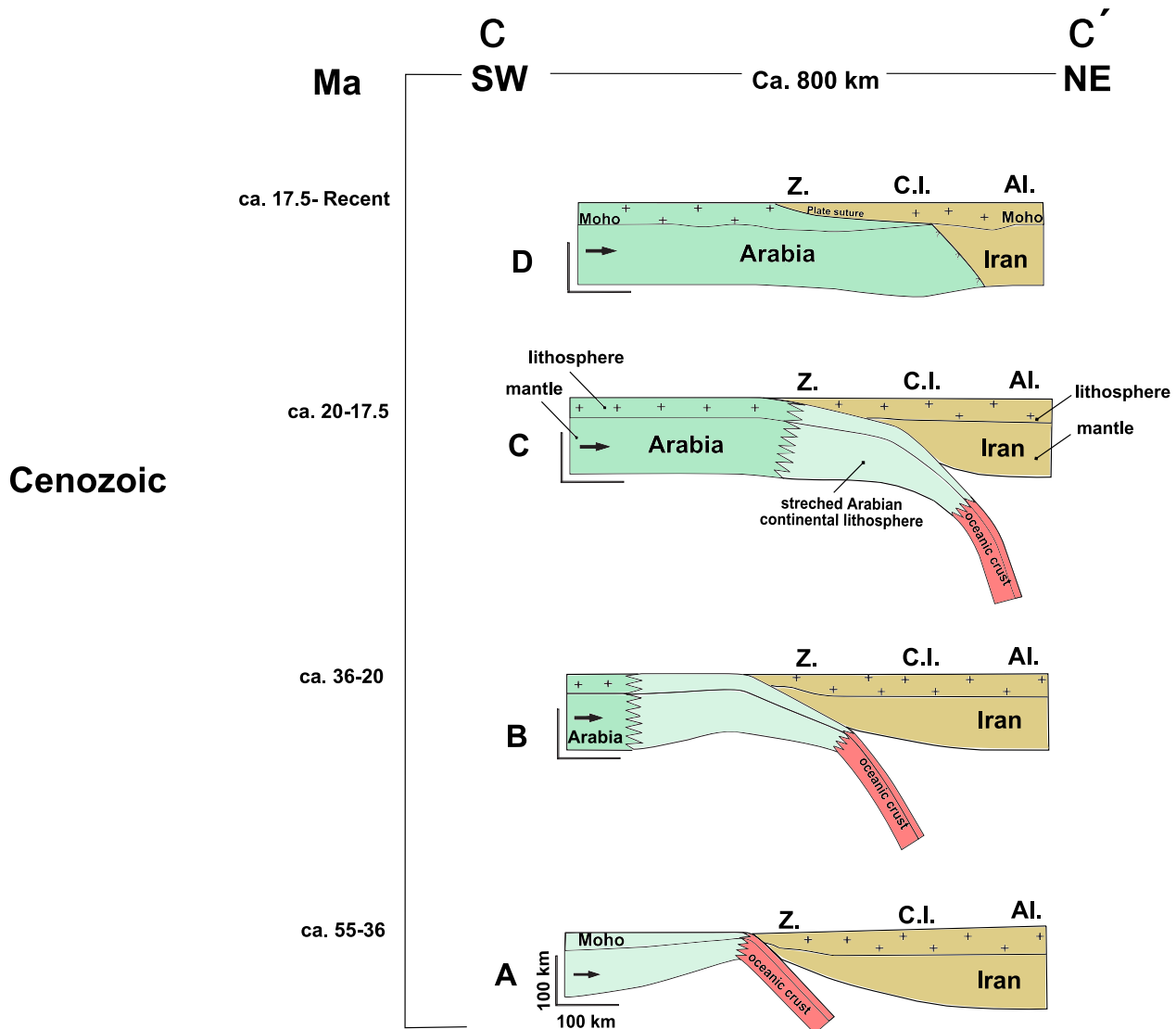


**Figure 2-5.** Cenozoic evolution of Iran and surroundings. This model focuses on geodynamic evolution between Iran and the Arabian Plate, Turan is out of this profile but it is connected to the right of Iran. A) Start of subduction of Arabia beneath Iran, B-C) continuation of the subduction and slab breakoff, D) start of collision. Zagros (Z.), Central Iran (C.I.), Alborz (Al.), after Ballato et al., 2011. See also Fig. 2-1 for the position of profile cc'.

Shortening took place across most of the present day deformation zone during the Latest Eocene to Early Oligocene (Ballato et al., 2011, Fig. 2-5). Taken together, tectonic processes during the Cenozoic consisted of two parts: continental subduction and plate suturing (e.g. Ballato et al., 2011). In the initial stage of continental collision, there was a primary continental subduction, and in this stage most of the plate convergence was absorbed by subduction processes. As a result, partial decoupling of sediments from the subducting continental crust, deformation along the accretionary prism, and melting of subducted continental crust at depth occurred (Chemenda et al., 1996, 2000; Regard et al., 2003; Toussaint et al., 2004).

Approximately 480 km of continental lithosphere was subducted between 36 and 20 Ma when the Arabian Plate motion slowed from 3 cm/yr to 2 cm/yr (McQuarrie et al., 2003). In other words, if subduction rate is 3 cm/yr, about 600 km will be subducted in ca. 20 Ma. Therefore a slow down can only begin at ca. 20 Ma and plate tectonic reconstructions for the Middle East do not reveal variations in convergence rates before ca. 20 Ma (Ballato et al., 2011).

Due to arid climatic conditions in the Arabia-Eurasia region, the effects of erosion and tectonic denudation have been limited. Consequently, exhumed remnants of subducted continental lithosphere have not been detected (Chemenda et al., 1996). Unequal crustal thickness, in the range of ~ 45 km and ~75 km across the suture zone of the Arabia-Eurasia collision could be a result of underthrusting of the Arabian Plate, which may have resulted in more than 30 km of crustal thickening (Paul et al., 2010).

As mentioned, from ca. 20 Ma onward, motion of the Arabian Plate slowed. Since this time, continental collision caused a plate suturing phase (Ballato et al., 2011). In this phase, as a result of the progressive severing of subduction process, the Arabia-Eurasia convergence rate was decreased (McQuarrie et al., 2003; Hatzfeld and Molnar, 2010). The time lag between the Late Eocene and Early Oligocene coincided with the onset of continental collision and continental accretion following the subduction of stretched continental lithosphere (Ballato et al., 2011).

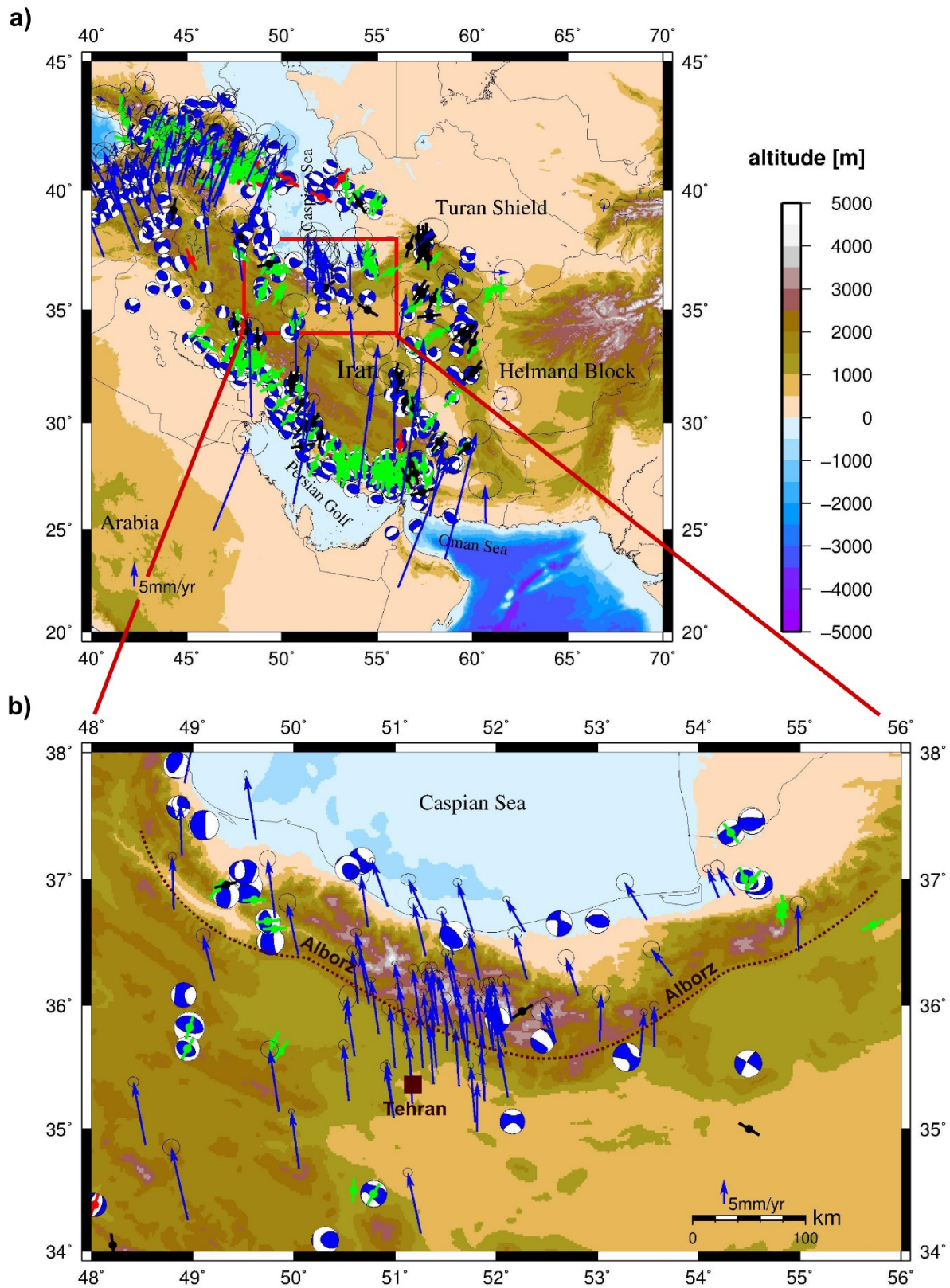


**Figure 2-6.** Map of stress regimes and shortening rates of Iran (a) /Alborz (b). Topography (DTU, Andersen and Knudsen, 2009), **blue arrows:** GPS velocity (Vernant et al., 2004 a, b), **beach balls:** Focal mechanism (CMT Catalogue, Ekström et al., 2012), stress regime (WSM Catalogue, Heidbach et al., 2008, WSM Symbols, **Red:** normal fault, **green:** thrust fault, **black:** strike slip fault).

## 2.4 Recent situation

To complete the proposed geodynamic model, information on recent tectonic activities is reviewed and linked with the presented geodynamic models. Studying of these present day activities accompanied by the knowledge of past events helps to understand, how previous geodynamic changes affect recent tectonic. These processes can deform the surface and depth of a region. Hence, surface and depth of the region need to be studied.

### 2.4.1 Near surface and crustal deformation

According to Mouthereau et al. (2012), deformation developed near the places of underthrusting and accretion of Arabian crust beneath Iran since ~25 Ma, then propagated after 15-10 Ma both southward to the Zagros Folded Belt (Gavillot et al., 2010; Khadivi et al., 2010, 2012) and northward in the Alborz (Guest et al., 2006 b), the Kopedagh, the South Caspian Basin (Hollingsworth et al., 2010; Shabanian et al., 2009 a,b), and in to Central Iran (Morley et al., 2009) in association with the uplift of the Iran Plate (Mouthereau et al., 2012).

Based on GPS data, present tectonics in Iran are best described as north-south convergence between the plates of Arabia to the southwest and Eurasia to the northeast at a rate of about 22 mm/yr (Fig. 2-6 a). Between Central Iran and the Arabian Plate, the shortening rate is about  $7\pm 2$  mm/yr. Shortening decreases in northern Zagros. North of Central Iran, the Alborz mountain range accommodates  $8\pm 2$  mm/yr of north-south compression (e.g. Vernant et al., 2004 a; Masson et al., 2006). According to Djamor et al. (2010), the GPS velocities in the Alborz region differ regionally. Velocites in western Alborz are ~3 mm/yr faster than in the eastern sites in the Eurasia fixed reference frame. To account for this difference, these authors reasoned that the GPS sites northeast of Alborz are farther away from the main active thrust fault than the northwestern GPS sites. Another explanation could be that western and eastern Alborz have different kinematics (Djamor et al., 2010; Fig. 2-6 b; table 2-1).

Active deformation at the northeastern boundary of the Arabia-Eurasia collision zone is taken up by strike-slip faults, which are oblique to the convergence direction in this boundary zone (Vernant et al., 2004 b; Reilinger et al., 2006). Masson et al. (2005), based on GPS data, found that the Arabia-Eurasia convergence is distributed within several regions as mountains belts and large strike-slip faults, but the seismotectonics of the Alborz range is largely controlled by major thrust faults (Jackson et al., 2002; Ashtari et al., 2005).

The WSM catalogue shows that the main active tectonic structures of Iran and Alborz are strike slip and thrust faults, thus a compressional regime dominates the area (Heidbach et al., 2008). This agrees with the results of e.g. Allen et al. (2003), Guest et al. (2006 a, b), Ritz et al. (2006), Berberian and Berberian, (1981), Priestley et al. (1994), and Jackson et al. (2002). Extensional structures represented by normal faults are not often visible on the map. The CMT catalogue (Ekström et al., 2012) affirms this, too (Fig. 2-6).



At present, active deformation is focused along the northern and southern margins of Alborz with the southern margin exhibiting major thrusts that emplace Paleozoic to Eocene rocks on Quaternary alluvial gravels (e.g. Annells et al., 1975, 1977; Haghypour et al., 1987). Active faulting along the northern margin of the Alborz is more difficult to assess due to the poor exposure and the limited amount of work that has been done in the region (Guest et al., 2007). However, the number and activity of faults in northern Alborz are lower than in southern Alborz (Stocklin, 1974; Guest et al., 2006 a, b).

**Table 2-1.** Shortening rate in the Alborz region.

	GPS measurements		Geological evidences
	Vernant et al., 2004 a, b	Djamour et al., 2010	
<b>Central Alborz</b>	8 ± 2 mm/yr Global left lateral rate: 4±2 mm/yr	-	N-E shortening oblique to the E-W structures of central Alborz in Pliocene and Quaternary (e.g. Jackson et al., 2002).
<b>North Alborz</b>	6 mm/yr	-	N-S compression between Central Iran and South Caspian basin in Miocene (e.g. Jackson et al., 2002).
<b>NW-Alborz</b>	14±2 mm/yr	Velocities in NW Alborz are ~3 mm/yr faster than eastern sites	~14 mm/yr (Jackson et al., 2002). 15-20 mm/yr (Jackson & McKenzie, 1984).
<b>NE- Alborz</b>	-	GPS coverage in NE is less than NW. Different kinematics of east and west of Alborz	-

## 2.4.2 Seismicity

Iran is a seismically highly active region. Since 1978, there have been at least five earthquakes with magnitudes of more than 6 that contributed substantial faulting (e.g. Mohajer-Ashjai and Nowroozi, 1979; Berberian, 1979 a, b, c; Nowroozi and Mohajer-Ashjai, 1981). Seismicity of Iran has been reported by a number of authors, e.g. Nabavi (1975), Nabavi and Partoazar (1977), Nowroozi (1971) Berberian (1976), and Ahmadi and Nowroozi (1980), Masson et al. (2005) and Engdahl (2006). According to these studies, seismicity of Iran does not show the same characteristics everywhere.

Three seismological zones are identified in Iran by Masson et al. (2005). Zone 1 corresponds to the Zagros and Sanandaj Sirjan. It is characterized by extensive seismicity and high geodetic strain. Zone 2, corresponding to Central Iran, shows low seismicity and no geodetic strain. Zone 3 is in between, i.e. this zone suffers low or moderate seismicity but a high geodetic strain. It corresponds to northwestern Iran, the Alborz, Kopedagh, and Lut regions (Fig. 2-1). This last group could be divided into two subzones, northwest Iran and the Alborz on one side and Kopedagh and Lut on the other side based on the number of earthquakes. The ratio of strain/number of earthquakes is generally higher in the Alborz and

northwest Iran than it is in the Lut and Kopedagh. All regions of zone 3 (Alborz) are crossed by large strike-slip faults (Masson et al., 2005).

Instrumental earthquake data of the Alborz shows that the most activity is concentrated along the mountain ranges (Fig. 2-7). Thus, several regions are vulnerable to destructive earthquakes (e.g. Tavakoli, 1996; Masson et al., 2005). Besides, for the Central Alborz numerous strong historical earthquakes (Tchalenko, 1975; Ambraseys and Melville, 1982; Berberian and Yeats 1999; 2001) are reported.

In addition to the seismological zones, which identified by Masson et al. (2005), seismotectonic provinces of Iran is studied by several investigators (e.g. Stoklin, 1968; Takin, 1972; Alavi, 1972; eftekharneshad 1980; Berberian, 1976, 1983; Nowroozi, 1976; Tavakoli 1996). Each seismotectonic province bounded by geological, tectonical and seismological features, which mark a difference in seismotectonic characteristics of one province from its neighboring provinces (e.g. Tavakoli, 1996). In the mentioned studies, different divisions for the seismotectonics provinces have been suggested. In each of them, the Alborz region is limited by different geographical boundaries.

The comparison of seismic and geodetic strain rates indicates that highly strained zones experience mainly aseismic deformation in southern Iran (3% seismic) and seismic deformation in northern Iran (30-100% seismic, Masson et al., 2005). Spatially, high seismic coupling zones correlate well with high-magnitude earthquake zones (Masson et al., 2005). Seismicity in northern Iran is mainly limited to the Alborz region with Central Iran and south Caspian basin (e.g. Priestley et al., 1994). Since many of the region's earthquakes were not associated with surface faulting, or damaged areas of many of these earthquakes are relatively large, locating active faults, which cause earthquakes, becomes complicated (Hessami and Jamali, 2006).

The bulk of seismicity in the Alborz region is shallow (<15 km) and partitioned into sinistral strike slip faults and thrust fault (e.g. Berberian and Berberian, 1981; Priestley et al., 1994; Jackson et al., 2002; Allen et al., 2003). According to the NEIC catalogue, more than 400 earthquakes occurred between 1900 and 2014. These earthquakes had magnitudes between 3 and 7.5. The NEIC catalogue shows a hypocentral depth of 1-60 km for the earthquakes, thus they are crustal earthquakes (Fig. 2-7). Epicenters are located in the Alborz mountain chains. This emphasizes that the area is active. Most of the earthquakes have hypocentral depth of 30-50 km. Two earthquakes were larger than magnitude seven. One of them was located in central Alborz with a hypocentral depth of 20-30 km (Fig. 2-7). It should be noted that Fig. 2-7 same as Fig. 1-3a, shows earthquake data but in larger coordinates in accordance with other maps of this chapter. Because all maps of this chapter will be correlated at the end of chapter.

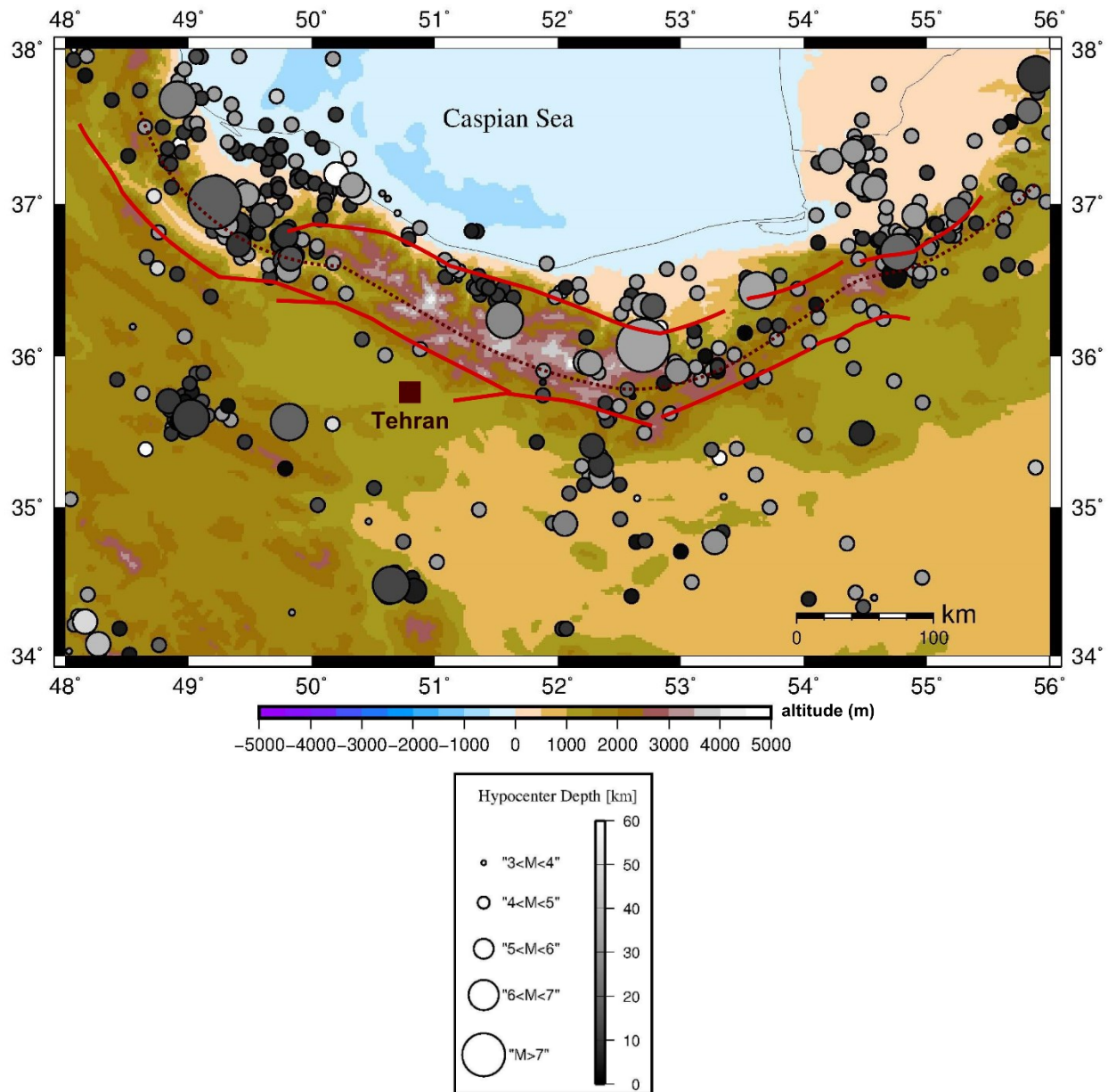


**Figure 2-7.** Earthquakes and main faults in the Alborz region. Red dotted line: water divide. Red line: main thrust faults (Berberian et al., 1993; Hind et al., 2001), topography (DTU, Andersen and Knudsen, 2009), earthquakes (NEIC catalogue 1900-2014). See also Fig. 2-6 b for the location of map.

### 2.4.3 Moho and upper mantle

Mouthereau et al. (2012) showed that the current elevation of the Iran Plate can be explained by the original differences in the initial thickness of the continental crust resulting from subduction and the related back-arc thinning events. Additional effects due to 1) small-scale convective removal of Iranian lithospheric mantle during roll-back of an originally flat slab or 2) slab detachment, may have also contributed to the current regional elevation (Mouthereau et al, 2012 and references therein).

Crustal thickness varies from 35 to 55 km in the Alborz region and surroundings (e.g. Molinaro et al., 2005; Hafkenscheid et al., 2006; Kaviani et al., 2007; Paul et al., 2010; Manaman and Shomali, 2010; Motavalli-Anbaran et al., 2011; Jiménez-Munt et al., 2012). However, there are different estimations about crustal thickness of the Alborz region:

A first group of studies estimated a thin crustal thickness (35-36 km) under the Alborz region (e.g. Dehghani and Makris, 1984; Guest et al., 2007; Sodoudi et al., 2009; Tatar, 2001) implying that the area is isostatically under-compensated at Moho level with no crustal roots (i.e. the base of crust does not move down in the mantle as the density of the crust increases).

A second group of studies proposed a thicker crust beneath the Alborz (Abbassi et al., 2010; Radjaee et al., 2007). Radjaee et al. (2007), using receiver functions from a temporary seismic network, obtained a crustal thickness of 46-48 km in the south of Alborz, 55 km in its central part and about 44 km at the northern flank of the Alborz region. Radjaee et al. (2010) proposed that the central Alborz Mountain chain has a moderately thick crustal root but that thickness is insufficient to compensate for the elevation of the range. Moho estimates resulting from using receiver functions can be reliable. The Moho depth estimated in the studies of the first group may be erroneous due to effects of data interpolation (Motavalli-Anbaran et al., 2011). However, results of the second group of studies are in agreement with new results of Motavalli Anbaran et al. (2013) and these estimates have been used for our study.

According to the results of Motavalli-Anbaran et al. (2013), the maximum Moho depth in the central Alborz is ~55 km, which indicates a root underneath the Alborz mountains, i.e. it seems that during the collision and consequently the forming of the orogen, the thickness of the crust increased. Besides, Moho depth in the central Alborz is deeper than west and east of this area (Fig. 2-8).

Figure 2-8 shows Moho depth in the Alborz region obtained from 3D joint inversion modeling of lithospheric density structure based on gravity, geoid and topographic data by Motavalli-Anbaran et al. (2013). At the center of the map (central Alborz), in an area of around 200 km<sup>2</sup>, a Moho depth of more than 50 km is visible. It decreases to the east and west of this area up to about 40 km (Fig. 2-8). A review of Moho depth studies of Iran and surrounding areas (e.g. Jiménez-Munt et al., 2012; Motavalli-Anbaran, 2013) shows that the mentioned difference between the minimum and the maximum depth of Moho (about 10 km) is recognizable in other places, such as the Zagros and the Caucasus, too.

It needs to be kept in mind that the collision phase of Alborz is older than that of Zagros, i.e. the collision phase which is happening in the Zagros region, had happened in the Alborz region in the Mesozoic (e.g., Ballato et al., 2011; Wilmsen et al., 2009). Thus, the Alborz can be viewed as a time window into the past to understand current tectonics in the Zagros region. It should be noted that Moho maps obtained from older studies are in fact large-scale maps with low resolution (e.g. Laske et al., 2013; Alinaghi et al., 2007). High resolution Moho maps for the Zagros region are not available, although it would be desirable to better know crustal thickness in the Zagros region. However, Moho depth in the central Alborz region

could infer that a new collision phase is at its initial stage. I speculate that a similar situation could be possible in the Zagros region in future.

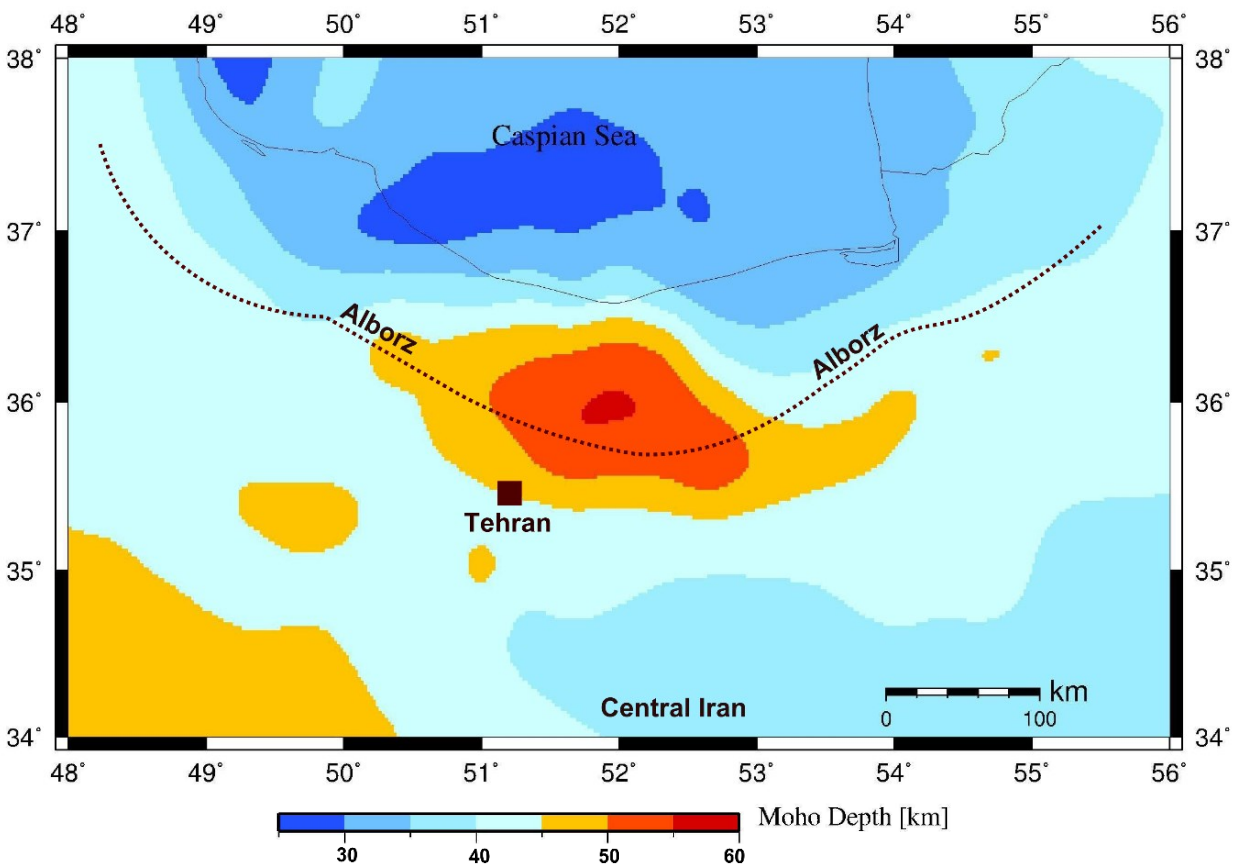


**Figure 2-8.** Moho depth of the Alborz region. Dotted line: water divide line, Moho data from Motavalli-Anbaran et al., 2013. See also Fig. 2-6 for the location of map.

Seismic tomography studies of the upper mantle of the Middle East show wide regions with high-velocity anomalies at depths of down to 2200 km (Bijwaard et al., 1998; Van der Voo et al., 1999). These anomalies have been inferred to correspond to the subducted slab of the Neotethys oceanic lithosphere beneath central and southern Iran. Local tomography studies in Iran suggest that along the Zagros mountains, Neotethyan slab remnants are only partially connected to the Arabian Plate (Alinaghi et al., 2007). Tomographic studies indicate also an anomalously high temperature of the uppermost mantle beneath central and northwestern Iran (Maggi and Priestley, 2005; Alinaghi et al., 2007). This suggests that subduction is no longer active now, and the Neotethys slab might have been partially detached following continental collision (Paul et al., 2010). Asthenosphere upwelling and consequently a new pulse of magmatic activity could take place as a result of slab break-off (Ballato et al., 2011).

## 2.5 Discussion

### 2.5.1 Present day tectonic situation

In order to study the Alborz region in the present time, the individually discussed data sets have been compiled and are described at a whole (Fig. 2-9). There is a spatial correlation between high GPS derived shortening rates, a deeper Moho, high seismicity and compressional regimes. GPS data show similar velocities and directions in the center of the Alborz region. Moho beneath the central Alborz is deeper than beneath the sides. Moment tensor solutions indicate strike slip and thrust faults.

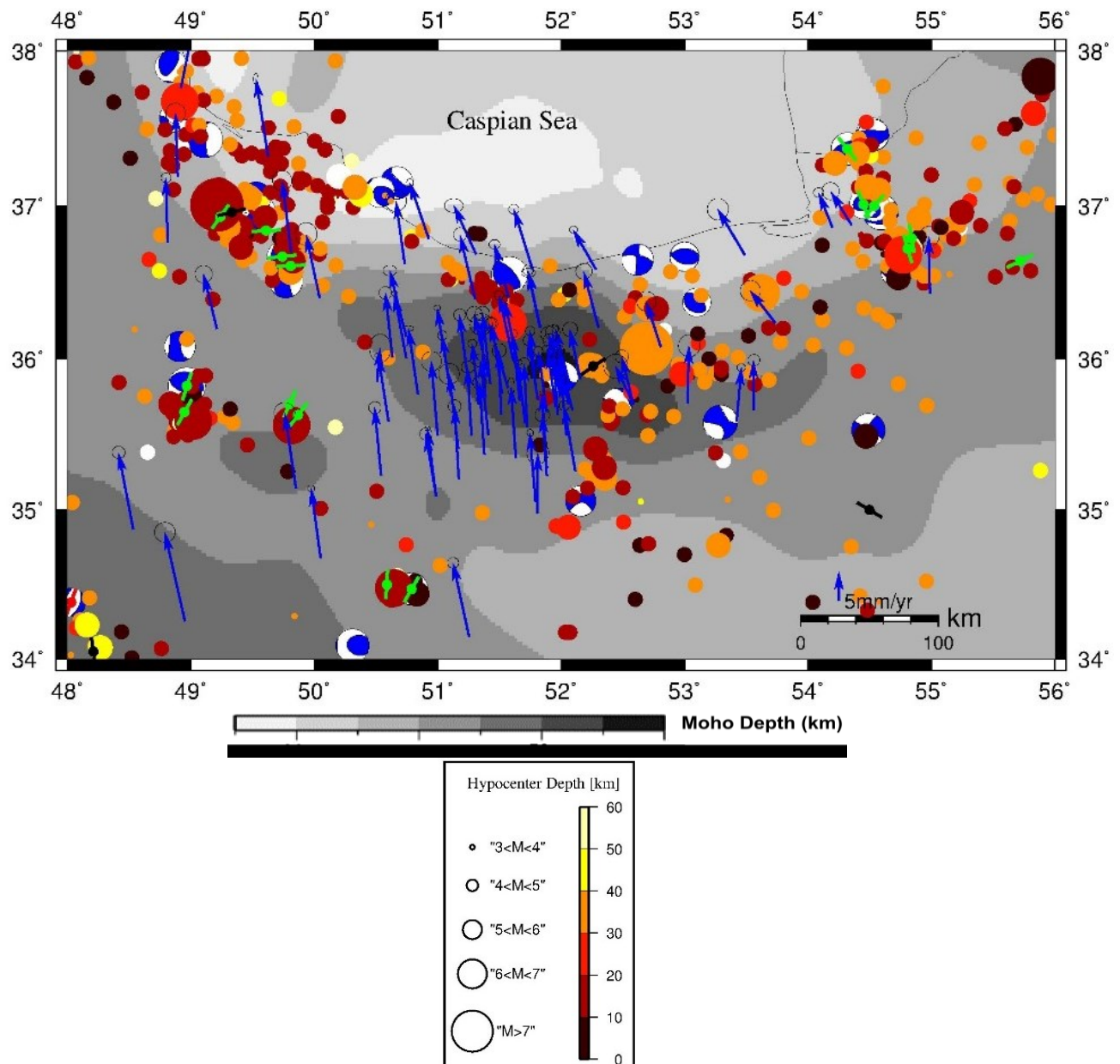


**Figure 2-9.** Map of stress regimes, Moho, and GPS velocities of the Alborz region. Moho data (Motavalli-Anbaran et al., 2013), earthquakes (NEIC catalogue, 1900-2014), **beach ball**: focal mechanism (CMT Catalogue, Ekström et al., 2012), **blue arrow**: GPS velocity (Vernant et al., 2004 a, b), stress regimes (WSM Catalogue, Heidbach et al., 2008, Symbols, **red**: normal fault, **green**: thrust fault, **black**: strike slip fault). See also Fig. 2-6 for the location of map.

All of the mentioned data imply a higher contractional regime in the center of the Alborz region. Additionally, a large earthquake with higher than magnitude 7 and a hypocenter depth of 30-40 km, took place at the center of the area. The observations show that a plate tectonic, such as a collision is happening in the center of the Alborz area (Fig. 2-9). Thus, the collision phase which started between the Iran Plate and the Turan Plate in the Mesozoic-Cenozoic may be continuing in present time. This is highly arguable if there is a region of collision, which is manifested in thickened and underthrust continental crust. As Moho deepening can occur as a result of crustal shortening and thickening during a collision phase, consequently region tectonic processes, such as shortening and seismic activity become larger. Thus, a higher collision rate in the center of the Alborz can be possible.

Furthermore, this collision area could develop towards the west and east of the Alborz region in the future, because if convergence continues, the shortened and thickened area may also increase. This means that Moho depth might increase from the center to the sides of the Alborz region. Accordingly, the thickness of lithosphere might increase from the center to the sides of the region. Thus, a wide collision area with a deep Moho and a thick lithosphere might arise in the entire Alborz region in the future.

### 2.5.2 Past tectonic situation

According to the geodynamic model proposed by Wilmsen et al. (2009), there were two subduction phases in Iran, and after each subduction, a collision phase arose. For example, in the Alborz region subduction and collision between the Iran and the Turan Plate took place. Wilmsen et al. (2009) argued that the detachment of the Iran Plate under the Turan Shield has occurred around 190 Ma (Early and Middle Jurassic). Vergés et al. (2011) suggested that there is no slab remnant under the Turan Shield. According to the compiled data sets (Moho, GPS, stress regimes, seismicity), there is a compressional phase in the region. If we assume that in the Alborz region (between the Iran Plate and the Turan Plate), a subduction phase was presented before ~190 Ma, and since ~190 Ma a collision phase has been presented, therefore a cycle of subduction-collision may explain the tectonic evolutionary of the Alborz region.

A similar collision cycle might also be a realistic solution for the Zagros region. Some authors, such as Vergés et al. (2011), suggested that the subduction of the Arabian Plate beneath Iran is continuing and the present day Arabian Plate boundary has a relatively sharp contact dipping about 50° to the northeast. Some authors (e.g. Hafkenscheid et al., 2006; Ballato et al., 2011) suggested that there is no connection between remnants of the slab and the surface. Hence, collision already takes place in this region (e.g. Ballato et al., 2011). However, my geodynamic model of Iran consists of two subduction-collision cycles (Fig. 2-10): the first such cycle occurred between the Iran and Turan platform and the second cycle occurred between the Arabian Plate and Iran. In the following sections, these cycles will be briefly outlined:

### 2.5.2.1 Subduction-collision cycle between Turan and Iran

This subduction-collision cycle started around the transition from the Paleozoic to the Mesozoic. At the boundary of the Mesozoic and the Cenozoic, slab detachment of Iran took place (Wilmsen et al., 2009; Ballato et al., 2011).

According to the tomographic results, there is no slab remnant under the Turan Shield now (Vergés et al., 2011). Thus, the subduction phase of the Iran Plate beneath the Turan Plate is completely finished. GPS data show a shortening of  $8\pm 2$  mm/yr between the Turan and Iran Plate (Vernant et al., 2004 a, b). This shortening indicates that a convergence phase, such as collision is happening in the Alborz region, now. Furthermore, earthquakes, stress regime data, and focal mechanism data all confirm the convergence in the Alborz region (Fig. 2-9).

### 2.5.2.2 Subduction-collision cycle between Arabian Plate and Iran

This subduction-collision cycle started in the Mesozoic and continues in the present time. After the Mesozoic, the slab of the Arabian Plate started to detach.

Tomographic studies show that along Zagros there is no connection in some places between the slab and the Arabian Plate (e.g. Hafkenscheid et al., 2006), but in some places partial connection has been seen (e.g. Alinaghi et al., 2007). This may indicate that subduction between the Arabian Plate and Iran is not still finished, completely. GPS data show a shortening of 4 -11 mm/yr along Zagros (Vernant et al., 2004 a, b). Additionally, stress regimes and focal mechanism data indicate that thrust faults dominate the Zagros region (Fig. 2-6 a). These data show that there is a contractional regime in the Zagros region.

However, this cycle is younger than the cycle between Turan and Iran and the events between Turan and Iran may occur between the Iran and Arabian Plate. Thus, in the future a collision phase would start and consequently a shortened plate can be expected for the Arabian Plate, Iran and Turan (Fig. 2-10). Figure 2-10 is a summary of the tectonic phases and provides a view of a schematic long-term geodynamic model as well as the subduction-collision cycles and the hypothesis of the tectonic situation in the future.

It should be noted that the movements of the Arabian, Iran, and Turan Plates arise from the Arabian-Eurasian collision (e.g. Aghanabati, 2004; Wilmsen et al., 2009; Ballato et al., 2011). During the first cycle, the Alborz ranges formed and during the second cycle, the Zagros ranges formed (Aghanabati, 2004; Wilmsen et al., 2009; Ballato et al., 2011). Between the Alborz and the Zagros ranges, Central Iran Block is located. It is characterized by coherent plate motion (internal deformation  $< 2$  mm/yr; Vernant et al., 2004 a, b) and comprises narrow mountain ranges. It has been considered as a relatively stable area between the Zagros and Alborz (e.g. Aghanabati, 2004; Axen et al., 2001).



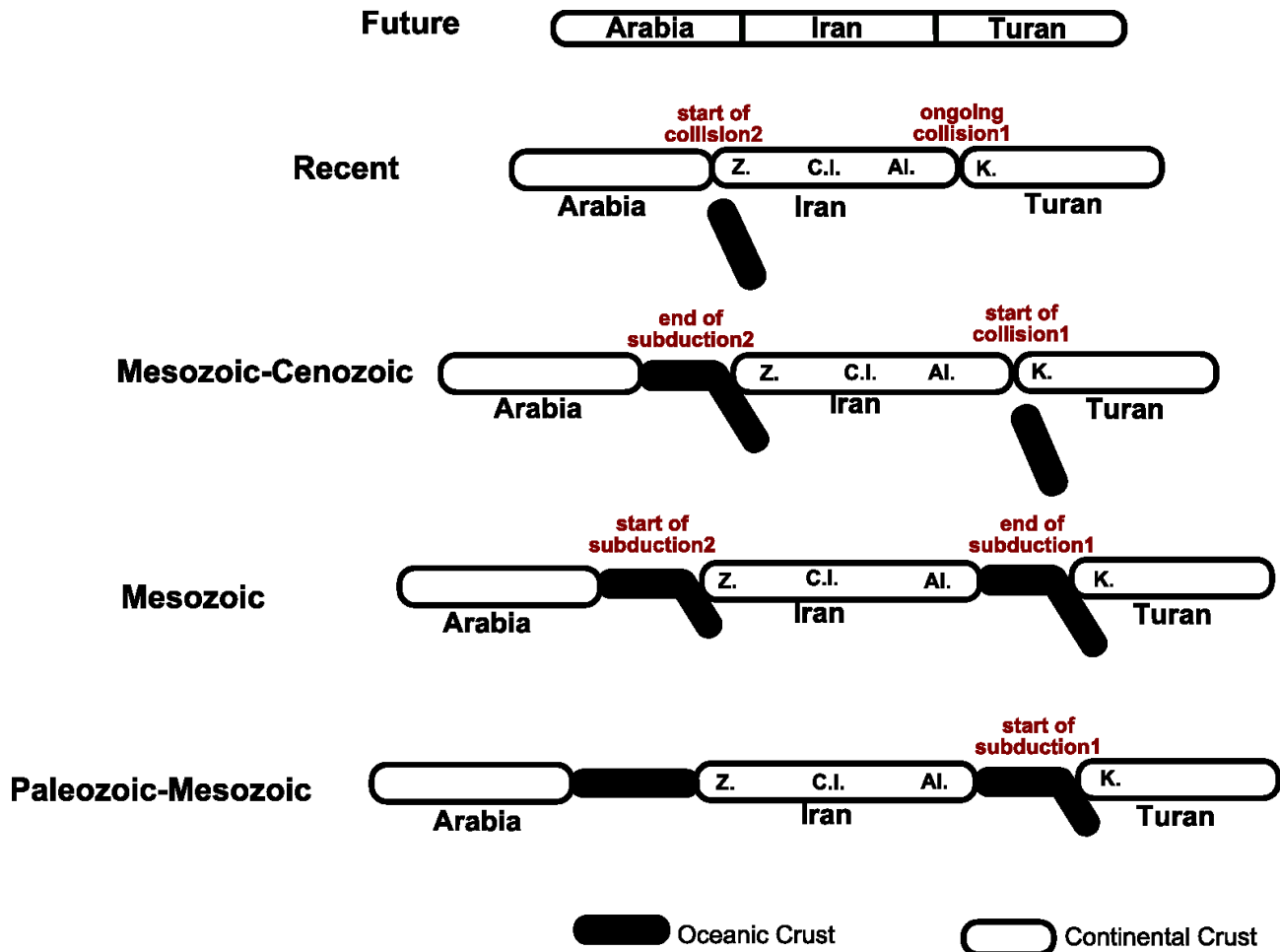


**Figure 2-10.** Sketch of long-term geodynamic model as well as the subduction-collision cycles from the Paleozoic. **Z.:** Zagros, **C.I.:** Central Iran, **Al.:** Alborz, **K.:** Kopedagh. The first phase of subduction (Iran beneath Turan) started in the Paleozoic and changed to a collision in the Cenozoic, whereas the second phase of subduction (Arabia beneath Iran) started in the Mesozoic and changed to a collision in the recent time. The image is schematic and not scaled.

Given the two similar subduction-collision cycles, the question follows, which parameters affect these cycles. Some parameters, such as climate and vegetation could affect these cycles considerably. It is useful to know, whether these parameters are similar during both cycles. If no, why are they different? Is it comparable with other place of the AHB, such as Caucasus? Answers to these questions are beyond the scope of this study and could be a topic for a later study.

### 2.5.3 Caucasus

Subduction-collision can also be observed in other places of the AHB, such as the Caucasus region. As is near the Alborz region (Fig. 2-11 a), it can be a relevant case to compare. In the following, the tectonic

situation of the Caucasus region has been reviewed and compared with the Alborz to find out if the plate tectonic evolution of these two regions shows any similarities.

The Caucasus comprises four main morphological and tectonic units: (1) the Ciscaucasian plain (Scythian platform) including the foredeeps of the Greater Caucasus (SP), (2) the Greater Caucasus (GC) itself, stretching in a WNW-ESE direction, (3) the Transcaucasian system of intermontane basins (TC), and (4) the Lesser Caucasus (LC) with an arcuate N-convex shape and the most heterogeneous structure (e.g. Khain, 1975, 1997; Eppelbaum and Khesin, 2012; Fig 2-11 a).

The Caucasus region, similar to Iran, is squeezed between the Arabian and Eurasian Plates. Thus the geodynamics of the GC orogen corresponds to an intercontinental collision zone inverting a deep Mesozoic-Cenozoic basin that is not located above a subduction regime, but bordered to the east and west by deep sedimentary basins that have their origin in the Mesozoic and are filled with Cenozoic-Quaternary sediments. To the north and south of GC, there are the foreland basins of the Terek-Kuban and the Kura-Kakheti-Kartli-Rioni, respectively (e.g. Ershov et al., 1999, 2003; Mikhailov et al., 1999; Ulmishek, 2001; Daukeev et al., 2002). To the east and west, the Caspian Sea and the Black Sea are located (e.g. Shikalibeily and Grigoriants, 1980; Ismail-Zade et al., 1987; Narimanov, 1992; Abrams and Narimanov, 1997; Mangino and Priestley, 1998; Allen et al., 2002; Brunet et al., 2003; Nikishin et al., 2003).

Present day Caucasus is dominated by thrust faulting due to continental collision. From the Jurassic to the Paleogene eras, subduction of the Tethyan seafloor occurred along the southern margin of the Turkish and Iranian blocks, resulting in calc-alkaline arc volcanism and a wide backarc basin system. The spread of the Red Sea began during the Early Miocene, and the Arabian Plate migrated northward, accompanied by a reduction in width of the Tethys. At ca. 20 Ma, subduction shifted to the north (e.g. Eppelbaum and Khesin, 2012). As a result of the indentation of the Arabian Plate, the continuous backarc basin was separated and the oceanic crust remained only in the Black Sea and the southern Caspian Sea. The continuous northward drift of the Anatolian Plate led to an initial continental collision expressed by the formation of the LC and the subsequent rebirth of the GC during the Middle Pliocene. Currently, continental convergence continues at a rate of up to ~30 mm/yr along thrust faults with strike slip component where most of the modern tectonic activity is localized (Eppelbaum and Khesin, 2012).

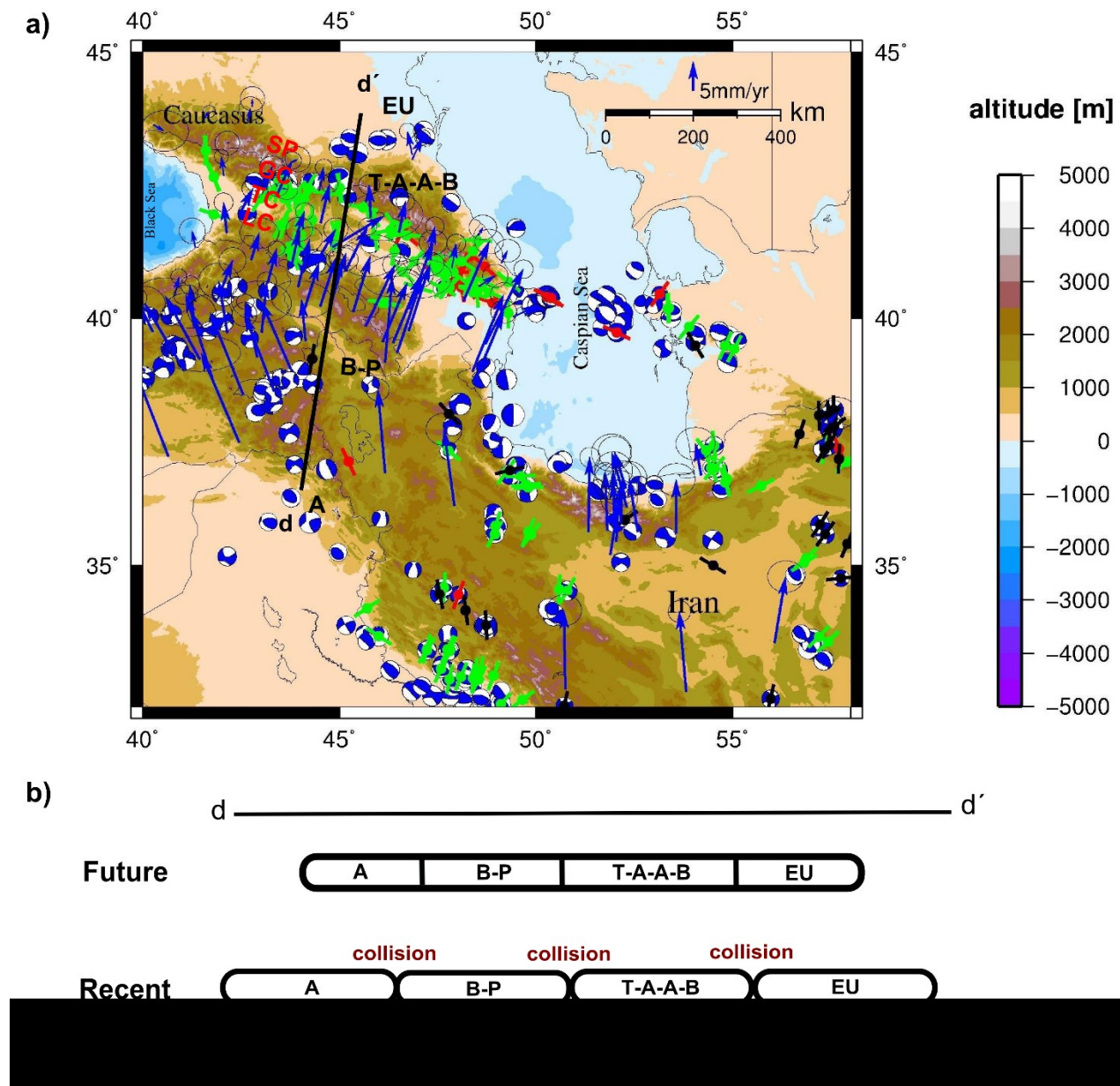


**Figure 2-11.** Recent tectonic situation of the Caucasus region. **a)** Caucasus and surroundings. Topography (DTU, Andersen and Knudsen, 2009), **blue arrows:** GPS velocity (Vernant et al., 2004 a, b), **beach balls:** Focal mechanism (CMT Catalogue, Ekström et al., 2012), stress regime (WSM Catalogue, Heidbach et al., 2008, WSM Symbols, **Red:** normal fault, **green:** thrust fault, **black:** strike slip fault). **A:** Arabian Plate, **B-P:** Bilits-Pürtürge, **T-A-A-B:** Tauride-Anatolide and Armenian Block, **EU:** Eurasian Plate. **SP:** Scythian Platform, **GC:** Greater Caucasus, **TC:** Transcaucasus, **LC:** Lesser Caucasus. **b)** Sketch of subduction-collision phases in the recent time and future. The sketch is not scaled.

Studies based on GPS data in the GC have confirmed the regional picture of convergence across the Caucasus region (McClusky et al., 2000; Nilforoushan et al., 2003; Reilinger et al., 2006). The average convergence of Arabia and Eurasia is 18-23 mm/yr. It led to deforming the GC, mainly in its southern part (Vernant et al., 2004 a, b; Fig. 2-11 a). During the Mesozoic and the Cenozoic, the Caucasus region experienced different tectonic phases. In the following, a geodynamic model of the Caucasus region, as developed by Saintot et al., (2006) is discussed:

**1)** In the Permo (?)–Triassic, rifting and volcanism were widespread in the fore-Caucasus region and in the northern part of the GC (Nazarevich et al., 1986; Lordkipanidze et al., 1989; Tikhomirov et al., 2004; Saintot et al., 2006). **2)** In the Late Triassic, the Eo-Cimmerian tectonic phase lead to a contractional regime (Nikishin et al., 1998 a, b, 2001; Gaetani et al., 2005) which probably was related to the collision-accretion of Gondwana-derived blocks, which together form the composite Iran plate (Saidi, 1995; Besse et al., 1998). **3)** In the Early-Middle Jurassic, a new rifting phase occurred (e.g. Zonenshain et al., 1990; Nikishin et al., 1998 a, b, 2001), which probably was related to north-dipping subduction, south of the Transcaucasus (i.e. LC). **4)** In the Bathonian, a Mid-Cimmerian orogenic event developed. For this time a unconformity has been identified, which was related either to the syn-to post-rift transition or to a collisional event at the active margin (e.g. Coward et al., 1987; Tankard and Balkwill, 1989; Frostick and Steel, 1993; Williams and Dobb, 1993; Busby and Ingersoll, 1995; Stephenson et al., 1996; Cloetingh et al., 1997; McCann and Saintot, 2003). **5)** From the Middle-Late Jurassic to the Eocene, post-rift subsidence dominated (e.g. Milanovsky and Khain, 1963; Lordkipanidze, 1980; Koronovsky, 1984; Adamia and Lordkipanidze, 1989; Zonenshain et al., 1990). **6)** From the Late Eocene, a main Cimmerian orogenic event developed (e.g. Shardanov and Peklo, 1959; Beliaevsky et al., 1961; Milanovsky and Khain, 1963; Khain, 1975, 1994). Additionally, an inversion of the basin related to the final closure of the Paleotetethys began in this time (Saintot et al., 2006). **7)** From the Late Miocene to the present time, a second shortening phase accompanied by uplift and magmatism and corresponding to the final stages of the Arabia-Eurasia collision dominated the region (e.g. Shardanov and Peklo, 1959; Beliaevsky et al., 1961; Milanovsky and Khain, 1963; Khain, 1975, 1994; Zonenshain et al. 1990; Nikishin et al. 1998 b).

Thus, the Caucasus like Iran has experienced several subduction and collision phases accompanied by shortening, uplift and magmatism during the Mesozoic-Cenozoic (e.g. Rolland et al., 2012; Saintot et al., 2006; Allen et al., 2004). A review of geodynamic models suggests that during the Mesozoic and Cenozoic, a collision phase took place after a subduction phase between the Arabian Plate and Bilitis-Prütürge, between the Bilitis-Prütürge and the Tauride-Anatolide-Armenian Block and finally between Tauride-Anatolide-Armenian Block and Eurasia. In recent times, a collision phase is prevailing in the Caucasus region (e.g. Rolland et al., 2012; Saintot et al., 2006).

GPS data reveal shortening rates similar to the Alborz region. According to the WSM catalogue (Heidbach et al., 2008), thrust and strike slip faults dominate in the Caucasus and there is a compressional regime in the region. Data from the NEIC catalogue reveal that this area has also experienced large earthquakes with magnitude >6. The maximum hypocenter depth is 50 km for this region (Fig. 2-11 a). Based on these data, tectonic regimes that are similar to those identified in Iran, especially in the Alborz region, may exist in the Caucasus region. Results of tomographic studies show that there is only a partial connection between slabs and subducted plates along the Europa-Caucasus-Arabian Plate (e.g. Hafkenscheid et al., 2006; Koulakov et al., 2012). It can be argued that subduction is ending and a collision phase is beginning now (Fig. 2-11 b).

## 2.6 Conclusion

A review of published geodynamics models suggests that the Iran Plate was subjected to two similar subduction-collision cycles from the Mesozoic to the recent time:

Cycle 1 took place between the Iran Plate and the Turan Plate and consists of 4 main parts: (a) start of subduction in the Paleozoic-Mesozoic (b) end of subduction in the Mesozoic-Cenozoic (c) slab break off in the Mesozoic-Cenozoic (d) start of collision in the recent time and future (Fig. 2-10). Cycle 2 took place between the Arabian Plate and the Iran Plate and consists of 4 main parts: (a) start of subduction in the Mesozoic (b) end of subduction in the Mesozoic-Cenozoic (c) slab break off in the recent time (d) start of collision in the recent time and future (Fig. 2-10). Thus, I propose that two collision phases already dominate in Iran which can be able to source the earthquakes of Iran and the Alborz region.

Based on resultant Moho data from Motavalli-Anbaran et al. (2013), and the suggested collision phase of the present day in the region, it can be speculated that by ongoing collision, Moho depth may increase from the center of the Alborz region to the sides (Fig. 2-8). Furthermore, if we accept that Moho increasing, collision, and suturing processes lead to increase crustal thickness (e.g. Dehghani and Makris, 1984; Guest et al., 2007; Sodoudi et al., 2009; Ballato et al., 2011), hence a thick and short crust could be expected for the Alborz region and then for the Arabian Plate, the Iran Plate, and the Turan Plate at the end of the two suggested cycles (Fig. 2-9, 2-10). Due to this compression and thickening, increasingly large earthquakes not only for Alborz but also for entire Iran could be expected in the future.

This study also suggests that a similar cycle of alternating subduction-collision may also have characterized the evolution of the Caucasus region.

### 3 CRITICAL TAPER ANALYSIS OF THE ALBORZ AND OTHER OROGENS OF THE ALPINE-HIMALAYAN BELT

#### Abstract

In this study, I investigate the mechanical properties of the Alborz orogen to analyse the geo-hazards in this seismically active region. For this purpose, the critical taper theory has been applied. While focusing on the Alborz, for comparison, a critical taper analysis has also been performed for other orogens of the Alpine-Himalayan Belt (AHB).

Surface slope ( $\alpha$ ) and basal dip ( $\beta$ ) have been estimated from topographic data and geological cross-sections, respectively.  $\alpha$ -values amount range from  $0^\circ$ -  $8^\circ$  in the Alborz and Caucasus region,  $0^\circ$ -  $3^\circ$  in the Apennines,  $-2^\circ$ -  $6^\circ$  in Himalayas, and  $-6^\circ$ -  $3.5^\circ$  in the Zagros. Beta values approximate  $\sim 3^\circ$  in the Alborz and  $\sim 5^\circ$  in the Caucasus,  $0^\circ$ - $2^\circ$  in the other AHB orogens.

Based on the estimated  $\alpha$  and  $\beta$  values, the strength parameter “F” has been estimated. This parameter changes from -0.20 to 0.35 in the entire AHB. However, the F-value solely can not determine the geohazards of the studied regions and the effect of some parameters, such as climate and lithology need also to be considered. By means of F-values and the mentioned parameters, I proposed a “critical to stable” situation for the Alborz and the entire AHB orogens.

#### 3.1 Introduction

Knowledge of the mechanical properties of a subduction or collision orogen is a means to shed light on the stability or non-stability of an orogenic wedge. Wedge stability may control geo-hazards, i.e. an unstable orogen can generate landslides or earthquakes. The critical taper theory has been successfully applied to explain the mechanics of a wedge (e.g. Davis et al., 1983; Dahlen, 1984) and the mechanical state of orogens, such as Taiwan (e.g. Suppe, 2007), the Hikurangi convergent margin (Kukowski et al., 2010), or the Swiss Alps (von Hagke et al., 2014). However, this theory has been not applied to the Alborz region and surroundings so far.

Mechanical properties of an orogen describe its geometry. The geometry of an orogen is a fundamental parameter for seismic and landslide hazard assessment studies (e.g. Hoth et al., 2007). Besides, natural factors such as climate can influence the geometry of orogen (e.g. Hoth et al., 2008). Tectonics, the geometry of an orogen, and climate are related subjects (Willet et al., 1993; Willet, 1999; Molnar and England, 1990), which may have an impact on seismicity (Molnar et al., 2007). This relationship has not yet been studied in the Alborz region.

For an active orogen, such as the Alborz region, which experiences many earthquakes and landslides and also is a populous area, it is necessary to identify the wedge stability and its relationship to geo-hazards by considering climate. Besides, this situation is to be compared with a neighboring orogen, i.e. Caucasus, to examine, if two neighboring orogens have a similar mechanical state. As the Alborz and the Caucasus regions are parts of the AHB, it is useful to compare these regions with other orogens of the AHB to understand, why the orogenic states are similar or different. Consequently, mechanical state for the entire AHB will be determined.

In this part, the following questions will be addressed: (a) What is the mechanical state of the Alborz mountains? (b) By which parameters is the mechanical state of orogen mostly affected? (c) Is the orogenic state of the Alborz similar to the neighboring orogen (Caucasus) and other orogens of the AHB?

### 3.2 Mechanical setting of a bivergent orogen

According to the mechanical model proposed by Willet et al. (1993), an underlying plate can slide beneath another plate (Fig. 3-1 a). This movement causes constant velocity boundary conditions at the base of the overlying layer. To the "left" of the singularity (towards the lower plate) the velocity of layers is constant and positive, whereas to the "right" of the singularity (towards the upper plate) it is zero. At the singularity point, effective stresses within the layer cause discontinuity in the horizontal boundary velocity. Due to basal velocity boundary conditions, two conjugate shear zones develop from the singularity to the surface (Fig. 3-1 a).

At first, the shear zones form at 45° relative to the direction of maximum compressive stress, which is approximately horizontal. The initial stress-strain rate fields lead to a symmetric geometry. Afterwards it changes to asymmetric conditions and remains so for three stages (Fig. 3-1 b). At first, the shear zones are located at the singularity. The region in between the shear zones forms a triangle, which then translates to the right to build an uplifted block. Deformation propagates outwards of the shear zones as the layer begins to slide on detachments that develop between the singularity and deformation front. A basal detachment forms first to the left of the singularity. It is named "pro" direction and also the overlying zone of deformation is named "pro-wedge". In contrast, downstream of the singularity is called the "retro" direction and its zone of deformation is called the "retro-wedge" (Willet et al., 1993).

In the next stage, the retro-wedge is detached from its base. The deformation front propagates significantly into the undeformed layer to the right and starts to form the formation of a lower taper wedge. In this stage, there is an asymmetric deformation and the strain in the pro-wedge is more separated than strain in the retro-wedge. It is caused by the movement of material through the movement of pro-wedge. In contrast, material deformed in the retro-wedge remains in place and trends to have concentrated deformation (Willet et al., 1993; Fig. 3-1 b).

It should be noted that natural processes, such as erosion, volcanism, deposition, or ground freezing could modify the basic model. As an important factor, erosion has to be taken into account. Surface erosion and denudation lead to large-scale removal of mass from an orogen and cause adjustment of the velocity field to replace eroded material by material from within (e.g. Molnar and Englan, 1990; Willet et al., 1993; 1999; Molnar et al., 2007; Hoth et al., 2008). Deformation can also adjust the replacement of removed material. Therefore, denuded zones exhibit increased exhumation rates. This leads to steady-state behavior of small collisional orogens undergoing asymmetrical denudation. This situation occurs, where precipitation is orographically controlled and orogen is wet, rapidly denuded, windward side and a dry side with little erosional denudation (Willet et al., 1993; 1999).

Steady-state retro-wedge denudation can change rock trajectories to exhume highest-grade metamorphic rocks at the retro-deformation front. It is joined by windward denudation. The replaced mass is derived from the pro-wedge. Therefore, the pressure temperature history of material in the orogen must reflect the path and time taken for mass to move across the entire width of the orogen. There is no net growth, uplift, or exhumation of the pro-wedge. In contrast, steady-state pro-wedge denudation creates a non-deforming, non-eroding retro-wedge against which pro-wedge material is decoupled and exhumed. This leads to reduce the path length and a resident situation for the orogen. Under steady-state pro-wedge denudation, the metamorphic grade of surface rocks increases across the pro-wedge (Willet et al., 1993; 1999; Fig. 3-1 c).

According to analog experiments, parameters, such as erosion and the type of an orogen's material can affect the mechanical setting of orogen (e.g. Lohrmann et al., 2003; Hoth et al., 2008). By changing the material in analog experiments, different kinematics or different behaviors of faults have been also observed (e.g. Lohrman et al., 2003). Besides, the type of material can determine the erodibility. Thus, material type and effect of erosion are two related parameters (e.g. Lohrman et al., 2003; Hoth, 2005). Applying erosion to bivergent wedges, Hoth et al. (2008) suggested that erosion of the retro-wedge affects the pro-wedge and vice versa. This means that erosion of the retro-wedge leads to retro-wedge deformation, pro-wedge internal deformation and lastly general effects, such as fault activity on the pro-wedge (Fig. 3-1 d). In nature, the effects of erosion and the orogen's material on the mechanical state of an orogen can be detected by studying climate and the lithology of an orogenic region, respectively.



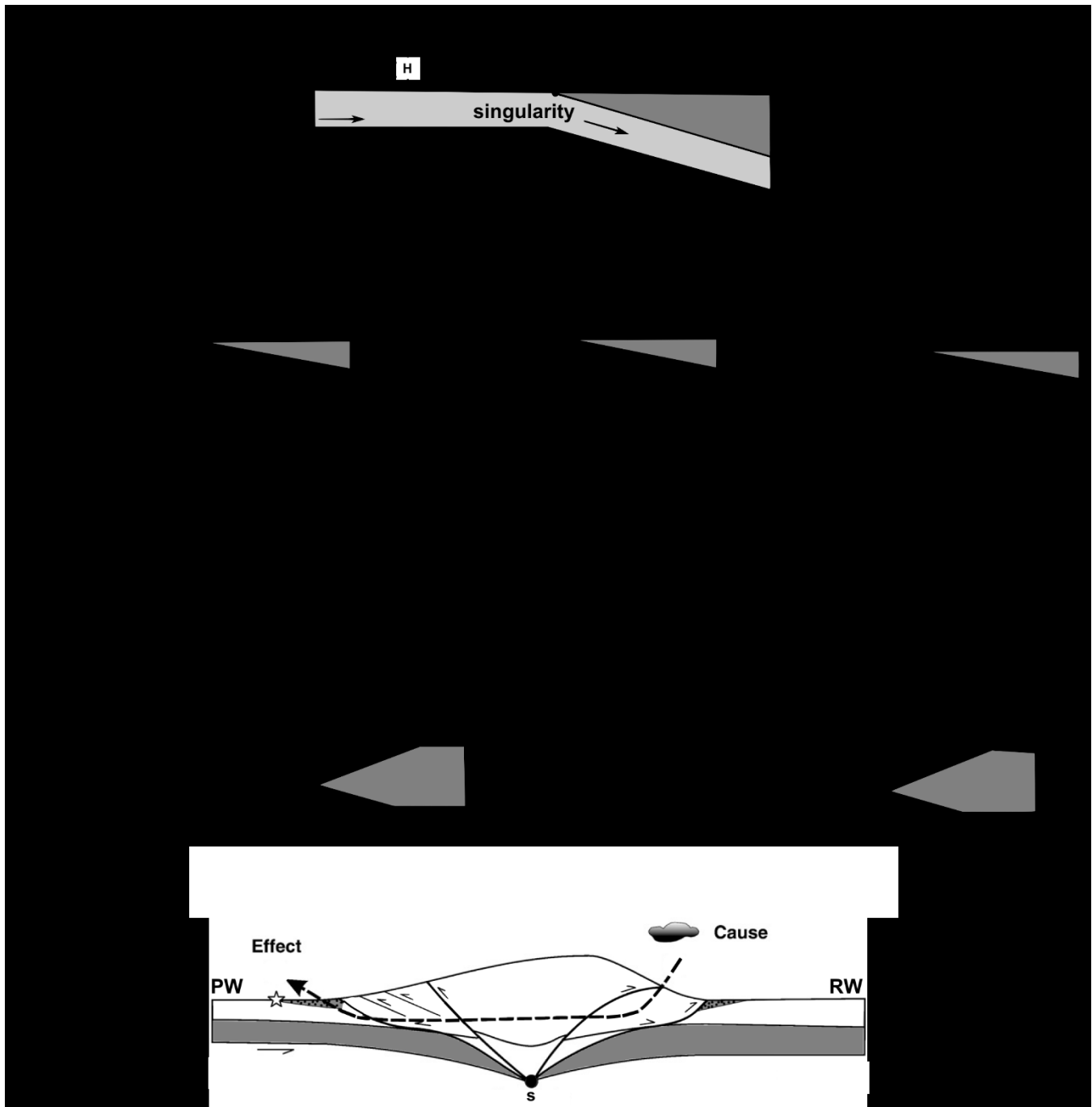


**Figure 3-1.** Bivergent setting. **a)** Bivergent setting with uniform crust extending from surface to depth ( $H$ ) is deformed under basal velocity boundary conditions. For these boundary conditions, there is not backstop, **b)** Stages of basic model development. **Shaded layer:** passive marker, **dotted lines:** instantaneous flow lines, not particle trajectories, **arrows:** proportional to velocity, **c)** Effect of steady-state erosion and denudation. Left: Retro-wedge denudation. Right: Pro-wedge denudation. Passive shaded layer shows exhumed position of middle crust. Lines are material trajectories, dots are progressive equal-time positions of points initially aligned vertically. Schematic metamorphic grade is for surface rocks assuming initial equilibrium conditions, after Willet et al. (1993), **d)** Erosion of the pro-wedge and its effect on the retro-wedge, after Hoth et al. (2008).

### 3.3 Method

#### 3.3.1 Critical taper theory

The subduction-accretion process leads to the formation of an orogenic wedge with a geometry controlled by its basal and internal mechanical properties (e.g. Davis et al., 1983; Willett et al., 2001). The critical taper theory is applied to understand the mechanical behaviour of such orogens (e.g. Davis et al., 1983; Dahlen, 1984, 1990).

To understand the mechanics of an orogen, it is thought of as a wedge that forms in front of a moving bulldozer or snowplough. Therefore, if a snowplough starts to move through a fresh layer of snow two scenarios can be considered: If the internal strength of the snow is lower than the basal friction (friction of the road), then the snow will be moved without internal deformation in front of the plow. If the internal strength is larger than the basal friction then the snow can move and deform internally and also its surface can incline (Davis et al., 1983; Hoth, 2005; Fig 3-2).

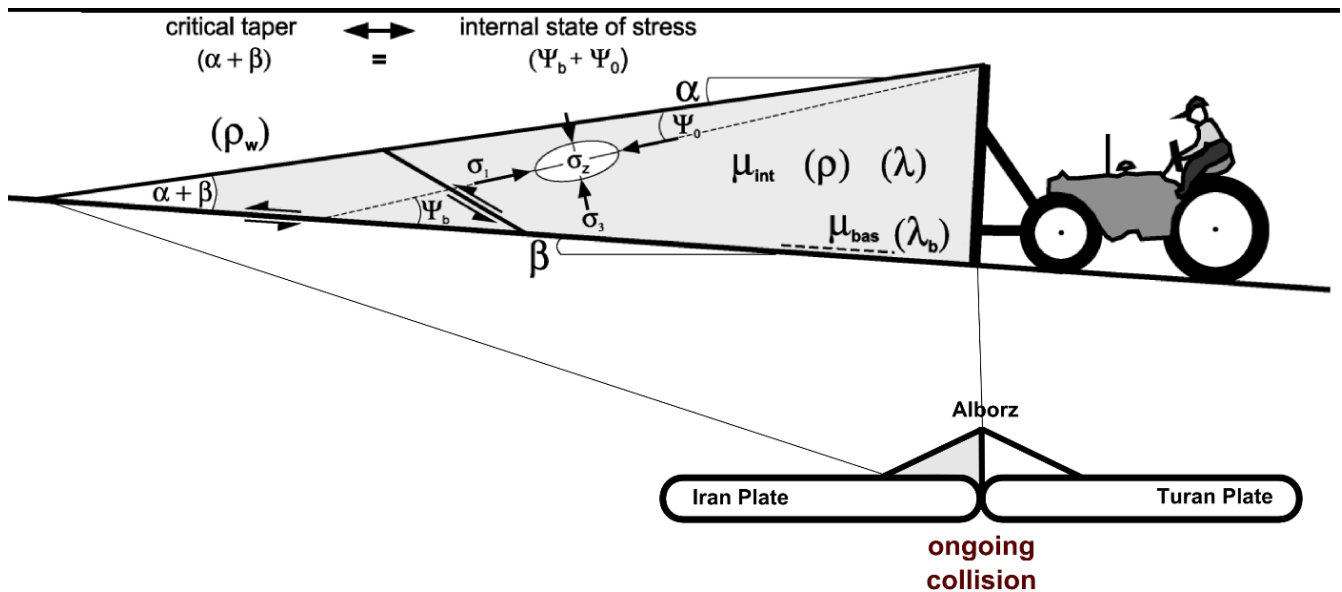


**Figure 3-2.** Convergent wedge and its controlling parameters (e.g. in the Alborz region formed between the Turan and Iran Plate).  $\alpha$ -surface slope;  $\beta$ -basal dip;  $\mu_{int}$ -coefficient of internal friction;  $\mu_{bas}$ -coefficient of basal friction;  $\lambda_{int}$ -internal pore pressure ratio;  $\lambda_{bas}$ -basal pore pressure ratio;  $\rho$ -density of rocks;  $\rho_w$ -density of seawater;  $\sigma_1$ -maximum principle stress;  $\sigma_3$ -minimum principle stress;  $\Psi_0$ -angle between  $\sigma_1$  and surface slope;  $\Psi_b$ -angle between  $\sigma_1$  and wedge base; after Davis et al. (1983).

According to the critical taper theory, four parameters characterise the geometry of a wedge: surface slope ( $\alpha$ ), basal dip ( $\beta$ ), coefficient of friction ( $\mu$ ) and pore pressure ratio ( $\lambda$ ) (Dahlen, 1984). In a mechanically homogeneous wedge, the critical taper equation using the small angle approximation is Dahlen (1990, equation 99):

$$(\alpha + \beta) \approx \frac{(1 - \rho_f/\rho)\beta + \mu_b(1 - \lambda_b) + S_b/\rho g H}{(1 - \rho_f/\rho) + 2(1 - \lambda)\left(\frac{\sin\phi}{1} - \sin\phi\right) + C/\rho g H} \quad (1)$$

Where  $\rho_f$  is the density of fluid above the wedge (water or air),  $\rho$  is the mean density of rock,  $\mu_b$  is the basal friction coefficient,  $\lambda_b$  is the basal pore fluid to lithostatic pressure ratio,  $S_b$  is basal cohesion,  $C$  is compressive wedge strength,  $\phi$  is the angle of internal friction, and  $H$  is wedge thickness. In simple terms, the critical taper angle ( $\alpha + \beta$ ) is dependent on the ratio of basal fault strength and wedge internal strength (von Hagke et al., 2014). This equation was also used as the main equation by von Hagke et al. (2014) to mechanically study the Swiss Alps. According to Suppe (2007), if we take “ $W$ ” to mean all wedge-strength term values and “ $F$ ” to mean all fault strength term values, then the reordered critical taper equation becomes:

$$F = \alpha(1 - \rho_f/\rho) + (\alpha + \beta)W \quad (2)$$

According to von Hagke et al (2014), since the Central Alps are a subaerial wedge,  $\rho_f/\rho$  will be negligible and it is possible to substitute  $(1 - \rho_f/\rho) \approx 1$ . Therefore, for the Alborz region and other orogens of the AHB, equation 2 can be simplified to

$$F = \alpha + (\alpha + \beta)W \quad W \approx 1 \quad (3)$$

$W$  (wedge strength) is a dimensionless parameter and a dimensionless measure of horizontal to vertical stress at failure.  $F$  is also analogous to  $W$ , dimensionless and a function of  $\mu_b$ .  $F$  is the normalized basal shear traction at failure of the detachment, or in other words is fault strength (Dahlen, 1990; Suppe, 2007).  $F$  and  $W$  in equation (3) are compatible with the critical taper theory and allow calculating the basal detachment strength only from determination of  $\alpha$  and  $\beta$ , under the assumption of the finite wedge-strength parameter  $W$  (Suppe, 2007; von Hagke et al., 2014).

### 3.3.2 Measurements

In order to determine the  $F$ -values of the Alborz orogen, two parameters have to be measured: the detachment dip ( $\beta$ ) and the slope ( $\alpha$ ).

### 3.3.2.1 basal dip ( $\beta$ )

In this study, the dip of detachment ( $\beta$ ) was obtained from geological cross-section. A geological cross-section is a conceptual model summarizing what is known about a certain region. It is compiled from various kinds of information, such as seismic profiles, seismological data, drill hole data, geological mapping, etc. It should be noted that the available cross-sections do not show the same information and the same quality and resolution. Additionally, for applying the critical taper theory, cross-sections which show the accretionary wedge are needed. This is not available for the entire AHB. In this study, I try to estimate the mechanical state with the help of the available cross-sections.

The available cross-sections are not numerous and for each orogen, there is only one cross-section (except Alborz with three cross-sections). Therefore, our results will be limited along the geological cross-section. To develop the study area, i.e. not only the area along the cross-section, but also its surroundings, according to von Hagke et al (2014), some profiles that are parallel and near to the available cross-sections and perpendicular to the orogen are added (Fig. 3-3). These help to better describe the taper analysis of the region.

Basal dip was graphically estimated from geological cross-sections available in the literature. To obtain the basal dip, lithological contents of sedimentary layers were compared. It shows which layer is weak and can slip and thus helps to find the detachment level. After that, the angle between the detachment and horizontal direction was measured, i.e. two points must be chosen on the detachment to get a line. The angle of this line and the horizon was measured. Normally a detachment level is not always linear, thus there is sometimes more than one possibility for determination of the line for a detachment (e.g. Fig. 3-7 b). Using all of the assumptive lines, it is possible to approach an error estimation for beta from each detachment.

For the Alborz region, three sections have been utilized in this study. Between these profiles, there are different distances (e.g. Fig. 3-3), between profile 1 (Allen et al., 2004) and profile 5 (Alavi, 1996) there is a distance of ~100 km. Three extra profiles between the place of available published cross-sections (profile 1 and 5) have been interpreted (Fig. 3-3). These profiles have been taken every ca. 40 km, as long or as parallel as side profiles and perpendicular to the orogenic range. This helps to analyse the surroundings of the main profiles, because from these extra profiles, topographic data and thus surface slope ( $\alpha$ ) can be obtained (Fig. 3-4). Along these extra added profiles, there is no beta value available because there is no cross-section for this region. As mentioned, to overcome this lack of beta value, there are two possibilities: a) using approximate beta from main profiles for the extra profiles (distance between two main profiles), b) using beta interpolation. For beta interpolation, the following equation has been used:

$$\beta_2 = \frac{\beta_1 \cdot b + \beta_5 \cdot a}{a+b} \quad (4)$$

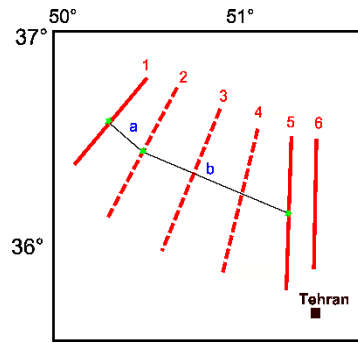


**Figure 3-3.** Beta interpolation between two studied profiles (1 and 5). **Green point:** water divide line, **red dashed line:** extra added profiles, **red line:** location of geological cross-section. See also Fig. 3-5 for the location of profiles.

It should be noted that beta interpolation can be applied only for the Alborz region, because for this region, in between two available geological cross-sections which showed different beta values, there is a wide area and hence it is difficult to estimate the beta value for its middle part. For the other orogens, there is only one geological cross-section and near this cross-section, some extra profiles have been lined parallel. Thus, for these other orogens the basal dip value of the main profile can be valid for the surrounding area. Hence, for these cases, no beta interpolation is needed.

Beta interpolation is tested for the Alborz region but the beta values resulting from this method are not used for the next steps of taper analysis. I just want to show that there is a possibility to estimate beta values of each point of a region. Beta values in this study are approximate values, which have been obtained from geological cross-sections, i.e., a beta value for the pro-wedge and a beta value for the retro-wedge have been used.

### 3.3.2.2 Slope ( $\alpha$ )

In order to measure the slope ( $\alpha$ ) along the geological cross-sections, topographic profiles based on SRTM 90 m (SRTM: Shuttle Radar Topography Mission) digital elevation data were examined. For this purpose, Arc-GIS software (arc map) was used. To obtain topographic profiles along a geological cross-section, coordinates of the cross-section need to be found in the topographic map (in arc map).

There are two possibilities to get the surface slope:

The first way is from a linear topographic profile. This way results in topographic profiles in 2D, i.e. only along the geological cross-section. The topographic profiles can be segmented in to general form (connection of big peaks of the topographic profile) or local form (connection of small peaks of the topographic profile) to estimate surface slope. In this study, general segmentation has been applied. Because the small peaks of profile can be existence of faults, river or erosion changes. To obtain the local

slope of the entire region, a local slope map is generated from the topographic map by Arc-GIS software. This map shows local slope of each point of orogen.

The second possibility to determine surface slope is to measure the surface slopes from each swath profile. From the topographic map, it is possible to get swath profiles (along each geological cross-section) which can show the 3D variation of elevation. From each swath, an average profile provides representative slopes along the swath. In order to get an average topographic profile, the digital elevation data of each swath have been computed in MATLAB. In the middle of each swath, the main profile is located.

Both the ways (2D and 3D) were tested in this study and similar results for surface slopes were obtained. Nevertheless, as in other studies, e.g. von Hagke et al (2014), the second way (3D variation of topography) was used for the taper analysis.

Every profile shows the geometry of an orogen which consists of different segments. These segments were formed during contractional regimes through the orogenic processes. Each segment has a certain slope. Thus, segmentation of orogen is important to estimate the slope of orogen. In order to obtain correct segments along each topographic profile, the water divide line or crest line should be considered as the highest point of orogen. The segmentation should be performed from the sides of profile to the middle (highest point of orogen).

The watershed is a geographic region within which water flows down into a specified body, such as a river, lake, etc. It can be outlined on a topographic map by tracing the points of highest elevation (usually ridge crests) between two adjacent stream valleys (e.g. Leopold et al., 1964). The runoff area of a large river usually contains many smaller streams, which is referred as a drainage basin. In the areas studied here, the crest of an orogen is usually coincident with the main watershed, but at some locations, the watershed line is located outside of the crest region. This indicates a variation of surface slope near to the crest of an orogen (e.g. Leopold et al., 1964). However, for critical taper analysis of an orogen, it is important to determine the main topographic border between the pro- and retro-wedge. For this goal, the detection of the crest of an orogen in SRTM maps is useful. To better detect the orogenic crest and better identify the surface of an orogen, different color scales have been tested for topographic maps but the black-white scale was more suitable for detection of the watershed (Fig. 3-4 a, b).

Additionally potential effects of faults, rivers or fluvial systems, erosional valleys, climate and lithology should be considered. There is a relationship between tectonics, climate and erosion rates. These parameters control the shaping of topography (e.g. Montgomery, 2003; Kirby and Whipple, 2012). Furthermore, erosion affects the variation of climate, vegetation, geology and tectonics (Riebe et al., 1991, a, b). Besides, changes in climate or tectonic forcing can variedly affect landscape scale erosion rates. In low-relief landscapes, the erosion is characterised by changes in hillslope steepness, whereas in high-relief landscapes, it is characterised by adjustments in the frequency of slope failure (Montgomery,

2003). However, the effect of all of the above mentioned phenomena on the original orogenic surface complicates the recognition of actual segments.

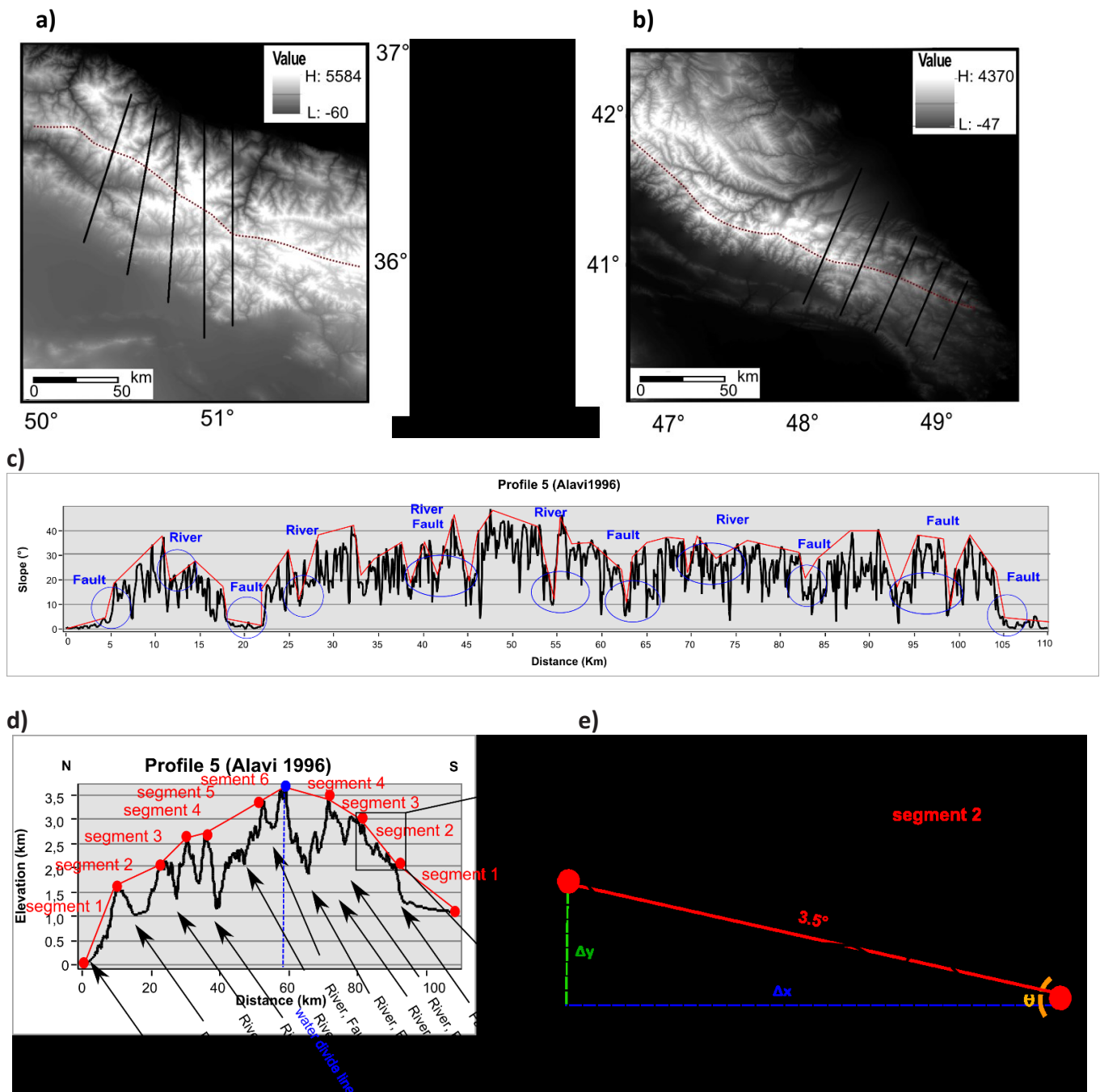


**Figure 3-4.** Surface slope estimation. Detection of orogenic crest in the Alborz region (a), and Caucasus (b) in the area of profiles, see also Fig. 3-20 c and 3-23 for the location of Fig. 3-4 a and b, respectively. c) Variation of slope ( $\alpha$ ) along a profile, d) Variation of elevation and general orogenic segments along studied profile by Alavi, 1996. e) Estimation of surface slope from topographic profile for one segment as an example. See also Fig. 3-5 for the location of profile.

For example, along the profile studied by Allen et al. (2004) in the Alborz region, thrust faults and V-shape rivers affected the surface and morphology through deformation and erosion (Fig. 3-10 c). In this profile between a distance of 33 km and 66 km, two valleys are visible. Each of them could be considered as a segment (green line in Fig 3-10 c). However, from a distance of 30-40 km and 50-60 km, there are two rivers and faults, which led to the formation of the above mentioned valleys. Hence, these valleys should not be considered as a segment of the orogen. In fact, the region from 20-77 km is the main segment. Hence, erosion complicates the identification of segments in nature. This identification is an important step to determine the alpha values. In this study, natural features, such as rivers, valley, or faults have been considered in segmentation. The slope of each segment was calculated (Fig. 3-4 d, e) by:

$$\text{Slope} = \Delta y / \Delta x = \tan(\theta) \quad (5)$$

As mentioned before, natural parameters deform the surface slope. It complicates segmentation. Therefore, in some places of an orogen, different possibilities for segmentation have been considered. Effect of these parameters, such as erosion makes it impossible to imagine the actual form of an orogen, i.e. the shape of orogen before the effect of erosion or other phenomena. Thus, segmentation of the slope in such region needs to be performed in a general form.

Climatic and lithological data were compiled to estimate erosion. In addition to topographic profiles, local slope profile also have been tested to identify faults and rivers (Fig. 3-4 c). These profiles can be obtained from the slope map, which has been produced from the obtained SRTM map. This profile as elevation profiles, illustrates the features similarly. Therefore, only elevation profile are used for identification of segments for all of the profiles and orogens (Fig. 3-4 d, e).

It should be noted that the slope values obtained from the topographic profiles, are average slope values. To get local slope values, local slope maps from topographic map (SRTM 90 m) were produced. Hence, both the local and regional slope are available for the Alborz region and also the AHB orogens.

Local slope maps show the local variation within the study area (entire an orogen). These maps illustrate slopes with 90 m resolution. Using other SRTM, such as 500m or 1 km, one can show smoother topography and thus lower variation of surface slope. In other words, the mentioned resolution (500m and 1000 m) can simplify the map, but this map can not show all the slopes. This is because in the map with 500-1000 resolutions, a lot of variation of slope are eliminated. As mentioned, SRTM 90 m illustrates change of slopes in every 90 m, but the other forms can show changes only in every 500 m or 1 km, which can remove main surface slopes. Thus, SRTM 90 m can be a suitable selection for this goal. Besides, by using the "Filter" tool in Arc-GIS (arc map), the resulting local slope maps have been tried to be smoothed by a lower data elimination, by more than 4 times, but only small differences have been observed. Because, the regions comprise high a variation of local slope values and the volume of data is anyway very large, therefore, it is difficult to have a clear look at the map.



### 3.3.2.3 Fault strength (F)

According to equation (3), for calculating normalized shear strength or fault strength ‘F’ of the detachment with retrieved “ $\alpha$ ” and corresponding “ $\beta$ ” values, a “W” value of 1.0 as determined for the European basement by Suppe (2007) was used. For the Alborz region there is no data about wedge strength (W) and therefore, it was assumed that the mentioned W-value (Suppe, 2007) may be valid also for other orogens, such as the Alborz. Equation (3) was used to obtain the F-value for each profile. Different types of “alpha” and “beta”, i.e. beta-approximate, beta-range, alpha-local, and alpha-regional, led to different F-values:

$$F = \alpha_{local} + (\alpha_{local} + \beta_{range})W \quad (6)$$

$$F = \alpha_{regional} + (\alpha_{regional} + \beta_{range})W \quad (7)$$

$$F = \alpha_{local} + (\alpha_{local} + \beta_{approx.})W \quad (8)$$

$$F = \alpha_{regional} + (\alpha_{regional} + \beta_{approx.})W \quad (9)$$

The F-maps obtained from the local slope values were not useful, because each point of the map shows a certain slope, which is different from the neighboring points. This difference decreases the resolution of the F-maps. Thus, the estimation of wedge stability becomes impossible. Hence, only the regional slope (mean alpha), and approximate beta (mean, minimum and maximum beta values) were used to produce the F-maps (Table 3-1).

In order to determine the effect of beta on F-maps, minimum and maximum beta values were replaced with mean beta values. Alpha values are from SRTM data and for each point, there is a defined alpha value. There is not much information available regarding the accuracy of SRTM data. However, probable errors can exist in SRTM data, but these errors can be considered comparatively small and can have only small effect on my results.

The resulted alpha and beta values from geological cross-sections and topographical profiles have just one dimension, i.e. there is only ‘x’ axis coordinate (longitude), but each profile has a depth which shows the border between pro- and retro-wedge. The pro- and retro-wedge of each profile have specific alpha and beta values. To use these alpha and beta values in map generating, 1D point of each profile has been transformed to 2D point ‘x, y’ (longitude and latitude) with MATLAB programming to plot these values on a map. Accordingly, for each point of a profile there are one mean alpha and three beta values (mean, minimum and maximum value). F-values between profiles can be correlated with GMT. After doing these processes, F-maps for each region were created.

In addition to the F-maps based on “regional” alpha, we can have a general view of F-value for the entire orogen with the local slope maps, which were obtained from SRTM 90 m (e.g. Fig. 3-20 a, b). In fact, these local slope maps show the local alpha, but can also show the variation of F-values. Since ‘F’ resulted

from  $2\alpha+\beta$  (equation 3), hence it means that alpha (slope) exerts the main effect on F-value, therefore with the variation of alpha values, different F-values can be determined.

### 3.4 Alborz

#### 3.4.1 Tectonic setting

Knowledge of the tectonics of an orogen helps to better identify the slope and basal dip of an orogen. A tectonic map, which shows the situation of plates, e.g. the situation of the pro- and retro-wedge and also the fault structure of a region, can provide a better determination of the basal detachment and surface slope, respectively.

As mentioned in chapter 2, the Alborz region has formed as a result of the convergence between the Iran Plate (in the south) and the Turan Plate (in the north). The southern flank of the Alborz is the pro-wedge and its northern flank is retro-wedge (e.g. Aghanabati 2004; Berberian and King 1981; Fig. 2-9).

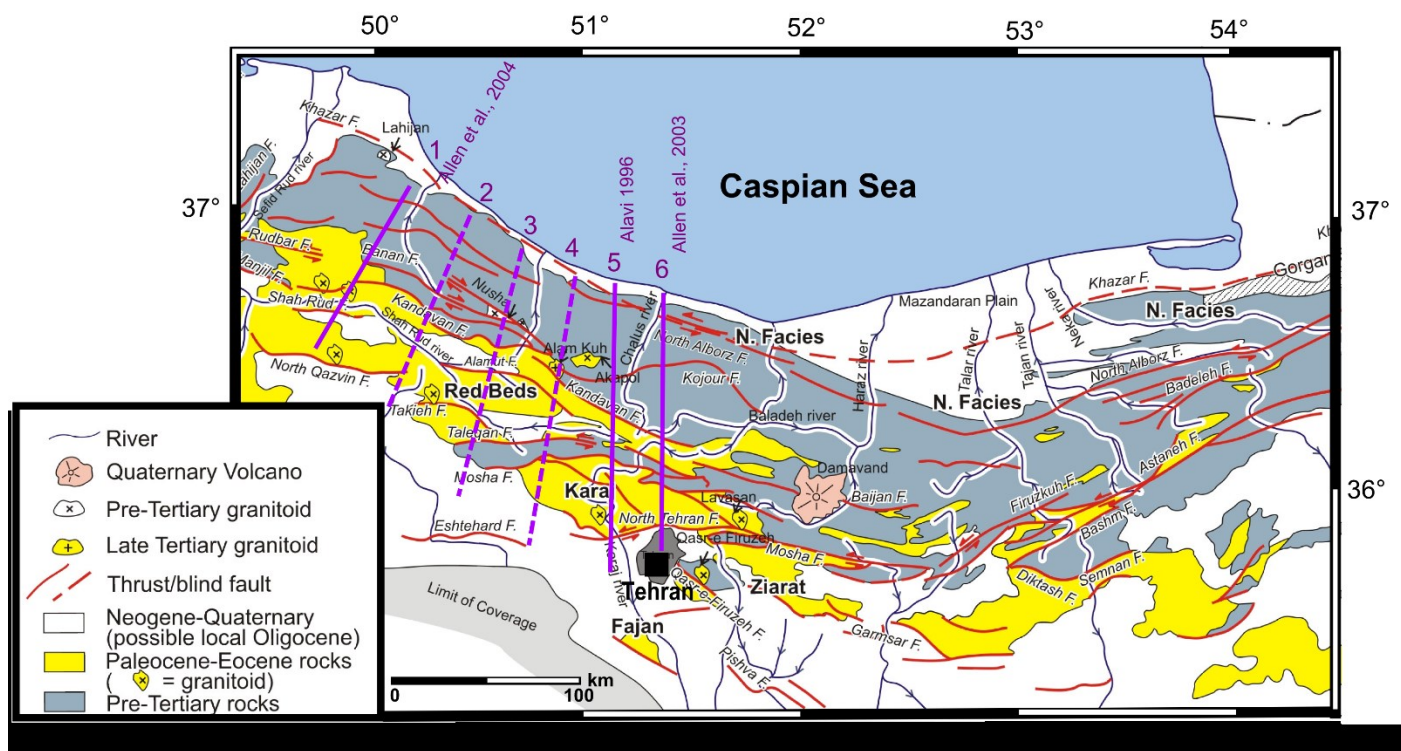


**Figure 3-5.** Generalized geological-structural map of the Alborz, after Rezaeian (2008). Profile 1: geological cross-section of Allen et al. (2004; Fig. 3-9), profile 2, 3 and 4: extra added profiles for better taper analysis, profile 5: geological cross-section of Alavi (1996; Fig. 3-8), profile 6: geological cross-section of Allen et al. (2003; Fig. 3-7).

In the entire Alborz, i.e. on its northern and southern flanks, different fault zones formed (e.g. Berberian et al., 1993, Berberian and Yeats, 1999; Guest et al., 2006 a, b; Ritz et al., 2006; Hessami and Jamali, 2006; Mokhtari and Kiarasi, 2008; Nazari et al., 2007, 2009, 2010; Landgraf et al., 2009; Solaymani Azad et al., 2011 a, b; Fig. 3-5). As mentioned in chapter 2, fault zones consist of thrust faults and strike slip

faults (Fig. 2-6). According to Berberian et al. (1993), major reverse faults in the study area are the Khazar fault, the North Tehran fault, the Mosha fault (with a strike slip component), the Banan fault (with strike slip component), the Kandevar fault, the North Qazvin fault and the Taleghan fault (with strike slip component). All of the mentioned faults are active except the Kandevar and the Banan fault, which might have turned inactive recently (Berberian et al., 1993; Fig. 3-5).

The WSM catalogue (Heidbach et al., 2008; Fig. 2-6 b) confirms that in the Alborz region the thrust faults dominate. From this data, it could be assumed that in this region, there is a general compressional regime. The strike slip component enables partitioning and potential local extension. Since these components are minor as compared to the reverse components, hence the thrust faults and the resulting compressional regimes have been considered for the tectonic phase of the Alborz region.

### 3.4.2 Lithology

Lithological data help to better identify the detachments. If we know about the lithology of the individual layers, we can assume, which layer may be relatively weaker than the others and thus can serve detachment. Based on lithofacies analyses, the Alborz has different tectonostratigraphic units and each unit includes several formations formed in a tectonically-controlled environment (Alavi, 1996). The units formed from the Precambrian to the end of Mesozoic (before the Cenozoic) have been named as Pre-Tertiary to simplify the lithological view of the region (Allen et al., 2003; Fig. 3-5). The below subsections describe the different units.

#### 3.4.2.1 Pre-Tertiary

These units consist of shallow water, rippled, tuffaceous shales, siltstones and sandstones which are interlayered with tuffs (Alavi, 1996) and possibly evaporates (Allen et al., 2003). The Proterozoic-Triassic platform succession is ~6 km thick along the section studied by Allen et al. (2003). They are overlain by alternating shales, dolomites, and dolomitic limestones containing the Precambrian-Cambrian boundary in the middle part (Hamdi et al., 1989), which grade upward into well-bedded, interbedded limestones and micaceous siltstones with several thin volcanic interlayers (e.g. Assereto, 1966; Alavi, 1996; Aghanabati, 2004). The Lower Jurassic consists of fluvial deltaic clastics, including coals. Marine Middle Jurassic-Early Cretaceous carbonates and clastics (Alavi, 1996) were followed by Late Cretaceous carbonates, basaltic and andesitic volcanic across a large part of the Alborz region (e.g. Alavi, 1996; Zanchi et al., 2009).

#### 3.4.2.2 Paleocene-Eocene

Paleocene units consist of conglomerate, and Eocene units consist of interbedded andesitic volcanics and clastics with locally gypsum and anhydrite, large scale slumps and mudstones rich in orogenic material indicating deposition in a deep-water basin (e.g. Alavi, 1996; Zanchi et al., 2009; Aghanabati, 2004). Volcanoclastic units consist of lavas and green tuffs with lesser amounts of shales, sandstone,

mudstones and calcareous tuff deposited in a marine deep-water system (Davoudzadeh et al., 1997; Ballato et al., 2008).

#### 3.4.2.3 Neogene-Quaternary

Neogene-Quaternary sediments show every aspect of fluvial regimes of sedimentation and include coarse to fine material: northward-coarsening, polymict fanglomerates, red argillites, and breccias with reworked sediments of Neogene age, as well as pebbles and boulders that are mainly derived from the Alborz magmatic assemblage. Neogene clastics cover Mesozoic strata disconformably. On the northern flank, there were not Lower Tertiary strata. It is questionable, if there were never any Tertiary strata, or if they were eroded prior to the Neogene (Allen et al., 2003). However, in a general lithological view, a hard lithology for the northern flank and a soft lithology for the southern flank of Alborz has been suggested (Rezaiean, 2008).

#### 3.4.3 Climate

Climate, especially rainfall, can affect pore fluid pressure, which is among the main parameters that control the mechanical state of a wedge (e.g. Dahlen, 1984). The Alborz mountains form a gently sinuous east-west mountain range across northern Iran, south of the Caspian Sea. They face the humid Caspian depression to the north and the arid plateau of Central Iran to the south (Naqinezhad et al., 2009; Rezaiean, 2008; Fig. 3-6). Steppic plant assemblages associated with the dry climate on the south-facing slope of the Alborz mountains (e.g. Klein, 2001) are very different from the forest vegetation associated with the wet climate of the north-facing side (e.g. Assadollahi et al., 1982; Frey and Probst, 1986; Zohary, 1973).

V-shape valleys are detectable at different elevations on the Alborz region, but in the northern flank, their number is higher. According to Rezaiean (2008), rivers and precipitation affect the surface of the Alborz region and lead to an annual erosion of up to 1.3 mm (Fig. 3-6 a). Erosion is not uniformly distributed across the Alborz mountains. There is a general trend from lower erosion rates in the east (up to 0.3 mm/y) to higher erosion rates (up to 1.3 mm/y) in the west. More remarkably, erosion rates are higher (up to 1.3 mm/y) on the southern flank of the mountain belt than on the northern flank (up to 0.3 mm/y), with the exception of a series of small, fast eroding catchments in the NW ranges. This is in strong contrast to the expectations based on precipitation patterns across the mountain belt.

The Alborz mountains have a wet northern flank and a (semi) arid southern flank with stream power being distributed even more asymmetrically. It is clear that climate is not the primary control for erosion at present. Strong rocks mostly exert low erodibility and vegetation can also decrease the effect of erosion. Hence, erosion rates on the steep and wet northern flank of the mountain belt is suppressed by the strength of rocks at the surface, and by the effects of dense vegetation cover (Rezaiean, 2008; Fig. 3-6 b).



On the southern flank of the mountain belt, strong rocks only cover some limited parts and the vegetation density is low, permitting whatever runoff that occurs to erode efficiently and in proportion to the local slope. Therefore, the pattern of erosion on the scale of the mountain belt is influenced by the erodibility of the substrate (Rezaeian, 2008).

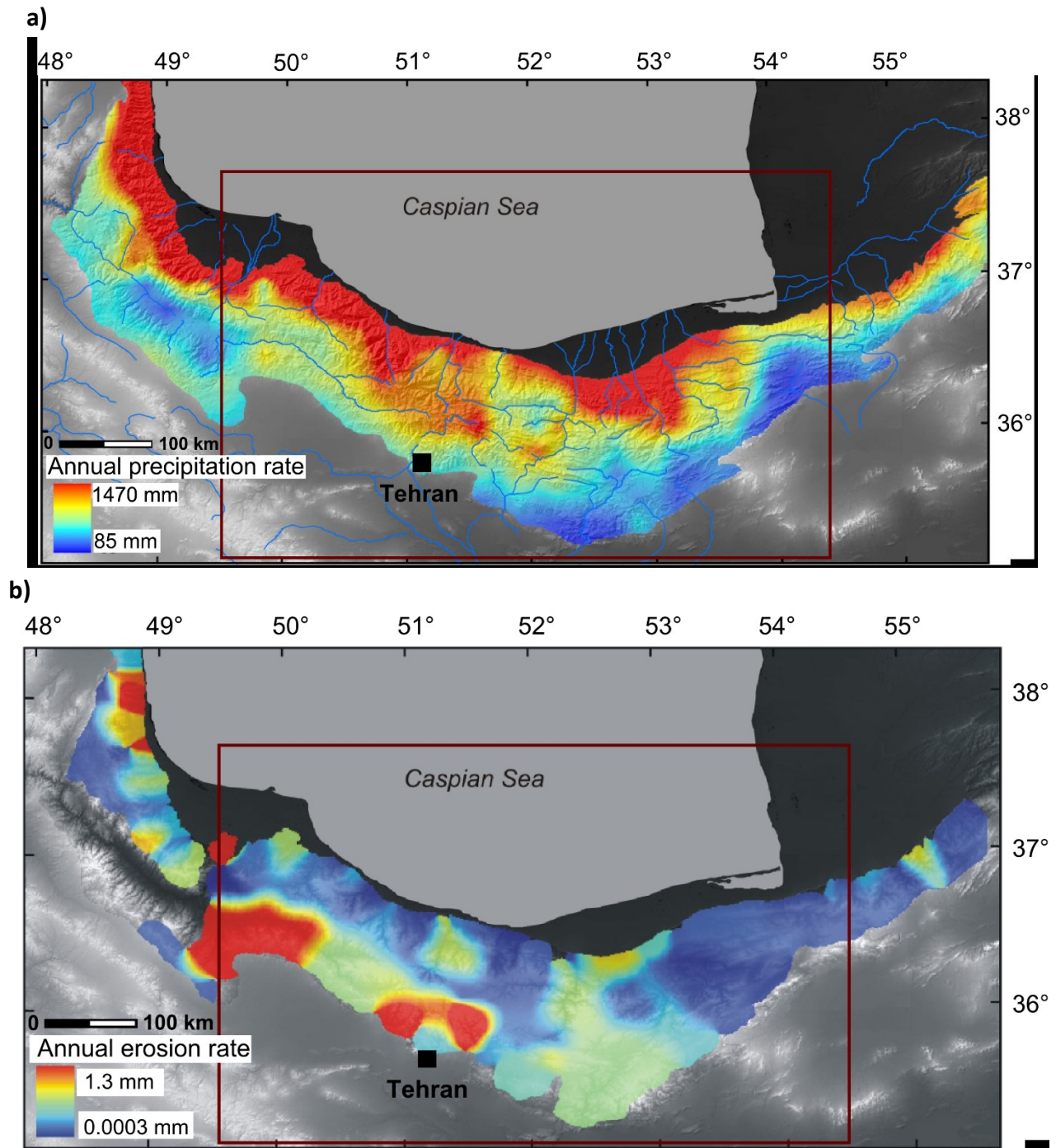


**Fig. 3-6.** Precipitation and erosion in the Alborz region (mm/yr). **a)** Total annual precipitation in the Alborz, derived from 877 meteorological stations (Rezaeian 2008). **b)** Spatial distribution of average annual erosion (Rezaeian, 2008), red frame: central Alborz (study area).

### 3.4.4 Parameters compiled for the critical taper analysis applied to the Alborz

#### 3.4.4.1 Basal dip ( $\beta$ )

In order to measure the basal dip of the Alborz region, all published cross-sections have been collected (Fig. 3-5, cross-section 1, 5, 6). As mentioned, these cross-sections do not have the same resolution. One of them (cross-section 6 - Allen et al., 2003) is a high resolution section and illustrates more layers in the sedimentary cover. So from all the collected cross-sections, only this cross-section is suitable for the assessment of basal dip. Nevertheless, basal dip in all of the available cross-sections has been measured (Table 3-1).

The cross-section published by Allen et al. (2003; Fig. 3-7): This cross-section is based on seismological data and geological studies. The décollement was identified at a depth of about 17 km, and the basement seems to be deformed. Thus, here, we consider thick-skinned tectonics. Above the basement, there are different lithological layers. The first layer is the Kahar Formation and according to Alavi (1996), this formation was formed in the Precambrian to the Lower Ordovician and consists of tuffaceous shale, siltstone, and sandstone with interlayered pyroclastics (such as tuff). Allen et al. (2003) illustrated a possible section of evaporates for the Kahar Formation.

The Cambrian-Middle Triassic section is a mixed layer of clastic carbonate (Fig. 3-7) and metamorphic (Gorgan schist as Paleotethyan collision, in the northeast). According to Alavi (1996) this section can consist of different formations (Kahar, Soltanieh, Barut, Mila, Dorud, Rute, Nessen, etc.), and each formation has its own properties. Altogether, the general lithology of the mentioned formations is clastic, carbonate and volcanic.

In this profile (Fig. 3-7) it is difficult to decide, which layer is weaker. This is because the lithostratigraphic data illustrated poorly the rock distribution of each unit. Besides, a precise lithostratigraphic profile for each layer is not available. Thus, it is only possible to get a general view regarding the durability of layers. For the cross-section of Allen et al. (2003), there are three possibilities for position of detachment as explained below.

- 1) If we think that the Kahar Formation consists of clastics with possible evaporative rocks, then this unit could be assumed as a weak layer in comparison to the basement. Therefore, it can be taken as a detachment, because its overlaying layers can slip on it (detachment A in Fig. 3-7 a).
- 2) a) If we consider that the Kahar Formation consists of evaporites, it can be assumed that the Cambrian-Middle Triassic section can slip on the Kahar Formation and the detachment would then be between them.
- b) If we think that the Kahar Formation has no evaporitic units and consists of Cambrian-Middle Triassic successions, then we have two layers with clastics and volcanics. But, how do we know, how much volcanics and how much clastics are there? The lithostratigraphic section just provides



For this cross-section for each detachment, there are three aspect lines, i.e. three possibilities for the place of the detachment line (Fig. 3-7 b). On the whole, for this profile there are nine different estimations for beta values. The average of them is  $2.7^\circ \pm 1^\circ$  for the RW and  $2^\circ \pm 1.8^\circ$  for the PW (Fig. 3-7 a, b).

The cross-section published by Alavi (1996; Fig. 3-8): This section is derived from geological and structural studies of Stocklin, (1968) and compiled by Alavi (1996). It reaches down to about 10 km depth. The basement is not included. This cross-section can be considered as a thin-skinned tectonic model that consists of Precambrian to the Quaternary units with different lithologies.

In this profile, just the border between the Precambrian and the sedimentary covers is observable. Hence, there is only one possibility to assume a detachment. The detachment can be considered between the Precambrian and the overlying layers (it is the same as detachment B in the profile of Allen et al. (2003)). For this detachment, there are three aspect lines to place the detachment line. The average of them is  $2.2^\circ \pm 1.5^\circ$  for the north and  $4^\circ \pm 1.1^\circ$  for the south (Fig. 3-8).

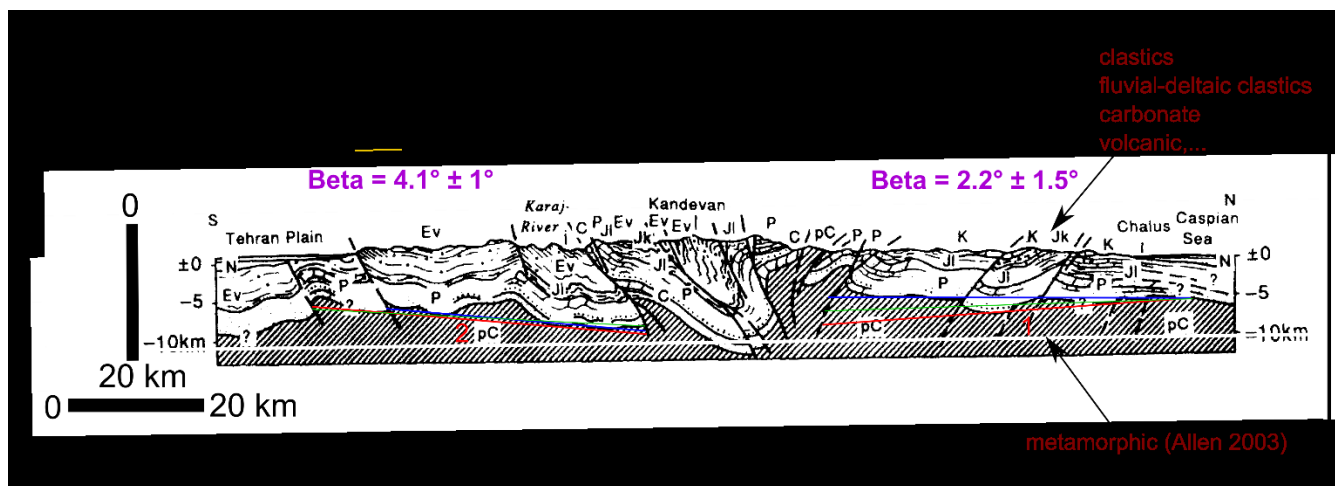


**Figure 3-8.** Measurement of basal dip in the Alborz, along the profile of Alavi (1996). Only one possibility to place the detachment for the northern (1) and the southern flank (2) has been identified. Beta values:  $2.2^\circ \pm 1.5^\circ$  for the RW and  $4^\circ \pm 1.1^\circ$  for the PW, lithological data (Alavi, 1996; Allen et al., 2003, 2004). See also Fig. 3-5 for the location of cross-section.

The cross-section published by Allen et al. (2004; Fig. 3-9): This section goes down to a depth of 40 km. It shows that there might be a deformation of the basement (thick-skinned model). It reaches from the Caspian Basin to the Zagros folded zone. From this section, a sub section (from the south of the Caspian Sea to the end of Alborz) has been clipped. The end point of this section is detectable in the topographic map (SRTM data) with the help of Arc-GIS (arc map).

In this cross section, only a border between the basement and the sedimentary cover is seen (Fig. 3-9). Therefore, it has been taken as detachment. Furthermore, there are two detachments for the PW. Both



of them have been measured and finally an average has been calculated. The average beta is  $0.7^\circ \pm 0.7^\circ$  for the north and  $4^\circ \pm 1.9^\circ$  for the south (Fig. 3-8). It should be noted that the Moho depth indicated in this profile is not compatible with more result estimations of Moho depth (Fig. 2-8).

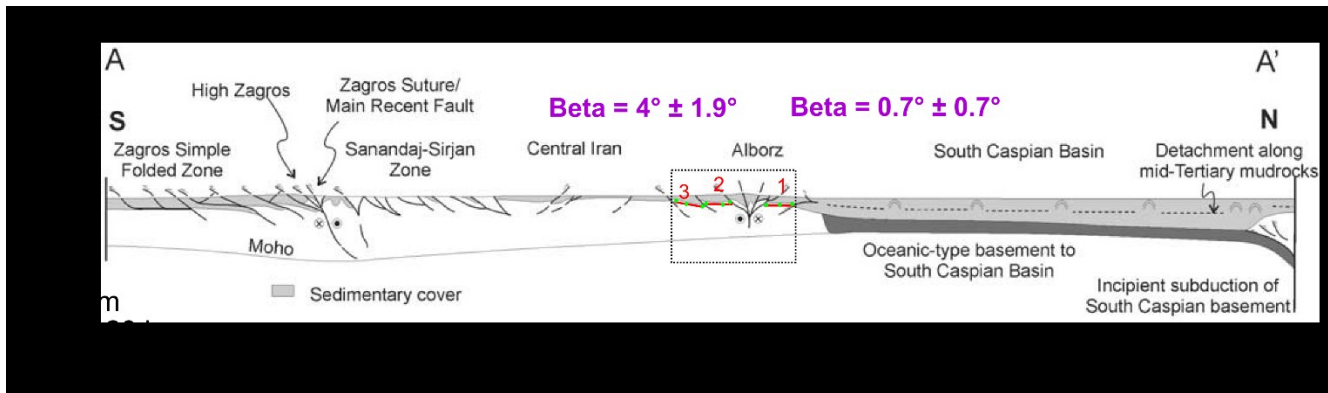


**Figure 3-9.** Measurement of basal dip in the Alborz, along the profile of Allen et al. (2004). One detachment for the northern (1) and two detachments for the southern flank (2, 3). Beta values:  $0.7^\circ \pm 0.7^\circ$  for the RW and  $4^\circ \pm 1.9^\circ$  for the PW, lithological data (Alavi, 1996; Allen et al., 2003, 2004). See also Fig. 3-5 for the location of cross-section.

As explained, since the first cross-section (Fig. 3-7) shows a clear sedimentary cover and enables to better identify the detachment, this cross-section has been regarded as the main cross-section to obtain beta values. Therefore, the beta values estimated from this cross-section have been considered as representative beta for the Alborz region. Altogether from the geological profiles, it can be suggested, that the PW detachment is dipping  $\sim 2^\circ - 4^\circ$ , whereas the RW detachment is dipping  $\sim 0.7^\circ - 2.7^\circ$  (Table 3-1).

#### 3.4.4.2. Slope ( $\alpha$ )

As noted, an orogen may consist of different segments, which were formed during convergence and orogenic processes. Each segment may have a certain average slope. Thus, in order to obtain the slope ( $\alpha$ ) of an orogenic wedge, potential segments have been identified. Each segment indicates an average slope and is valid up to the next variation of average slope. The border between two segments is characterised by abrupt difference of slope. Topographic profiles of each cross-section have been produced to identify a potential segmentation of the wedge. In such a profile, the main peaks have been connected. The small peaks of topographic profile may be formed due to the effect of faults, rivers, or erosion. The structural map/cross-section and SRTM data of the region can also help to identify surface phenomena and segments. Whereas in some places the identification of segments is easy, in other places (such as 22-44 km in profile 6, Fig. 3-10 a) different possibilities for a segmentation can be considered. Below is an overview of the surface slope along the three geological cross-sections.

Along the cross-section constructed by Allen et al. (2003), thrust faults and V-shape rivers (Fig. 3-6 a) affect the orogenic surface and consequently the values of alpha. In this region, there is also an erosion effect, which on the northern side is smaller than on the southern side (Rezaeian, 2008; 3-6 b).

In the obtained topographic profiles (Fig. 3-10 a) two sections are identified, but within the distances of 22-44 km and 60-88 km there are two possibilities for the segmentation:

- 1) Regional segmentation: if we assume that the big V-shape (in distance of 22 to 33 km) could be a faulted area or formed as a result of effect of erosion (red line).
- 2) Local segmentation: if we assume that the V-shape is formed due to the orogenic event without the effect of erosion (green line).

Along this profile, from the north (left) to the south (right), six segments with different average slopes have been identified (Fig. 3-10 a).

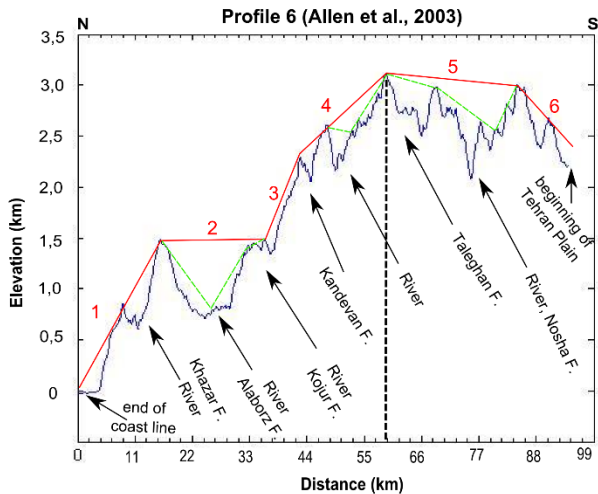
Along the cross-section of Alavi (1996), some valleys, which can be a location of faults or rivers, are visible. At the distance of ~95 km, a border between the orogen and the Tehran plain is obvious, but it is difficult to identify the real shape of the orogen, because erosion or sedimentation in foreland could deform the surface of orogen. Additionally, the material fall from top of the orogen can change the real border between orogen and plain. For this profile, from the north (left) to the south (right), nine surface slopes (alphas) have been identified (Fig. 3-10 b).

Along the cross-section of Allen et al. (2004), there are also thrust faults and large V-shape valleys. This would lead to two possibilities for the segmentation (Fig. 3-10 c):

- 1) Local segmentation: if we assume that each big V-shape as a segment without considering the role of faults and rivers, which can deform the surface, then in Fig. 3-10 c the green dashed line can be taken for the segmentation.
- 2) Regional segmentation: we consider that faults or rivers deformed the surface of region, also the first assumption can be false. Moreover, in the southern flank, which has soft stones, the effect of erosion is much more than in the northern flank (Rezaeian, 2008). Thus, a regional segmentation is reasonable for this section (red lines in Fig. 3-10 c).

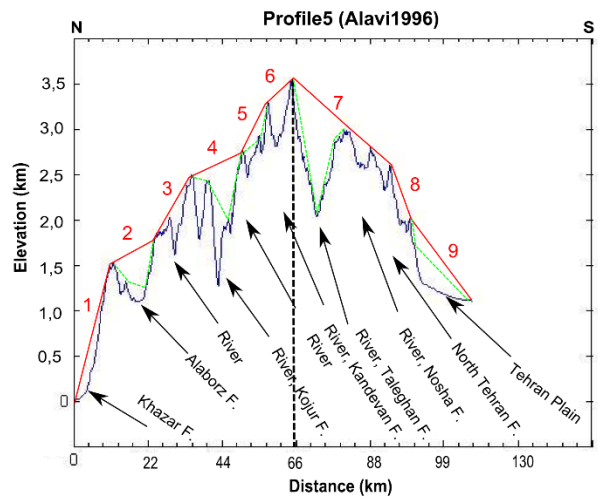
For this red line, two surface slopes (alphas) have been obtained (Fig.3-10 c). The values from the profiles in between are available in the appendix (Fig. 6-1).

a)



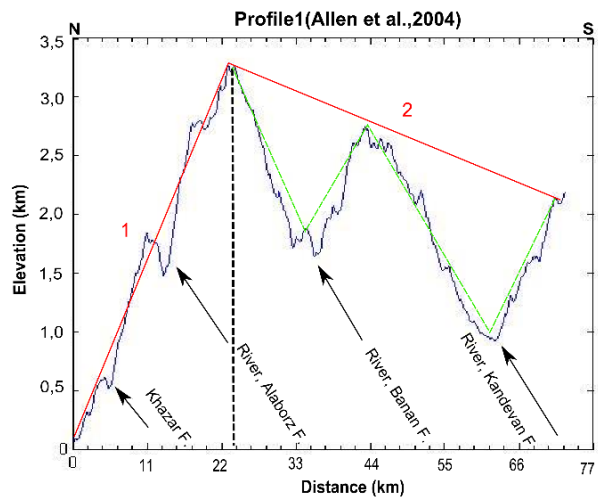
	X	Y	Z	Slope (°)
1	51.3000	36.7000	-29.0000	5.42
2	51.3000	36.5320	1478.3907	-0.03
3	51.3000	36.3200	1464.6290	6.59
4	51.3000	36.2447	2286.7464	2.72
5	51.3000	36.0680	3082.1031	0.19
6	51.3000	35.8004	2998.0897	4.74
Min. slope : -0.03° Max. slope : 6.59° Mean slope : 2.97°				

b)



	X	Y	Z	Slope (°)
1	51.2000	36.7000	-2.1261	7.32
2	51.2000	36.5902	1528.1423	1.19
3	51.2000	36.4751	1789.2999	3.59
4	51.2000	36.3746	2475.0099	0.90
5	51.2000	36.2348	2715.2897	4.16
6	51.2000	36.1622	3288.7201	1.70
7	51.2000	36.0993	3491.7962	1.74
8	51.2000	35.8266	2593.1131	5.71
9	51.2000	35.7694	1972.2384	2.70
Min. slope : 0.90° Max. slope : 7.32° Mean slope : 3.06°				

c)



	X	Y	Z	Slope (°)
1	50.5000	36.9000	45.3874	7.91
2	50.4053	36.7422	3270.1811	1.23
Min. slope : 1.23° Max. slope : 7.91° Mean slope : 3.34°				

**Figure 3-10.** Regional slope along the studied profile in the Alborz, as well as the table of coordinates and  $\alpha$ -values of the segments. The  $\alpha$ -values of extra profiles are available in the appendix (6-1). **a)** Along the profile of Allen et al. (2003; Fig. 3-7), **b)** Along the profile of Alavi (1996; Fig. 3-8), **c)** Along the profile of Allen et al. (2004; Fig. 3-9), **black dashed line:** crest of orogen, **red line:** general segmentation, **green dashed line:** local segmentation.

## 3.5 Caucasus

The Caucasus is a neighboring orogen to the Alborz, which is in a similar tectonic and geodynamic situation as the Alborz. Here, the Caucasus region is addressed within the framework of mechanical properties. Then, the mechanical properties of this orogen is compared with the mechanical properties of the Alborz region. As for the Alborz, average values of  $\alpha$  and  $\beta$  will be estimated from SRTM data and geological cross-sections, respectively.

### 3.5.1 Tectonic setting

The Caucasus is located between the Black Sea to the west and the Caspian Sea to the east. As shown in chapter 2, similar to Iran, the Caucasus lies between the converging the Eurasian Plate in the north and the Arabian Plate in the south. Due to the northward motion of the Arabian Plate, the Caucasus mountains have been formed and are characterized by a complex crustal structure (e.g. Saintot et al., 2006; Fig. 2-11).

The Greater Caucasus (GC) is the northern extent of the Arabia-Eurasia collision zone and represents the main place of shortening within the center of the collision zone between 40° and 48°E. Since the Plio-Pleistocene, much of the shortening in the eastern part of the Caucasus has taken place in the Kura fold-thrust belt along the southeastern margin of the GC (Forte et al., 2013).

The GC is composed of Precambrian and Paleozoic volcanic and metamorphic units (e.g. Triep et al., 1995; Zonenshain et al., 1990), which are a result of the Paleozoic ocean continent-collisions of the Paleotethys Ocean with the margins of the Eurasian and the Gondwana/Africa-Arabian Plate. According to Triep et al. (1995), Zonenshain et al. (1990), and Zonenshain and Le Pichon (1986), mainly back arc basin sediments have been deposited at the southern slope of the GC northbound to the Lesser Caucasus (LC). This mountain range is characterized by fold-and-thrust-belts and shows considerable seismic and volcanic activity (Mosar et al., 2010; Triep et al., 1995).

The structural inventory of the GC reveals a complicated interaction between deformation, syn-tectonic sedimentation, and erosion. Therefore, the GC underwent a very heterogeneous structural and stratigraphic development along strike and structures show variability even on the local scale (Forte et al., 2013).

According to the WSM catalogue (Heidbach et al., 2008), the main active structures in the GC are thrust faults. Some normal faults can be detected in the GC, but a compressional regime prevails (Fig. 2-11). These structures have been also reported by Ruppe and McNutt, (1990), Milanovsky and Khain, (1963), and Dotduyev, (1987).

### 3.5.2 Lithology

According to the geological map of the region, Paleozoic units are outcropping only in the west, but Mesozoic and Cenozoic rocks are found all over the GC. Mesozoic units consist of Jurassic and Cretaceous strata (Fig. 3-11).

The Jurassic sedimentary succession of the GC basin can be subdivided into two large lithological packages divided by an unconformity (Ruban, 2007 a, b). The lower lithological package comprises of the siliciclastic dominated deposits up to 10 km thick, the age of which ranges from the Sinemurian to the Bathonian. The upper lithological package includes Callovian-Tithonian carbonate- and evaporite-dominated deposits with a total thickness of up to 3 km (Ruban, 2008). Tertiary sediments are known as Molasse type successions, which may consist of conglomerate, sandstone and shales. There are also Quaternary volcanic rocks in the GC (Dotduyev, 1987). The axial zone of the GC includes Jurassic sedimentary rocks (Azerbaijan), a pre-Mesozoic basement (Georgia, Russia), and Pliocene intrusions. Both, the external fold-and-thrust belts consist mainly of Cretaceous and Cenozoic sedimentary rocks (Khain, 1997).

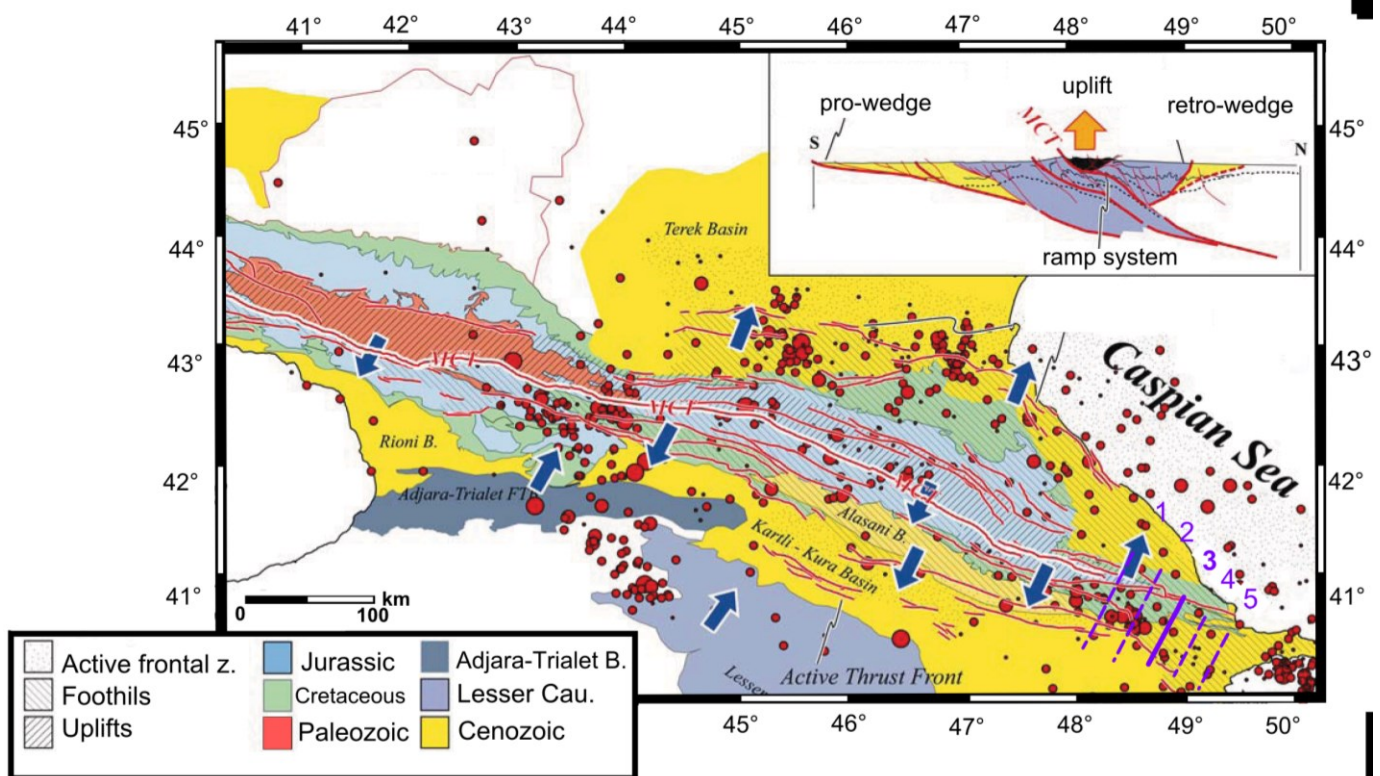


**Figure 3-11.** Geological and structural map of the Caucasus, after Mosar et al. (2010). Profile 3: studied geological cross-section by Mosar et al. (2010), profile 1, 2, 4 and 5: extra added profiles for better taper analysis.

In the study area of Mosar et al. (2010) from the center to the sides, Mesozoic (Jurassic, Cretaceous) and Cenozoic (Tertiary) units are visible. According to the geological map, on both the flanks of orogen,

Mesozoic and Cenozoic units with different lithological hardness are spread, but toward the crest of orogen first the Cenozoic units and then Mesozoic units are located (Mosar et al., 2010; Fig. 3-11).

### 3.5.3 Climate

The climate of the Caucasus region varies both vertically (according to elevation) and horizontally (by latitude and location). Temperature generally decreases with elevation. This region is known for a high amount of snowfall. The GC mountains are covered with forests at higher elevations. Some of the lowest areas of the region are covered with steppes and grasslands (Kvavadze and Rukhadze, 1989). The littoral zones have a humid subtropical climate with mild winters and hot summers. Facing strong westerly winds, this area receives high precipitation of 1300-1500 mm per annum, mostly in autumn and winter (Arslanov et al., 2007).

As a result of high levels of precipitation and the melting of snow, many V-shape valleys are developed in the Caucasus region. The flow of most rivers in the GC is dependent on season. Additionally, in the rivers facing south, flood during the spring period, snowmelt and rainfall reach their peak. Summer floods are very common among rivers facing north at higher elevations (Coene, 2010). During other periods of the year, many rivers tend to dry up. Most Caucasian rivers flowing into the Black Sea are relatively short but extremely numerous where the mountains region almost touches the coastline. In contrast, the rivers flowing into the Caspian Sea are generally much longer (Coene, 2010).

On the whole, according to the NOAA images (e.g. Amante and Eaklins, 2009), vegetation in the western part of the Caucasus, especially close to the Black Sea is denser than in the east. Different climates dominate the area, but a comparison of the NE and SW parts of the GC with the Alborz indicates almost the same conditions for the both orogens. In general, the distribution of forest and rivers in NE and SW can be considered almost the same.

### 3.5.4 Parameters compiled for the critical taper analysis applied to the Caucasus

#### 3.5.4.1 Basal dip ( $\beta$ )

In order to estimate the dip of the detachment for the Caucasus, a cross-section (Mosar et al., 2010; Egan et al., 2009; Fig. 3-12) has been used. In this profile, Mosar et al. (2010) illustrated the place of the pro- and the retro-wedge in the Caucasus. They suggested that the northern flank of the Caucasus is the retro-wedge whereas the southern flank is considered to be the pro-wedge (first model). In contrast, the geodynamic models of the region obtained by e.g. Saintot et al. (2006) and Mumladze et al. (2015) place the pro-wedge in the north and the retro-wedge in the south of the region (second model).



According to Eppelbaum and Khesin (2004), the depth of the Moho decreases from the center to the south and north of the GC. Beneath the northern flank, the Moho depth is higher than beneath the southern flank. This indicates that the basal dip of the northern flank may be higher than the southern flank and consequently, the northern flank can be considered as retro-wedge and the southern flank as pro-wedge. This affirms the first model.

In contrast, according to the topography of the GC, a pro-wedge for the northern flank and a retro-wedge for the southern flank can be considered. This matches with the second model. But it is to be noted that this inversion could have happened as a result of constant and focused erosion at the same time in the southern and northern flank. Therefore, the pro-wedge has a higher surface slope but the retro-wedge has a lower surface slope. While the Caucasus region is located between two seas and has a wet climate (Kvavadze and Rundhadze), the effect of erosion on both flanks could be a compelling reason for this feature. Hence, according to the geodynamic models (e.g. Mosar et al., 2010; Saintot et al., 2006), Moho shape (Eppelbaum and Khesin, 2004), and considering the effect of wet climate (Kvavadze and Rundhadze, 1989) in the Caucasus, it can be considered that there are more convincing reasons to accept the first model to take the northern flank of the GC as the retro-wedge and its southern flank as the pro-wedge.

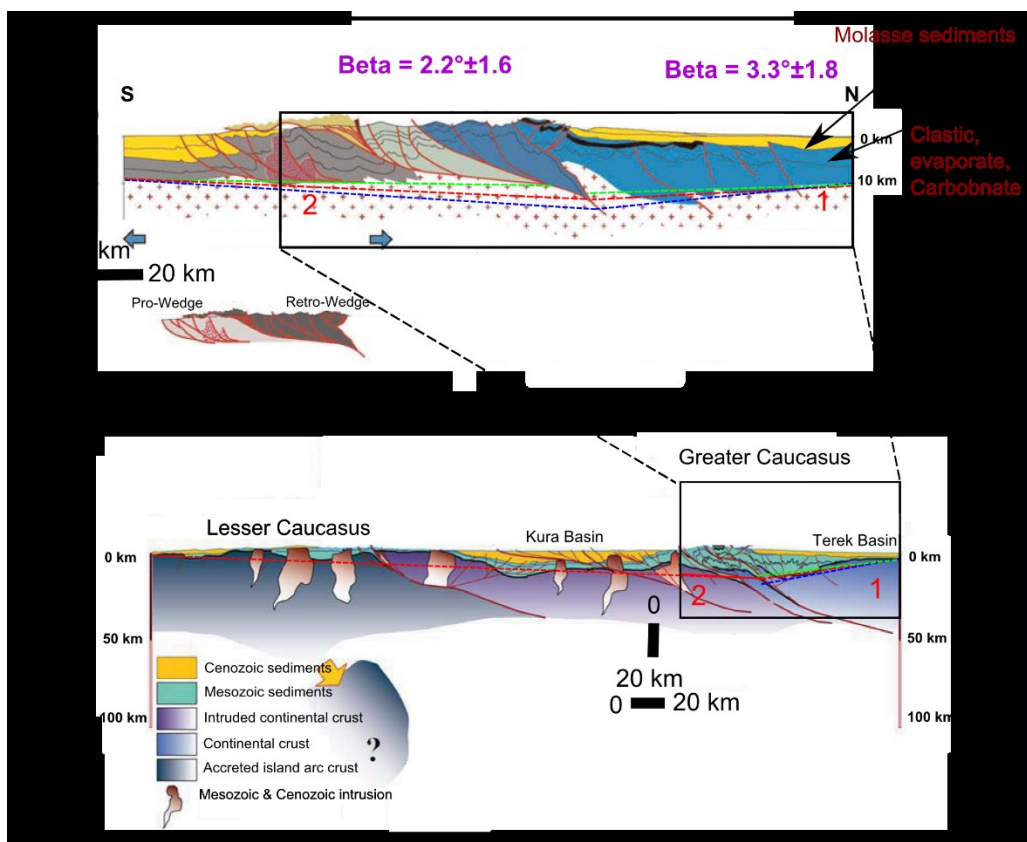


**Figure 3-12.** Measurement of basal dip in the Caucasus along the profile of Egan et al. (2009)-the below cross-section and Mosar et al. (2010)-the above cross-section. Beta values:  $3.3^{\circ} \pm 1.8^{\circ}$  for the RW and  $2.2^{\circ} \pm 1.6^{\circ}$  for the PW, lithological data (Mosar et al., 2012). See also Fig. 3-11 for the location of cross-section.

In the cross-section of Mosar et al. (2010), a detachment is visible between basement and sediment layers. This detachment is clear and may be a suitable level for estimating  $\beta$ . From this detachment, for the retro-wedge a beta value of  $3.3 \pm 1.8^\circ$  and for the pro-wedge a beta value of  $2.2 \pm 1.6^\circ$  was estimated (Table 3-1). For this orogen, we have beta values only along one profile. To taper analyse in the surrounding area of the profile, four extra profiles have been added near and parallel to the main profile (e.g. Fig. 3-20 a).

#### 3.5.4.2. Slope ( $\alpha$ )

Along this section, such as for the Alborz region, the effect of faults, especially thrust faults and also V-shape rivers are to be considered. In this section, as in the previous section, considering the effect of thrust faults and rivers, a general segmentation is presented (red lines in Fig. 3-19 a). In this profile from the north (left) to the south (right) seven values for the regional slopes have been estimated. The resultant values from the extra profiles are available in the appendix (Fig. 6-2).

### 3.6 Other orogens of the Alpine-Himalayan Belt

A comparison of critical taper parameter values (surface slope, basal dip and fault strength) in the Alborz and Caucasus indicates that these regions may be in a similar mechanical situation. As discussed in chapter 2, this may be the result of a similar tectonic history.

As the Alborz and Caucasus regions are parts of the AHB, the question follows, whether other orogens on this belt exhibit a similar mechanical behaviour. For this purpose three more orogens, the Zagros, the Apennines, and the Himalayas are studied. In the following, the critical taper parameters as well as tectonics, lithology and climate are compiled for the other regions of the AHB. At the end, all of the studied orogens are compared in detail (Table 3-2).

#### 3.6.1 Zagros

##### 3.6.1.1 Tectonics, Lithology and Climate

In the general context of the Alpine-Himalayan orogenic system, the Zagros fold-thrust belt (ZFTB) is the most recent result of the convergence and closure of the Neotethys oceanic domain between Arabia and Eurasia (Takin, 1972; Haynes and McQuillan, 1974; Ricou et al., 1977; Alavi, 1994; Stampfli et al., 2001). In the ZFTB, the Arabian passive margin sequence has been decoupled from its basement and deformed by large-scale folding and thrusting. According to seismicity records, within the underlying Pan African basement, shortening is presently accommodated by reverse faulting (Jackson and Fitch, 1981; Berberian, 1995). The ZFTB is characterized by a relatively intense seismic activity increasing from NW to SE. All earthquakes in Zagros are limited to depths shallower than about 20 km (Maggi et al., 2000; Talebian and Jackson, 2004).



Numerous blind faults are known to be active beneath the sedimentary cover. In particular, the active Mountain Front Fault (MFF) and High Zagros Fault (HZF) are considered as major segmented reverse faults, whose seismogenic and morphologic signature is recognized throughout the Zagros orogen (Berberian, 1995). The movement accumulated by the ensemble of these faults has generated a total vertical displacement in the order of up to 6 km (Berberian, 1995; Molinaro et al., 2005). The WSM catalogue shows strike slip and thrust faults with a domination of thrust faults (Heidbach et al., 2008; Fig. 2-6 a).

In the region where the cross-section published by Molinaro et al. (2005) is located, there are units from the Paleozoic to the Cenozoic (Fig. 3-13). On the basement, the Lower Mobile Group is detectable which represents the Late Precambrian Hormuz evaporite layers. This level forms the main regional décollement level for most of the larger folds within the ZFTB (Colman-Sadd, 1978; Kent, 1979). Subsequent Zagros folding has remobilized the salt, which flows from the synclines toward the cores of the anticlines. Therefore, its present thickness must be highly variable, ranging from almost zero beneath the synclines to perhaps thousands of meters in the cores of the anticlines (Edgell, 1996).

A 4-5 km-thick Cambrian to the Lower Miocene sequence forms the Competent Group. Apart from the initial Cambrian-Carboniferous clastic formations, the majority of this group until the Upper Cretaceous consists of massive platform carbonate rocks (e.g. James and Wynd, 1965; Sharland et al., 2001). The upper part of the group is lithologically more variable. Approximately 400 m of Upper Cretaceous marine marls (Gurpi formation) are overlain by 400-600 m of competent Eocene limestone and dolomite (Asmari-Jahrum formation) and 50-100 m of lower Miocene gypsiferous red marl (Razak formation). Polymictic conglomerates are visible within this latter formation, suggesting an important change of the depositional environment possibly related to early regional tectonic movements. (e.g. Edgell, 1996).

**Table 3-1.** Beta values of several orogens of the AHB

orogens	beta range PW/RW	beta mean (PW/RW)	beta minimum (PW/RW)	beta maximum (PW/RW)
<b>Alborz</b>	2.0°±1.8°/2.7°±1°	2.0°/2.7°	0.2°/1.7°	3.8°/3.7°
<b>Caucasus</b>	2.2°±1.6°/3.3°±1.8°	2.2°/3.3°	0.6°/1.5°	3.8°/5.1°
<b>Apennines</b>	0°/1.4°±1.5°	0°/1.4°	0°/-0.1°	0°/2.9°
<b>Zagros</b>	1.1°±1.2°	1.1°	-0.1°	2.3°
<b>Himalayas</b>	1.7°±0.6°	1.7°	1.1°	2.3°

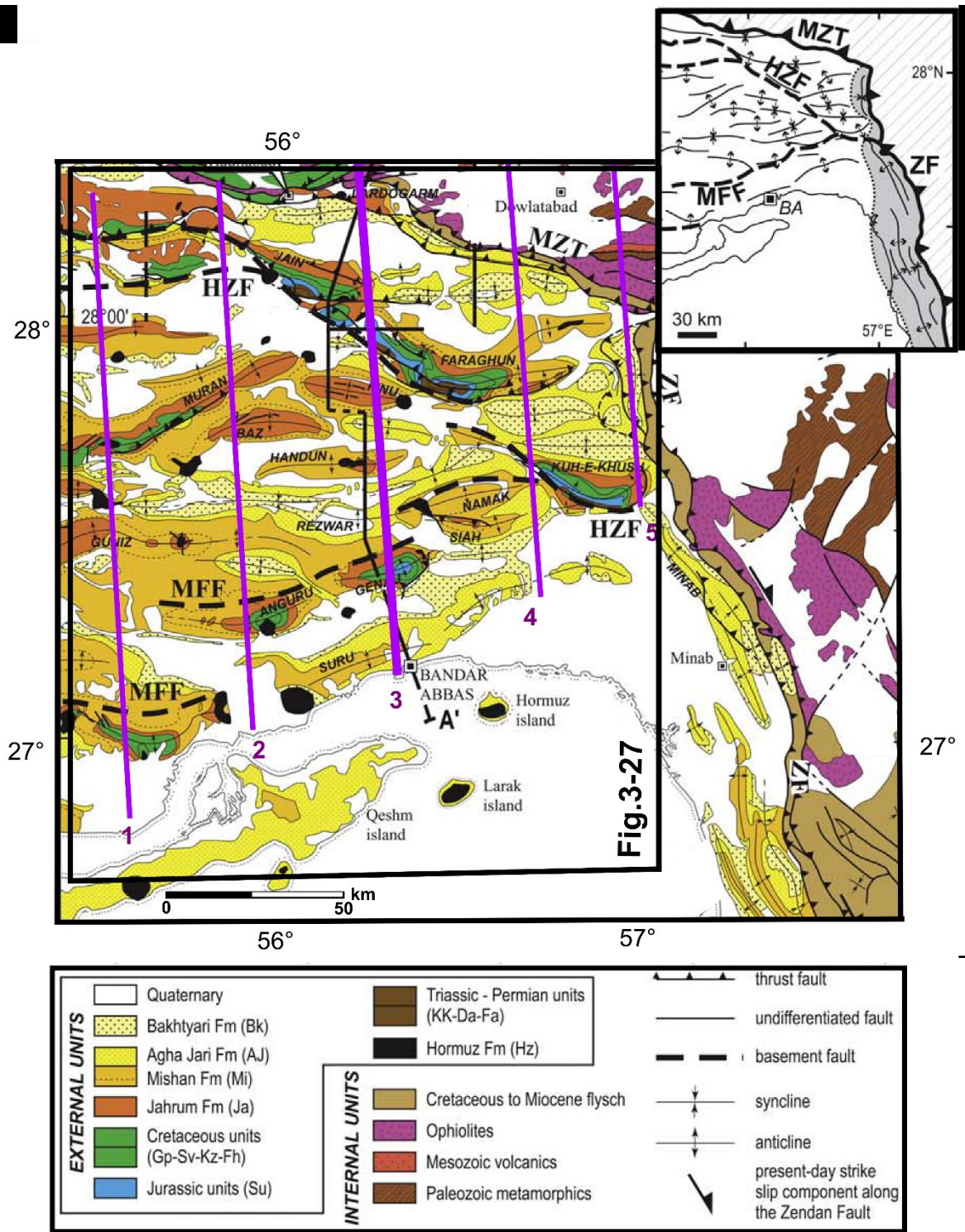


**Figure 3-13.** Geological map of the Zagros, after Molinaro et al. (2005). Profile 3: cross-section of Molinaro et al. (2005), profile 1, 2, 4 and 5: extra added profiles for better taper analysis.

From a structural point of view, the Cambrian to Upper Cretaceous sequence is the main unit underlying the large wavelength anticlines of the region. The remainder of the stratigraphic sequence is represented by Middle Miocene to the recent Cretaceous clastic sediments. These molasse-type sediments, derived from the uplift and erosion of the Zagros mountains, show a coarsening upward evolution from marine clastics to

continental clastics (Agha Jari Formation) and coarse conglomerates (Bakhtyari Formation) at the top. Structures observed within these formations include small-scale thrusting and thrust-related folds soling out into the Mishan marls (Molinaro et al., 2005; Fig. 3-13).

The Zagros mountains are exposed to different climates. Prominent among them are the forest and forest steppe areas with a semi-arid climate. The annual precipitation ranges from 400 mm to 800 mm and falls mostly in winter and spring. Winters are severe with temperatures often below  $-25^{\circ}\text{C}$ . The region exemplifies a continental variation of the Mediterranean climate pattern, with a snowy, cold winter and mild rainy spring followed by a dry summer and autumn (Frey and Probst, 1986). According to Kottek et al. (2006) the region is a hot and arid area. Rivers and precipitation affect the surface of the Zagros region causing V-shape valleys and erosion respectively, but the effect of tectonics may be higher.

#### 3.6.1.2 Parameters compiled for a critical taper theory applied to the Zagros

Basal dip ( $\beta$ ): The cross-section published by Molinaro et al. (2005) constructed from geological and seismological data shows a thick-skinned section (Fig. 3-14). From this cross-section, the basal detachment can be identified reasonably well. The evaporative unit between the basement and the deformed sediments can be assumed as a weak layer, which serves as detachment. This cross-section consists of two parts: the Zagros simple fault and the high Zagros belt. This study only focuses on the simple fault zone, because the high Zagros is incompletely illustrated in this cross-section. It should be noted that in this cross-section, only the pro-wedge of the simple fault zone (south side of the Zagros orogen) is illustrated.

The cross-sections published by Tunini et al. (2015) are large scale profiles and the sedimentary layers and structures, such as faults and folds and also the near surface deformation are not clearly illustrated. Therefore, these profiles have not been used.

Slope ( $\alpha$ ): in the topographical profile along the chosen Zagros cross-section (Fig. 3-19 b), two main basement faults and rivers were identified. These two faults have changed the surface of the region. Thus, to segment the orogen on the topographic profiles the effect of these faults and rivers has been considered (Fig. 3-19 b, red dashed line). In Fig. 3-19 b, the segment of the northern side is unclear (segment 1). This part could not be retro-wedge. It seems that near to the first peak from the north, there is another peak but this peak is out of the section. Therefore, there is a negative slope for the first segment. The values resulting from the extra profiles are available in the appendix (Fig. 6-3).

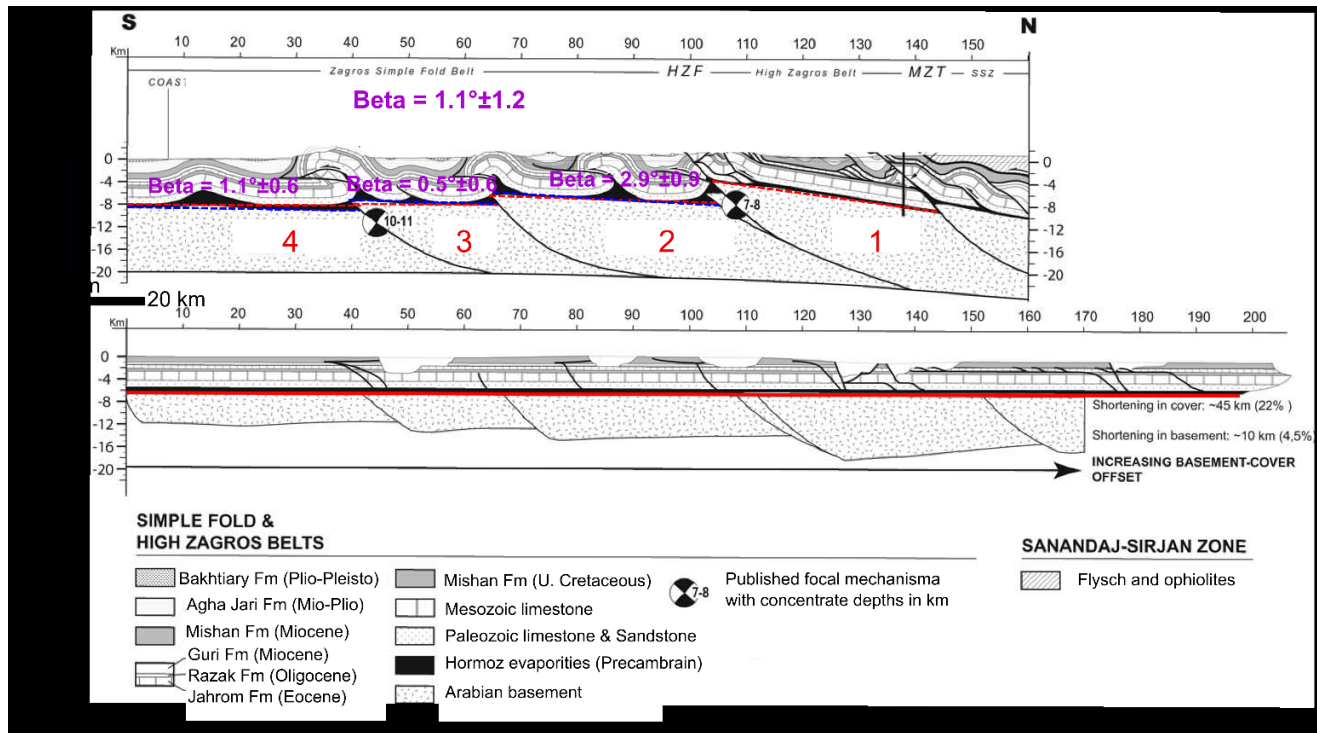


**Figure 3-14.** Measurement of basal dip in the Zagros region, along the profile of Molinaro et al. (2005). Beta values:  $1.1^{\circ} \pm 1.2^{\circ}$  for the entire profile, See also Fig. 3-13 for the location of cross-section.

## 3.6.2 Himalayas

### 3.6.2.1 Tectonics, Lithology and Climate

The closing and subduction of the Paleotethys Ocean located between India and Asia during the Paleozoic, followed by collision of the continents, produced the present day structures and lithologies in the Himalayas. Consequently, the mountains and surrounding regions are characterized by a variety of deformed lithologies and several phases of tectonic and deformational events (Windley, 1995). Heim and Gansser (1939) and Gansser (1964) divided the rocks of the Himalayan fold-and-thrust belt in Nepal into four tectonostratigraphic zones that are characterized by distinctive stratigraphy and physiography. From the south to the north, there are the Subhimalayan, the Lesser Himalayan, the Greater Himalayan, and the Tibetan Himalayan zones (Fig. 3-15).

**Subhimalayan zone:** The topographic front of the Himalayas rises from elevations of 150-250 m in the active foreland basin system to form the Subhimalayan zone, which is the frontal part of the fold-thrust belt (e.g. Nakata, 1989; Powers et al., 1998). The Subhimalayan zone is a 10 to 25 km area consists of Neogene Siwalik (or Churia) Group rocks that crop out in several northward dipping thrust sheets (e.g. Gansser, 1964; Valdiya, 1980; Powers et al., 1998).

**Lesser Himalaya:** This zone is bounded by the Main Central Thrust (MCT) to the north and the Main Boundary Thrust (MBT) to the south. Unlike the higher Himalaya, the lessers only experienced



metamorphism up to the green schist facies. The rock types outcropping here are different. They are primarily sedimentary rocks from the Indian platform. Rock units here also show a series of anticlines and synclines that in many cases are quite sheared. Fossils have been found in this zone, but they do not occur at the same frequency as Tehtyan zone fossils (e.g. DeCelles et al., 2001; Fuchs and Frank, 1970; Frank and Fuchs, 1970; Valdiya, 1980; Stöcklin, 1980).

Higher Himalaya: This zone consist of paragneiss schists, migmatites, marbles, and orthogneisses. To the north of the Main Central thrust, rocks are metamorphosed to amphibolite facies, whereas the rocks of the Dadelhdhura thrust sheet are generally in the upper greenschist facies (e.g., DeCelles et al., 2001; Sorkhabi and Macfarlane, 1999).

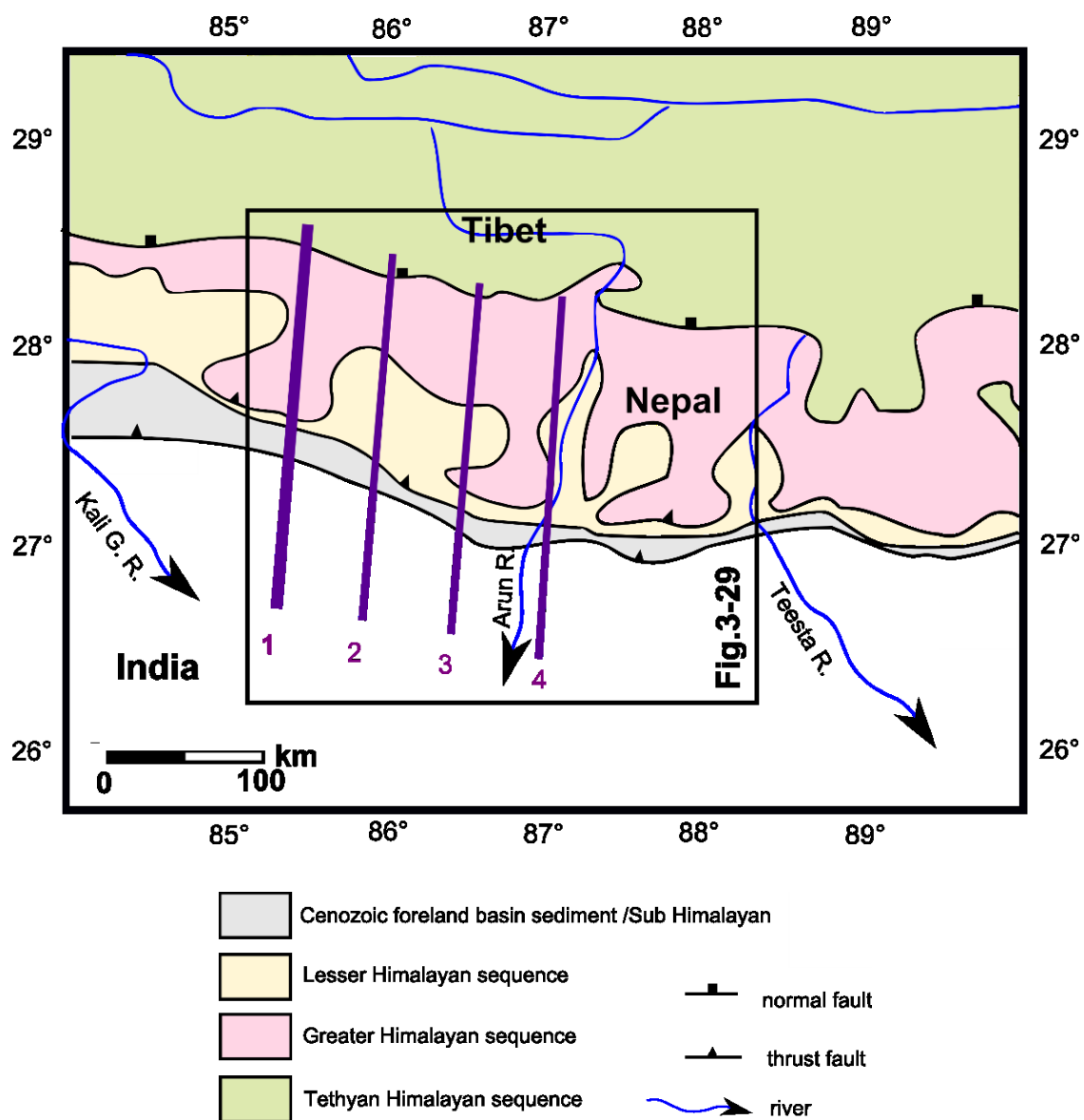


**Figure 3-15.** Geological map of the Himalayas, after Yin et al. (2010). Profile 1: geological cross-section of Lavé and Auouac, 2000 (Fig. 3-16), profile 2, 3 and 4: extra added profiles for better taper analysis.

Tibetan-Himalaya: The Tethyan Himalayas consist of 10-17km marine sediments that were deposited on the continental shelf and slope of the Indian continent. This occurred when India was drifting still in the southern hemisphere (Verma, 1997). Sediments are largely unmetamorphosed, which consist of synclinal basins fossils. Some regions have experienced greenschist facies deformation (Windley, 1995). Altogether, a lot of studies on the Himalayas (e.g. Gansser, 1964; Sorkhabi and Macfarlane, 1999; DeCells et al., 2001) show that the lithology of the northern Himalayas is mechanically harder than those of the southern Himalayas. Annual precipitation ranges from 200 to 5000 mm/yr. In the region dry climate dominates. Vegetation in the southern Himalayas is denser than the northern Himalayas (Kottek et al., 2006; NOAA images).

### 3.6.2.2 Parameters compiled for a critical taper theory applied to the Himalayas

Basal dip ( $\beta$ ): There are several studies about the depth of the Himalayas detachment but all of them have used a common cross-section, which has been studied by Lavé and Avouac (2000) and is also used for this study (Fig. 3-16). This cross-section constructed from geological and seismological data shows basement and sedimentary layers. Along this section, the units from the Paleozoic to the Tertiary are detectable (Fig. 3-15). For this section, there are different possibilities to place the basal dip:

- 1) Along the MFT (main frontal fault) slipping can occur. If we take it as a detachment, beta is between  $6^\circ$  and  $9^\circ$ . It seems that this value for beta is unusually large. Thus, this possibility can be eliminated.
- 2) A detachment can be assumed between the metasediment unit and the basement (detachment B). This metasediment unit consists of phyllite, philitic siltstone, chloritic schist, which could be weaker than the basement. It leads to slipping of the metasediment member above the upper crust. The beta value for this detachment is estimated  $1.7^\circ \pm 0.6^\circ$ .
- 3) A weak boundary can be assumed between the Paleozoic and the overlaying sediments (detachment A). The sediment unit consists of claystone, siltstone, sandstone and conglomerate. The boundary between this unit and Paleozoic layer can be considered as a weak plate, which has a beta value the same as the detachment B ( $1.7^\circ \pm 0.6^\circ$ ).

For this cross-section beta values of about  $1.7^\circ \pm 0.6^\circ$  have been estimated (table 3-1). These values are for PW (southern side).

Slope ( $\alpha$ ): Along the mentioned cross-section, there are normal and thrust faults and also V-shaped valleys. Therefore, as for the other orogens, a regional segmentation was identified to find  $\alpha$ . Precipitation and vegetation affected the surface of the region. In the south of the area, climate is humid and vegetation is dense but dry climate dominates in the region. According to Vance et al. (2003) the maximum erosion rate for this region is 10 mm/yr. Considering the mentioned parameters, a regional segmentation (red line) has been identified (Fig. 3-19 c). The values resulting from the extra profiles are available in the appendix (Fig. 6-4).

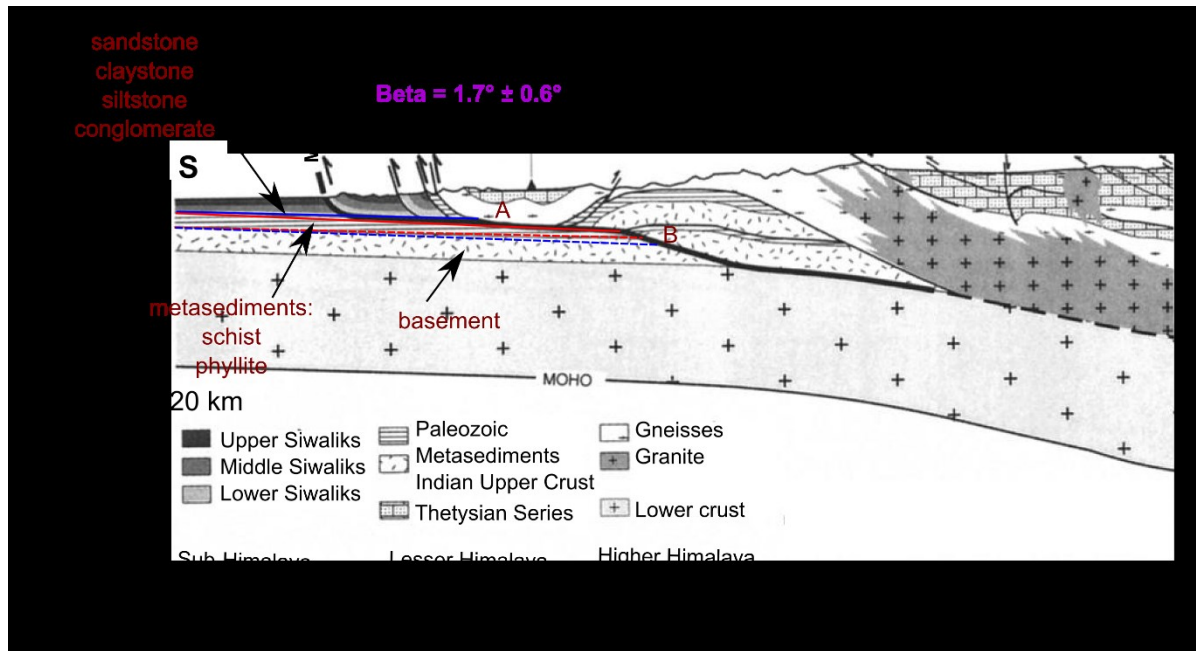


**Figure 3-16.** Measurement of basal dip in the Himalayas, along the profile of Lavé and Avouac (2000). Beta values:  $1.7^\circ \pm 0.6^\circ$  for the entire profile, lithological data (Lavé and Avouac., 2000). See also Fig. 3-15 for the location of cross-section.

### 3.6.3 Apennines

#### 3.6.3.1 Tectonics, Lithology and Climate

The southern Apennines fold and thrust belt results from the convergence between the Africa-Apulian and the European plates since the Late Cretaceous (Mazzoli and Helman, 1994, and references therein). The Apennine orogen comprises several tectonic units characterized by Mesozoic-Tertiary shallow water to slope-facies carbonates (Apennines and Apulian carbonate platforms) and pelagic basin (Lagonegro) successions. They originate from the deformation of the Apulian continental paleomargin, as well as unconformably overlying Miocene-Pliocene wedge-top and foredeep basin deposits (Bonardi et al., 2009; Mazzoli et al., 2008). The orogenic mass is tectonically covered by remnants of an accretionary wedge, which was superposed onto the Apennine Platform domain in the Early Miocene (Bonardi et al., 2009; Ciarcia et al., 2009).

Generally, the area comprises southern Tethys passive margin sediments, basins, ramps and structural highs of Triassic to Miocene age (Parotto and Pratlurion, 1975). These are dominated by various carbonate facies (platform, margin and basin) that are dissected by Cenozoic and Mesozoic faults. Between the major thrust-related culminations of these carbonates, Late Miocene and Pliocene siliciclastics (flysch) overlie them. From the south-west to the north-east, the onlap of progressively younger flysch onto the pre-tectonic carbonates has been used to support a model of piggy-back thrusting that migrated towards the north-east (Cipollari and Cosentino, 1995). In a general view, this region from the south to the north consists of hard to soft lithological units (Fig.3-17).

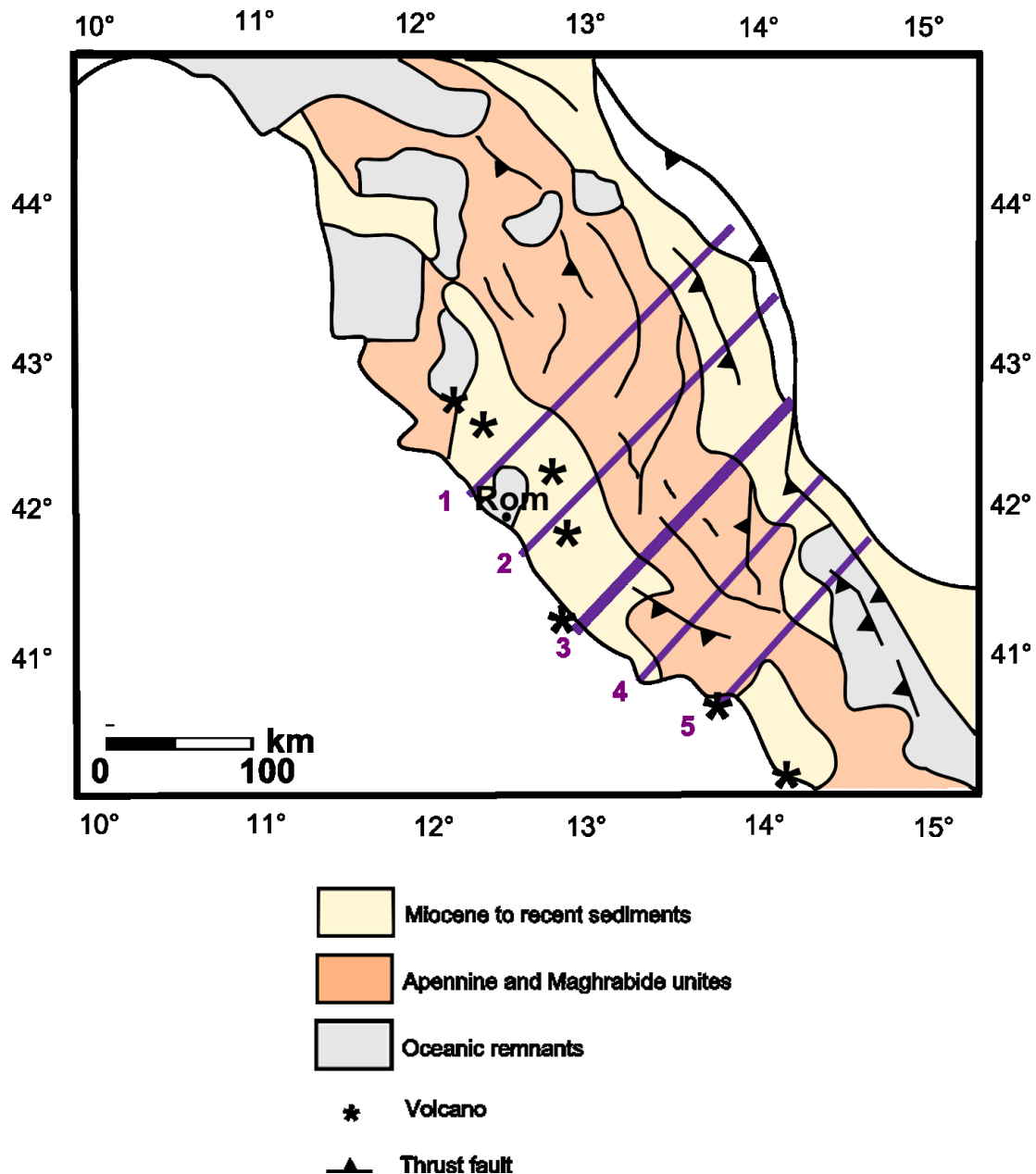


**Figure 3-17.** Geological map of central Italy, after Rosenbaum et al. (2002). Profile 3: studied cross-section by Tozer et al. (2002, Fig. 3-18), profile 1, 2, 4 and 5: extra added profiles for better taper analysis.

Italy has a variety of climate systems. Between the north and the south, there can be a considerable difference in temperature. The east coast of Italy is not as wet as the west coast, but it is usually colder in winter. The east coast is occasionally affected by cold winds in winter and spring. Precipitation rate is different in the entire region, but mostly a wet climate dominates (Kottke et al., 2006).



## 3.6.3.2 Parameters compiled for the critical taper theory applied to the Apennines

Basal dip ( $\beta$ ): The cross-section published by Tozer et al. (2000) consists of different layers, such as carbonate of Triassic-Middle Miocene, alluvial sediment of the Pliocene-Quaternary and also flysch of the Miocene-Pliocene and some volcanic of the Pleistocene (Fig. 3-18), which can be considered as a thin-skinned model. The detachment can be assumed between the basement and the basal Triassic layers. For this detachment, beta values of  $1.4^\circ$  for the retro-wedge and  $0^\circ$  for the pro-wedge have been estimated.

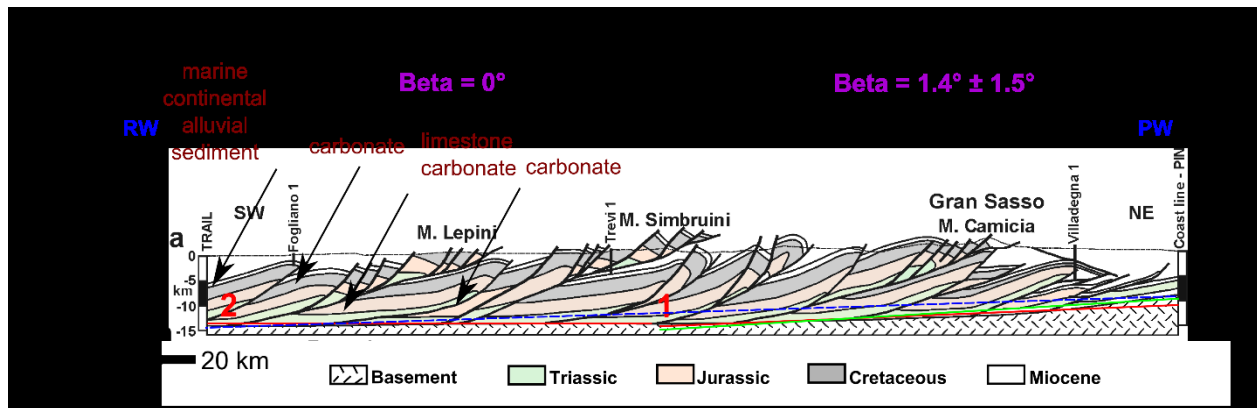
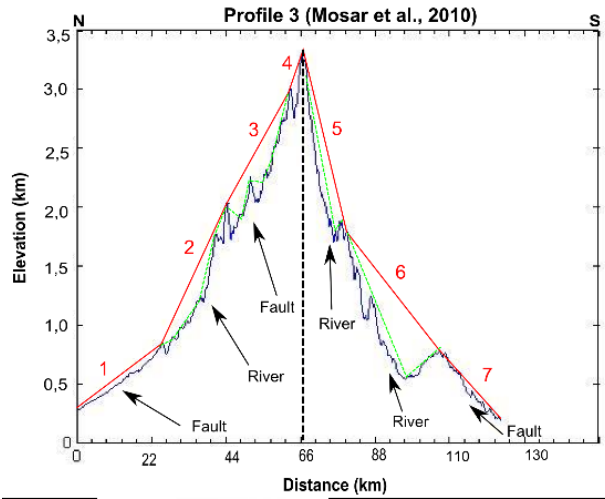


**Figure 3-18.** Measurement of basal dip in the Apennines, along the profile of Tozer et al. (2002). Beta values:  $1.4^\circ \pm 1.5^\circ$  for the RW and  $0^\circ$  for the PW, lithological data (Tozer et al., 2002). See also Fig. 3-17 for the location of cross-section.

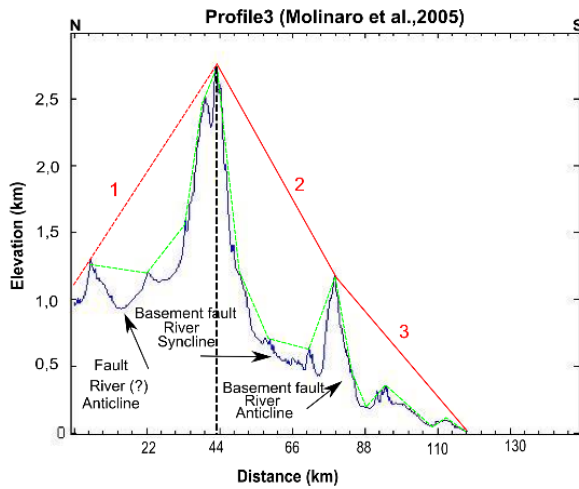
Slope ( $\alpha$ ): Along the mentioned cross-section, thrust faults dominate especially on the NE side and affect the surface slope. V-shape rivers also are detectable along the profiles. Thus, like for the other regions, a regional segmentation has been identified from the topographic profile along the geological cross-section (Fig. 3-19 d, red dashed line).  $\alpha$ -values from the extra profiles are available in the appendix (Fig. 6-5). The  $\alpha$  and  $\beta$  estimated for the Apennines indicate that the retro-wedge is coincident with the northern flank and pro-wedge with the southern flank which is compatible with Moho data and the geometry of the orogen (Piana and Amato, 2009).

a)



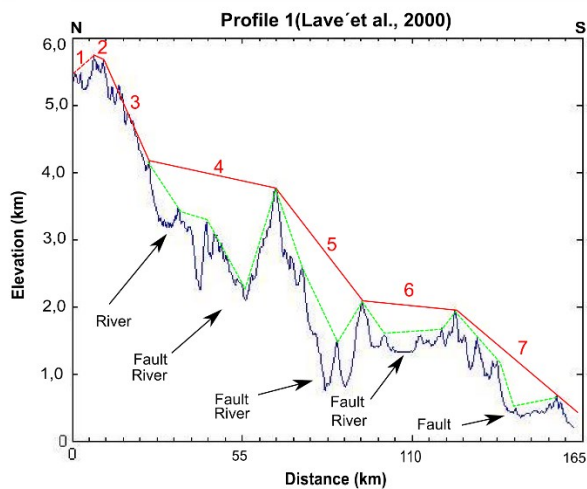
	X	Y	Z (m)	Slope (°)
1	48.6000	41.5000	266.5227	1.27
2	48.4569	41.3160	838.0704	3.58
3	48.3511	41.1800	2028.5969	2.96
4	48.2466	41.0456	3000.7369	4.87
5	48.2265	41.0197	3308.3883	6.98
6	48.1604	40.9349	1856.3602	2.17
7	48.0003	40.7290	763.6015	1.73
Min. slope : 1.27° Max. slope : 6.98° Mean slope : 3.01°				

b)



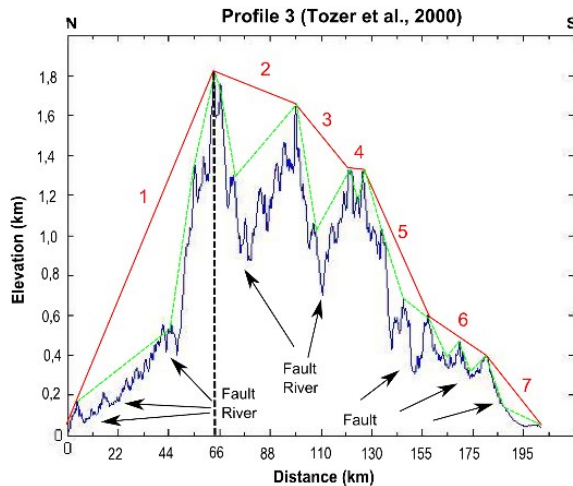
	X	Y	Z	Slope (°)
1	56.2000	28.2000	1064.1899	-2.17
2	56.2361	27.8389	2708.8227	2.42
3	56.2649	27.5363	1172.0310	1.64
Min. slope : -2.17° Max. slope : 2.42° Mean slope : 2.01°				

c)



	X	Y	Z	Slope (°)
1	85.3000	28.3000	5411.5605	-2.5
2	85.2957	28.2913	5719.7684	1.2
3	85.2939	28.2398	5656.0976	5.7
4	85.2847	28.2143	4130.2993	0.51
5	85.2595	28.0857	3756.6191	3.40
6	85.2422	27.7325	2070.7949	0.26
7	85.2033	27.2322	640.2755	2.21
Min. slope : -2.5° Max. slope : 5.7° Mean slope : 1.74°				

d)



	X	Y	Z (m)	Slope (°)
1	13.9500	42.8000	3.6530	1.61
2	13.5321	42.3666	1811.3874	0.27
3	13.2978	42.1237	1638.1286	0.76
4	13.1428	41.9629	1321.2745	0.07
5	13.1057	41.9245	1314.0352	2.09
6	13.0517	41.7334	593.3720	0.44
7	12.75	41.5580	390.4798	0.86
Min. slope : 0.07° Max. slope : 2.09° Mean slope : 0.98°				

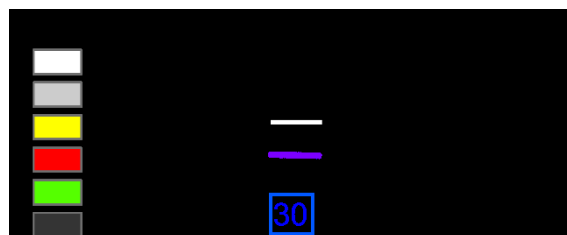
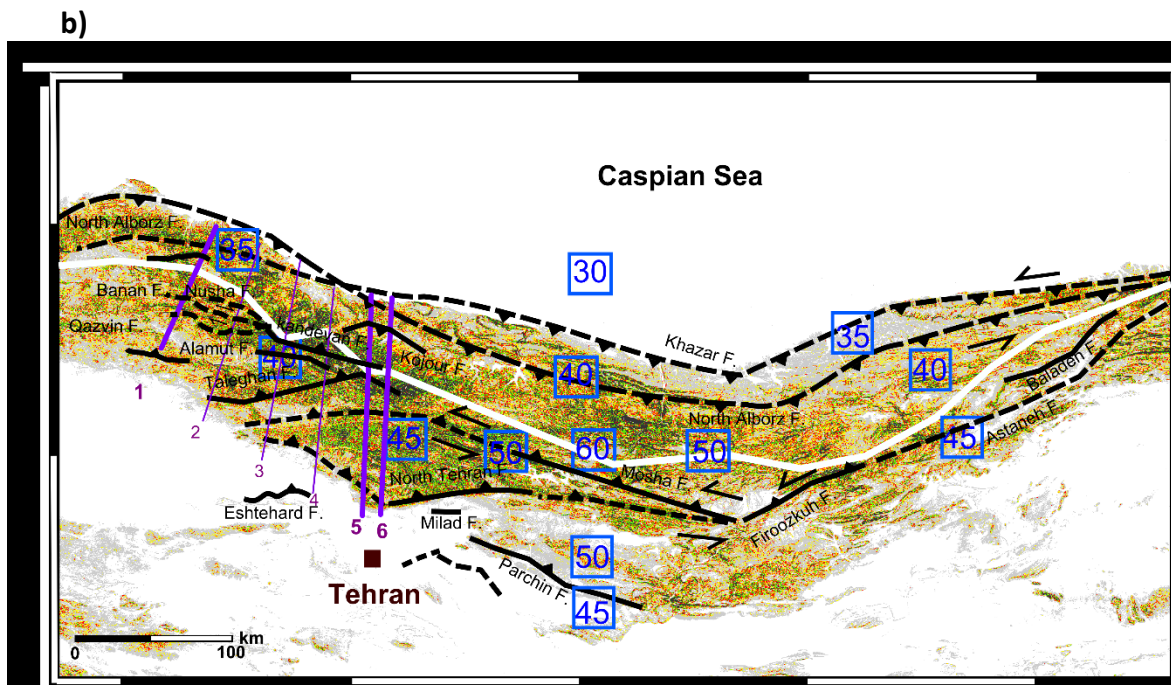
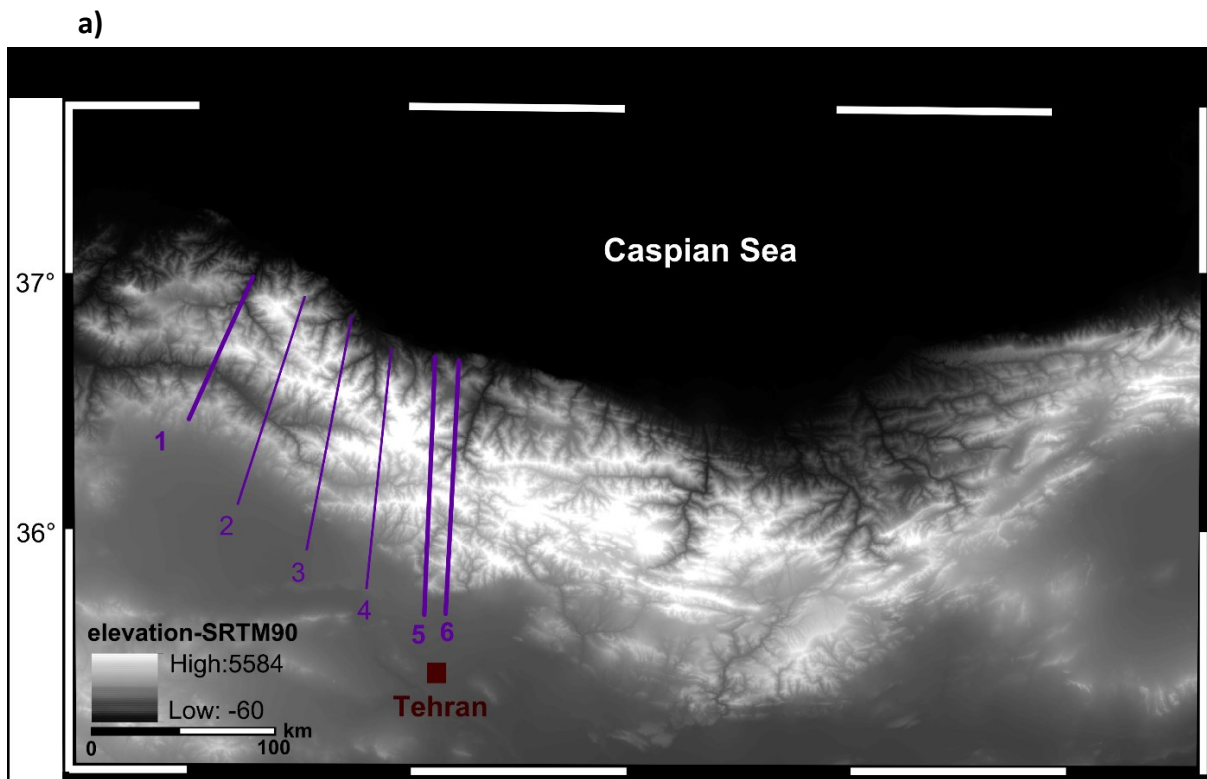
**Figure 3-19.** Regional slope along the main profiles, as well as the table of coordinates and  $\alpha$ -values of the segments. The  $\alpha$ -values of the extra profiles are given in the appendix. Regional slope of **a)** the Caucasus (along the profile of Mosar et al., 2010; Fig. 3-11), **b)** the Zagros (along the profile of Molinaro et al., 2005; Fig. 3-13), **c)** the Himalayas (along the profile of Lavé and Avouac, 2000; Fig. 3-15), **d)** the Apennines (along the profile of Tozer et al., 2002; Fig. 3-17), **black dashed line:** crest of orogen, **red line:** general segmentation, **green dashed line:** local segmentation.

### 3.7 Critical taper analysis

In the following, I present a critical taper analysis for the Alborz and other orogens of the AHB in terms of computing F-value maps. Then, I argue, if the F-maps can show the wedge stability of the Alborz and other orogens of the AHB. For this purpose, all compiled data, such as tectonics, lithology, climate, earthquakes and landslides have been used. Since this study mainly focuses on the Alborz, extensive data have been compiled for this region and then for the Caucasus region. For some regions, the available data are local not regional.

#### 3.7.1 Alborz

In western Alborz, the number of faults are higher than on its eastern side (Fig. 3-20 b). According to the critical taper theory, the faults can be a result of internal deformation of orogen. According to the local slope map (Fig. 3-20 b), on the western side, local slope can be higher than  $30^\circ$ , but on the eastern side, these values are up to  $20^\circ$ . Increasing slope ( $\alpha$ ) leads to an increase in the F-value (von Hagke et al., 2014). Therefore, by means of the local slope map, it is possible to estimate the local F values. Thus, if the local slope map shows high values in a location, it means that this location has high local F-values (Fig. 3-20 b). The local slope values are higher in western Alborz. This can indicate a higher wedge stability for the western part than the eastern part. Given the mentioned data, a non-uniform mechanical wedge state can be expected for the Alborz.



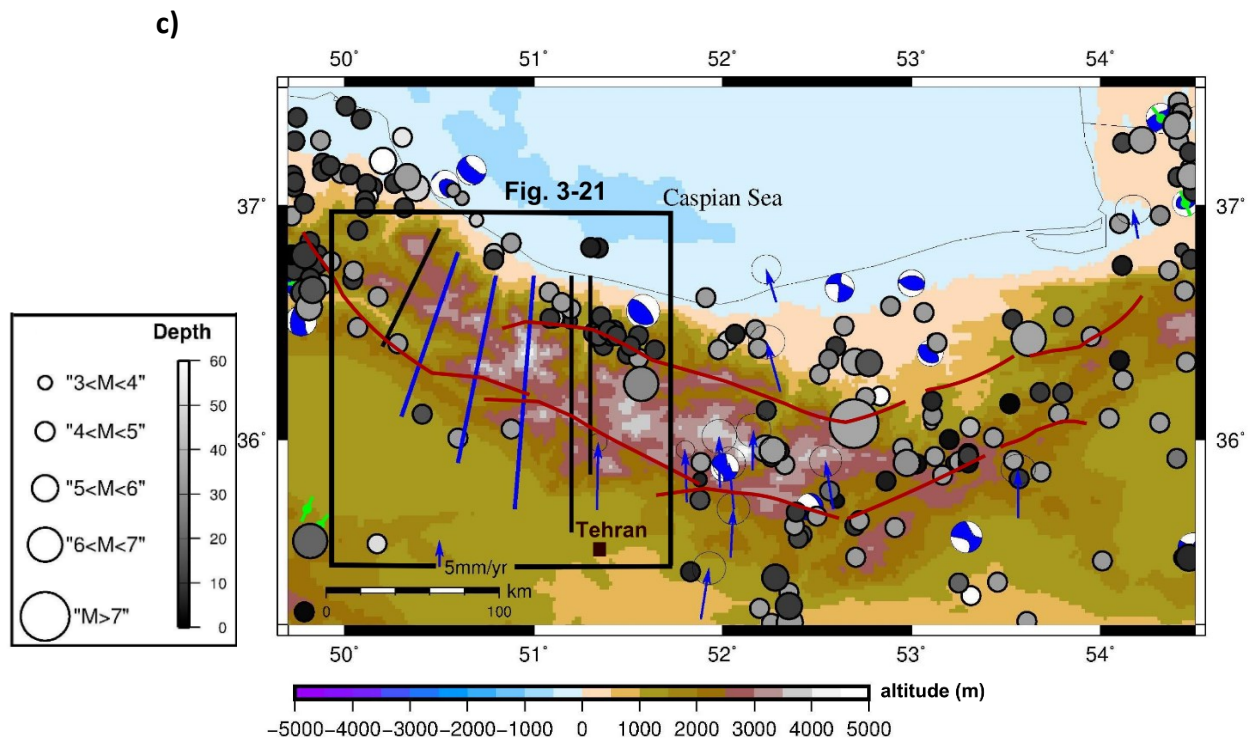


**Figure 3-20.** Elevation, local slope and earthquakes of the Alborz region. **a)** Elevation map from SRTM 90 m, **b)** Local slope from elevation map. Faults: Berberian et al.(1993); Hinds et al. (2001); Allen et al. (2003), Guest et al. (2006 a, b); Nazari et al. (2007), Moho: Motavalli-Anbaran et al. (2013), **c)** Earthquakes and stress regimes and location of F-maps, earthquakes (NEIC catalogue, 1900 to 2014 ), **red lines:** main faults (Berberian et al., 1993; Hind et al, 2001; Allen et al., 2003), **blue arrows:** GPS velocity (Vernant et al., 2004 a, b), focal mechanism (CMT Catalogue, Ekström et al., 2012), stress data (WSM Catalogue, Heidbach et al., 2008, **green:** thrust fault), black line: location of geological cross-section, **blue line:** location of topographic profile.

A high frequency of earthquakes is obvious in eastern Alborz (Fig. 3-20 c). It shows that this part of the Alborz may have a relatively lower wedge stability. Besides, a higher number of landslides appear in eastern Alborz (Fig. 1-4 a). It should be noted that a regional map of landslides, which shows the size and volume of landslides, is not available for the Alborz region. There is just data about the location of landslides in the Alborz. Furthermore, for a small section, there are data about the size and volume of some giant landslides, which are located mostly in northern Alborz (Fig. 1-4 b). Additionally, more rivers are observed in eastern Alborz than in western Alborz (Fig. 3-6 a). Rivers can be taken as wetness, which could increase the pore fluid ratio. Where the pore fluid ratio is high, effective friction is low (e.g. Dahlen, 1984).

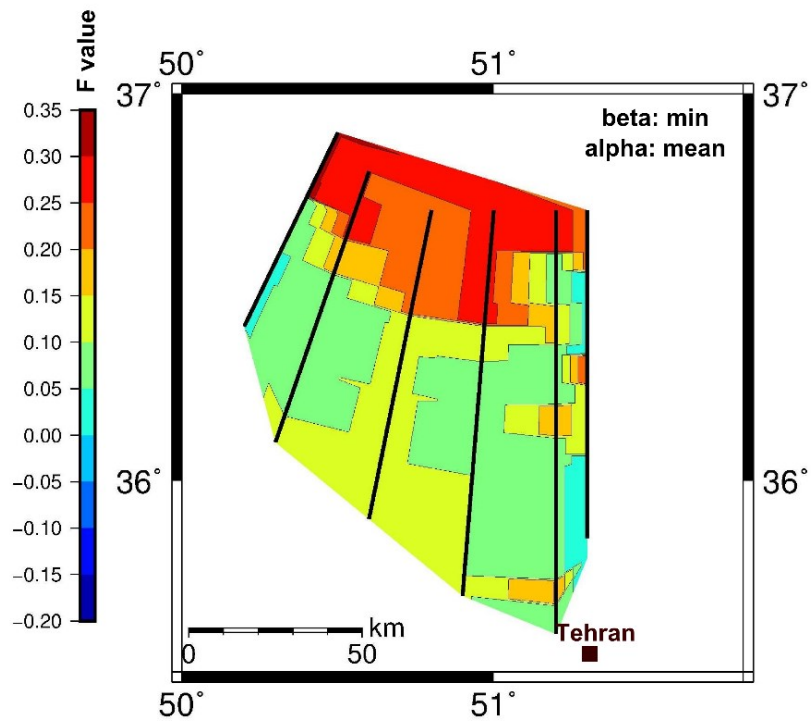
With the obtained values of "alpha" and "beta" and with the help of equation (3), the F-value for the Alborz region has been calculated. If in this equation, we consider  $W=1$ , then we have  $F = 2\alpha + \beta$ . The F-maps are based on regional alpha (mean alpha) but different beta values (minimum; Fig. 3-21 a, mean; Fig. 3-21 b, and maximum; Fig. 3-21 c). According to the equation (3), any change in "beta" has in fact a little effect on the obtained F-values, but every change in "alpha" can change F-values, effectively. The

obtained F-maps show that F-values range from 0.03 to 0.35 in the region. The lowest F-values (0.03-0.10) appear in the east and west of the region (Fig. 3-21 a, b, c). In the north and some places of the south, F-values are greater than 0.15. The highest F-values are mostly visible in the NW. However, all F-maps show a relatively higher F-value in northern Alborz (retro-wedge; Fig. 3-21 a, b, c).

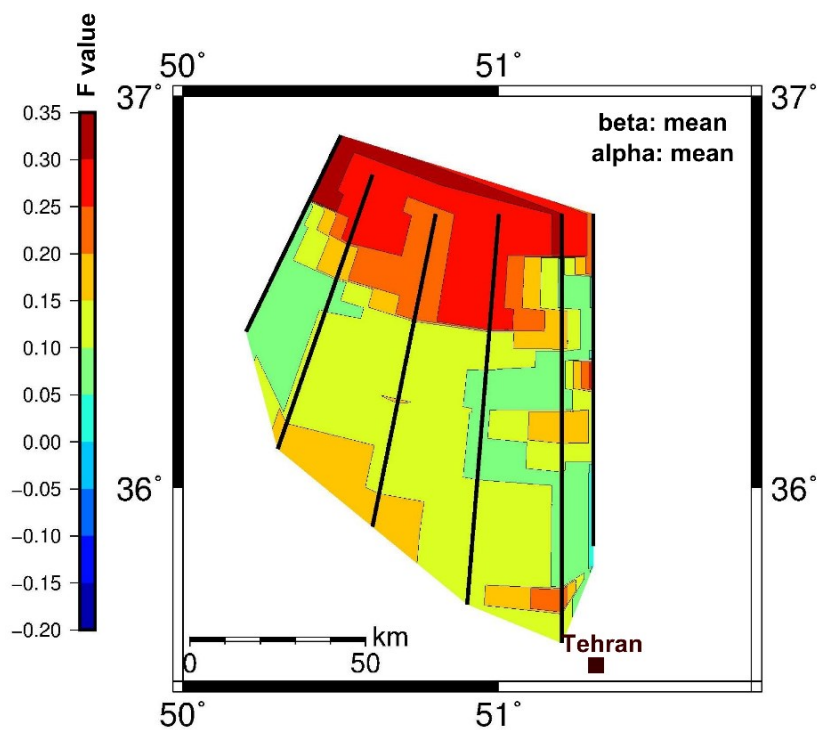
The minimum F-value is comparable with result of Suppe (2007) for Taiwan (0.08) and Niger delta in Nigeria (0.04) based on the  $W$ -value of 0.6 and 0.7, respectively. F-values of Taiwan were between 0.07 and 0.11, if  $W=1$  (Suppe, 2007), which is less than in the Alborz region. According to the obtained F-maps of the Alborz, in the region of studied profiles, fault strength may be higher in northern Alborz than in southern Alborz. If we consider that the F-values are in fact an equivalent of basal friction ( $\mu_b$ ) (e.g. von Hagke et al., 2014), then, there is relatively higher friction ( $\mu_b$ ) in northern Alborz, consequently northern Alborz may be more stable than southern Alborz (Fig. 3-21 a, b, c).



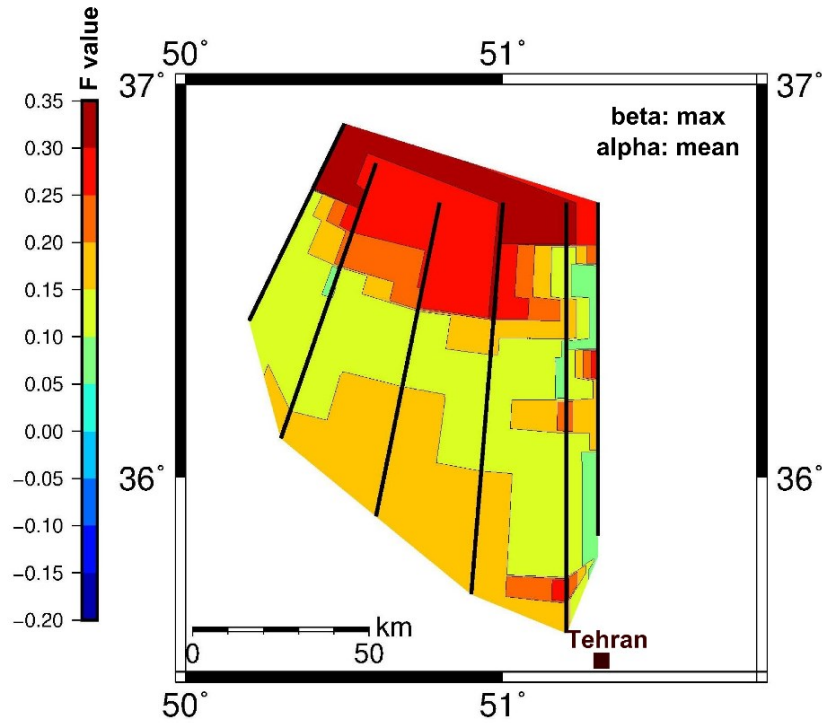
a)



b)



c)



d)

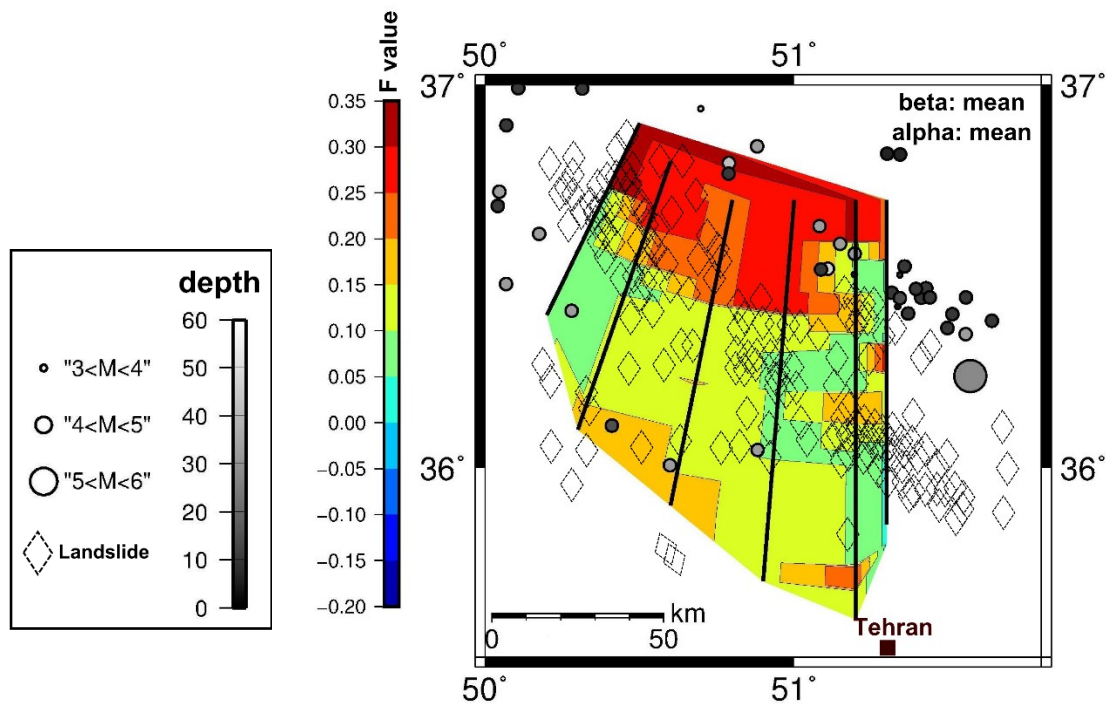


**Figure 3-21.** Map of F-values in the Alborz region. Higher F-values in the north of the area based on mean alpha and minimum beta values (a), mean alpha and mean beta values (b), mean alpha and maximum beta values (c), mean alpha and beta with geo-hazards (earthquakes: NEIC Catalogue, 1900 - 31.05.2015; landslides: Hafezi and ghafoori, 2007) (d). See also Fig. 3-20 c for the location of maps.

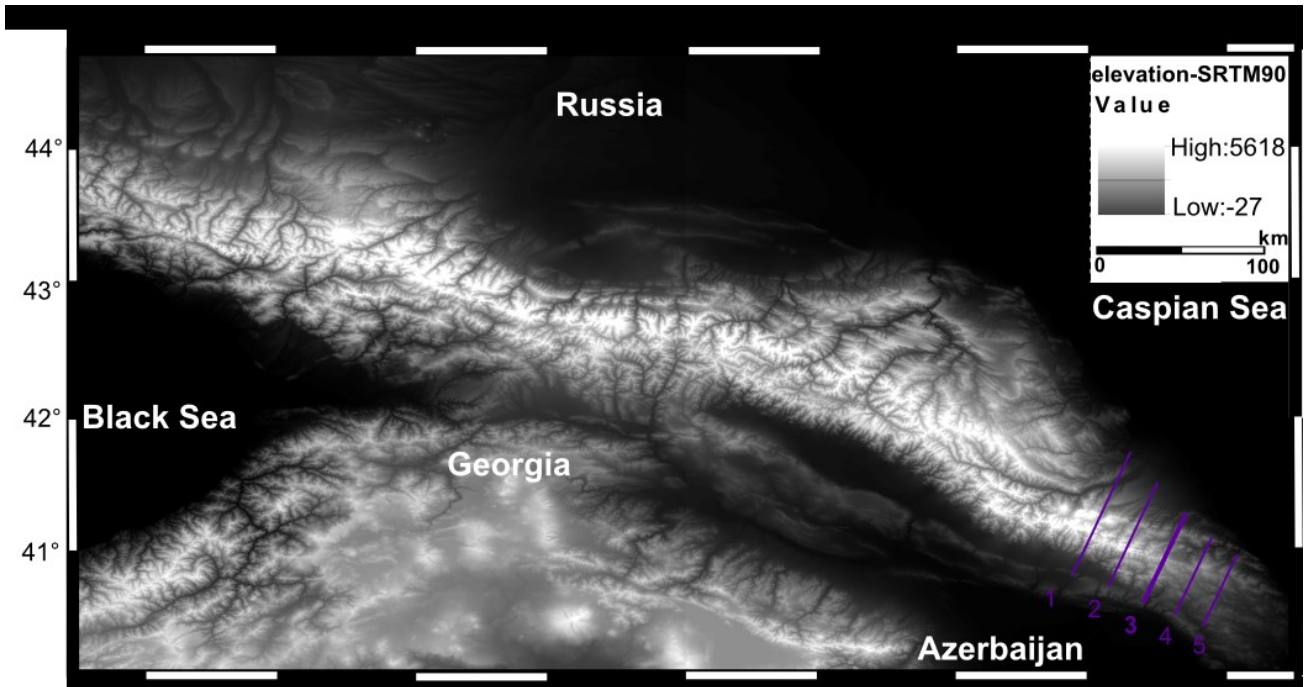


To analyse if hazard is related to orogen mechanics, especially F-values of the Alborz, and geo-hazard, i.e. earthquakes and landslides are plotted on the F-maps (Fig. 3-21 d). As mentioned, the obtained F-maps showed a relatively higher stability in northern Alborz. It is comparable with the geo-hazards distribution in the region. There are some landslides and earthquakes in northern and southern Alborz, but a high frequency of landslides is observed in a trend of NW-SE area in the middle part of the region. To complete the comparison of F-value and geo-hazards and thus for a better interpretation of wedge stability, to study of micro earthquakes is necessary. For the Alborz region, in the coordinate of F-maps, there are no microseismic data available, but for another part of Alborz (west part) microseismic data from 1900 to 2011 were available (Fig. 1-3 b). Taken together, based on the F-maps, earthquakes and microseismicity, it can be explained that in northern Alborz the F-values are higher. Therefore, the northern Alborz may be more stable than southern Alborz in the location of F-maps.

### 3.7.2 Caucasus

In this region, the variation of local slope or local F-values is the same as Alborz and is between  $0^{\circ}$ - $35^{\circ}$ . The maximum local F-values are detectable in the entire orogen (Fig. 3-22 a, b). Faults, especially thrusts, are detectable along the orogenic line but in the center, near to the west part, smaller faults also are visible (Fig. 3-22 b). The entire Caucasus experiences earthquakes and landslides (Fig. 3-23, 3-24), but a high frequency of earthquakes and large landslides are observed mostly on the southern side of the orogen (the pro-wedge). The Entire Caucasus (pro- and retro-wedge) is covered by forest and a wet climate dominates in the region (Kvavadze and Rukhadze, 1989; Kottek et al., 2006). F-maps show a general variation between 0 and 30 radian. In mostly three parts of the map, i.e., in the NE, E, and middle part of the region high F-values are observed (3-25 a, b, c)

a)



c)

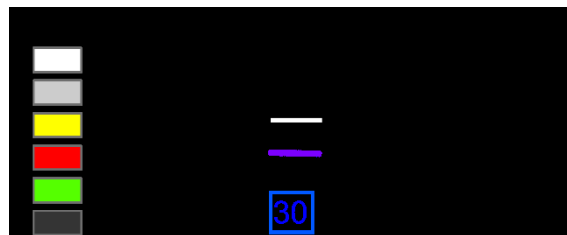
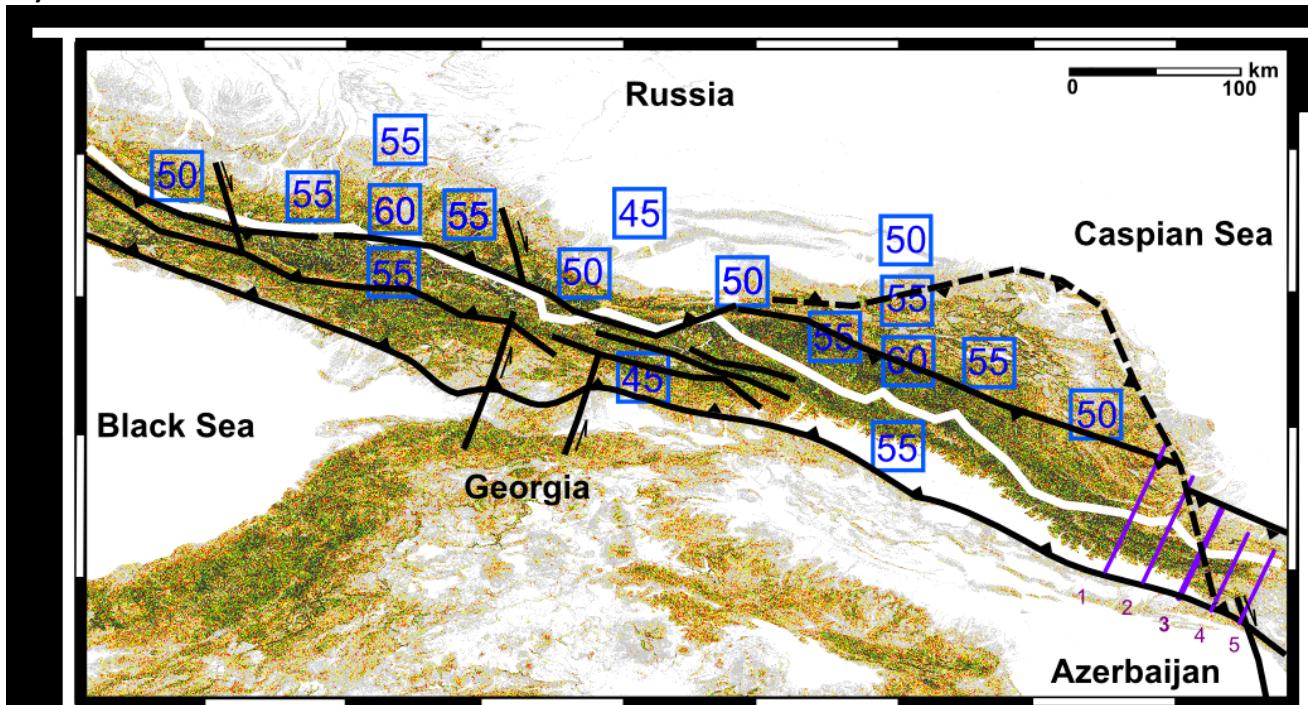


**Figure 3-22.** Elevation and local slope in the Caucasus region. **a)** Elevation map from SRTM 90 m, **b)** Local slope from the elevation map. Faults: Saintot et al. (2006), Moho: Eppelbaum and Khesin (2012).



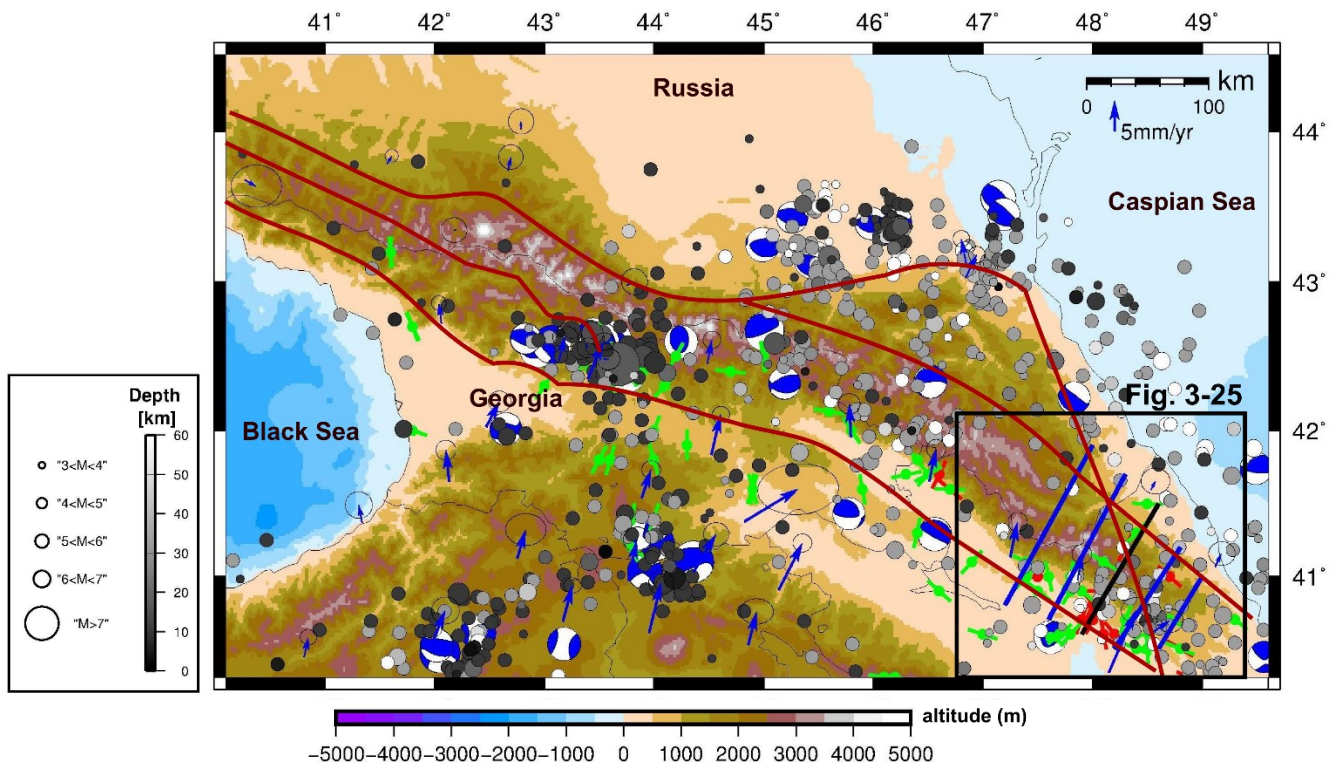


**Figure 3-23.** Map of earthquakes and tectonic regimes in the Caucasus. Topography (DTU, Andersen and Knudsen, 2009), **blue arrows:** GPS velocity (Vernant et al., 2004 a, b), **beach balls:** Focal mechanism (CMT Catalogue, Ekström et al., 2012), stress regime (WSM Catalogue, Heidbach et al., 2008, WSM Symbols, **Red:** normal fault, **green:** thrust fault), **red line:** main thrust fault, **black line:** location of geological cross-section, **blue line:** location of topographic profile.

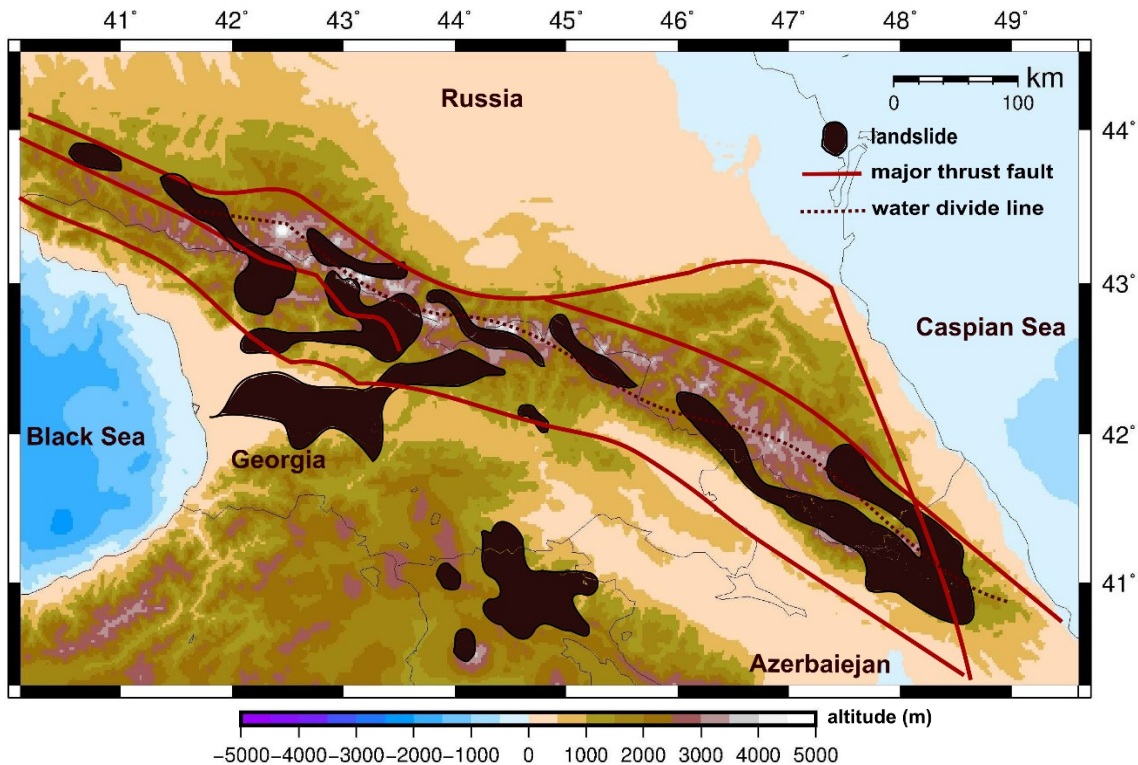


**Figure 3-24.** Landslide map of the Caucasus region, after Armenian second national communication 2010 (<http://www.undp-alm.org>).

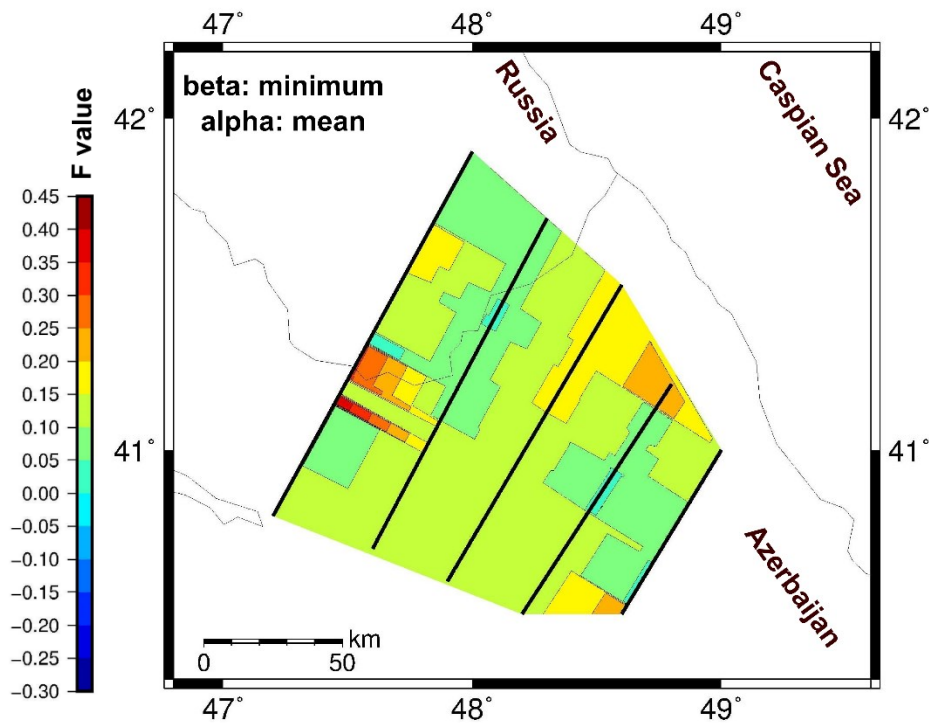
F-maps based on alpha (mean) and beta (mean, minimum and maximum value) (Fig. 3-25) show values between 0.05 and 0.35 radian for the Caucasus region. This is lower than the F-values of Taiwan (0.07-0.11 radian, Suppe, 2007).

According to the F-maps, a high F-value (greater than 0.15) region in NE, W and the center of the Caucasus is detectable. The other regions are almost between 0.05 and 0.15. Altogether, it can be interpreted that in the east Caucasus the higher F-values are detectable in the northern and southern sides of the orogen, but they may be relative higher in the northern side, i.e. the retro-wedge (Fig. 3-25 a, b, c).

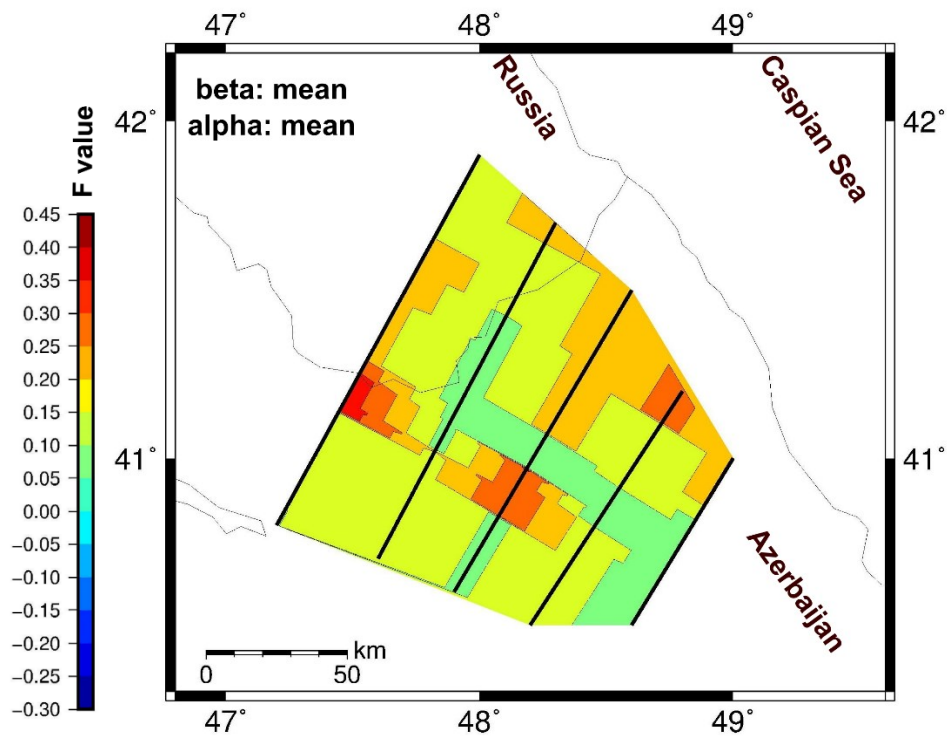
If we accept that the northern flank of the Caucasus orogen has higher F-values, then it can be assumed that the northern flank can have a higher basal friction ( $\mu_b$ ) and may be more stable than the other parts of Caucasus orogen. This result is almost the same as for the Alborz region (Fig. 3-21 a, b, c), i.e. in the Alborz region, F-values on the northern flank (RW) are higher than on the southern flank (PW).

Furthermore, similar to the Alborz, earthquakes and landslides are more numerous in the southern part of the Caucasus (Fig. 3-25 d), which is not in agreement with the distribution of F-values. It means that I expected a higher number of earthquakes in the lower F-value parts of the Caucasus but the higher F-value parts also experienced earthquakes and landslides. This may depend on some natural factors, such as differences in lithology and climate. As mentioned, lithology and climate of the Caucasus are not similar to the Alborz and on both the northern and southern flanks, are mostly the same. However, for this region in the compiled data (lithology, climate, tectonics, surface slope, earthquakes, landslide) and F-maps, no specific differences between pro- and retro-wedge have been identified. It can be assumed that the mechanical state of the wedge is the same in the entire region.

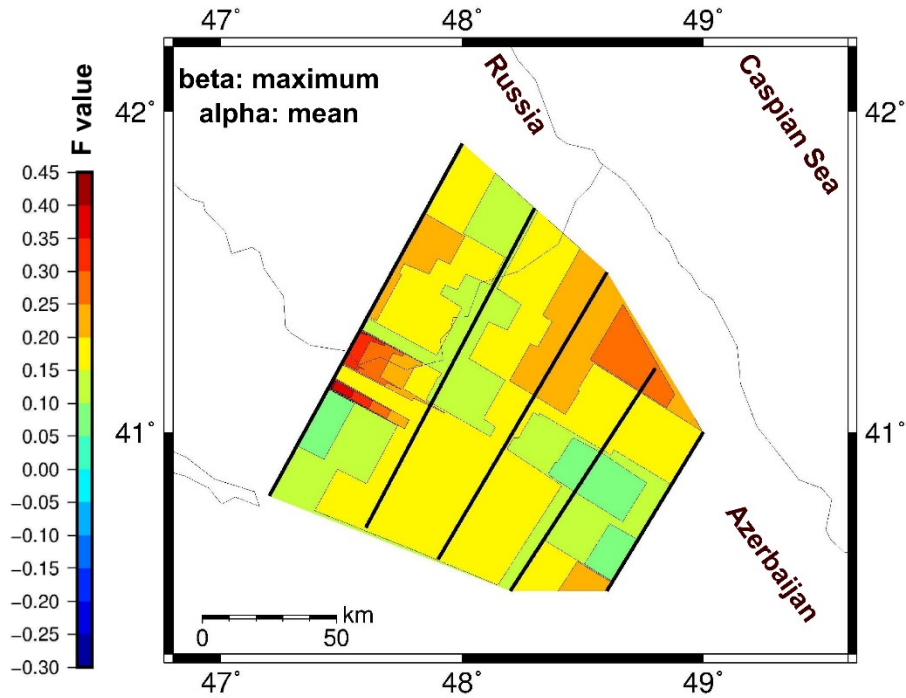
a)



b)



c)



d)

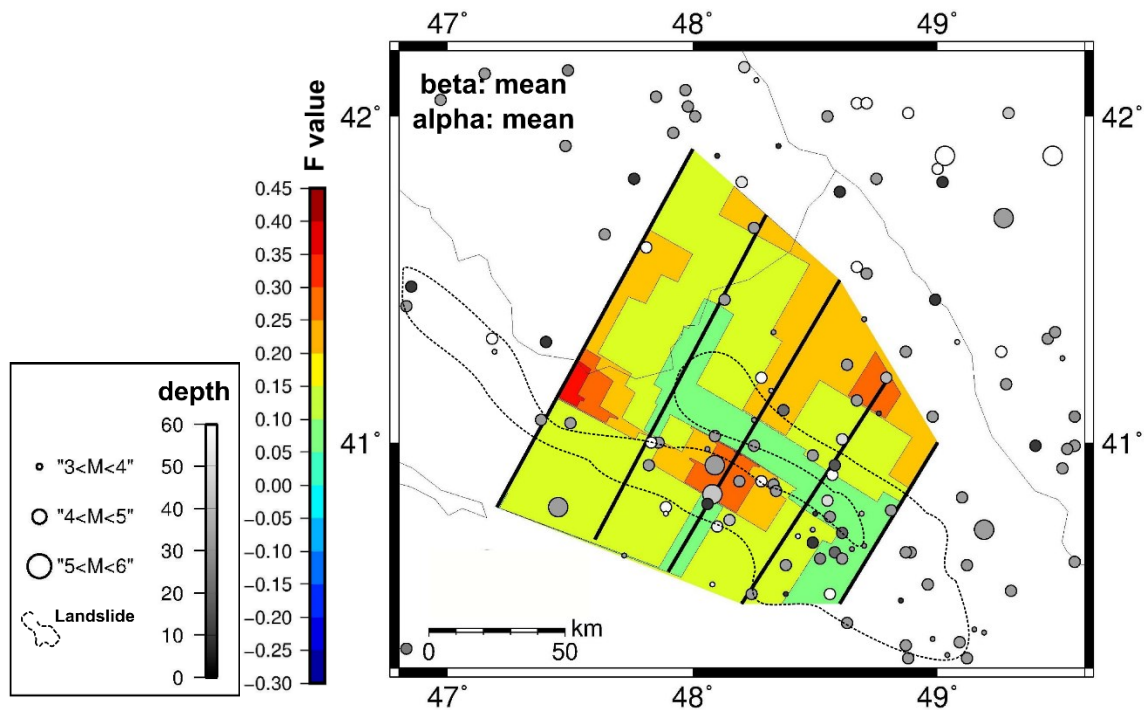


**Figure 3-25.** Map of F-values in the Caucasus region. Higher F-values in the northeast and in the small location of the west and center, based on mean alpha and minimum beta values (a), mean alpha and mean beta values (b), mean alpha and maximum beta values (c), mean alpha and mean beta with geo-hazards (earthquakes: NEIC Catalogue 1900-31.05.2015; landslides: Armenian second national communication 2010 (d)). See also Fig.3-23 for the location of maps.



### 3.7.3 Zagros

As shown, the region of the Zagros is a part of a bivergent orogen, i.e. the pro-wedge part. Faults have almost a NW-SE trend in this region and a higher number of these faults are obvious in the NE and W of the region (Fig. 3-26). The dominant local slope values are between 5°-25° and local slope values higher than 30° are presented in some limited small areas near the faults (Fig. 3-26). The lithological map of the region indicates that the eastern part has mechanically stronger units in comparison to the western part (Fig. 3-13). According to the NOAA images and the Köppen Geiger climate classification, this region has an arid climate (Kottek et al., 2006).

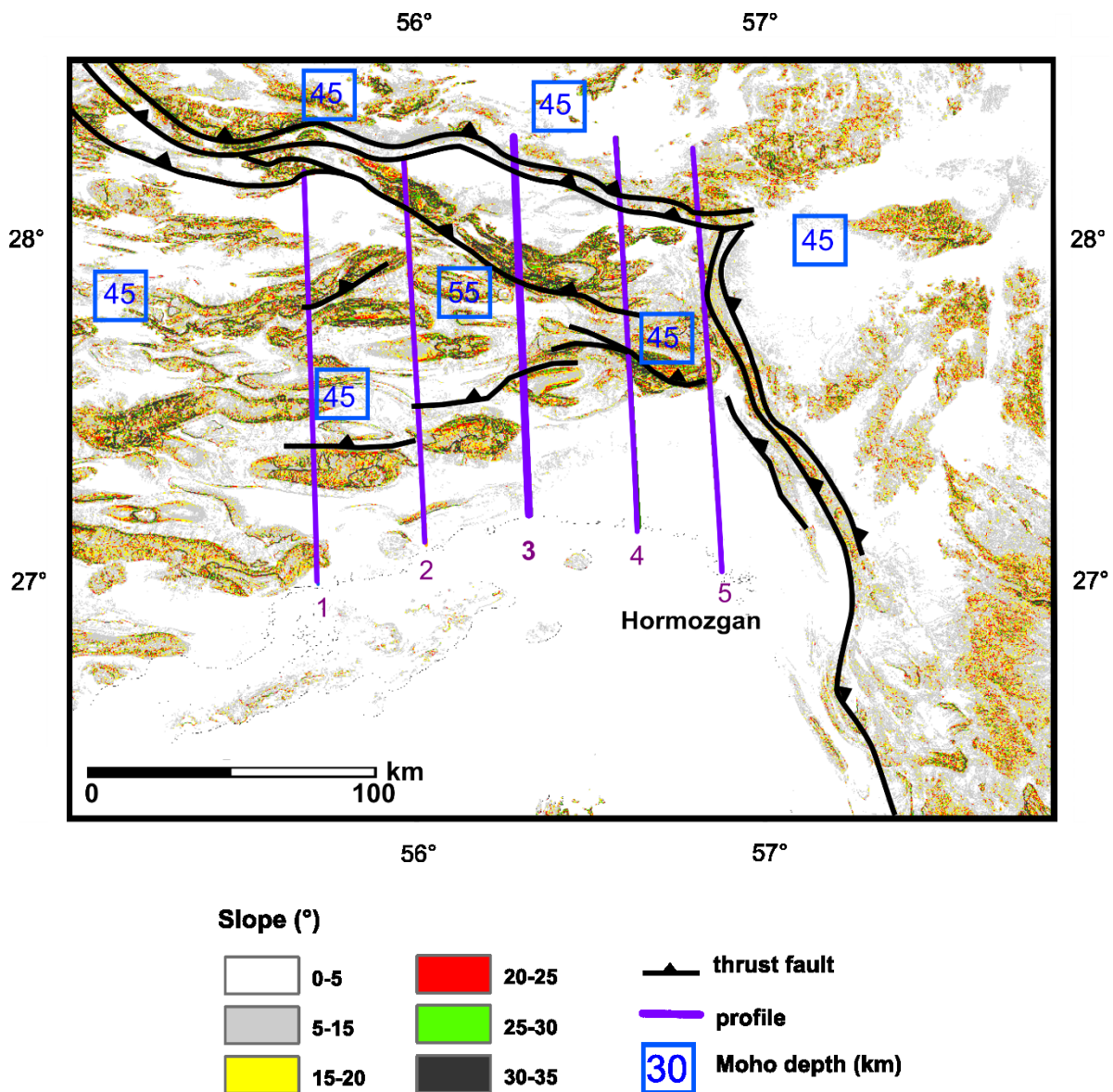


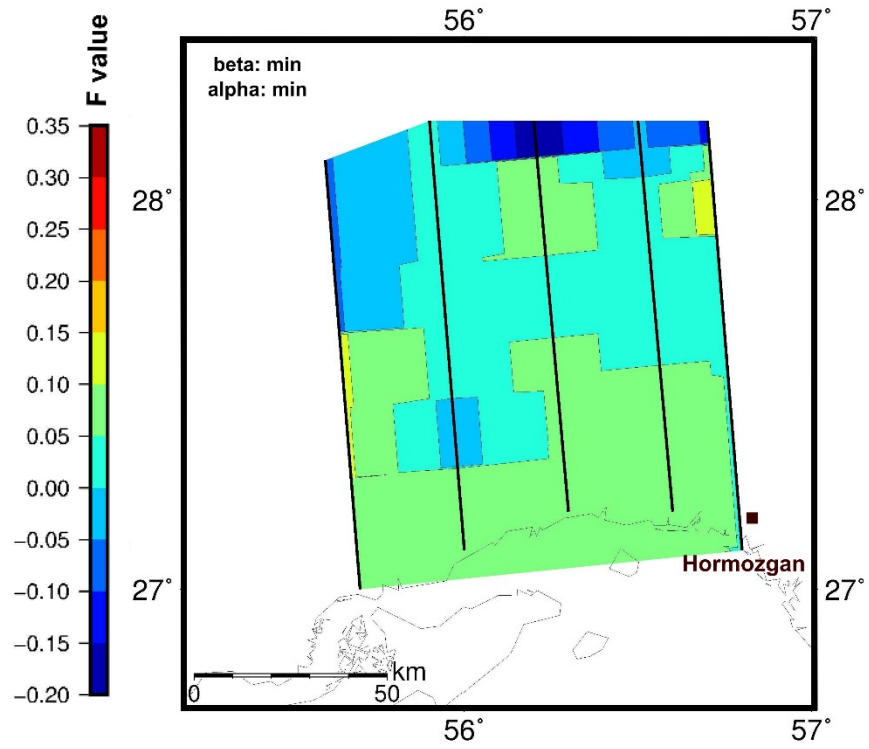
**Figure 3-26.** Local slope map of the Zagros region. Slope data from SRTM 90, Faults: Molinaro et al. (2005), Moho: Manaman et al. (2011), Nasrabadi et al. (2008).

The obtained F-maps of the Zagros region show a variation of F-values between -0.20 and 0.15. Based on the minimum, mean and maximum F-values, the south of the area and some locations in the west and east have relatively higher F-values (Fig. 3-27 a, b, c). This indicates that mostly the south of the Zagros region may have a higher basal friction ( $\mu_b$ ) and consequently may have a higher wedge stability in comparison to the north of the region. Since this section shows a part of bivergent orogen, I do not compare this section with the section of the Alborz. The lowest F-values are obtained for the northern part of the profiles (Fig. 3-27 a, b, c). Plotting earthquakes epicenters on an F-map (Fig. 3-27 d) indicates high epicenters in the middle to the eastern part of this region (F-value of 0 - 0.1). This is in agreement with the local slope map and the number of faults (Fig. 3-26). In the eastern part, the number of large faults are lower than the western part. Besides, the high local slope values are rarely detectable in the eastern part. This means the eastern part may have a low stability.

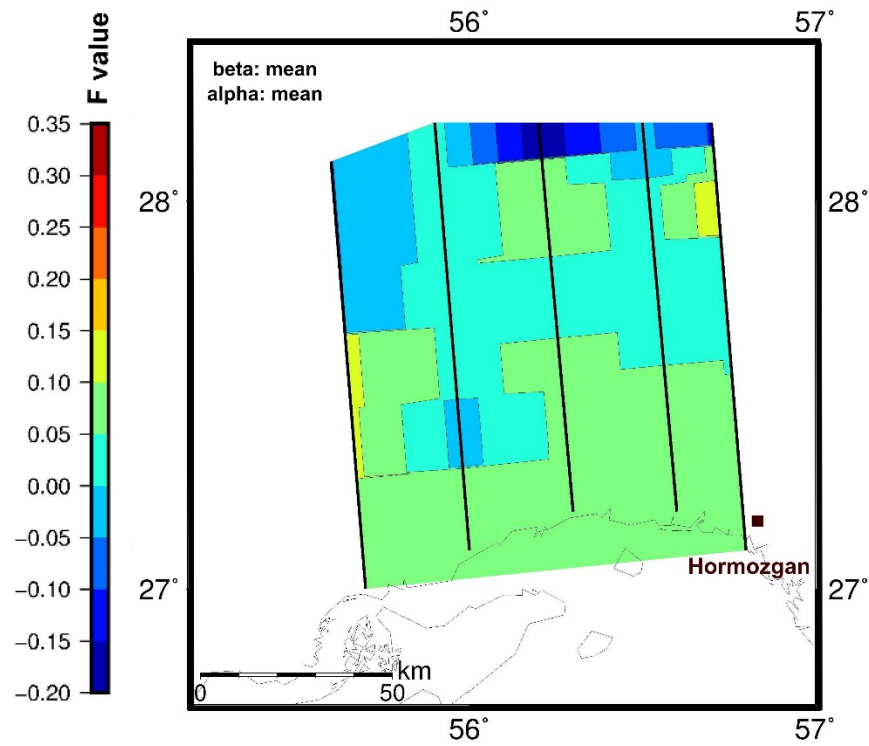
According to Hafezi and Ghafoori (2007), the studied Zagros region experienced a lower number of landslides (less than 5). However, complete data with coordinates and size of the landslides are not available. Thus landslides are not shown on the F-maps and are not correlated with the F-values.



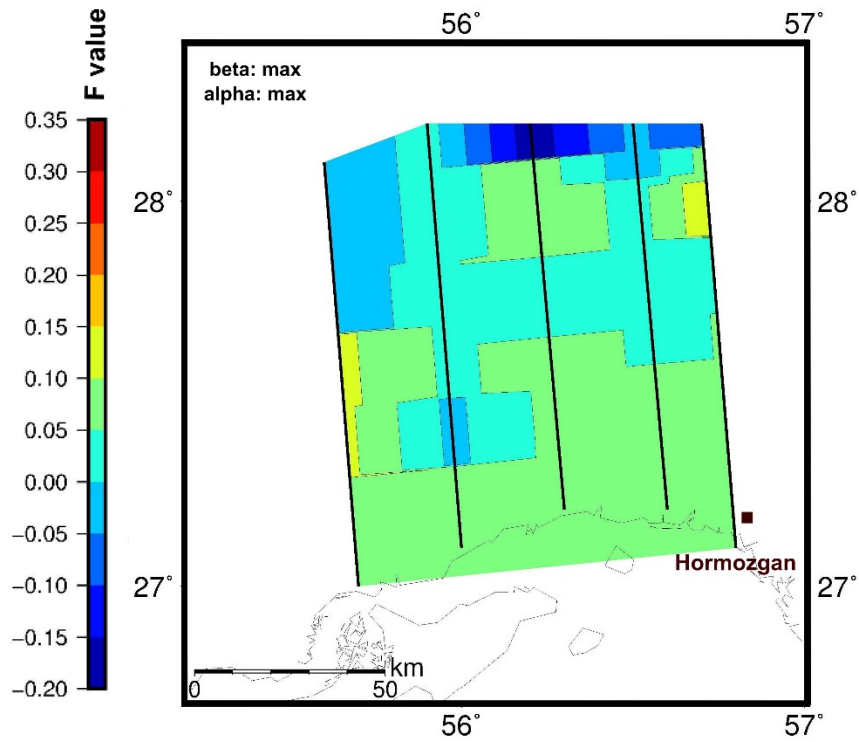
a)



b)



c)



d)

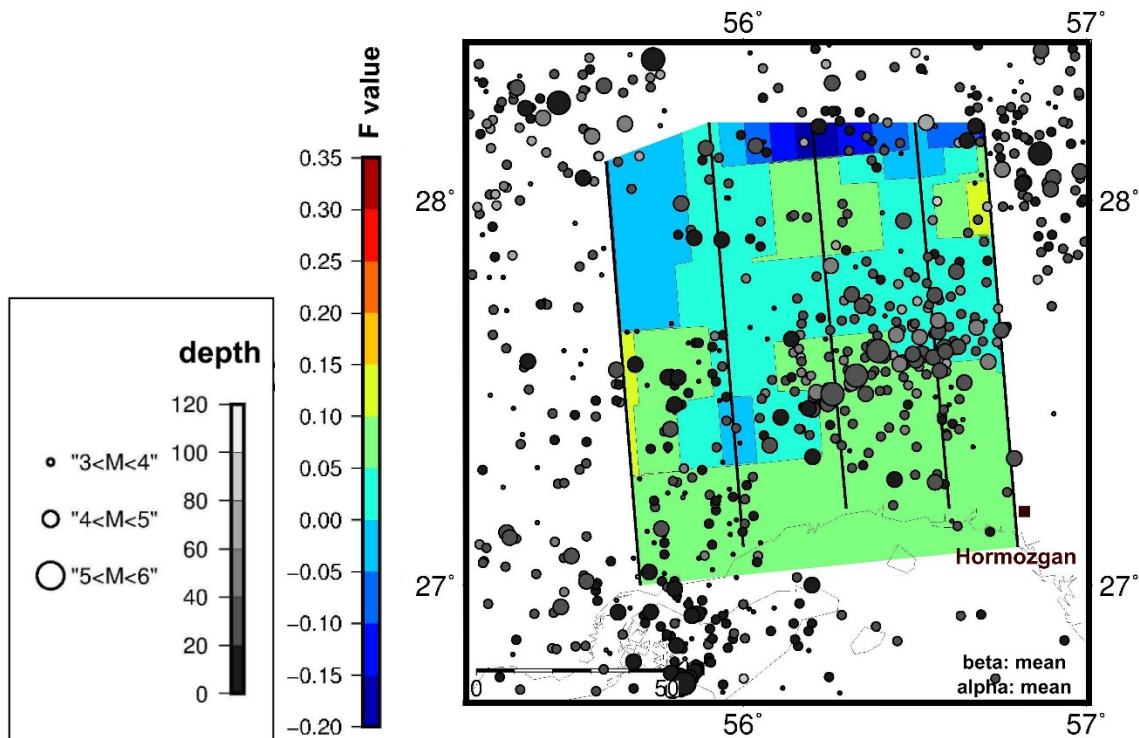


**Figure 3-27.** Map of F-values in the Zagros region. Higher F-values in the south, based on mean alpha and minimum beta values (a), mean alpha and mean beta values (b), mean alpha and maximum beta values (c), mean alpha and mean beta with earthquakes (NEIC Catalogue, 1900- 31.05.2015) (d). See also Fig. 3-13 for the location of maps.

### 3.7.4 Himalayas

The studied part of the Himalayas, is located within the pro-wedge. Thrust faults dominate in this region and generally show an E-W trend and are equally frequent all over the study area. Only one normal fault with the same trend was located in to the north of the studied region. This means that the thrust faults dominate in the region (Fig. 3-28). Besides, higher local F-values are obvious in the middle part of the region in a trend of east-west (Fig. 3-28). It can be assumed that in the region of thrust faults, i.e in the middle part as a result of a compressional regime and higher local slope, higher friction along these faults may exist. The lithological map of the region shows a relatively stronger northern part in comparison to the southern part (Fig. 3-15). There are some landslide areas in this region (Ives and Messerli, 1989), but a regional map, which shows the coordinates and size of them is not available. NOAA images and Köppen Geiger climate classification reveal an arid area for Himalayas (Kottek et al., 2006).

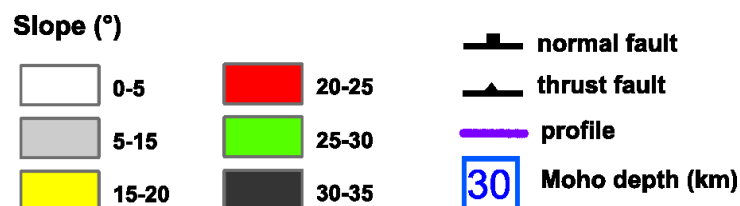
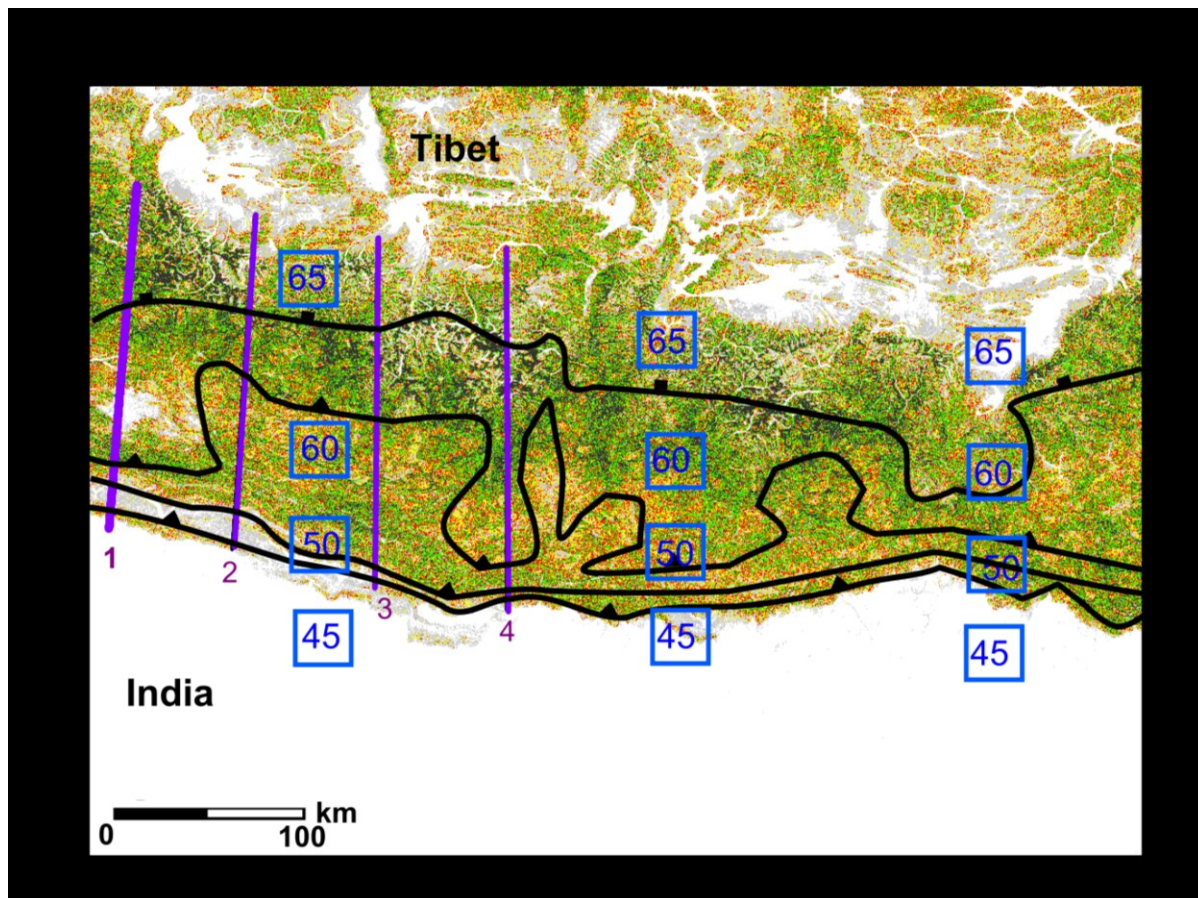
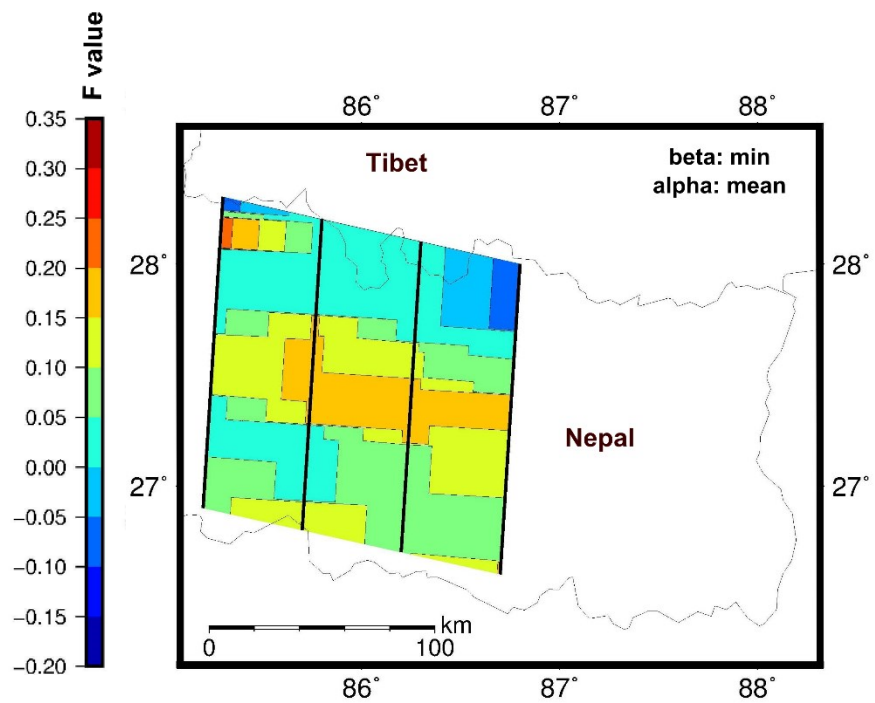


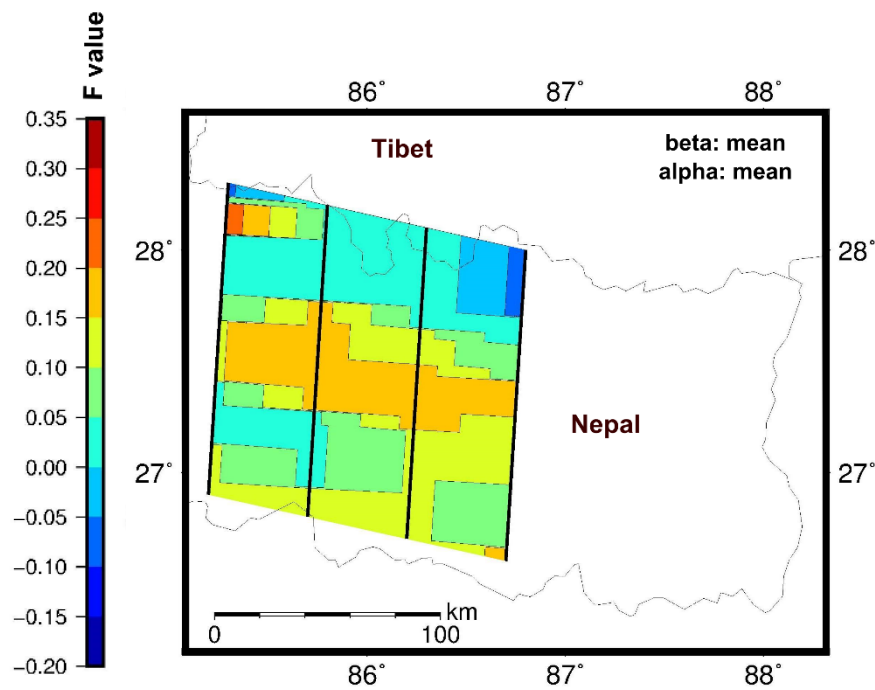
**Figure 3-28.** Local slope map of the Himalayan region. Slope data from SRTM 90, Faults: Lavé and Auouac (2000), Zhao et al., 1993; Yin et al, (2010), Moho: Zhao et al. (1993).

According to the obtained F-maps, a variation of F-values from -0.05 up to 0.25 are observable in the Himalayas. In the middle part of the region, in a NW-SE trend, the highest F-values are obvious. This indicates that these locations may have a higher basal friction ( $\mu_b$ ) and consequently may have a higher wedge stability. The lowest F-value is visible in two sections of the northern part. These negative values are a result of negative surface slope in equation (3). F-values between 0.05 and 0.20 dominate in the region (Fig. 3-29 a, b, c). The region has experienced many earthquakes (Fig. 3-29 d). Plotting earthquake epicenters on an F-map indicates that at the higher F-value locations, epicenters are rarely detectable (Fig. 3-29 d). Earthquakes concentrate almost in the northern part of the region, which shows lower F-values. For this orogen, no specific differences have been detected within the region. It can be assumed that the entire Himalaya region may have a same wedge stability.

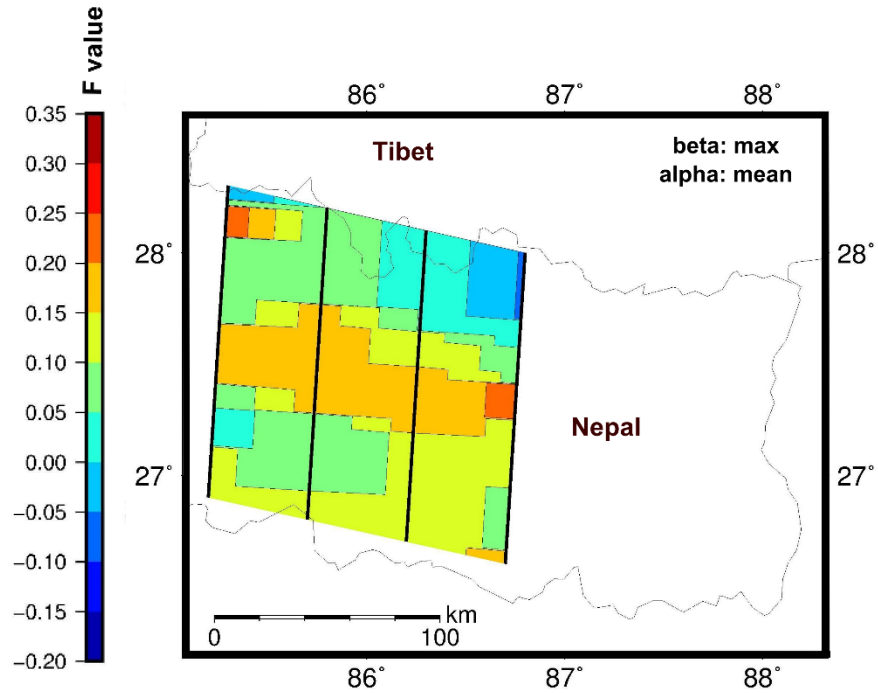
a)



b)



c)



d)

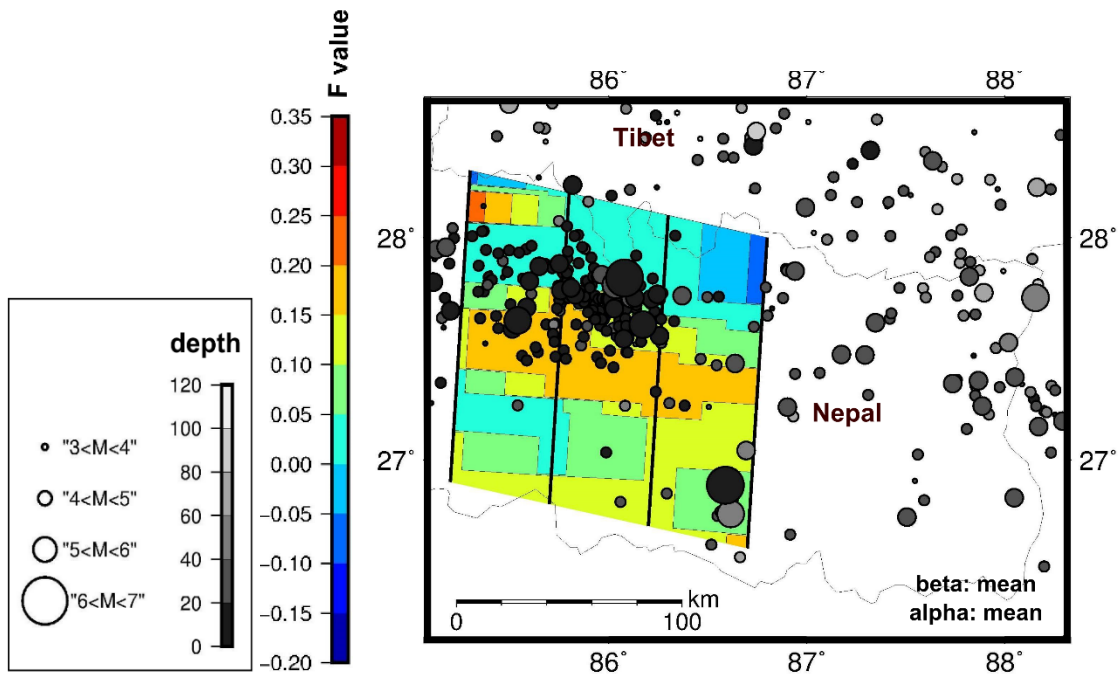


**Figure 3-29.** Map of F-values in the Himalayan region. Higher F-values in a trend of W-E and also in the south, based on mean alpha and mean beta values (a), mean alpha and minimum beta values (b), mean alpha and minimum beta values (c), mean alpha and mean beta with earthquakes (NEIC Catalogue, 1900- 31.05.2015) (d). See also Fig. 3-15 for the location of maps.



### 3.7.5 Apennines

Faults are located with a trend of NW-SE the entire region to the NE. A variation of local slope values between 20° and 30° is observed in the region and values higher than 30° are limited to small areas in some places, mostly in the east (Fig. 3-30). These may indicate to a relatively higher friction in the eastern part. The lithological map indicates that the southern part of this region is mechanically stronger than the northern part (Fig. 3-17). NOAA images and the Köppen Geiger climate classification reveal a wet climate for the region (Kottek et al., 2006).

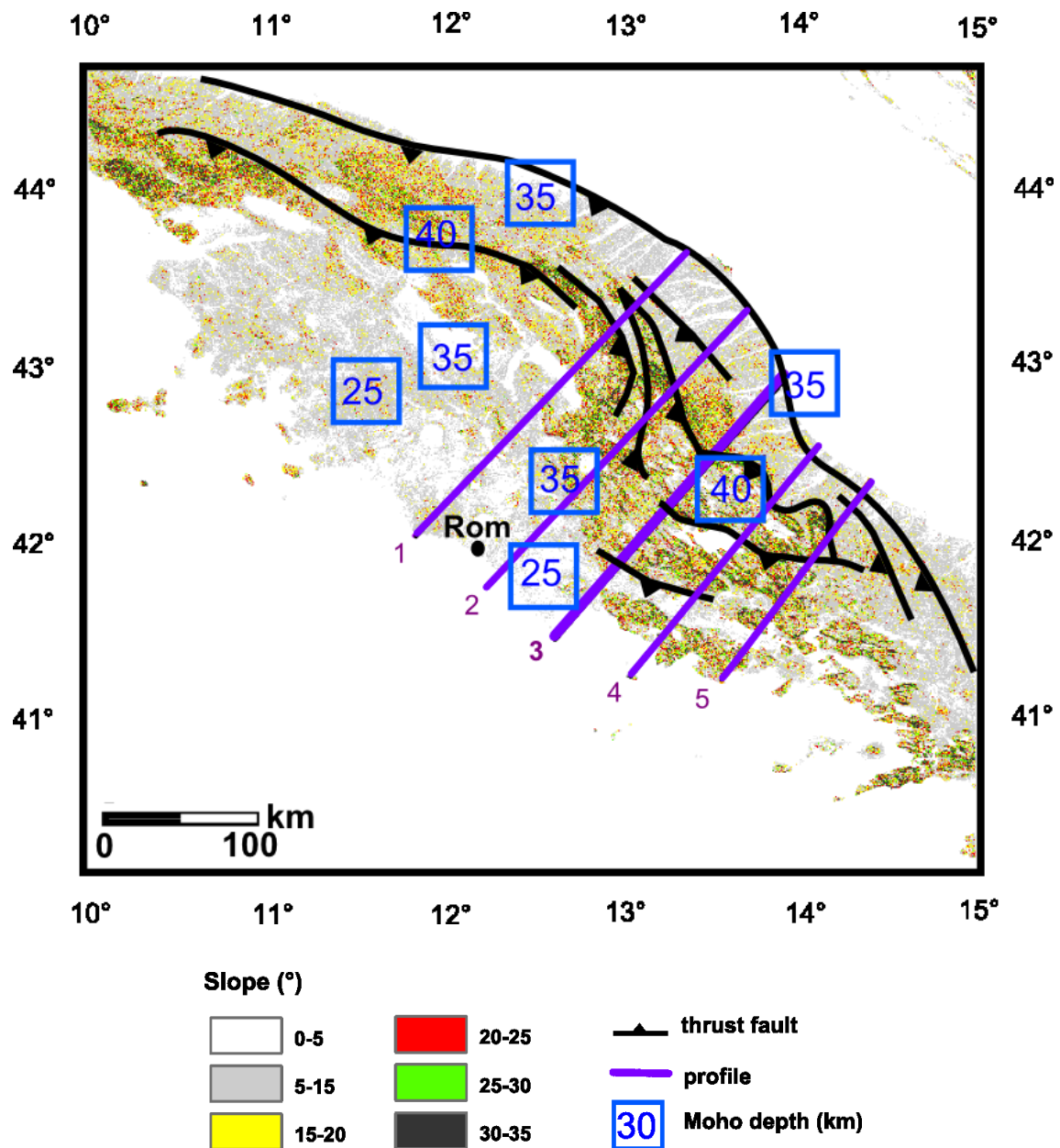


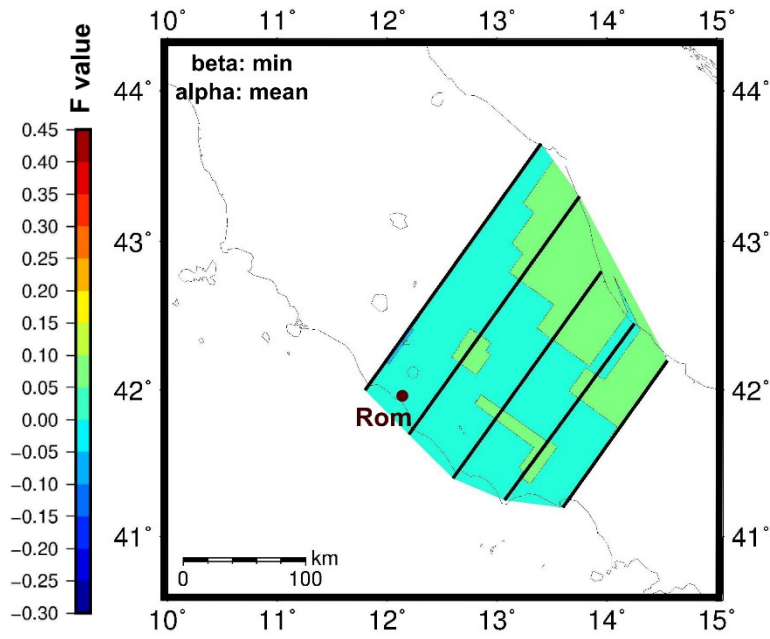
**Figure 3-30.** Local slope map of the Apennines region. Slope data from SRTM 90 m, Faults: Tozer et al. (2002), Calamita et al. (2014); Moho: Piana and Amato (2009).

According to the obtained F-maps, a variation of the F-value from 0 to 0.10 is observed for the Apennines region. The northern flank shows maximum F-values. In contrast, the southern flank shows minimum F-values (Fig. 3-31 a, b, c). This indicates that the north of the region may have a higher basal friction ( $\mu_b$ ) and consequently may have a higher stability. This is comparable with the northern Alborz region, which shows a higher wedge stability. F-values between 0 and 0.05 dominate the Apennines region (Fig. 3-31 a, b, c). Plotting earthquake epicentres on an F-map shows that in the north of the region, some epicenters are detectable, but they are numerous in a NW-SE trend in the middle part of the region. The northeast of this region has higher F-values, but a lower number of earthquakes. It is compatible with the faults number and the local slope values (Fig. 3-30), which may indicate more stability for the northeastern part, i.e. for the retro-wedge of the orogen (Fig. 3-29 d). The entire Apennines is in a landslide hazard region (Guzzetti et al., 2005), but a general map with coordinates of the landslides was not available. Thus, they are not plotted on the F-maps.

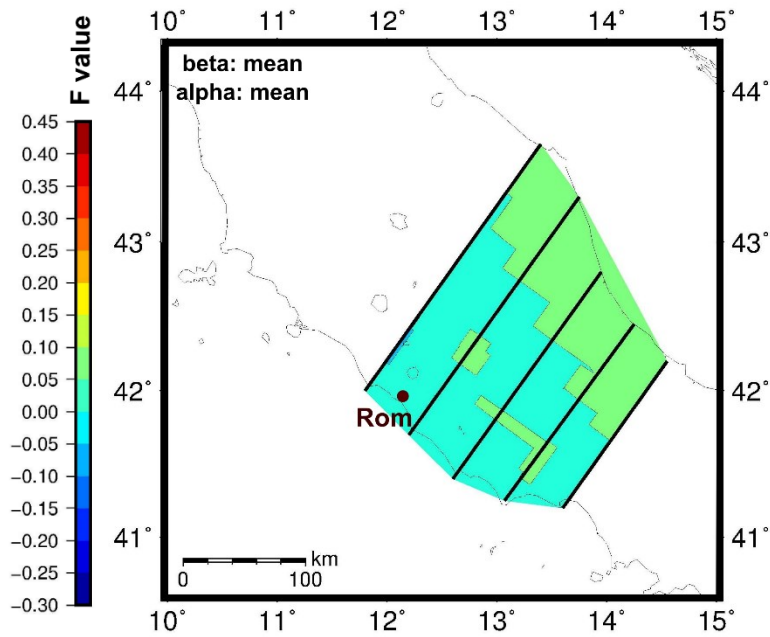
In the next sections, I compare the wedge stability of all of the the AHB orogens from different viewpoints.



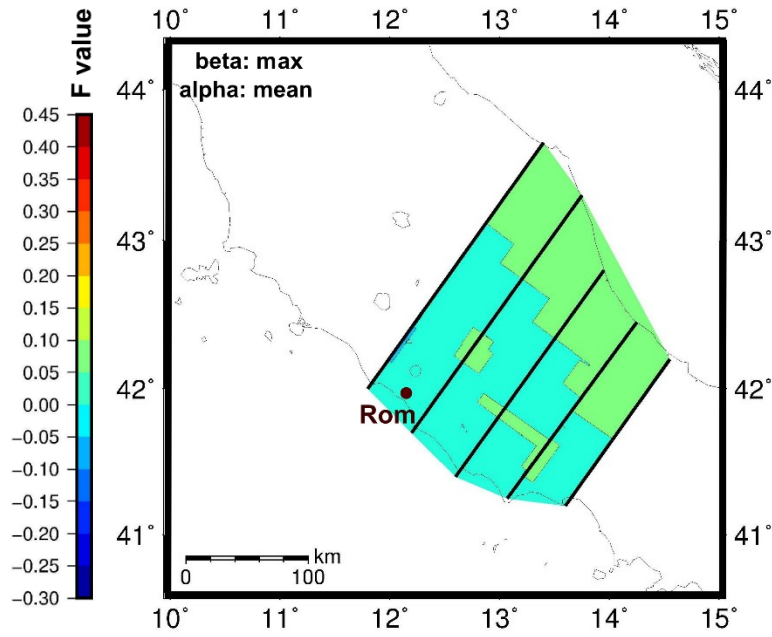
a)



b)



c)



d)

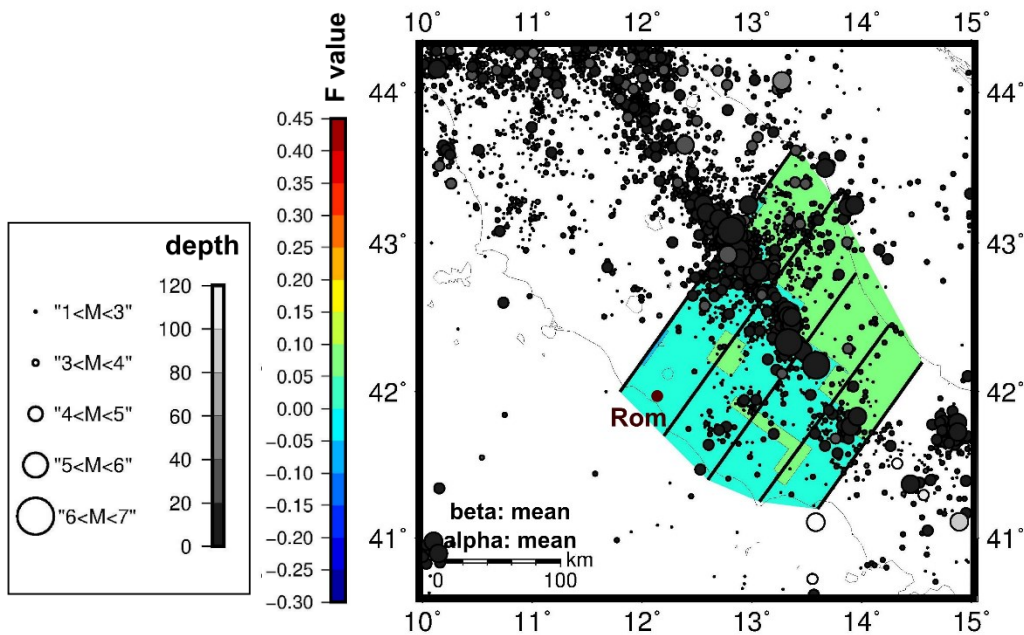


**Figure 3-31.** Map of F-values in the Apennines region. Higher F-values in NE based on mean alpha and mean beta values (a), mean alpha and minimum beta values (b), mean alpha and minimum beta values (c), mean alpha and mean beta with earthquakes (NEIC Catalogue, 1900-31.05.2015) (d).

**Table 3-2.** Comparison of the AHB orogens (black: finding from literature review; blue: result of this research).

	Alborz	Caucasus	Zagros	Himalayas	Apennines	Alps
<b>Local slope</b>	0-35° east: 5-25°/West: 25-35°, in PW slope value bigger than 30° is more than RW (Fig. 3-20 b).	0-35° same distribution for east and west in PW slope value bigger than 30° is more than RW (Fig. 3-22 b).	0-35° slope 0-5° dominate the area, slope 25°-35° in west and center is higher than E and NE (Fig. 3-26).	0-45° slope 25°-45° in west and center of orogen is higher, Center and south is steeper than north (Fig. 3-28).	0-35° 0-15° dominate the area, slope 15°-35° in the area of profiles is higher (Fig. 3-30).	0-5° (von Hagke et al., 2014)
<b>Regional slope (mean)</b>	0 - 8° in some profile RW is steeper than PW, in some profile invers (Fig. 3-19, 6-1).	0 - 7° in some profile PW is steeper than RW, but in some of those are invers (Fig. 3-19 a, 6-2).	-6°-3.5° in some profile more segment (Fig. 3-19 b, 6-3).	-2.7°- 6° in some profile more segment (Fig. 3-19 c, 6-4).	0°-2.5° more segmentation in PW (Fig. 3-19 d, 6-5).	
<b>Basal detachment (mean)</b>	Pw: 2.7° ± 1° Rw: 2° ± 1.8° (Fig. 3-7)	Pw: 2.2° ± 1.6° Rw: 3.3° ± 1.8° (Fig. 3-12)	PW: 1.1° ± 1.2° (Fig. 3-14)	PW: 1.7° ± 0.6° (Fig. 3-16)	Pw: 0° Rw: 1.4° ± 1.5° (Fig. 3-18)	2.9° (von Hagke et al., 2014)
<b>Lithology</b>	east and west almost same hardness. S to N weak to strong units (Fig. 3-5).	center of orogen is stronger than north and south, same hardness for PW and RW (Fig. 3-11).	almost same, but sometimes in north is stronger than south. West is stronger than east (Fig. 3-13).	south to north: weak to strong (Fig. 3-15).	south to north: weak to strong (Fig. 3-17).	south to north: strong to weak
<b>Moho</b>	30-60 km (Fig. 2-8; Motavalli-Anb. et al., 2013)	40-60 km (Fig. 3-22b Eppelbaum&Khesi n, 2012)	45-55 km (Fig. 3-26; e.g. Manaman et a., 2011)	55-65 km (Fig. 3-28; Zaho et al., 1993)	25-40 km (Fig. 3-30; Piana&Amato, 2009)	30-45 km (Molinari et al., 2012)
<b>Climate</b>	east & west: same PW/RW: arid/wet	east & west: same Pw & RW: wet	arid	arid	Pw & RW: wet	Pw & RW: wet
<b>F</b>	0 - 0.35 (Fig. 3-21)	0 - 0.30 (Fig. 3-25)	-0.20 - 0.15 (Fig. 3-27)	-0.05 - 0.30 (Fig. 3-29)	0 - 0.10 (Fig. 3-31)	0 - 0.5 (von Hagke et al., 2014)
<b>General wedge state</b>	critical-stable (Fig. 3-32)	critical-stable (Fig. 3-32)	critical-stable (Fig. 3-32)	critical-stable (Fig. 3-32)	critical-stable (Fig. 3-32)	critical (von Hagke et al., 2014)
<b>Landslide</b>	in PW and RW, but some landslides in RW (Fig. 1-4).	Pw & RW in the profile area have landslides (Fig. 3-24).	in southern Iran they have Concentration in the profile region,	entire Himalayas, but concentration of high landslides in south	entire Apennines, same distribution in the region of profiles	
<b>Shortening rate (mm/yr)</b>	8±2 (Vernant et al., 2004 a,b)	14±2 (Vernant et al., 2004 a, b)	9±2 (Vernant et al., 2004 a,b)	19±2.5 (Bettinelli et al., 2006)	8.85±0.61 (Basili & Barba, 2007)	0,5 (Pfiffner, 2009) or up to 1,7 (Delacou & Champagnac 2004).
<b>Earthquake (according to USGS)</b>	in RW and PW, but in the profile area concentration in RW. Max depth: 60km. Max mag: M>7, (Fig. 3-21 d)	in RW and PW, but concentration in RW Max depth: 60km. Max mag: M>7 (Fig. 3-25 d)	entire Zagros, (it seems) a higher concentration in the center-east Max depth: 150km Max mag: M>7 (Fig 3-27 d)	entire Himalayas, with higher concentration in the center. Max depth: 150km Max mag: M>7 (3-29 d)	entire Apennines, Max depth: 150km (in profiles area). Max depth entire Apennines: 500km Max mag: M>7 (Fig. 3-31 d)	Max. depth: 50km  Max mag: M<7

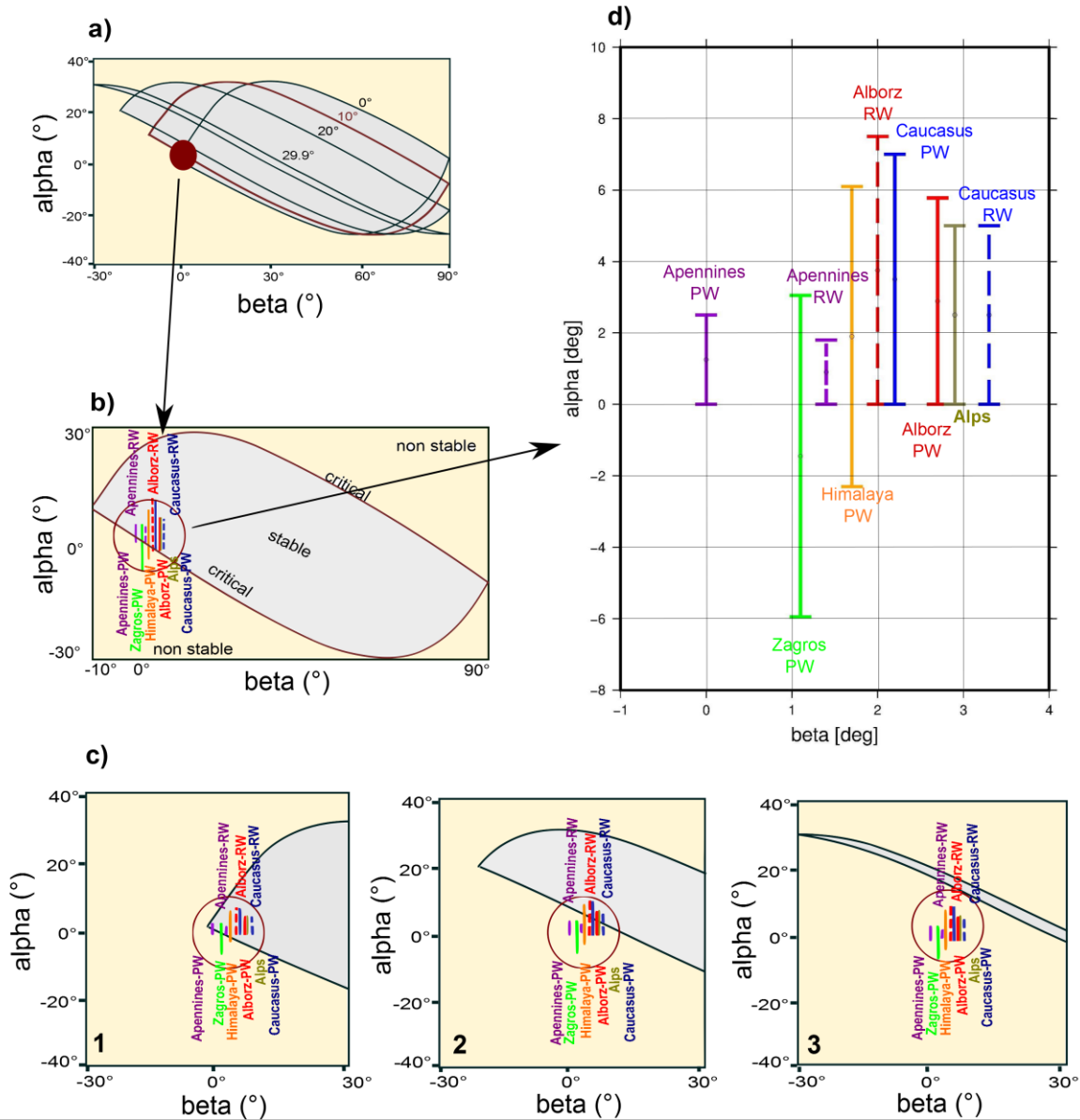


**Figure 3-32.** Stability diagram. **a)** State of wedges for the orogens of the AHB based on different  $\phi_b$  (angles of basal friction) value; **b)** State of wedges if  $\lambda = \lambda_b = 0$ ,  $\phi = 30^\circ$ ,  $\phi_b = 10^\circ$ , after Dahlen (1984); **c)** state of wedges based on different basal friction angles ( $\phi_b$ ): 1-  $\phi_b = 0^\circ$ ; 2-  $\phi_b = 20^\circ$ ; 3-  $\phi_b = 30^\circ$ . **d)** Zooming of minimum and maximum  $\alpha$  and  $\beta$  values.  $\alpha$  and  $\beta$  values of the Alps are from the study of von Hagke et al. (2014). See also Fig. 1-1 for the location of each orogen.

## 3.8 Discussion

### 3.8.1 Mechanical state of orogens based on critical taper analysis

Based on alpha (approximate surface slope) and beta (approximate basal dip) for the pro- and retro-wedge, respectively F-values for each orogen have been estimated. According to these values, among the AHB orogens, the maximum average alpha was obtained to the Alborz and Caucasus region ( $8^\circ$ ), whereas Zagros had the minimum alpha value ( $-6^\circ$ ). The Zagros region indicated relatively higher negative values for alpha (Table 3-2). In southern Iran, i.e. Zagros and its surroundings, salt plays an important role for the structural development of the orogen (e.g. Kent, 1979; Talbot and Jarvis, 1984; Jahani et al., 2009) and could affect the surface slope, thus the negative values for alpha could be a result of existence of the salt zones. The beta values of the AHB orogens vary from  $0^\circ$  to  $3.3^\circ$  (Table 3-2). The maximum and minimum beta values obtained in this study were for the retro-wedge of the Caucasus region ( $\sim 3.3^\circ$ ) and the pro-wedge of the Apennines region ( $0^\circ$ ), respectively (Fig. 3-32 d).

As mentioned, with the help of the alpha and beta values and equation (3), an estimation of the wedge state for each orogen is possible (Fig. 3-32 a). For this purpose, alpha and beta are used in equation (3) to illustrate the stability diagram suggested by Dahlen (1984). By varying alpha and beta, the angle of friction ( $\phi_b$ ) will be also varied. However, in this diagram, almost all of the AHB orogens are in the same state, i.e. in a critical-stable state (Fig. 3-32 b).

If we consider  $\phi_b$  in a range of  $0^\circ$  to  $10^\circ$ , then some orogens are located in the stable region and some of them in the unstable (under-critical) region and also on the border between the stable and unstable state, i.e. they may be critical. With  $\phi_b$  of more than  $10^\circ$  (e.g.  $20^\circ$ ), the orogens are located mostly in the non-stable part. If  $\phi_b=30^\circ$ , then all the orogens are located in the non-stable region (Fig. 3-32 c).

Taking everything together,  $\phi_b$  in a range of  $0^\circ$  to  $10^\circ$  is realistic for the AHB orogens and thus in Fig. 3-32 b, c, the obtained curves of  $\phi_b$  is similar for all orogens. If we consider  $\phi_b$  to be  $10^\circ$ , then it can be suggested that the Alborz and Caucasus region, especially the pro-wedge of the Alborz and the retro-wedge of the Caucasus are more stable than the other orogens of the AHB. It should be noted that the data of the Alps are based on the study of von Hagke et al. (2014). In their results, beta is  $2.9^\circ$ , which only addressed the Alps pro-wedge (Fig. 3-32 a, b, d).

### 3.8.2. Wedge state of orogens based on F-value, lithology, slope and climate

In this part, I apply my findings to obtain the natural wedge state, i.e. F-values correlated with some natural factors. These factors are lithology, local slope, faults, rivers, precipitation and climate. All of these parameters help to better identify the mechanical state of wedges. For example, the F-map illustrates basal friction ( $\mu_b$ , e.g. von Hagke et al., 2014), which is impossible to measure in nature. Faults can also be an indicator for friction. Slope map give hints to local wedge stability. All of these parameters should be compared with the F-values. This also helps to show a local wedge state. For this goal, three classes can be represented (Fig. 3-33):

- a) Situation of the pro- and retro-wedge based on only alpha-beta values.
- b) Situation of the pro- and retro-wedge based on climate and lithology.
- c) Situation of the pro- and retro-wedge based on local slope and faults.

The first classification (a) has been explained already earlier (Fig. 3-32). It is based on the alpha values, which have been estimated from topographic profiles (SRTM data), and also beta values, which have been estimated from geological profiles. According to this classification, all of the orogens are in a critical-stable state. This situation does not seem to depend on the geographic location, because from the east to the west of the AHB no special systematic change is observable (Fig. 3-33 a).

The second classification (b) is based on lithology and climate type (Fig. 3-33 b). As mentioned, wet climate and weak lithology lead to lower stability and in contrast, arid climate and strong lithology lead to higher stability. Lithology or material of an orogen relates to the friction of the orogen (e.g. Lohrman et al., 2003), i.e a “hard” lithology may have a higher coefficient of friction than a “soft” lithology. Wet climate with precipitation and humidity can reduce the friction of an orogen (e.g. Dahlen, 1984). In contrast, an arid climate can lead to higher friction. Friction plays a crucial role in controlling thrust faulting and wedge stability (e.g. Dahlen et al., 1984).

Classification (b) indicates that the northern Alborz (retro-wedge) with a strong lithology and wet climate may be more stable than the southern side (pro-wedge). This result is comparable with the F-maps of the Alborz region. These maps and also the distribution of earthquakes and landslides (Fig. 1-3, 1-4 and 3-21) indicate that the northern Alborz is more stable than its southern side.

Based on classification (b), the southern Apennines (pro-wedge) has a relatively “harder” lithology and could be more stable than its northern side (retro-wedge). According to the geological map illustrated by Rosenbaum et al. (2002) it seems that the southern part consists of a relatively stronger lithology. Earthquakes (Fig. 3-31 d) are more numerous in the center and NE part of this region. This is compatible with the F-maps. F-values do not change very much in the entire Apennines, but in the retro-wedge, F-values are relatively higher and indicate that the retro-wedge of Apennines can be more stable than the pro-wedge.

According to the second classification (b), the northern Alps (pro-wedge) has a wet climate and weak lithology, thus making it potentially weaker than the southern side (retro-wedge), which has a wet climate and strong lithology. It is interesting to note that all of these orogens have a N-S difference in lithology. However, in this classification, because of the lack of regional data for the Zagros, the Caucasus and the Himalayas, the interpretation of the wedge state is difficult. Altogether, this classification shows a critical-stable wedge state for all of the orogens.

The third classification (c) is based on fault distribution and local slope. Faults can be considered as an indicator of internal deformation and also movement along two walls. Besides, by means of local slope maps we can have a view of general the F-values. As mentioned, F-value is an equivalent of basal friction ( $\mu_b$ ). Hence, according to the classification (c), the entire Alborz is not similar. Based on faults and the local slope map, it can be demonstrated that the western Alborz may have a relatively higher stability than its eastern part (Fig. 3-33 c).

This wedge state is valid also for the Zagros region. According to the local slope map and fault distribution (Fig. 3-26), eastern Zagros is more stable than western Zagros. This is confirmed by the F-maps of this region (Fig. 3-27). Variation of lithology and climate is difficult to distinguish within the area. For the Apennines region, based on local slope maps and fault distribution (Fig. 3-30), it can be suggested that the eastern part has a relatively higher stability than the western part. This is confirmed with the F-values (Fig. 3-31), but lithology data indicated that the pro-wedge has a strong lithology and thus may be more stable (Fig. 3-33 b).

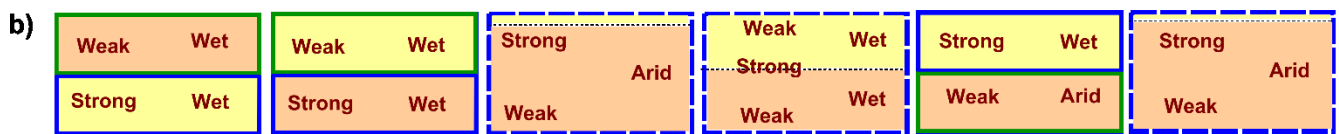
Classification (c) also reveals a critical-stable state for all of the orogens. There is no relation between geographic locations (west or east orientation) and the wedge state in the entire AHB. This may be also valid within Iran, because the Alborz and the Zagros show the same east-west differences of local wedge state. As mentioned, for the Alps, a critical state was obtained by von Hagke et al. (2014). For the Caucasus and the Himalayas region, because of unclear data, to determine the local wedge state is not possible, but it can be assumed that these regions are similar to the other AHB orogens an equal mechanical state (critical-stable) dominates.

WEST ————— EAST

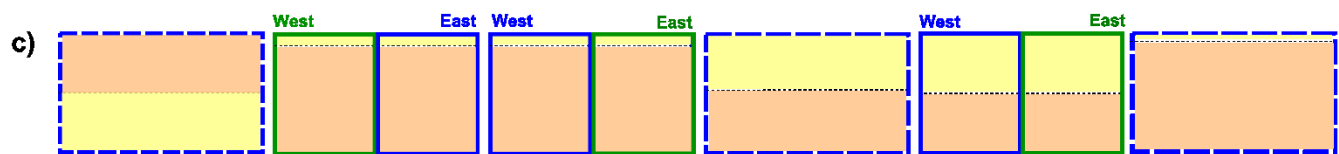
**Classification (a)** (based on alpha and beta values)



**Classification (b)** (based on lithology and climate type)



**Classification (c)** (based on local slope and faults)



———— critical-stable    ——— critical    RW    PW

**Figure 3-33.** Local wedge state. Situation of pro- and retro-wedge based on alpha-beta values (a) as well as natural factors such as lithology and climate (b). Situation of pro- and retro-wedge according to the local slope and fault distribution (c). Rectangulars with dashed line are regions with poor or unclear data for local wedge state estimation.

With the help of these three classifications, a comparison of the wedge state of the AHB orogens based on all of the studied factors is possible. Additionally, with the help of the suggested classifications, a local wedge state of the orogens can be determined (final classification, Fig. 3-34 a).

As mentioned, according to the stability diagram (Fig. 3-32), all of the AHB orogens are in a critical-stable state. The Alborz region, based on classification (b), has a more stable northern side or retro-wedge, whereas based on classification (c), its western part is more stable than the eastern part. If these data can be correlated, then it can be suggested that the Alborz region is in a critical-stable situation, but the pro-wedge of the eastern part is mostly in a critical state. For this location, the generation of new hazard (earthquakes and landslides) regions and also the reactivation of old hazard regions could be expected



more likely than for other regions of the Alborz, because friction seems to be lower here. This is comparable with the F-maps (Fig. 3-21) and nature. According to Fig. 3-21 d, the entire Alborz experiences earthquakes and landslides but in critical locations, their frequency and magnitude are much higher. In other words, these high geo-hazard may be a result of the critical state of the wedge (Fig. 3-34 a, b).

The Apennines region, based on the classification (**b**), has a more stable pro-wedge (the southern part), but according to the classification (**c**) has a more stable western part. By correlating of these data, it can be suggested that this orogen is also in a critical-stable situation, but the retro-wedge of the western part has a relatively more critical state and in this location, we can expect more geo-hazards than in other locations (Fig. 3-34 a).

The Zagros region, based on the classification (**c**), has a more stable western part, which is compatible with the F-maps (Fig. 3-27) and thus in the eastern part, more geo-hazards can be expected than in the western part (Fig. 3-34 b). In other orogens, such as the Caucasus, the Himalayas and the Alps no difference within the regions has been detected. Thus, about the mechanical situation of these orogens, only based on alpha and beta can be suggested that they are in a critical-stable state, whereas the local state of orogens is difficult to assess.

According to the all of the mentioned data, classifications, and their correlation with nature, for the study area (the Alborz region), it can be suggested that this region is in a critical-stable state, but southeastern Alborz may be in a critical state. Therefore, the entire Alborz experienced geohazard (earthquakes and landslides), but most earthquakes and landslides are occurring in the southeastern part. Furthermore, an earthquake with magnitude higher than 7 has been observed here, which may emphasize the difference of this part compared to other parts of the Alborz orogen (Fig. 3-34 b). Hence, the mechanical wedge state obtained from the taper analysis, the compiled data of lithology, climate, tectonics, and classification is compatible with the natural mechanical wedge state and geo-hazard in the region.

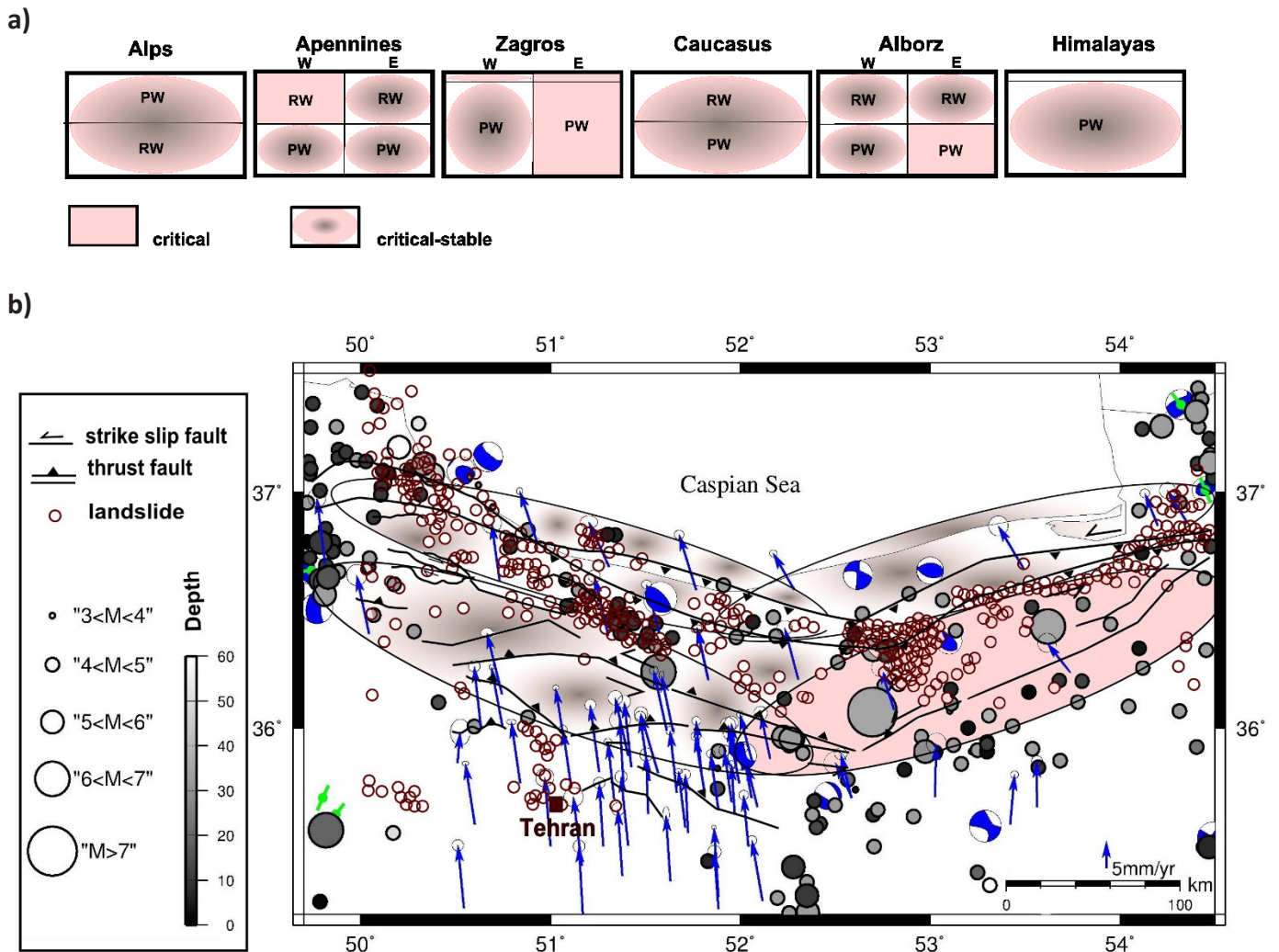


**Figure 3-34.** Local wedge state based on final correlation. **a)** Final classification, situation of the pro- and retro-wedge based on alpha-beta values as well as all natural factors together, **b)** Comparison of the local orogenic state with the Alborz region.

### 3.8.3 Comparison with analog experiments

The results of laboratory sandbox experiments indicate that parameters, such as erosion can affect the shape and size of a wedge. Besides, erosion on one part of wedge, e.g. the pro-wedge may affect the other part of a bivergent orogen (retro-wedge, Hoth et al., 2008). More specifically, pro- and retro-wedge erosion retard the lateral growth of the pro-wedge. This effect is higher for pro-wedge erosion. Similarly, pro- and retro-wedge erosion delay the lateral growth of the retro-wedge. In this case, the effect is stronger for retro-wedge erosion. Retro-wedge erosion increases vertical growth, whereas pro-wedge erosion significantly decreases it. Hence, every change of deformation in e.g. pro-wedge can cause of erosion in the retro-wedge and vice versa (Hoth et al., 2008).

The influence of erosion on an orogenic wedge is well confirmed from the critical taper theory (e.g. Davis et al., 1983). Erosion of a critically tapered wedge may lead to internal deformation, thus changing  $\alpha$  (surface slope) and  $\beta$  (detachment dip) by a shift of the center of the orogenic load towards the interior

of the orogen. This in turn may modify the amount and distribution of erosion. Additionally, changing the load configuration of e.g. the pro-wedge, has a direct influence on the geometry of deformation within the retro-wedge and the retroforeland basin. With the help of this concept the Pyrenean Mountain belt (Spanish-France) has been interpreted as a natural observation (Hoth et al., 2008). This can be applied for the studies region (the Alborz orogen) too.

In the Alborz region, erosion on the southern flank is higher than on the northern flank (Fig. 3-6 b; Rezaeian, 2008), i.e. the pro-wedge erosion is higher than the retro-wedge erosion. The retro-wedge area in the western Alborz is more narrow than the pro-wedge area. Besides, local slopes higher than 30° are visible on the southern flank of the western Alborz (Fig. 3-20 b). The shape and deformation in the retro-wedge can be caused due to the erosion of the pro-wedge. This could also change fault kinematics in the retro-wedge. Hoth et al. (2008) demonstrated that the impact of pro-wedge erosion is most dominant within the pro-wedge but also modifies the shape and size of retro-wedge, which in turn changes the geometry and propagation velocity of retro-foreland basin and vice versa.

Some authors (e.g. Axen et al., 2001; Jackson et al., 2002; Allen et al., 2003; Ritz et al., 2006; Ballato et al., 2008; Hollingsworth et al., 2010) considered a regional change in kinematics during the Neogene for the Alborz region. Additionally, Stocklin (1974) and Guest et al. (2006 a, b) suggested that in the northern part of the Alborz faults are smaller and less active than in the southern part. If we compare this orogen with the analog experimental results of Hoth et al. (2008) related to the erosion factor, it can be interpreted that the relatively lower fault activity in the retro-wedge of the Alborz may be due to the erosion processes of the pro-wedge, i.e. the erosion of the pro-wedge may change the shape and fault activity in the retro-wedge.

### 3.9 Conclusions

The obtained values of ' $\alpha$ ', ' $\beta$ ' and consequently 'F' values for the Alborz and Caucasus regions are almost the same. The local slope values (local alpha values) are between  $0^\circ$  and  $35^\circ$ , and the mean Alpha values of both Alborz and Caucasus orogens are between  $0^\circ$  and  $8^\circ$  in both of the orogens. Beta values of the Alborz are around  $2.7^\circ$  for the retro-wedge and  $2^\circ$  for the pro-wedge, and for the Caucasus  $2.2^\circ$  for the pro-wedge and  $3.3^\circ$  for the retro-wedge. Based on these values, F-values between 0 and  $0.35^\circ$  for the Alborz and the Caucasus regions have been estimated (Table 3-2). This similarity could be a result of the same tectonic situation (as concluded in chapter 2). These values are different in the other orogens of the AHB. This difference can also be due to the different situations, mainly with regard to tectonics, lithology and climate.

The beta values of the AHB orogens are between  $0^\circ$  and  $3.3^\circ$ . The values are higher for the retro-wedges than for the pro-wedges. The difference between the pro- and retro-wedges is between  $0.7^\circ$  and  $1.4^\circ$  for all of the orogens. This difference is  $0.7^\circ$  for the Alborz and for the Caucasus  $1.1^\circ$ . The maximum and the minimum beta values belong to the Caucasus and the Apennines, respectively (Table 3-1). These values do not depend on Moho depth. Moho is even deeper beneath the Himalayas, but this orogen does not have the highest beta values. Its beta value is almost the same as the beta values of Apennines ( $0^\circ$ - $1.4^\circ$ ), which has the shallowest Moho (Table 3-2).

The alpha values of the AHB orogens are between  $-6^\circ$  and  $8^\circ$  from the regional slope, and between  $0^\circ$  and  $45^\circ$  from the local slope. The Zagros region shows the highest negative values for alpha. These negative values could be caused as a result of the existence of the salt layers in the region, which can affect the amount of alpha. The maximum local slope can be detected in Himalayas ( $45^\circ$ ), but in the other orogens the dominant local slope is up to  $35^\circ$ . The regional slope (mean value) for the Alborz and the Caucasus is more than  $8^\circ$  and can be considered as the maximum value of the AHB (Table 3-1).

The F-values of the all AHB orogens are between 0 and 0.15. In comparison to the other orogens, the Alborz region has the maximum F-value after the Alps. It can be suggested that this region has a relatively high basal friction ( $\mu_b$ ). After that, the Caucasus and Apennines with a maximum F-value of 0.3 can be placed. It should be noted that the climate of these regions are not similar. The Alps have an F-value between 0 and 0.5 as shown by von Hagke et al. (2014).

Based on only alpha and beta values, if  $\lambda = \lambda_b = 0$ ,  $\phi = 30^\circ$ ,  $\phi_b = 10^\circ$ , it can be suggested that the AHB orogens are in a "critical-stable" state. According to the alpha-beta diagram (Fig. 3-32), the AHB is located at the border between "critical" and "stable". In this order, the Caucasus, the Alborz and the Alps are the first orogens, which are in the "stable" area. Thus, it can be suggested that the Caucasus and the Alborz are relatively more stable than the other orogens. The Himalayas and the Zagros are the last orogens, which are located mostly in the critical area. These orogens could have a relative low stability (Fig. 3-32).

Fault strength and rainfalls are two important parameters, which affect the wedge state. 'F' as fault strength or basal friction ( $\mu_b$ ) and rainfalls and humidity as basal pore fluid pressure ( $\lambda_b$ ) can be considered in nature. Besides, the effect of some factors, such as lithology, tectonics, fault distribution and climate should not be neglected. Based on all of the mentioned factors it can be suggested that although all of the AHB orogens are in a "critical-stable" situation, the pro-wedge of the eastern Alborz, pro-wedge of the eastern Zagros and retro-wedge of the western Apennines are mostly in a critical state. Therefore, in the critical state locations (pink), friction may be low, thus leading to higher geohazard (earthquakes and landslides; Fig. 3-34 a, b).

All of the AHB orogens are in a "critical-stable" state but have different behaviors in the generation or reactivation of geo-hazards, such as earthquakes. This difference depends on the effect of tectonics, lithology and climate, mainly.

## 4 SYNTHESIS AND OUTLOOK

The tectonic situation and geometry of an orogen both can cause geohazard (e.g. Berberian 1976; Ritz et al., 2006; Landgraf et al., 2009; von Hagke et al., 2014). Therefore, to better analyze geo-hazard of an active region, such as the Alborz, the relationship between the mentioned parameters (tectonics and mechanics) and geo-hazard has been studied in this research.

### 4.1 Tectonic evolution of Alborz

The study of the long-term geological Earth history of Iran showed that two similar tectonic cycles are detectable. There are several studies about the tectonic evolution (e.g. Berberian and King, 1981; Wilmsen et al., 2009; Ballato et al., 2011), but they do not focus on a long-term tectonic evolution model and the tectonic cycles. However, according to the detected tectonic cycles, two main collision phases dominated the region: Cycle 1) Collision phase between the Arabian Plate and the Iran Plate, which formed the Alborz ranges, and Cycle 2) Collision phase between the Iran Plate and the Turan Plate, which formed the Zagros ranges (Fig. 4-1).

Cycle 2 is out of the Alborz region. By focusing on cycle 1, which formed the Alborz region, it is interpreted that since the Middle Mesozoic (190 Ma), a collision phase dominated the Alborz region (e.g. Aghanabati, 2004; Wilmsen et al., 2009). Before collision, there were subduction phases in Iran, which could shape the collision phase and in other words, the collision phase can be considered as a consequence of subduction. Whereas this collision phase is after a subduction phase, it can be assumed that this collision phase is developing now (Fig.4-1). However, the mentioned collision phase and its different crustal shortening rates can be considered as the primary source of the recent fault structures (thrust and strike slip faults) of the region, which can cause the earthquakes and landslides of the Alborz region (Fig. 1-3, 1-4).

The mentioned earthquakes triggered landslides in some areas of the Alborz (e.g. Asadi and Zare, 2014). There are also landslides, which are not related to fault activity (Hafezi and Ghafoori 2007). Thus, we cannot consider only the tectonic effect for the cause of geo-hazards, but potentially also the geometry of an orogen. Geometry and slope of an orogen can affect fault activity (e.g. Lohrmann et al., 2003; Hoth et al., 2007) and geo-hazards.

The mechanical orogenic state may not have always been the same throughout the mentioned period of time, and since 190 Ma a cycle of wedge state may happen (Fig. 4-1). In an orogenic wedge during a collision phase, faults could show different behaviors, such as activation, non-activation and re-activation phases (Hoth et al., 2007). In the Alborz region, most of the faults are active currently (e.g. Berberian 1976) but the mentioned behaviour is observed by the recurrence time of earthquakes (e.g. Berberian, 1976; Ambraseys and Melville, 1982), i.e. the active faults generated several earthquakes, mostly, but they were also without seismicity in a certain period of time.

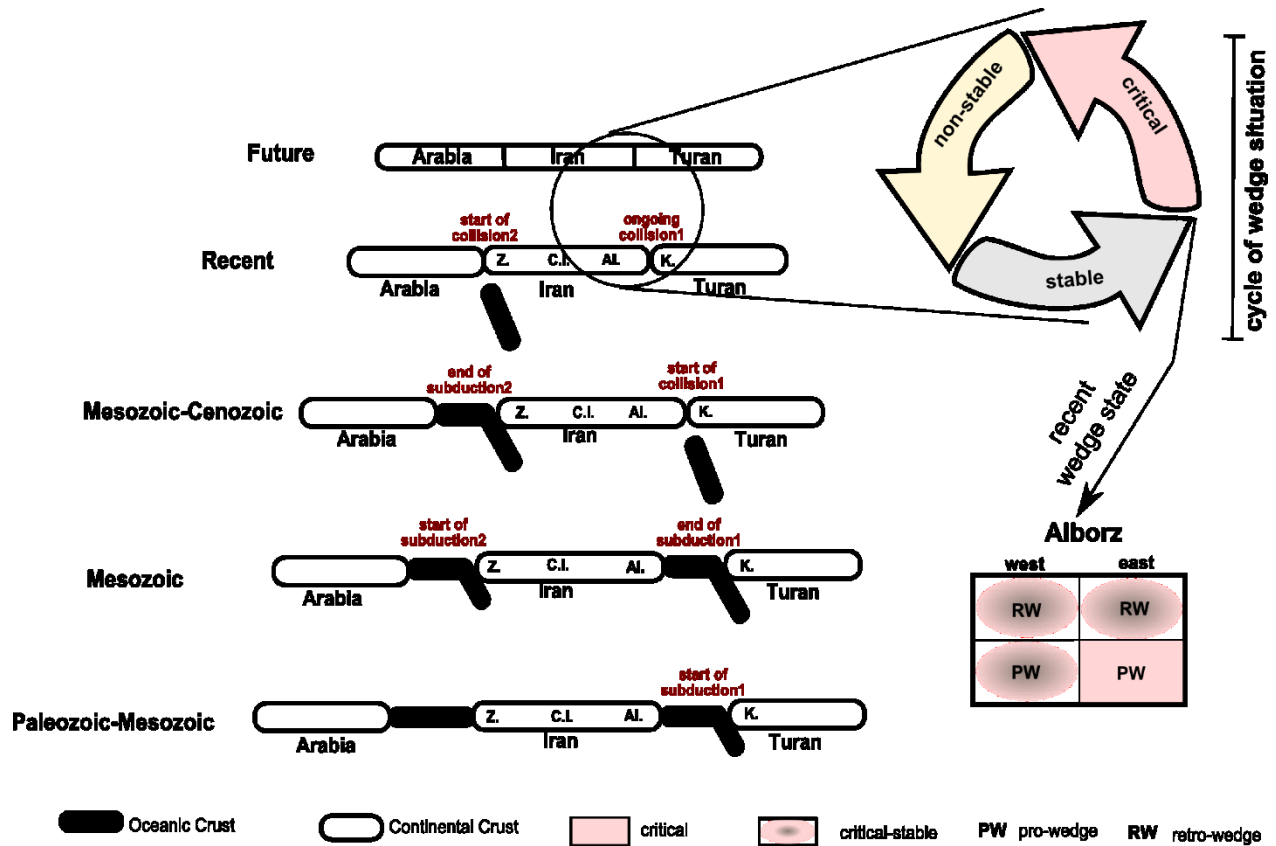


Figure 4-1. Cycle of wedge state in the collision phase of the Alborz region and the recent mechanical state of orogen.

The fault activity and geometry of orogen are parameters depending on the other and each of them can affect the other. If the geometry of an orogen controls fault activity (e.g. Hoth, 2005; Hoth et al., 2007; Lohrmann et al., 2003), the mechanical state of an orogen could be a key to understand fault activity and its relation with geo-hazards. The concept of critical taper has been studied by many authors (e.g. Davis et al., 1983; Dahlen, 1984; Lohrmann et al., 2003; Hoth, 2005; Hoth et al., 2007, 2008) to address different questions, but it was not applied to the Alborz region before this research.

To study the tectonic evolution helps to determine the effect of past events on present tectonic events and also analyse the situation of orogenic regions. Furthermore, for the recent time, different data, such as the stress regime, Moho depth, GPS and earthquakes data were compiled to determine the recent tectonics regimes (Chapter 2). According to this review, the Alborz mountains formed as a result of subduction of the Iran Plate (in the south) beneath Tutan Plate (in the north). This phase is finished and since ~190 Ma dominated a collision phase.

To complete our data set for the recent situation and also to better analyse the recent geo-hazard, I also included the present mechanical wedge state of the Alborz orogen, which can be considered as another cause of earthquakes or landslides (Chapter 3).



## 4.2 Mechanical analysis of Alborz

The southern flank of the Alborz orogen is the pro-wedge and the northern flank is the retro-wedge. Average basal dip values of the southern flank were lower than the northern flank (Fig. 3-7) and average slope values of the northern flank were almost higher than those of the southern flank (Fig. 3-10).

Basal dip ( $\beta$ ) values were estimated between 2°- 3° for the Alborz region. Surface slope ( $\alpha$ ) values of the Alborz region, were estimated between 0°- 8°. According to these results and with the help of the stability diagram of Dahlen (1984), considering internal friction of 30° and basal friction values between 0° and 10°, a “critical-stable” state has been suggested for the Alborz orogen. By increasing the angle of basal friction (up to 30°), the wedge was located in the non-stable parts (Fig. 3-32).

Based on the resulting “alpha” and “beta” and by means of the equation ( $F= 2\alpha+\beta$ ), the fault strength (F) of the orogen was also estimated. This parameter is equivalent to the effective friction ( $\mu$ ) (von Hagke et al., 2014). It amounts from 0.05 to 0.35 radian and shows that the northern Alborz has higher F- values. This means that the friction of this part is higher and thus it may be more stable than the other parts. Nevertheless, earthquakes and landslides are concentrated also in the middle and east of the Alborz (Fig. 3-21 d). Pore pressure ratio ( $\lambda$ ), especially basal pore pressure ( $\lambda_{bas}$ ), is impossible to measure in nature, because it is difficult to access the basal detachment. However, in this research pore pressure is assessed qualitatively from some factors, such as precipitation. For example, in a wet regions, the effect of pore pressure can be considered higher than in an arid region. It can affect the effective friction, the higher the pore pressure, the lower the friction.

A comparison of Alborz with its neighboring orogen (the Caucasus) showed that these two orogens experienced a similar tectonic evolution. The study of surface deformation (GPS velocity, stress regimes, and seismicity) and depth (Moho and tomography) of the region indicated that the Caucasus is like the Alborz, in the same recent tectonic situation, i.e. a collision phase dominated in the present time and led to the development of the thrust faults and earthquakes (Fig. 2-11). Additionally, from the framework of mechanics or taper analysis, they are in the same wedge state, i.e. “critical-stable” state (Fig. 3-32).

Based on the estimated “alpha” and “beta” and the stability diagram (Dahlen, 1984), the AHB orogens are located in a border region between the “critical” and the “stable” state. The Caucasus, the Alborz and the Alps plot rather in the “stable” area. Therefore, it can be suggested that the Caucasus and the Alborz are more stable than other orogens of the AHB. The Himalayas and the Zagros rather plot in the “critical” area. The latter orogens therefore might be less stable (Fig. 3-32).

Since the Middle Mesozoic collision dominated and developed in the Alborz region (e.g. Aghanabati, 2004; Wilmsen et al., 2009), hence the mechanical state of the Alborz could change from one form to other form (e.g. stable to critical state, or critical to unstable). It can be assumed that a mechanical cycle of stable-critical-unstable has been repeating since the forming of orogen, consistently (Fig. 4-1).

Therefore, a frequent reshaping of the mechanical state of the Alborz can be expected. It could repeat also in the present and future time. However, for the recent mechanical state of the Alborz orogen a critical-stable state is estimated (Fig. 4-1). This hypothesis can be applied to the Alborz region and other regions with a contractional regime, such as the AHB orogens. The velocity of this repetition could depend up on the velocity of convergence or the shortening rate of orogen. This relation should be studied in detail in future studies so as to address the following questions:

- How long does the stability/unstability phase take place in the Alborz region?
- Is it comparable with the other orogens of the AHB?
- Which parameters affect the duration of the mechanical state of an orogenic wedge?
- Are they the same in the other orogens of the AHB?

However, according to the stability diagram (Fig. 3-32 b), the Alborz is in a stable-critical state and along every profile, the surface slope values ( $\alpha$ ) decrease from the north to the south. Consequently, the values of fault strength ( $F$ ) decrease from the north to the south of each profile, but the distribution of the geo-hazards is not equal along them (Fig. 3-21 d). In the southeast of Alborz a concentration of epicenters and landslides appears. In contrast, a lower amount of earthquakes and landslides is obvious in the southwest of Alborz (Fig. 3-34). Therefore, solely  $F$  values cannot explain geo-hazard. While some natural factors, such as erosion, lithology can affect the wedge state (e.g. Hoth, 2005; Hoth et al., 2007; Molnar et al., 2007; Lohrmann et al., 2003; Willet et al., 1993; Willet, 1999), hence in addition to  $F$  values, the effect of climate, lithology, etc. on the mechanics of orogen and its impact on geo-hazard was considered.

### 4.3 Impact of the mechanical state of an orogen on geo-hazard

My critical taper analysis showed that the Alborz region as part of the AHB is in a “critical-stable” state. This state is estimated also for all of the AHB orogens, but in every region, it has different effects on the generation of geo-hazards. As mentioned, this difference can be a result of the different effects of natural parameters, such as climate or erosion (e.g. Hoth et al., 2007; Molnar et al., 2007).

Mountain topography in convergent orogens is a result of a balance between tectonics, uplift and erosion (e.g. Willet et al., 1993; Willet, 1999; Molnar et al., 2007). Climate, especially rainfall can affect pore fluid pressure and fault strength, which then control the wedge state (e.g. Dahlen, 1984). Additionally, lithology or materials of an orogen affect erodibility (e.g. Rezaiean, 2008) and friction (e.g. Lohrmann et al., 2003).

The Alborz mountains have a wet northern flank and (semi) arid southern flank. Strong rocks mostly exert low erodibility and vegetation can also decrease the effect of the erosion. Hence, erosion rates on the steep and wet northern flank of this mountain belt are suppressed by the strength of rocks at the surface, and the effects of the dense vegetation cover (Rezaiean, 2008; Fig. 3-6 b). On the southern flank, strong rocks have limited coverage, and the vegetation density is low, permitting whatever runoff occurs

to erode efficiently and in proportion to the local slope. Therefore, the pattern of erosion on the scale of the mountain belt is set by the erodibility of the substrate rather than the erosivity of the climate and its derivatives (Rezaeian 2008). Thus, lithological and climate data indicate that the Alborz region has a more stable northern flank.

With regard to geo-hazards, in the northern part, the frequency and location of landslides and earthquakes is not the same as in the southern part of Alborz. According to Fig. 3-34 b, the northern part experienced earthquakes with magnitude  $<5$ , generally. The numbers of earthquakes and landslides are different in the northeastern and northwestern part. In the northeastern part, it is lower than the in northwestern part. Moreover, the depth of earthquakes on the northwest part is lower (20 km) than that on the northeast part (more than 40 km). The magnitude of earthquakes is almostly similar to the entire northern part (Fig. 3-34).

In the southern part, especially the southeastern part, frequent landslides and earthquakes have occurred. The number and magnitude of earthquakes in this part of the Alborz are higher than in other parts of this region. Some earthquakes with magnitudes  $>5$ , two earthquakes with magnitudes  $>6$ , and  $>7$  have occurred here. The depth of hypocenters is up to 50 km. In the southwestern part, the number of landslides and earthquakes is lower than in the southeastern and northwestern part of the Alborz. Besides, according to Fig. 3-5, the number of faults in southeast Alborz is lower than in southwest Alborz, but the number of earthquakes and landslides in southeast Alborz is higher than in southwest Alborz (Fig. 3-34).

Taken together, in south Alborz the number and magnitude of earthquakes and frequency of landslides are higher than in north Alborz, but some differences are visible between east and west Alborz. Thus, east and west Alborz could be affected by other parameters, such as fault distribution and local slope.

Fault distribution and local slope may qualitatively indicate stability of a wedge. Fault strength ( $F$ ) can be used as an indicator of friction (von Hagke et al., 2014). According to von Hagke et al. (2014), by increasing the slope of orogen the  $F$ -values increase ( $F=2\alpha+\beta$ ), which refers to higher stability. The values of the local slope ( $\alpha$ ) in the western part of Alborz are higher than the eastern part and the number of faults are higher, thus it seems that the western part of Alborz is more stable than the eastern part, which would explain the lower frequency of earthquakes and landslides here (Fig. 3-34).

In eastern Alborz, the number of rivers and amount of precipitation are higher than in western Alborz. As mentioned, precipitation and rivers can lead to increase pore fluid pressure and decrease effective friction. Therefore, the pore fluid pressure is higher and effective friction is lower in the eastern part (Fig. 3-6 a). In contrast, the effect of precipitation and rivers is lower in western Alborz, consequently a higher wedge stability for western Alborz can be expected. Moreover, according to the local slope map, on the western side, local slopes of more than  $30^\circ$  are observed. But on the eastern side, the average local slope is up to maximum  $20^\circ$  (Fig. 3-20 b). Hence, as a result of the effect of precipitation and the amount of

local fault strength, the frequency of earthquakes and landslides in the eastern part is lower than the western part of Alborz.

Taken together, the recent collision phase may be responsible for the recent mechanical state of the Alborz region. However, considering natural parameters, such as lithology, climate, tectonics and fault distribution, it is suggested that although the Alborz region is in a “critical-stable” state in the recent time (Fig. 4-1), the pro-wedge of the eastern Alborz (southeast Alborz) is rather in a “critical” state and frequency of landslides and earthquakes with magnitudes >6 is higher at this region. This indicates that stability and friction here is lower than in other parts of the Alborz.

Solely critical taper analysis can not explain the geo-hazard of an orogen completely and hence additional analysis of natural parameters, such as climate, lithology, and faults is mandatory. The effects of these parameters need to be correlated. These parameters and probably other unknown parameters may change the mechanical state of a wedge. Accordingly, the more natural parameters can be evaluated, the better the mechanical state of wedge can be estimated.

According to published analogue experiments, during convergence, horizontal and vertical changes of the wedge and consequently inactivity and reactivity of faults occurred (e.g. Lohrmann et al., 2003). As mentioned, changing the geometric situation of a wedge leads to changes in fault activity. Hence, during the orogenic processes, faults may activate or reactivate (e.g. Lohrmann et al, 2003; Hoth et al., 2007). This activity can be accompanied by earthquakes and landslides (e.g. Berberian, 1976; Aghanabati, 2004; Nazari and Ritz, 2008). Thus, if changes of the mechanics of an orogenic wedge affect fault activity, fault activity or earthquakes could be also a key to assess the local wedge state.

In this regard, the detection of very small earthquakes with local networks may be suitable to identify fault activity. For this goal, long-range observation of micro seismicity is needed. Migration of epicenters during a certain period of time (e.g. 100 years) could indicate local temporal changes of the mechanical state. This means that the concentration of epicenters in a location shows fault activity and thus, migration of epicenters during a period of time can show the path of fault activities. Whereas fault activity relates to the mechanical state of an orogen, accordingly by studying microseismicity, it is possible to obtain local-temporal changes of mechanical state of orogen. This detection could also illustrate a dominant tendency of the mechanical state during the period of time (e.g. critical-stable, but rather to stable state). This parameter also helps to correlate to the other parameters (lithology, climate, etc).

Given the mentioned assumptions, the following questions can be addressed:

- Which relationship exists between the local wedge state and number, magnitude and intensity of micro-seismic activities in a certain period of time e.g. 100 year?
- Can the micro-seismic activities show the tendency of wedge state, quantitatively?

The mentioned questions should be addressed in future studies, first for the Alborz region, then for the AHB orogens.

## 5 REFERENCES

- Abbassi, A., Nasrabadi, A., Tatar, M., Yaminifard, F., Abbassi, M.R., Hatzfeld, D., Priestley, K., 2010.** Crustal velocity structure in the southern edge of the Central Alborz (Iran). *Journal of Geodynamics*, 49 (2), 68-78.
- Abrams, M.A., and Narimanov, A.A., 1997.** Geochemical evaluation of hydrocarbons and their potential sources in the western South Caspian depression, Republic of Azerbaijan. *Marine and Petroleum Geology*, 14, 451-468.
- Adamia, S.A., and Lordkipanidze, M.B., 1989.** An outline of Georgian geological structure. In: Rakus, M., Dercourt, J. & Narin, A. E. M. (eds) IGCP Project 198: Evolution of the Northern Margin of Tethys. *Mémoires de la Société Géologique de France, Nouvelle Série*, 154(II), 63-66.
- Agard, A., Omrani, J., Jolivet, L., Mouthereau, F., 2005.** Convergence history across Zagros (Iran): constraints from collisional and earlier deformation. *International Journal of Earth Sciences*, 94, 401-419, doi: 10.1007/s00531-005-0481-4.
- Aghanabati, A., (ed) 2004.** Geology of Iran, Ministry of Industry and Mines, Geological Survey of Iran, 1-650 (in Persian), available from <http://palaeontology.blogfa.com/post/17>, accessed 10.07.2012.
- Ahmadi, G., and Nowroozi, A.A., 1980.** Earthquake Risk Analysis of Iran. Annual meeting of Iranian Petroleum Institute, Tehran.
- Alavi, M., 1972.** Etude géologique de la région de Djam, Geological Survey of Iran, Report 23, 1-288.
- Alavi, M., 1994.** Tectonics of the Zagros orogenic belt of Iran: New data and interpretations, *Tectonophysics*, 229, 211-238.
- Alavi, M., 1996.** Tectonostratigraphic synthesis and structural style of the Alborz mountain system in northern Iran, *Journal of Geodynamics*, 21, 1-33, doi: 10.1016/0264-3707(95)00009-7.
- Alinaghi, A., Koulakov, I., Thybo, H., 2007.** Seismic tomographic imaging of *P*- and *S*-waves velocity perturbations in the upper mantle beneath Iran, *Geophysical Journal International*, 169, 1089-1102, doi: 10.1111/j.1365-246X.2007.03317.x.
- Allen, M.B., Jones, S., Ismail-Zadeh, A., Simmons, M., Anderson, L., 2002.** Onset of subduction as the cause of rapid Pliocene–Quaternary subsidence in the South Caspian basin, *Geology*, 30, 775-778.
- Allen, M., Ghassemi, M.R., Shahrabi, M., Qorashi, M., 2003.** Accommodation of late Cenozoic oblique shortening in the Alborz range, northern Iran, *Journal of Structural Geology*, 25, 659-672, doi: 10.1016/S0191-8141(02)00064-0.
- Allen, M., Jackson, J., Walker, R., 2004.** Late Cenozoic reorganization of the Arabia-Eurasia collision and the comparison of short-term and long-term deformation rates, *Tectonics*, 23, doi: 10.1029/2003TC001530.
- Allmann, B.P., and Shearer, P.M., 2009.** Global variations of stress drop for moderate to large earthquakes, *Journal of Geophysical Research* 114, B01310, doi: 10.1029/2008JB005821.
- Amante, C., and Eakins, B.W., 2009.** ETOPO1 1 ARC-MINUTE global relief model, National Geophysical Data Center Marine Geology and Geophysics Division Boulder, Colorado, global relief, <http://www.ngdc.noaa.gov/mgg/global/global.html>, accessed 30.06.2015.
- Ambraseys, N.N., and Melville, C.P., (eds) 1982.** A history of Persian earthquakes, Cambridge University Press, 20-213.
- Andersen, O.B., and Knudsen, P., 2009.** The DNSC08 mean sea surface and mean dynamic topography, *Journal of Geophysical Research* 114, C11, doi: 10.1029/2008JC005179, DTU Space, National Space Institute, Technical University of Denmark, global mean dynamic topography, <http://www.space.dtu.dk>, accessed 28.12.2014.
- Anells, R.N., Arthurton, R.S., Bazley, R.A., Davies, R.G., 1975.** Qazvin and Rasht; 1:250,000 scale geological quadrangle map of Iran, Geological survey of Iran.
- Anells, R.N., Arthurton, R.S., Bazley, R.A., Davis, R.G., Hamed, M.A.R., Rahimzadeh, F., 1977.** Geological map of Shakran, scale 1:100,000, GSI. Shakran sheet 6162. 1:100,000, Tehran, Geological map of Iran, Geological survey of Iran.
- Armenian second national communication 2010.** Landslides, <http://www.undp-alm.org>, accessed 28.12.2014.
- Arslanov, Kh.A., Dolukhanov, P.M., Gei, N.A., 2007.** Climate, Black Sea levels and human settlements in Caucasus Littoral 50,000–9000 BP, *Quaternary International* 167-168, 121-127.

- Asadi, Z., and Zare, M., 2014.** Estimating magnitudes of prehistoric earthquakes and seismic capability of fault from landslide data in Noor valley (central Alborz, Iran), *Natural Hazards*, 74, 445-461, doi: 10.1007/s11069-014-1186-4.
- Ashtari, M., Hatzfeld, D. Kamalian, N., 2005.** Microseismicity in the region of Tehran, *Tectonophysics*, 395, 193-208.
- Assadollahi, F., Barbéro, M., Quézel, P., 1982.** Les écosystèmes forestiers et préforestiers de l'Iran (Colloque: Définition et Localisation des Ecosystèmes méditerranéens terrestres), *Ecol.Medit.* 8, 365-379.
- Assereto, R., (ed) 1966,** Explanatory notes on the geological map of Upper Dadjerud and Lar valleys (central Elburz, Iran), scale 1:50000, 86 pp., Institut of Geology University of Milan, Italy, 1-86.
- Axen, G.J., Lam, P.J., Grove, M., Stockli, D.F., Hassanzadeh, J., 2001.** Exhumation of the west-central Alborz Mountains, Iran, Caspian subsidence, and collision-related tectonics, *Geology*, 29, 559-562, doi: 10.1130/0091 7613.
- Ballato, P., Nowaczyk, N.R., Landgraf, A., Strecker, M.R., Friedrich, A., Tabatabaei, S.H., 2008.** Tectonic control on sedimentary facies pattern and sediment accumulation rates in the Miocene foreland basin of the southern Alborz Mountains, northern Iran, *Tectonics*, 27, 1-20, doi: 10.1029/2008TC002278.
- Ballato, P., Uba, C., Landgraf, A., Strecker, M.R., Sudo, M., Stockli, D.F., Friedrich, A., Tabatabaei, S.H., 2011.** Arabia-Eurasia continental collision; Insights from late Tertiary foreland-basin evolution in the Alborz Mountains, northern Iran, *Geological Society of America Bulletin* 123,1-2, 106-131, doi: 10.1130/B30091.1.
- Basili, R., and Barba, S., 2007.** Migration and shortening rates in the northern Apennines, Italy: implications for seismic hazard, *Terra Nova*, 19, 462-468, doi: 10.1111/j.1365-3121.2007.00772.x.
- Beliaevsky, N.A., Verechtchagin, V.N., Krasny, L.I., 1961.** Tectonics. In: Markovsky, A. P. (ed.) *Geological Structures of USSR*. CNRS, Paris (in French).
- Berberian, M., 1976.** Contribution to the seismotectonics of Iran-Part II, Technical Report No. 39, Geological Survey of Iran.
- Berberian, M., 1979 a.** Tabas-e-Golshan (Iran) catastrophic earthquake of 16 September 1978: a preliminary fieldreport, *Disaster*, 2, 207-219.
- Berberian, M., 1979 b.** Earthquake faulting and bedding thrust associated with the Tabas-e-Golshan (Iran) earthquake of September 16, 1978, *Bulletin Seismological Society of America*, 69, 1861-1887.
- Berberian, M., 1979 c.** Evaluation of the instrumental and relocated epicentres of Iranian earthquakes, *Royal Astronomical Society*, 58, 625-630.
- Berberian, F., and Berberian, M., 1981.** Tectono-plutonic episodes in Iran. In: Delany, F.M. (Ed.), *Zagros-Hindu Kush-Himalaya Geodynamic Evolution*, Geodynamics Series, American Geophysical Union, Washington, D.C., 5-32.
- Berberian, M., and King, G.C.P., 1981.** Toward a paleogeography and tectonic evolution of Iran, *Canadian Journal of Earth Science*, 18 (1981), 210-265.
- Berberian, M., 1983.** The southern Caspian: a compressional depression floored by a trapped, modified oceanic crust, *Canadian Journal of the Earth Science*, 20(2), 163-183.
- Berberian, M., Ghorashi, M., Arzhangraves, B., Mohajer-Ashjai, A., 1993.** Seismotectonic and earthquake-fault hazard investigations in the greater Qazvin region, Geological Survey of Iran, report No. 61 (in pershian).
- Berberian, M., 1995.** Master "blind" thrust faults hidden under the Zagros folds: Active basement tectonics and surface morphotectonics, *Tectonophysics*, 241, 193-224.
- Berberian, M., and Yeats, R.S., 1999.** Patterns of historical earthquake rupture in the Iranian plateau, *Bulletin Seismological Society of America*, 89, 120-139.
- Berberian, M., and Yeats, R.S., 2001.** Contribution of archaeological data to studies of earthquake history in the Iranian Plateau. Paul Hancock Memorial Issue, *Journal of Structural Geology*, 23, 536-584.

- Besse, J., Torcq, F., Gallet, Y., Ricou, L.E., Krystyn, L., Sidi, A., 1998.** Late Permian to Late Triassic palaeomagnetic data from Iran; constraints on the migration of the Iranian Block through the Tethyan Ocean and initial destruction of Pangaea, *Geophysical Journal International*, 135, 77-92.
- Bettinelli, P., Avouac, J.P., Flouzat, M., Jouanne, F., Bollinger, L., Willis, P., Chitrakar, G.R., 2006.** Plate motion of India and interseismic strain in the Nepal Himalaya from GPS and DORIS measurements, *Journal of Geodesy*, 80, 567-589.
- Bijwaard, H., and Spakman, W., 1998.** Closing the gap between regional and global travel time Tomography, *Journal of Geophysical Research*, 103, 30,055-30, 078D.
- Blanckenburg, F., and Davies, J.H., 1995.** Slab breakoff: a model for syncollisional magmatism and tectonics in the Alps, *Tectonics*, 14, 120-131.
- Bonardi, G., Ciarcia, S., Di Nocera, S., Matano, F., Sgrosso, I., Torre, M., 2009.** Carta delle principali Unità Cinematiche dell'Appennino meridionale, *Boll. Società Geologica Italiana*, 128 pl. f. t.
- Brunet, M.F., Korotaev, M.V., Ershov, A.V., Nikishin, A.M., 2003.** The South Caspian Basin: a review of its evolution from subsidence modelling. *Sediment, Geology*, 156, 119-148.
- Busby, C.J., and Ingersoll, R.V., (eds) 1995.** *Tectonics of Sedimentary Basins*, Blackwell Science, Oxford, 3-31.
- Calamita, F., Satolli, S., Scisciani, V., Esestime, P., Pace, P., 2014.** Contrasting styles of fault reactivation in curved orogenic belts: Examples from the Central Apennines (Italy), *Geological Society of America Bulletin*; 123, 5-6; 1097-1111), doi: 10.1130/B30276.1
- Chemenda, A.I., Mattauer, M., Bokun, A.N., 1996.** Continental subduction and mechanism for exhumation of high-pressure metamorphic rocks: New modeling and field data from Oman, *Earth and Planetary Science Letters*, 143, 173-182.
- Chemenda, A.I., Burg, J.P., Mattauer, M., 2000.** Evolutionary model of the Himalaya Tibet system: Geopem based on new modelling, geological and geophysical data, *Earth and Planetary Science Letters*, 174, 397-409, doi: 10.1016/S0012-821X(99)00277-0.
- Ciarcia, S., Vitale, S., Di Staso, A., Iannace, A., Mazzoli, S., Torre, M., 2009.** Stratigraphy and tectonics of an 'Internal' Unit of the southern Apennines: implications for the geodynamic evolution of the peri-Tyrrhenian mountain belt, *Terra Nova*, 21, 88-96.
- Cipollari, P., and Cosentino, D., 1995.** Miocene unconformities in the Central Apennines: geodynamic significance and sedimentary basin evolution, *Tectonophysics*, 252, 375-389.
- Cloetingh, S., Fernández, M., Munoz, J.A., Sassi, W., Horváth, F., 1997.** Structural controls on sedimentary basin evolution, *Tectonophysics*, 282.
- Coene, F., 2010.** *The Caucasus - An Introduction*, Routledge Taylor and Friedrics Group, London and Newyork, 11-12.
- Colman-Sadd, S.P., 1978.** Fold development in Zagros simply folded belt, southwest Iran, *American Association of Petroleum Geologists Bulletin*, 62, 984-1003.
- Coward, M.P., Dewey, J.F., Hancock, P.L., (eds) 1987.** *Continental Extensional Tectonics*, Geological Society, London, Special Publications, 28.
- Dahlen F.A., 1984.** Noncohesive critical coulomb wedge: an exact solution, *Journal of Geophysical Rearearch*, 89, B12, 10,125-10,133.
- Dahlen, F.A., 1990.** Critical taper model of fold-and-thrust belts and accretionary wedges, *Annual Review of Earth and Planetary Science*, 18, 55-99.
- Daukeev, S.Z., Uzhkenov, B.S., Miletenko, N.V., Morozov, A.F., Leonov, Y.G., Wang, F., Akhmedov, N.A., Abdullayev, E.K., Murzagaziyev, S.M., Orifov, A.O., and Ali-Zade, A.A., 2002.** *Atlas of Lithology-Paleogeographical, Structural, Palinspastic and Geoenviromental Maps of Central Asia*, Scientific Research Institute of Natural Resources YUGGEO, Almaty (Kazakhstan).
- Davis, D., Suppe, J., Dahlen, F.A., 1983.** Mechanics of fold-and-thrust belts and accretionary wedges, *Journal of Geophysical Research*, 88(B2), 1153-1172.
- Davoudzadeh, M., Lammerer B., Weber-Diefenbach, K., 1997.** Paleogeography, stratigraphy, and tectonics of the Tertiary of Iran, *Neues Jahrbuch Geologie und Paläontologie Abh.*, 205, 33-67.
- DeCelles, P.G., and Giles, K.A., 1996.** Foreland basin systems, *Basin Research*, 8, 105-123, doi: 10.1046/j.1365-2117.1996.01491.x.



- DeCelles, P.G., Robinson, D.M., Quade, J., Ojha, T.P., Garzzone, C.N., Cope-land, P., Upreti, B.N., 2001.** Stratigraphy, structure, and tectonic evolution of the Himalayan fold-thrust belt in western Nepal, *Tectonics*, 20, 487-509.
- Dehghani, G., and Makris, J., 1984.** The gravity field and crustal structure of Iran, *Neues Jahrbuch Geologie und Paläontologie Abh.*, 168, 215-229.
- Delacou, B., Sue, C., Champagnac, J.D., Burkhard, M., 2004.** Present-day geodynamics in the bend of the western and central Alps as constrained by earthquake analysis, *Geophysics Journal of International*, 158, doi: 10.1111/j.1365-246X.2004.02320.x, 753-774.
- Dewey, J.F., and Bird J.M., 1970.** Mountain belts and the new global tectonics, *Journal of Geophysical Research*, 75, 2625-2647, doi: 10.1029/JB075i014p02625.
- Dewey, J.F., Pitman, W.C., Ryan, W.B.F, Bonnin, J., 1973.** Plate tectonics and the evolution of the Alpine system, *Geological Society of America Bulletin*, 84, 3137-3180.
- Djamor, Y., Vernant, P., Bayer, R., Nankali, H.R., Ritz, J.F., Hinderer, J., Hatam, Y., Luck, B.L., Moigen, N., Sedhighi, M., Khorrami, F., 2010.** GPS and gravity constraints on continental deformation in the Alborz Mountain range, Iran. *Geophysical Journal International*, doi: 10.1111/j.1365-246X.2010.04811.x.
- Dotduyev, S.I., 1987.** Nappe structure of the Greater Caucasus Range, *Geotectonics*, 20, 420-430.
- Edgell, H.S., 1996.** Salt tectonism in the Persian Gulf Basin, in *Salt Tectonics*, edited by J. L. Alsop, D. J. Blundell, and I. Davison, The Geological Society of London Special Publication, 100, 129-151.
- Eftekharneshad, J., 1980.** Tectonic divisions of different parts of Iran regarding sedimentary basins. *Journal of Oil Society*, 82, 19-28.
- Egan, S.S., Mosar, J., Brunet, M.F., Kangarli, T., 2009.** Subsidence and uplift mechanisms within the South Caspian Basin: insights from the onshore and offshore Azerbaijan region. From Brunet, M.F., Wilm-sen, M. and Granath J.W. (eds.) *South Caspian to Central Iran Basins*. The Geological Society of London Special Publication, 312, 219-240.
- Ekström, G., Nettles, M., Dziewonski, A.M., 2012.** The global CMT project 2004-2010: Centroid-moment tensors for 13,017 earthquakes, *Phys. Earth Planet. Inter.*, 200-201, 1-9, doi: 10.1016/j.pepi.2012.04.002. **CMT Catalogue**, <http://www.globalcmt.org/CMTsearch.html>, accessed 28.12.2014.
- Engdahl, E.R., 2006.** Application of an improved algorithm to high precision relocation of ISC test events, *Physics of the Earth and Planetary Interiors*, 158, 14-18.
- Eppelbaum L.V., and Khesin E.B., (eds) 2012.** *Geophysical Studies in the Caucasus*, Lecture Notes in Earth System Sciences, doi: 10.1007/978-3-540-76619-3\_2, Springer-Verlag Berlin Heidelberg, 19-37.
- Ershov, A.V., Brunet, M.F., Korotaev, M.V., Nikishin, A.M., Bolotov, S.N., 1999.** Late Cenozoic burial history and dynamics of Northern Caucasus molasse basin: implications for foreland basin modelling, *Tectonophysics*, 313, 219-241.
- Ershov, A.V., Brunet, M.F., Nikishin, A.M., Bolotov, S.N., Nazarevich, B.P. Korotaev, M.V., 2003.** Northern Caucasus basin: thermal history and synthesis of subsidence models, *Sedimentary Geology*, 156, 95-118.
- Forte, A., Cowgill, E., Murtuzayev, I., Kangarli, T., Stoica, M., 2013.** Structural geometries and magnitude of shortening in the eastern Kura fold-thrust belt, Azerbaijan: Implications for the development of the Greater Caucasus Mountains, *Tectonics*, 32, 688-717, doi:10.1002/tect.20032.
- Frank, W., and Fuchs, G.R., 1970.** Geological investigations in west Nepal and their significance for the geology of Himalayas, *Geologische Rundschau*, 59, 522.
- Frey, W., and Probst, W., 1986.** A synopsis of the vegetation of Iran, In: Kürschner, H. (ed), *Contribution to the Vegetation of Southwest Asia*. Dr. Ludwig Reichert, Wiesbaden, 1-43.
- Frostick, L.E., and Steel, R.J., (eds) 1993.** *Tectonic Controls and Signatures in Sedimentary Successions*, International Association of Sedimentologists, Special Publications, 20.

- Fürsich, F.T., Wilmsen, M., Seyed-Emami, K., Cecca F., Majidifard, M.R., 2005 a.** The upper Shemshak Formation (Toarcian-Aalenian) of the Eastern Alborz (Iran): Biota and palaeoenvironments during a transgressive-regressive cycle. *Facies*, 51, 365-384, doi: 10.1007/s10347-005-0051-z.
- Fürsich, F.T., Hautmann, M., Senowbari-Daryan, B., Seyed-Emami, K., 2005 b.** The Upper Triassic Nayband and Darkuh formations of east-central Iran: stratigraphy, facies patterns and biota of extensional basins on an accreted terrane, *Beringeria*, 35, 53-133.
- Fürsich, F.T., Wilmsen, M., Seyed-Emami, K., Majidifard, M.R., 2009 a.** Lithostratigraphy of the Upper Triassic-Middle Jurassic Shemshak Group of northern Iran. In: *South Caspian to Central Iran Basins* (M. F. Brunet, M. Wilmsen and J. Granath, eds), Geological Society London, Special Publication, 312, 129-160, doi: 10.1144/SP312.6.
- Fürsich, F.T., Wilmsen, M., Seyed-Emami, K., Majidifard, M.R., 2009 b.** The Mid-Cimmerian tectonic event (Bajocian) in the Alborz Mountains, northern Iran: Evidence of the break-up unconformity of the South Caspian Basin. In: *South Caspian to Central Iran Basins* (M. F. Brunet, M. Wilmsen and J. Granath, eds), Geological Society London, Special Publication, 312, 189-203, doi: 10.1144/SP312.9.
- Fuchs, G., and Frank, W., 1970.** The Geology of West Nepal between the rivers Kali Gandaki and Thulo Bheri, *Jahrbuch der Geologischen Bundesanstalt*, 18: 1-103, Wien.
- Gaetani, M., Garzanti, E., Polino, R., Kiricko, Y., 2005.** Stratigraphic evidence for Cimmerian events in NW Caucasus (Russia), *Bulletin de la Société Géologique de France*, 176(3), 283-299.
- Galewsky, J., 1998.** The dynamics of foreland basin carbonate platforms: tectonic and eustatic controls, *Basin Research*, 10, 409-416, doi: 10.1046/j.1365-2117.1998.00079.x.
- Gansser, A., (ed) 1964.** *Geology of the Himalayas*. London/New York/Sydney: Wiley Interscience, 289.
- Garfunkel, Z., and Greiling, R.O., 2002.** The implications of foreland basins for the causative tectonic loads, *EGU Stephan Mueller Special Publication*, 1, 3-16.
- Gavillot, Y., Axen, G.J., Stockli, D.F., Horton, B.K., Fakhari, M.D., 2010.** Timing of thrust activity in the High Zagros fold-thrust belt, Iran, from (U-Th)/He thermochronometry, *Tectonics*, 29, TC4025, doi: 10.1029/2009TC002484.
- Golonka, J., 2004.** Plate tectonic evolution of the southern margin of Eurasia in the Mesozoic and Cenozoic, *Tectonophysics*, 381, 235-273, doi: 10.1016/j.tecto.2002.06.004.
- Guest, B., Axen, G.J., Lam, P.S., Hassanzadeh, J., 2006 a.** Late Cenozoic shortening in the west-central Alborz Mountains, northern Iran, by combined conjugate strike-slip and thin-skinned deformation, *Geosphere*, 2 (1), 35-52.
- Guest, B., Stockli, D.F., Grove, M., Axen, G.J., Lam, P., Hassanzadeh, J., 2006 b.** Thermal histories from the central Alborz Mountains, northern Iran: implications for the spatial and temporal distribution of deformation in northern Iran, *Geological Society of America Bulletin*, 118 (11/12), 1507-1521, doi: 10.1130/B25819.1.
- Guest, B., Guest, A., Axen, G., 2007.** Late tertiary tectonic evolution of northern Iran: a case for simple crustal folding, *Global Planet Change*, 58, 435-453.
- Guzzetti, F., Stark, C.P., Salvati, P., 2005.** Evaluation of flood and landslide risk to the population of Italy, *Environmental Management*, 36(1), 15-36.
- Hafezi, M.N., and Ghafoori, M., 2007.** Investigation of the distributions and causes of land slides in central Alborz, Iran, *World Applied Sciences Journal*, 2, 652-657.
- Hafkenscheid, E., Wortel, M.J.R., Spakman, W., 2006.** Subduction history of the Tethyan region derived from seismic tomography and tectonic reconstructions, *Journal of Geophysical Research*, 111, doi: 10.1029/2005JB003791.
- Haghipour, A., Taraz, H., Vahdati Daneshmand, F., 1987.** Tehran, Geological quadrangle map of Iran. 1:250,000, Tehran, Geological Survey of Iran.
- Hamdi, B., Brasier, M.D., Jiang, Zh., 1989.** Earliest skeletal fossils from Precambrian-Cambrian boundary strata, Elburz Mountains, Iran, *Geology*, 126, 283-289.
- Hatzfeld, D., and Molnar, P., 2010.** Comparisons of the kinematics and deep structures of the Zagros and Himalaya and of the Iranian and Tibetan plateaus and geodynamic implications, *Review of Geophysics*, 48, doi: 10.1029/2009RG000304.

- Haynes, S.J., and McQuillan, H., 1974.** Evolution of the Zagros Suture Zone, Southern Iran, *Geological Society of America Bulletin*, 85, 739 - 744.
- Heidbach, O., Tingay, M., Barth, A., Reinecker, J., Kurfeß, D., Müller, B., 2008.** The World Stress Map database release 2008, doi: 10.1594/GFZ, **WSM catalogue**, <http://dc-app3-14.gfz-potsdam.de>, accessed 28.12.2014.
- Heim, A., and Gansser, A., 1939.** Central Himalaya Geological Observations of Swiss Expedition, 1936, 246.
- Hessami, Kh., and Jamali, F., 2006.** Explanatory notes to the map of Major Active Faults of Iran, *Journal of Seismology and Earthquake Engineering* 8 (1), 1-11.
- Hinds, D.J., Simmons, M.D., Allen, M.B., Aliyeva, E., 2001.** Architecture variability within the Pereriva and Balakhany suites of the Neogene Productive Series, Azerbaijan: implications for reservoir quality. *American Association of Petroleum Geologists*, Memoir in press.
- Hollingsworth, J., Fattahi, M., Walker, R., Talebian, M., Bahroudi, A., Bolourchi, M.J., Jackson, J., Copley, A., 2010.** Oroclinal bending, distributed thrust and strike-slip faulting, and the accommodation of Arabia–Eurasia convergence in NE Iran since the Oligocene. *Geophysical Journal International* 181 (3), 1214-1246, doi: 10.1111/j.1365-246X.2010.04591.x.
- Hoth, S., 2005.** Deformation, erosion and natural resources in continental collision zones, Insight from scaled sandbox simulations (Dissertation). *GeoForschungsZentrum Potsdam*, ISSN 1610-0956.
- Hoth, S., Hoffmann-Rothe, A., Kukowski, N., 2007.** Frontal accretion: an internal clock for bivergent wedge deformation and surface uplift, *Journal of Geophysics Research*, 112 (B06408), 1-17.
- Hoth, S., Kukowski, N., Oncken, O., 2008.** Distant effects in bivergent orogenic belts - How retro-wedge erosion triggers resource formation in pro-foreland basins, *Earth and Planetary Science Letters*, 273, 28-37.
- Ismail-Zade, T.A., Gadjiev, T.G., Guseinov, A.N., Akhmedov, A.M., Yusufzade, H.B., 1987.** Atlas of Oil and Gas Bearing and Perspective Structures of Azerbaijan, USSR Ministry of Geology.
- Ives, J.D., and Messerli, B., 1989.** The Himalayan Dilemma, reconciling development and conservation *Routledge*, Google e Book, p 9-12.
- Jackson, J.A., and Fitch, T., 1981.** Basement faulting and the focal depths of the larger earthquakes in the Zagros Mountains (Iran), *Geophysics Journal Research astronomy soc.*, 64, 561-586.
- Jackson, J.A., and McKenzie, D.P., 1984.** Active tectonics of the Alpine-Himalayan Belt between western Turkey and Pakistan, *Geophysics Journal Research, astronomy soc*, 77, 185-246.
- Jackson, J.A., Priestley, K., Allen, M., Berberian, M., 2002.** Active tectonics of the South Caspian Basin, *Geophysical Journal International* 148, 214-245, doi: 10.1046/j.1365-246X.2002.01588.x.
- Jahani, S., Callot, J.P., Letouzey, J., Frizon de Lamotte, D., 2009.** The eastern termination of the Zagros Fold-and-Thrust Belt, Iran: Structures, evolution, and relationships between salt plugs, folding, and faulting, *Tectonics* 28, 6, doi: 10.1029/2008TC002418.
- James, G.A., and Wynd, J.G., 1965.** Stratigraphic nomenclature of Iranian oil consortium agreement area *American Association of Petroleum Geologists Bulletin*, 49, 2162-2245.
- Jiménez-Munt, I., Fernández, M., Saura, E., Vergés, J., García-Castellanos, D., 2012.** 3-D lithospheric structure and regional/residual Bouguer anomalies in the Arabia–Eurasia collision (Iran), *Geophysical Journal International* 190, 1311-13, doi: 10.1111/j.1365-246X.2012.05580.x.
- Kaviani, A., Paul, A., Bourova, E., Hatzfeld, D., Pedersen, H., Mokhtari, M., 2007.** A strong seismic velocity contrast in the shallow mantle across the Zagros collision zone (Iran). *Geophysical Journal International* 171 (1), 399-410, doi: 10.1111/j.1365-246X.2007.03535.x.
- Kent, P.E., 1979.** The emergent Hormuz salt plugs of southern Iran, *Journal of Petroleum Geologists*, 2, 117-144.
- Khadivi, S., Mouthereau, F., Larrasoña, J.C., Vergés, J., Lacombe, O., Khademi, E., Beamud, E., Melinte-Dobrinescu, M., Suc, J.P., 2010.** Magnetochronology of synorogenic Miocene foreland sediments in the Fars arc of the Zagros Folded Belt (SW Iran), *Basin Research* 22(6), 918-932.

- Khadivi, S., Mouthereau, F., Barbarand, J., Adatte, T., Lacombe, O., 2012.** Constraints on paleodrainage evolution induced by uplift and exhumation on the southern flank of the Zagros–Iranian Plateau, *Journal of the Geological Society* 169 (1), doi: 10.1144/0016-76492011-031.
- Khain, V.E., 1975.** Structure and main stages in the tectono-magmatic development of the Caucasus: an attempt at geodynamic interpretation, *American Journal of Science*, 275-A, 131-156.
- Khain, V.E., (ed) 1994.** *Geology of Northern Eurasia*. Borntraeger, Stuttgart, 443 (in German).
- Khain, V.E., 1997.** Azerbaijan – Greater Caucasus. In: Moores, E. M. & Fairbridge, R.W. (eds), *Encyclopedia of European and Asian Regional Geology*. Chapman and Hall, London, 60-63.
- Khodaverdian, A., Zafarani, H., Rahimian, M., 2015.** Long term Fault slip rates, distributed deformation rates and forecast of seismicity in the Iranian Plateau, *American Geophysical Union*, 34, 10, doi: 10.1002/2014TC003796.
- Kirby, E., and Whipple, K.X., 2012.** Expression of active tectonics in erosional landscapes, *Journal of Structural Geology* 44, 54-75, doi: org/10.1016/j.jsg.2012.07.009.
- Klein, J.C., 2001.** Lavégétation altitudinale de Alborz Central (Iran): Entre les régions Irano-Touranienne et Euro-sibérienne, *Institut Français de Recherche en Iran, Téhéran*.
- Koronovsky, N.V., (ed) 1984.** *Geology of the USSR*. Moscow State University Press, Moscow (in Russian).
- Korup, O., Clague, J.J., Hermanns, R.L., Hewitt, K., Strom, A.L., Weidinger, J.T., 2007.** Giant landslides, topography and erosion, *Earth Planet Science Letters* 261:578-589.
- Koulakov, I., Tychkov, S., Bushenkova, N., Vasilevskiy, A., 2002.** Structure and dynamics of the upper mantle beneath the Alpine-Himalayan orogenic belt, from teleseismic tomography, *Tectonophysics*, 358, 77-96.
- Koulakov, I., Zabelina, I., Amanatashvili, I., Meskhia, V., 2012.** Nature of orogenesis and volcanism in the Caucasus region based on results of regional tomography, *Solid Earth*, 3, 327-337, doi: 10.5194/se-3-327.
- Kottek, M., Grieser, J., Beck, C., Rudolf, B., Rubel, F., 2006.** World Map of the Köppen-Geiger climate classification updated, *Meteorologische Zeitschrift*, 15, 259-263, doi: 10.1127/0941-2948/2006/0130.
- Kukowski, N., Greinert, J., Henrys, S., 2010.** Morphometric and critical taper analysis of the Rock Garden region, Hikurangi Margin, New Zealand: Implications for slope stability and potential tsunami generation, *Marine Geology* 272, 141-153, doi: 10.1016/j.margeo.2009.06.004.
- Kvavadze, E.V., and Rukhadze, L.P., (eds) 1989.** *Vegetation and climate of the Holocene Abkhazia*. Tbilisi, Metsniereba, 138 (in Russian).
- Landgraf, A., Ballato, P., Strecker, M.R., Friedrich, A., Tabatabaei, S.H., Shahpasandzadeh, M., 2009.** Fault-kinematic and geomorphic observations along the North Tehran Thrust and Mosha-Fasham Fault, Alborz mountains Iran: implications for fault-system evolution and interaction in a changing tectonic regime, *Geophysical Journal International* 177, 676-690.
- Laske, G., Masters, G., Reif, C., 2013.** A New Global Crustal Model at 2x2 Degrees, <http://mahi.uscd.edu/Gabi/rem.html>, accessed 10.07.2013.
- Lavé, J., and Avouac, J.P., 2000.** Active folding of fluvial terraces across the Siwaliks Hills, Himalayas of central Nepal, *Journal of Geophysical Research*, 105, 5735-5770.
- Leopold, L.B., Wolman, M.G., Miller, J.P., 1964.** *Fluvial processes in geomorphology*. United States of America, Dover publications, 462-475.
- Lordkipanidze, M.B., 1980.** The Alpidic volcanism and geodynamics of the central segment of the Mediterranean fold belt. *Trudy Geologicheskoy Institut im A.I. Dzhanelidze, Metsniereba, Tbilisi, USSR*, 69 (in Russian).
- Lordkipanidze, M.B., Melikstein, B., Djarbashian, R., 1989.** Mesozoic–Cenozoic magmatic evolution of the Pontian–Crimean–Caucasian region. In: Rakaú S. M., Dercourt, J., Narin, A. E. M. (eds) IGCP Project no. 198: Evolution of the Northern Margin of Tethys, *Mémoires de la Société Géologique de France, Nouvelle Série*, 154(II), 103-124.
- Lohrmann, J., Kukowski, N., Adam, J., Oncken, O., 2003.** The impact of analogue material properties on the geometry, kinematics, and dynamics of convergent sand wedges, *Journal of Structural Geology*, 25 (10), 1691-1711.

- Maggi, A., Jackson, J.A., Priestley, K., and Baker, C., 2000.** A reassessment of focal depth distributions in southern Iran, the TienShan and northern India: Do earthquakes really occur in the continental mantle, *Geophysical Journal International*, 143, 629-661, doi: 10.1046/j.1365-246X.2000.00254.x.
- Maggi, A., and Priestley, K., 2005.** Surface waveform tomography of the Turkish-Iranian plateau, *Geophysical Journal International*, 160, 1068-1080, doi: 10.1111/j.1365-246X.2005.02505.x.
- Manaman, N.S., and Shomali, H., 2010.** Upper mantle S-velocity structure and Moho depth variations across Zagros belt, Arabian-Eurasian plate boundary, *Physics of the Earth and Planetary Interiors* 180 (1-2), 92-103, doi: 10.1016/j.pepi.2010.01.011.
- Manaman, N.S., Shomali, H., Koyi, H., 2011.** New constraints on uppermantle S-velocity structure and crustal thickness of the Iranian plateau using partitioned waveform inversion, *Geophysical Journal International*, 184, 247-267, doi: 10.1111/j.1365-246X.2010.04822.x.
- Mangino, S., and Priestley, K., 1998.** The crustal structure of the southern Caspian region, *Geophysical Journal International*, 133, 630- 648, doi: 10.1046/j.1365-246X.1998.00520.x.
- Masson, F., Chéry, J., Hatzfeld, D., Martinod, J., Vernant, P., Tavakoli, F., Ghafory-Ashtiani, M., 2005.** Seismic versus aseismic deformation in Iran inferred from earthquakes and geodetic data, *Geophysical Journal International*, 160, 217-226.
- Masson, F., Djamour, Y., Van Gorp, S., Chéry, J., Tatar, M., Tavakoli, M., Nankali, H., Vernant, P., 2006.** Extension in NW Iran driven by the motion of the South Caspian Basin, *Earth and Planetary Science Letters* 252, 180-188, doi: 10.1016 /j.epsl .2006 .09.038.
- Mazzoli, S., and Helman, M., 1994.** Neogene patterns of relative plate motion for Africa–Europe: some implications for recent central Mediterranean tectonics, *Geologische Rundschau* 83, 464-468.
- Mazzoli, S., D’Errico, M., Aldega, L., Corrado, S., Invernizzi, C., Shiner, P., Zattin, M., 2008.** Tectonic burial and young (<10 Ma) exhumation in the southern Apennines fold and thrust belt (Italy), *Geology* 36, 243- 246.
- McCann, T., and Saintot, A., (eds) 2003.** *Tracing Tectonic Deformation Using the Sedimentary Record*, Geological Society London, Special Publications, 208.
- McClusky, S., Balassania, S., Barka, A., Demir, C., Ergintav, S., Georgiev, I., Gurkan, O., Hamburger, M., Hurst, K., Kahle, H., Kastens, L., Kekelidze, G., King, R.W., Kotzev, V., Lenk, O., Mahmoud, S., Mishin, A., Nadariya, M., Ouzounis, A., Paradissis, D., Peter, Y., Prilepin, M., Reilinger, R., Sanli, I., Seeger, H., Taelieb, A., Toksoz, M.N., Veis, G., 2000.** GPS constraints on plate motions and deformation in the Eastern Mediterranean: Implications for plate dynamics, *Journal of Geophysical Research*, 105, 5695-5719.
- McQuarrie, N., Stock, J.M., Verdel, C., Wernicke, B.P., 2003.** Cenozoic evolution of Neotethys and implications for the causes of plate motions, *Geophysical Research Letters*, 30, 20, 2036, doi: 10.1029/2003GL017992.
- Milanovsky, E.E., and Khain, V.E., 1963 (eds).** *Geological Structure of Caucasus*. MGU, Moscow, 357 (in Russian).
- Mikhailov, V., Panina, L.V., Polino, R., Koronovsky, N.V., Kiseleva, E.A., Klavdieva, N.V., Smolyaninova, E.I., 1999.** Evolution of the North Caucasus foredeep: constraints based on the analysis of subsidence curves, *Tectonophysics*, 307, 361-379.
- Mohajer-Ashjai, A., and Nowroozi, A.A., 1979.** The Tabas earthquake of September 16, 1978 in East-Central Iran, a preliminary field report, *Geophysical Research Letters* 6, doi: 10.1029/GL006i009p00689.
- Mokhtari, M., and Kiarasi, S., 2008.** The pattern and magnitude of rotational piezomagnetic anomalies along the dip-slip Moshafault, Northern Tehran, Iran, *Natural Hazards and Earth System Sciences*, 8, 1293-1297, doi: 10.5194/nhess-8-1293-2008.
- Molinari, I., Raileanu, V., Morelli, A., 2012.** A Crustal Model for the Eastern Alps Region and a New Moho Map in Southeastern Europe, *Geophysics* 169, 1575-1588, doi: 10.1007/s00024-011-0431-y.
- Molinaro, M., Leturmy, P., Guézou, J.C., Frizon de Lamotte, D., 2005.** The structure and kinematics of the south-eastern Zagros fold-thrust belt, Iran: from thin-skinned to thick-skinned tectonics, *Tectonics*, 24, TC3007, doi: 10.1029/2004TC001633.
- Molnar, P., and Englan, P., 1990.** Late Cenozoic uplift of mountain ranges and global climate change: chicken or egg? *Nature*, 346,29.
- Molnar, P., Anderson, R.S., Prestrud Anderson, S., 2007.** Tectonics, fracturing of rock, and erosion, *Journal of Geophysical Research*, 112, doi: 10.1029/2005JF000433.

- Montgomery, D.R., 2003.** Predicting landscape-scale erosion rates using digital elevation models, *Comptes Rendus Geoscience*, 335, 16, 1121-1130, doi: 10.1016/j.crte.2003.10.005.
- Morley, C.K., Kongwung, B., Julapour, A.A., Abdolghafourian, M., Hajian, M., Waples, D., Warren, J., Otterdoom, H., Srisuriyon, K., Kazemi, H., 2009.** Structural development of a major late Cenozoic basin and transpressional belt in central Iran: the Central Basin in the Qom–Saveh area, *Geosphere* 5 (4), 325-362, doi: 10.1130/ges00223.1.
- Mosar, J., Kangari, T., Bochud, M., Glasmacher, U.A., Rast, A., Brunet, M.F., Sosson, M., 2010.** Cenozoic-Recent tectonics and uplift in the Greater Caucasus: a perspective from Azerbaijan, *The Geological Society of London, Special Publications*, 340, 261-280.
- Motavalli-Anbaran, S.H., Zeyen, H., Brunet, M.F., Ebrahimzadeh Ardestani, V., 2011.** Crustal and lithospheric structure of the Alborz Mountains, Iran, and surrounding areas from integrated geophysical modeling, *Tectonics*, 30, TC5012, doi: 10.1029/2011TC002934.
- Motavalli-Anbaran S.H., Zeyen, H., Ebrahimzadeh Ardestani, V., 2013.** 3D joint inversion modeling of the lithospheric density structure based on gravity, geoid and topography data — Application to the Alborz Mountains (Iran) and South Caspian Basin region, *Tectonophysics* 586, 192-205.
- Mouthereau, F., Lacombe, O., Meyer, B., 2006.** The Zagros folded belt (Fars, Iran): constraints from topography and critical wedge modelling, *Geophysical Journal International* 165, 336-356.
- Mouthereau, F., Lacombe, O., Verges, J., 2012.** Building the Zagros collisional orogen: Timing, strain distribution and the dynamics of Arabia/Eurasia plate convergence, *Tectonophysics*, 532-535.
- Mumladze, T., Forte, A.M., Cowgill, E.S., Trexler, C.C., Niemi, N.A., Burak Yikilmaz, M., Kellogg, L.H., 2015.** Subducted, detached, and torn slabs beneath the Greater Caucasus, *GeoResJ* 536-46, doi: org/10.1016/j.grj.2014.09.004.
- Muttoni, G., Mattei, M., Balini, M., Zanchi, A., Gaetani, M., Berra, F., 2009.** The drift history of Iran from the Ordovician to the Triassic. In: *South Caspian to Central Iran Basins* (M.F. Brunet, M. Wilmsen and J. Granath, eds), *Geological Society London, Special Publication*, 312, 7-29, doi: 10.1144/SP312.2.
- Nabavi, M., (ed) 1975.** Geological history of Iran, ministry of Industry and Mines, Geological Survey of Iran, 20-150 (in Persian).
- Nabavi, M., and Partoazar, H., 1977.** Report of Neocomian in Biarjmand – Kerman, Geological Survey of Iran, unpublished.
- Nakata, T., 1989.** Active faults of the Himalayas of India and Nepal, *Geological Society of America, Special Paper*, 32, 243-264, doi: 10.1130/spe232-p243.
- Naqinezhad, A., Jalili, A., Attar, F., Ghahreman, A., Wheele, B.D., Hodgson, J.G., Shaw, S.C., Maassoumi, A., 2009.** Floristic characteristics of the wetland sites on dry southern slopes of the Alborz Mts., N. Iran: The role of altitude in floristic composition, *Flora Morphol. Distrib. Functional Ecology of Plants*, 204, 254-269.
- Narimanov, N.P., 1992.** Tectonic regionalization of offshore of South Caspian depression, *Geologiya Nefti i Gaza*, 11, 22-24.
- Nasrabadi, A., Tatar, M., Priestley, K., Sepahvand, M.R., 2008.** Continental lithosphere structure beneath the Iranian Plateau, from analysis of receiver functions and surface waves dispersion. The 14th World Conference on Earthquake Engineering, October 12-17, Beijing, China.
- Nazarevich, B.P., Nazarevich, I.A., Shvydko, N.I., 1986.** The Upper Triassic Nogai volcano-sedimentary formation of Eastern Fore-Caucasus: composition, constitution, and relations to earlier and later-formed volcanics. In: Timofeev, P. P. and Boulin, YU. K. (eds) *The Formations of Sedimentary Basins*. Nauka, Moscow, 67-86 (in Russian).
- Nazari, H., and Bozorgnia, Y., 1992.** The 1990 Manjil, Iran, earthquake: geology and seismology overview, PGA attenuation, and observed damage, *Bulletin of Seismological Society of America*, 82, 2, 774.
- Nazari, H., Ritz, J.F., Salamati, R., Solaymani, S., Balescu, S., Michelot, J.L., Ghasemi, A., 2007.** Paleoseismological Analysis in Central Alborz, (The 1957 Geobi-Attay Earthquake Commemorating Conference, Ulaanbaatar-Mongolia).
- Nazari, H., and Ritz, J.F., 2008.** Neotectonic in Central Alborz, *Geosciences*, 17, 1.
- Nazari, H., Ritz, J.F., Shafei, A., Ghassemi, A., Salamati, R., Michelot, J.L., Massault, M., 2009.** Morphological and paleoseismological analyses of the Taleghan fault, Alborz, Iran, *Geophysical Journal International*, 178, 1028-1041.
- Nazari, H., Ritz, J.F., Salamati, R., Shahidi, A., Habibi, H., Ghorashi, M., Karimi Bavandpur, A., 2010.** Distinguishing between fault scarps and shorelines: the question of the nature of the Kahrizak, North Rey and South Rey features in the Tehran plain (Iran), *Terra Nova*, 22, 227-237, doi: 10.1111/j.1365-3121.2010.00938.x.

- Nikishin, A.M., Cloething, S., Bolotov, S.N. Baraboshkin, E.Yu, Kopaevich, L.F., Nazarevich, B.P., Panov, D.I., Brunet, M.F., Ershov, A.V., Iliina, V.V., Kosova, S.S., Stephenson, R.A., 1998 a.** Scythian platform, chronostratigraphy and polyphase stage of tectonic history. In: Crasquin-Soleau, S. and Barrier, E. (eds) Peri-Tethys Memoir 3, Stratigraphy and Evolution of the Peri-Tethyan The Mesozoic-Cenozoic tectonic evolution of the Greater Caucasus 287 Platforms, Mémoires du Muséum National d'Histoire Naturelle, 177,151-162.
- Nikishin, A.M., Cloetingh, S., Brunet, M.F., Stephenson, R.A., Bolotov, S.N., Ershov, A.V., 1998 b.** Scythian platform, Caucasus and Black sea region: Mesozoic-Cenozoic tectonic history and dynamics. In: Crasquin, S. & Barrier, E. (eds) Peri-Tethys Memoir 3, Stratigraphy and Evolution of Peri-Tethyan Platforms, Mémoires du Muséum National d'Histoire Naturelle, 177, 163-176.
- Nikishin, A.M., Ziegler, P.A., Panov, D.I., Nazarevich, B.P., Brunet, M.F., Stephenson, R.A., Bolotov, S.N., Korotaev, M.V., Tikhomirov, P.L., 2001.** Mesozoic and Cenozoic evolution of the Scythian Platform–Black Sea–Caucasus domain. In: Ziegler, P. A., Cavazza, W., Roberston, A. H. F., Crasquin-Soleau, S. (eds) Peri-Tethys Memoir 6, Peri-Tethyan Rift/Wrench Basins and Passive Margins, Mémoires du Muséum National d'Histoire Naturelle, 186, 295-346.
- Nikishin, A.M., Korotaev, M.V., Ershov, A.V., Brunet, M.F., 2003.** The Black Sea basin: tectonic history and Neogene–Quaternary rapid subsidence modelling, *Sedimentary Geology*, 156, 149-168.
- Nilforoushan, F., Masson, F., Vernant, P., Vigny, C., Martinod, J., Abbassi, M., Nankali, H., Hatzfeld, D., Bayer, R., Tavakoli, F., Ashtiani, A., Doerflinger, E., Daignières. M., Collard, P., Chéry, J., 2003.** GPS network monitors the Arabia-Eurasia collision deformation in Iran, *Journal of Geodesy* 77, 411-422, doi: 10.1007/s00190-003-0326-5.
- NOAA images**, National Oceanic And Atmospheric Administration, <http://www.noaa.gov>, accessed 30.07.2014.
- Nowroozi, A.A., 1971.** Seismo-tectonics of the Persian Plateau, eastern Turkey, Caucasus and Hindu-Kush region, *Bulletin of the Seismological Society of America*, 61, 311-341.
- Nowroozi, A.A., 1976.** Seismotectonic Provinces of Iran, *Bulletin of the Seismological Society of America*, 66, 1249-1276.
- Nowroozi, A.A., and Mohajer-Ashjai, A., 1981.** Faulting of Kurizan and Koli (Iran) earthquake of November 1979, Field Report, *Bulletin du Bureau de Recherches Géologiques et Minières (2nd series) 2*, TV, 91-99.
- Parotto, M., and Praturlon, A., 1975.** Geological summary of the Central Apennines. *Quaderni de “La ricerca scientifica”*, 90, 258-311.
- Paul, A., Hatzfeld, D., Kaviani, A., Tatar, M., Péquegnat, C., 2010.** Seismic imaging of the lithospheric structure of the Zagros mountain belt (Iran), *Geological Society, London, Special Publications*, 330, 5-18, doi: 10.1144/SP330.2.
- Pfiffner, O.A., (ed) 2009.** *Geologie der Alpen*, Haupt Verlag, 359, available from [http://www.amazon.de/Geologie-Alpen-O-Adrian-Pfiffner/dp/3825284166#reader\\_3825284166](http://www.amazon.de/Geologie-Alpen-O-Adrian-Pfiffner/dp/3825284166#reader_3825284166), accessed 10.03.2014
- Piana, A.N., and Amato, A., 2009.** Moho depth and Vp/Vs ratio in peninsular Italy from teleseismic receiver functions, *Journal of Geophysical Research*, 114, B06303, doi: 10.1029/2008JB005899.
- Pinto, L., Hérail, I.G., Sepúlveda, S.A., Krop, P., 2008.** A Neogene giant landslide in Tarapacá, northern Chile: asignal of instability of the westernmost Altiplano and palaeoseismicity effects, *Geomorphology* 102,532-541.
- Powers, P.M., Lillie, R.J., Yeats, R.S., 1998.** Structure and shortening of the Kangra and Dehra Dun reentrants, Sub-Himalaya, India, *Geological Society of America Bulletin*, 110, 1010-1027.
- Priestley, K., Baker, C., Jackson, J., 1994.** Implications of earthquake focal mechanism data for the active tectonics of the south Caspian basin and surrounding regions, *International Journal of Geophysics*, 118, 111-141.
- Radjaee, A.H., Mokhtari, M., Priestley, K., Hatzfeld, D., 2007.** Variation of Moho depth in the central Alborz (in Persian), *Geosciences, Geological Survey of Iran* 64.
- Radjaee, A.H., Rham, D., Mokhtari, M., Tatar, M., Priestley, K., Hatzfeld, D., 2010.** Variation of Moho depth in the central part of the Alborz Mountains, northern Iran, *Geophysical Journal International* 181 (1), 173-184, doi: 10.1111/j.1365-246X. 2010. 0 4518.x.
- Regard, V., Faccenna, C., Martinod, J., Bellier, O., and Thomas, J.C., 2003.** From subduction to collision: Control of deep processes on the evolution of convergent plate boundary, *Journal of Geophysical Research*, 108, 42208, 1-13, doi: 10.1029/2002JB001943.



- Regard, V., Faccenna, C., Bellier, O. and Martinod, J., 2008.** Laboratory experiments of slab-break-off and slab dip reversal: insight into the Alpine Oligocene reorganization, *Terra Nova*, 20, 267-273, doi: 10.1111/j.1365-3121.2008.00815.x.
- Reilinger, R., McClusky S., Vernant P., Shawn L., Ergintav S., Cakmak, R., Ozener, H., Kadirov, F., Guliev, I., Stepanyan, R., Nadariya, M., Hahubia, G., Mahmoud, S., Sakr, K., ArRajehi, A., Paradissis, D., Al-Aydrus, A., Prilepin, M., Guseva, T., Evren, E., Dmitrotsa, A., Filikov, S.V., Gomez, F., Riad Al-Ghazzi, R., Gebran Karam, G., 2006.** GPS constraints on continental deformation in the Africa–Arabia–Eurasia continental collision zone and implications for the dynamics of plate interactions. *Journal of Geophysical Research, Solid Earth*, 111.
- Rezaeian, M., 2008.** Coupled tectonics, erosion and climate in the Alborz Mountains, Iran. PhD thesis, University of Cambridge, 219.
- Ricou, L., Braud, J., Brunn, J.H., 1977.** Le Zagros, *Mémoires de la Société géologique de France*, 8, 33-52.
- Riebe, C.S., Kirchner, J.W., Granger, D.E., Finkel, R.C., 1991 a.** Minimal climatic control on erosion rates in the Sierra Nevada, California, *Geology* 29, 447-450.
- Riebe, C.S., Kirchner, J.W., Granger, D.E., Finkel, R.C., 1991 b.** Strong tectonic and weak climatic control of long-term chemical weathering rates, *Geology* 29, 511-514.
- Ritz, J.F., Nazari, H., Ghassemi, A., Salamati, R., Shafei, A., Solaymani, S., Vernant, P., 2006.** Active transtension inside central Alborz: a new insight into northern Iran–southern Caspian geodynamics, *Geology* 34, 477-490, doi: 10.1130/G22319.1.
- Robertson, A.H.F., 1987.** Upper Cretaceous Muti Formation: transition of a Mesozoic carbonate platform to a foreland basin in the Oman Mountains, *Sedimentology*, 34, 1123-1142, doi: 10.1144/GSL.MEM.2006.032.01.14.
- Robertson, A.H.F., 1994.** Role of the tectonic facies concept in orogenic analysis and its application to Tethys in the Eastern Mediterranean region, *Earth Science Reviews Journal*, 37, 139-213.
- Robertson, A.H.F., 2004.** Contrasting mode of ophiolite emplacement in the Eastern Mediterranean region, *European Lithosphere Dynamics* (D.G. Gee and R.A. Stephenson, eds), *Geological Society of London*, 32, 235-261.
- Rolland, Y., Perinek, D., Kaymakci, N., Sosson, M., Barrier, E., Avagyan, A., 2012.** Evidence for ~80-75 Ma subduction jump during Anatolide–Tauride–Armenian block accretion and ~48 Ma Arabia–Eurasia collision in Lesser Caucasus-East Anatolia, *Journal of Geodynamics* 56-57, doi: 10.1016/j.jog.2011.08.006.
- Rosenbaum, G., Lister, G.S., and Duboz, C., 2002.** Reconstruction of the tectonic evolution of the western Mediterranean since the Oligocene. In: Rosenbaum, G. and Lister, G. S. 2002. Reconstruction of the evolution of the Alpine-Himalayan Orogen, *Journal of the Virtual Explorer*, 8, 107-130.
- Ruban, D.A., 2007 a.** Jurassic transgressions and regressions in the Caucasus (northern Neotethys Ocean) and their influences on the marine biodiversity. *Palaeogeography, Palaeoclimatology, Palaeoecology*, 251, 422-436.
- Ruban, D.A., 2007 b.** Major Paleozoic-Mesozoic unconformities in the Greater Caucasus and their tectonic re-interpretation, a synthesis, *GeoActa*, 6, 91-102.
- Ruban, D.A., 2008.** The Jurassic events in the Greater Caucasus basin (northern Neotethys) and the Neuquén basin (West Gondwana), a comparison, *Revista de la Asociación Geológica Argentina*, 63, 766-775.
- Ruppe, C., and McNutt, M., 1990.** Regional compensation of the Greater Caucasus Mountains based on an analysis of Bouguer gravity data, *Earth and Planetary Science Letters*, 98, 360-379.
- Saidi, A., 1995.** Calendrier de la migration permo-triasique et morcellement mésozoïque des éléments continentaux de l'Iran. PhD thesis, Université P. & M. Curie, Paris.
- Saintot, A., Brunet, M., Yakovelv, F., Sebrier, M., Stephenson, R., Ershov, A., Charlot-Prat, F., Mccann, T., 2006.** The Mesozoic–Cenozoic tectonic evolution of the Greater Caucasus, *Geological Society, London, Memoirs*, 32, 277-289.
- Shabanian, E., Bellier, O., Siame, L., Arnaud, N., Abbassi, M.R., Cocheme, J.J., 2009 a.** New tectonic configuration in NE Iran: active strike-slip faulting between the Kopeh Dag and Binalud mountains, *Tectonics* 28, TC5002, doi: 10.1029/2008tc002444.
- Shabanian, E., Siame, L., Bellier, O., Benedetti, L., Abbassi, M.R., 2009 b.** Quaternary slip rates along the northeastern boundary of the Arabia–Eurasia collision zone (Kopeh Dag Mountains, Northeast Iran), *Geophysical Journal International* 178 (2), 1055-1077, doi: 10.1111/j.1365-246X.2009.04183.x.

- Shardanov, A.N., and Peklo, V.P., 1959.** Tectonics and history of formation of buried folds on southern flank of western Kuban trough and hydrocarbon potential of Mesozoic deposits, Gostoptekhizdat, Moscow, 3-27 (in Russian).
- Sharland, P.R., Archer, R., Casey, D.M., Davies, R.B., Hall, S.H., Hewerd, A.P., Horbury, A.D., Simmons, M. D., 2001.** Arabian plate sequence stratigraphy, GeoArabia Special Publication 2, Gulf. PetroLink, Bahrain.
- Shikalibeily, E.S., and Grigoriant, B.V., 1980.** Principal features of the crustal structure of the South-Caspian Basin and the conditions of its formation, Tectonophysics, 69, 113-121.
- Sinclair, H.D., 1997 a.** Tectonostratigraphic model for underfilled peripheral foreland basins: an Alpine perspective, Geological Society of America Bulletin, 109, 324-346, doi: 10.1130/0016-7606.
- Sinclair, H.D., 1997 b.** Flysch to molasse transition in peripheral foreland basins: the role of the passive margin versus slab breakoff. Geology, 25, 1123-1126, doi: 10.1130/0091-7613.
- Smith, A.G., 1971.** Alpine deformation and oceanic areas of the Tethys, Mediterranean and Atlantic, Geological Society of America Bulletin, 82, 20139-2070.
- Soudouy, F., Yuan, X., Kind, R., Heit, B., Sadidkhouy, A., 2009.** Evidence for a missing crustal root and a thin lithosphere beneath the Central Alborz by receiver function studies, Geophysical Journal International, 177 (2), 733-742, doi: 10.1111/j.1365 246X.2009.04115.x.
- Solaymani Azad, S., Dominguez, S., Philip, H., Hessami, K., Forutan, M. R., Shahpasan Zadeh, M., Ritz, J.F., 2011 a.** The Zandjan fault system: Morphological and tectonic evidences of a new active fault network in the NW of Iran, Tectonophysics, 506, 73-85, doi: 10.1016/j.tecto.2011.04.012.
- Solaymani Azad, S., Ritz, J.F., Abbassi, M.R., 2011 b.** Left-lateral active deformation along the Mosha–North Tehran fault system (Iran), Morphotectonics and paleoseismological investigations, Tectonophysics, 497, 1-14, doi: 10.1016 /j.tecto. 2010. 09.013.
- Sorkhabi, R., and Macfarlane, A., 1999.** Himalaya and Tibet: Mountain roots to mountain tops, in Macfarlane, A., Sorkhabi, R.B, and Quade, J., eds., Himalaya and Tibet: Mountain Roots to Mountain Tops, Geological Survey of America, Special Paper, 328, 1-8.
- SRTM data, CGIAR - Consortium for Spatial Information (CGIAR-CSI), 2004.** <http://srtm.csi.cgiar.org>, accessed 28.12.2014.
- Stampfli, G.M., 1996.** The intra-Alpine terrain: a Palaeotethyan remnant in the Alpine Variscides. Eclogae Geologicae Helvetiae, 89, 13-42.
- Stampfli, G.M., 2000.** Tethyan oceans. In: Tectonics and Magmatism in Turkey and the Surrounding Area (E. Bozkurt, J.A., Winchester, J.D.A. Piper, eds), Geological Society of London Special Publication, 173, 1-23, doi: 10. 1144 /GSL.SP. 2000. 173.01.01.
- Stampfli, G.M., Mosar, J., Favre, P., Pillecuit, A., Vannay, J.C., 2001.** Permo-Mesozoic evolution of the western Tethys realm, The Neo-Tethys East Mediterranean Basin connection, in Peri-Tethyan Rift/ Wrench Basins and Passive Margins, Peri-Tethys Mem., 6, edited by P.A. Ziegler et al., Memoires du Museum National d'histoire Naturelle, 186, 51-108.
- Stampfli, G.M., and Borel, G.D., 2002.** A plate tectonic model for the Paleozoic and Mesozoic constrained by dynamic plate boundaries and restored synthetic oceanic isochrones, Earth and Planetary Science Letters, 196, 17-33.
- Stephenson, R.A., Wilson, M., De boorder, H., Starostenko, V.I., (eds) 1996.** EUROPROBE: intraplate tectonics and basin dynamics of the Eastern European Platform, Tectonophysics, 268. Stöcklin, Journal Structural history and tectonics of Iran, a review. AAPG Bulletin, 52(7), 1229-1258.
- Stocklin, J., 1968.** Structural history and tectonics of Iran: A review, American Association of Petroleum Geologist Bulletin 52. 1229-1258.
- Stocklin, J., 1974.** Northern Iran: Alborz Mountains. In: Spencer, A.M. (Ed.), Mesozoic–Cenozoic Orogenic Belts; Data for Orogenic Studies; Alpine–Himalayan Orogens, Special Publication Geological Society of London, 213-234.
- Storetvedt, K.M., 1990.** The Tethys Sea and the Alpine-Himalayan orogenic belt; mega-elements in a new global tectonic system, Physics of the Earth and Planetary Interiors, 62, 1-2, 141-184.
- Stöcklin J., 1980.** Geology of the Nepal and its regional frame, Journal of the Geological Society of London, 137, 1-34.
- Suppe, J., 2007.** Absolute fault and crustal strength from wedge tapers, Geology, 35(12), 1127-1130.

- Taheri, J., Fürsich, F.T., Wilmsen, M., 2009.** Stratigraphy, depositional environments, and geodynamic significance of the Upper Bajocian-Bathonian Kashafrud Formation (NE Iran). In: South Caspian to Central Iran Basins (M. F. Brunet, M. Wilmsen and J. Granath, eds), Geological Society of London, Special Publication, 312, 205-218, doi: 10.1144/SP312.10.
- Takin, M., 1972.** Iranian Geology and continental drift in the Middle East, *Nature*, 235, 5334, 147-150.
- Talbot, C.J., and Jarvis, R.J., 1984.** Age, budget and dynamics of an active salt extrusion in Iran, *Journal of Structural Geology*, 6, 5, 521-533, doi: 10.1016/0191-8141(84)90062-2.
- Talebian, M., and Jackson, J., 2004.** A reappraisal of earthquake focal mechanisms and active shortening in the Zagros mountains of Iran, *Geophysical Journal International*, 156, 506-526.
- Tankard, A.J., and Balkwill, H.R., (eds) 1989.** Extensional Tectonics and Stratigraphy of the North Atlantic Margins, AAPG, Memoirs, 46.
- Tatar, M., 2001.** Étude sismotectonique de deux zones de collision continentale: le Zagros Central et l'Alborz (Iran). PhD Thesis, Université de Grenoble, Grenoble, France.
- Tavakoli, B., 1996.** Major seismotectonic provinces of Iran, unpublished map, International Institute of Earthquake Engineering and Seismology (IIEES) internal document.
- Tavakoli, B., and Ghafari-Ashtiani, M., 1999.** Seismic hazard assessment of Iran, *Annali Di Geofisica* 42(6) 1013-1021.
- Tchalenko, J.S., 1975.** Seismicity and Structure of the North Tehran Fault, *Tectonophysics*, 29, 411-420.
- Toussaint, G., Burov, E., Avouac, J.P., 2004.** Tectonic evolution of a continental collision zone: A thermomechanical numerical model, *Tectonics*, 23, TC6003, 1-24, doi: 10.1029/2003TC001604.
- Tikhomirov, P.L., Charlot-Prat, F., Nazarevich, B.P., 2004.** Triassic volcanism in the eastern Fore-Caucasus: evolution and geodynamic interpretation, *Tectonophysics*, 381, 119-142.
- Tozer, R.S.J., Butler, R.W.H., Corrado, S., 2002.** Comparing thin- and thick-skinned thrust tectonic models of the Central Apennines, Italy, *EGU Stephan Mueller Special Publication Series*, 1, 181-194.
- Triep, E.G., Abers, G.A., Lerner-Lam, A.L., 1995.** Active Thrust Front of the Greater Caucasus: The April 29, 1991, Racha earthquake sequence and its tectonic implications, *Journal of Geophysical Research*, 100, B3, 4011-4033.
- Tunini, L., Jiménez-Munt, I., Fernandez, M., Vergés, J., Villaseñor, A., 2015.** Lithospheric mantle heterogeneities beneath the Zagros Mountains and the Iranian Plateau: a petrological-geophysical study, *Geophysical Journal International* 200, 596-614, doi: 10.1093/gji/ggu418.
- Ulmishek, G.F., 2001.** Petroleum geology and resources of the Middle Caspian Basin, former Soviet Union. U.S. Geological Survey Bulletin, 2201-A, 38.
- United State Geological Survey (USGS), earthquakes hazard program, NEIC catalogue,** <http://earthquake.usgs.gov/earthquakes/search/>, accessed 30.07.2015.
- Valdiya, K.S., 1980.** Geology of Kumaun Lesser Himalaya. Dehra Dun, India. Wadia Institute of Himalayan Geology, 291.
- Vance, D., Bickle, M., Ivy-Ochs, S., Kubik, P.W., 2003.** Erosion and exhumation in the Himalaya from cosmogenic isotope inventories of river sediments, *Earth and Planetary Science Letters*, 206, 273-288, doi: 10.1016/S0012-821X(02)01102-0.
- Van der Voo, R., Spakman, W., Bijwaard, H., 1999.** Tethyan subducted slabs under India, *Earth and Planetary Science Letters*, 171, 7-20.
- Vergés, J., Saura, E., Casciello, E., Fernández, M., Villaseñor, A., Jiménez-Munt, I., García-Castellanos, D., 2011.** Crustal-scale cross-sections across the NW Zagros belt: implications for the Arabian margin reconstruction, *Geological Magazine* 148 (5-6), 2011, 739-761, doi: 10.1017/S0016756811000331.
- Verma, R.K., 1997.** Paleomagnetism from Parts of Tethys Himalaya, Indus Suture Zone, Ladakh and South Tibet: Implications for Collision between Indian and Eurasian Plate, *Himalayan, Geology*, 18, 93-102.

- Vernant, Ph., Nilforoushan, F., Chery, J., Bayer, R., Djamour, Y., Masson, F., Nankali, H., Ritz, J.F., Sdighi, M., Tavakoli, F., 2004 a.** Deciphering oblique shortening of central Alborz in Iran using geodetic data, *Earth and planetary science letters*, 223, doi: 10.1016/j.epsl.2004.04.017.
- Vernant, Ph., Nilforoushan, F., Hatzfeld, D., Abbassi, M.R., Vigny, C., Masson, F., Nankali, H., Martinod, J., Ashtiani, A., Bayer, R., Tavakoli, F., Chery, J., 2004 b.** Present-day crustal deformation and plate kinematics in the Middle East constrained by GPS measurements in Iran and northern Oman, *Geophysical Journal International*, 157, 381-398, doi: 10.1111/j.1365-246X.2004.02222.x.
- Von Hagke, C., Oncken, O., Evseev, S., 2014.** Critical taper analysis reveals lithological control of variations in detachment strength: An analysis of the Alpine basal detachment (Swiss Alps), *Geochemistry, Geophysics, Geosystems*, 15 (1), 176-191, ISSN 1525-2027.
- Walker, R.T., Bergman, E., Jackson, J., Ghorashi, M., Talebian, M., 2005.** The 2002 June 22 Changureh (Avaj) earthquake in Qazvin province, northwest Iran: epicentral relocation, source parameters, surface deformation and geomorphology, *Geophysical Journal International*, 160, 707-720, doi: 10.1111/j.1365-246X.2005.02516.x.
- Wessel, P., and Smith, W.H.F., 2010.** The Generic Mapping Tools, Version 4.5.5, <http://gmt.soest.hawaii.edu/>, accessed 01.03.2012-2015.
- Williams, G.D., and Dobb, A., (eds) 1993.** *Tectonics and Seismic Sequence Stratigraphy*, Geological Society, London, Special Publications, 71.
- Willett, S., Beaumont, C., Fullsack, P., 1993.** Mechanical model for the tectonics of doubly vergent compressional orogens, *Gology*, 21, 371-374.
- Willett, S., 1999.** Orogeny and orography: The effects of erosion on the structure of mountain belts, *Journal of Geophysical Research*, 104, 12, 28,957-28,981.
- Wilmsen, M., Fürsich, F.T., Seyed-Emami, K., Majidifard, M., Taheri, T., 2009.** The Cimmerian Orogeny in northern Iran: tectono-stratigraphic evidence from the foreland, *Terra Nova*, 21, 211-218, 2009, doi: 10.1111/j.1365-3121.2009.00876.x.
- Windley, B.F., (ed) 1995.** *The Evolving Continents*, third Edition, John Wiley & Sons, Chichester, 526.
- Yin, A., Dubey, C.S., Kelty, T.K., Webb, A.A.G., Harrison, T.M., Chou, C.Y., Célérier, J., 2010.** Himalaya Structural geology, geochronology, and tectonic evolution of the Eastern Geologic correlation of the Himalayan orogen and Indian craton: Part 2, *Geological Society of America Bulletin*; 122; 360-395, doi: 10.1130/B26461.1.
- Zaho, W., Nelson, K.D., and Project INDEPTH team, 1993.** Deep seismic reflection evidence for continental underthrusting beneath southern Tibet. *Nature*, 366.
- Zanchi, A., Zanchetta, S., Berra, F., Mattei, M., Garzanti, E., Molyneux, S., Nawab, A., Sabouri, J., 2009.** The Eo-Cimmerian (Late? Triassic) orogeny in north Iran. In: *South Caspian to Central Iran Basins* (M.F. Brunet, M. Wilmsen and J. Granath, eds), Geological Society of London, Special Publication, 312, 31-55.
- Zohary, M., (ed) 1973.** *Geobotanical Foundations of the Middle East*, 2 volumes. Fischer, Stuttgart, Amsterdam, 765.
- Zonenshain, L.P., and Le Pichon, X., 1986.** Deep basins of the Black Sea and Caspian Sea as remnants of Mesozoic back arc basins.
- Zonenshain, L.P., Kuzmin, M.I., Natapov, L.M., 1990.** *Geology of the USSR, a plate tectonics synthesis*, American Geophysical Union, Geodynamics Series, 21.

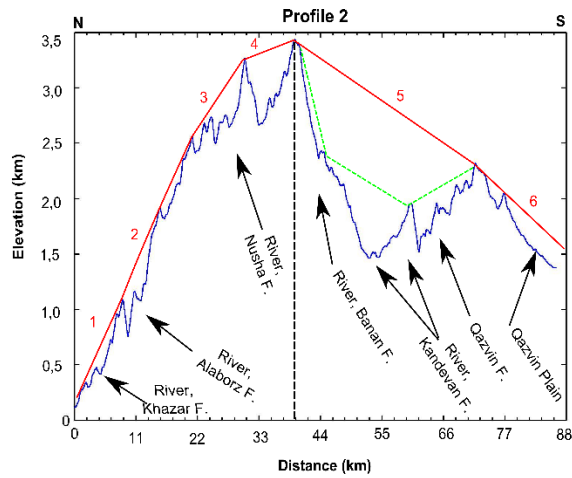
## **Acknowledgement**

I would like to use this opportunity to express my gratitude to everyone who supported me throughout this doctoral study.

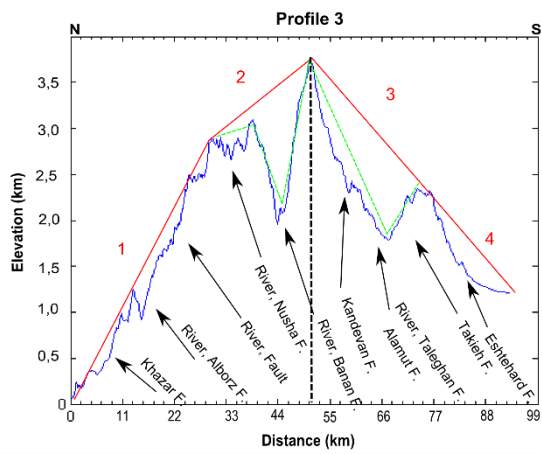
Above all, I wish to express thanks to my parents for their support and encouragement. I would like to acknowledge my supervisor Prof. Nina Kukowski and Dr. Silvan Hoth for their guidance. I would also like to extend special thanks to Roland Hendel and Peter Schindler for the programming support and the GMT advises, respectively.

My appreciation also extend to Dr. Seyed-Hani Motavalli-Anbaran for making available the digital Moho data and Prof. Phippe Vernant for the digital GPS data during this research.

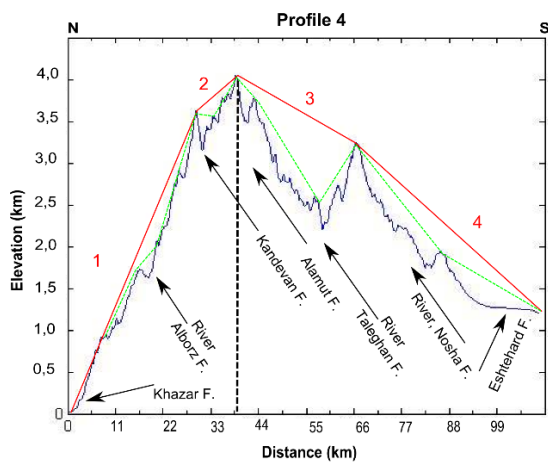
6 APPENDIX



	X	Y	Z (m)	Slope (°)
1	50.6000	36.8000	110.0452	6.34
2	50.5698	36.7296	1083.8392	6.74
3	50.5269	36.6294	2556.3982	4.22
4	50.4937	36.5519	3257.5464	0.97
5	50.4624	36.4790	3412.2281	1.93
6	50.3501	36.2169	2314.7501	3.72
Min. slope : 0.97° Max. slope : 6.74° Mean slope : 3.51°				

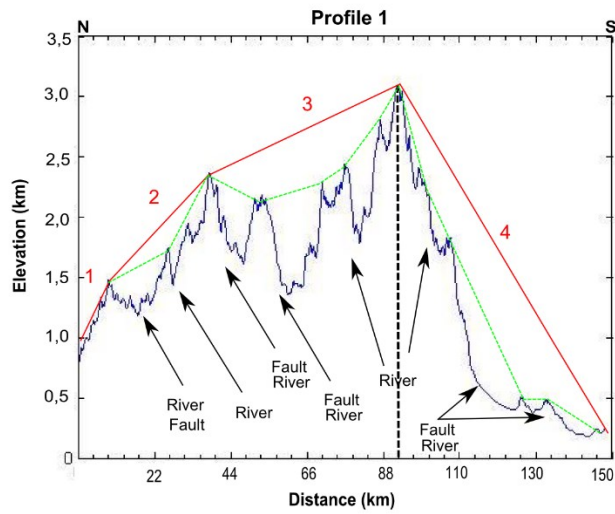


	X	Y	Z (m)	Slope (°)
1	50.8000	36.7000	54.2169	5.38
2	50.7353	36.4413	2892.8359	2.31
3	50.6904	36.2617	3745.1186	3.22
4	50.6345	36.0380	2262.2113	3.76
Min. slope : 2.31° Max. slope : 5.38° Mean slope : 4.12°				

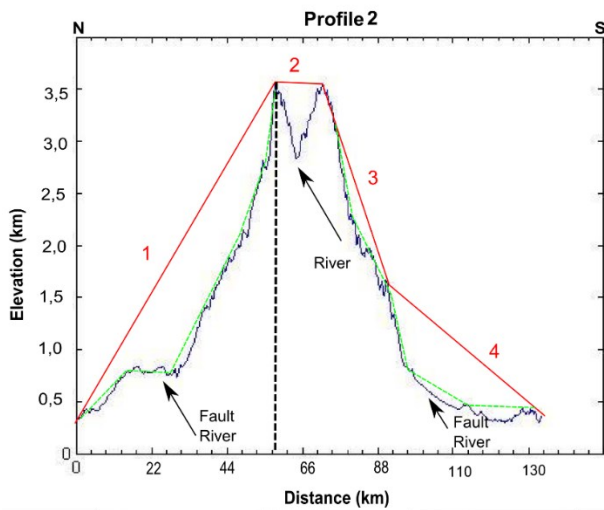


	X	Y	Z (m)	Slope (°)
1	51.0000	36.7000	12.4751	6.85
2	50.9727	36.4251	3613.0144	2.61
3	50.9644	36.3419	4027.2167	1.61
4	50.9384	36.0807	3222.8416	2.77
Min. slope : 1.61° Max. slope : 6.85° Mean slope : 3.57°				

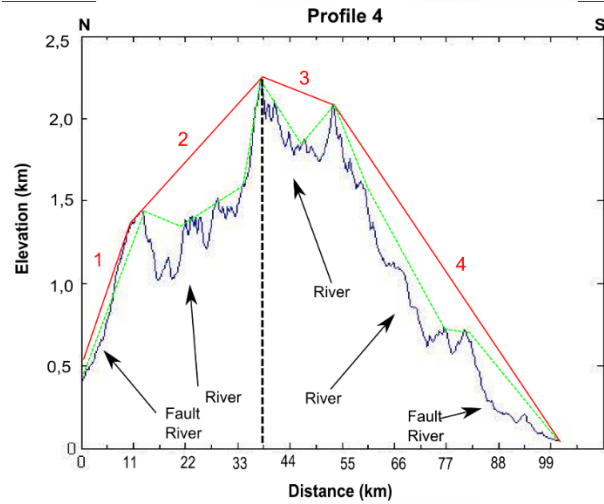
Figure 6-1. Alborz, regional slope for the extra profiles, as well as table of coordinates and  $\alpha$ -values of the segments. Dashed line: crest of orogen. See Fig 3-5 for the location of profiles.



	X	Y	Z (m)	Slope (°)
1	48.0000	41.9000	894.7230	3.70
2	47.9545	41.8375	1457.9725	1.76
3	47.8005	41.6257	2366.0638	0.75
4	47.5136	41.2312	3092.6212	2.71
Min. slope : 0.75° Max. slope : 3.70° Mean slope : 1.88°				

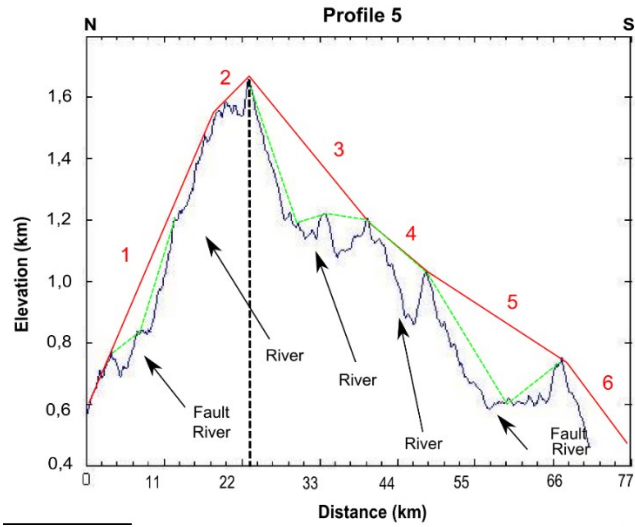


	X	Y	Z (m)	Slope(°)
1	48.3000	41.7000	333.7481	3.13
2	48.0013	41.2733	3536.4313	0.06
3	47.9293	41.1705	3552.9491	5.79
4	47.8337	41.0339	1654.3769	1.62
Min. slope : 0.06° Max. slope : 5.79° Mean slope : 2.83°				



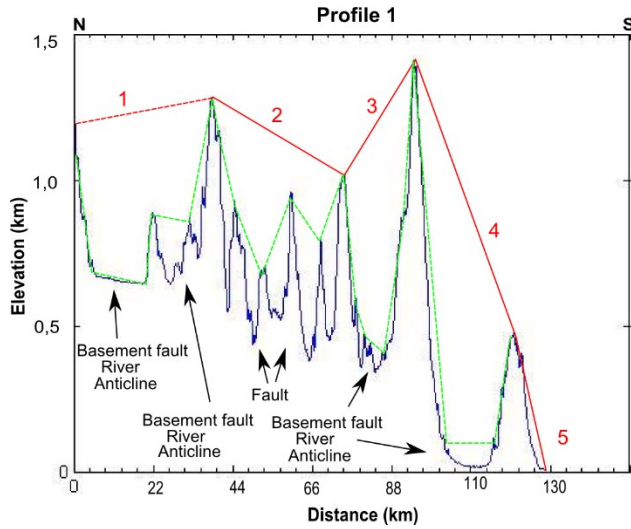
	X	Y	Z (m)	Slope (°)
1	48.0000	41.2000	419.8867	4.42
2	48.7223	41.1093	1436.6347	1.81
3	48.5734	41.9356	2233.0733	0.60
4	48.4835	40.8308	2072.1668	2.42
Min. slope : 0.6° Max. slope : 4.42° Mean slope : 1.98°				



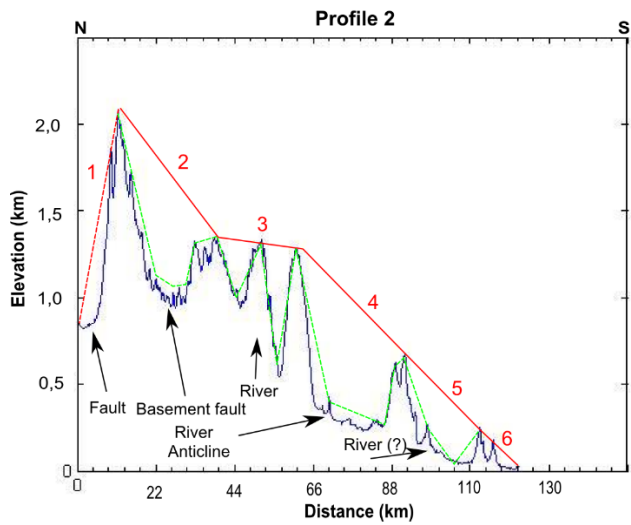


	X	Y	Z (m)	Slope (°)
1	49.0000	41.0000	559.1082	3.04
2	48.8960	40.8700	1551.5852	1.37
3	48.8713	40.8353	1658.3653	1.54
4	48.7756	40.7194	1193.4833	1.17
5	48.7308	40.6635	1028.6694	0.81
6	48.6226	40.5283	751.8502	4.12
Min. slope : 0.81°				
Max. slope : 4.12°				
Mean slope : 1.40°				

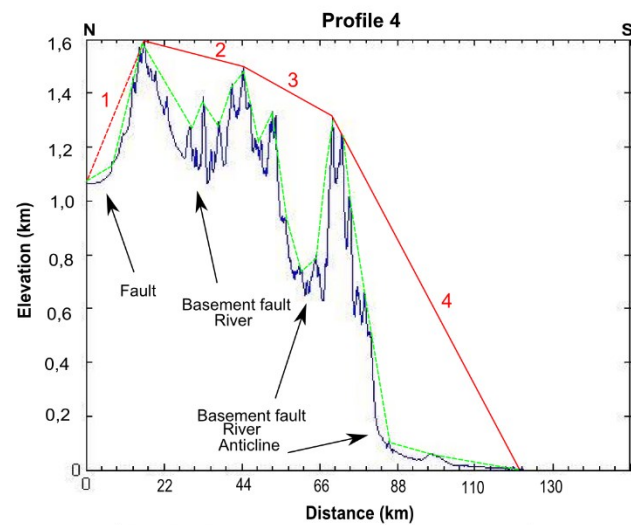
**Figure 6-2. The Caucasus**, regional slope for the extra profiles, as well as table of coordinates and  $\alpha$ -values of the segments. Dashed line: crest of orogen. See also Fig. 3-11 for the location of profiles.



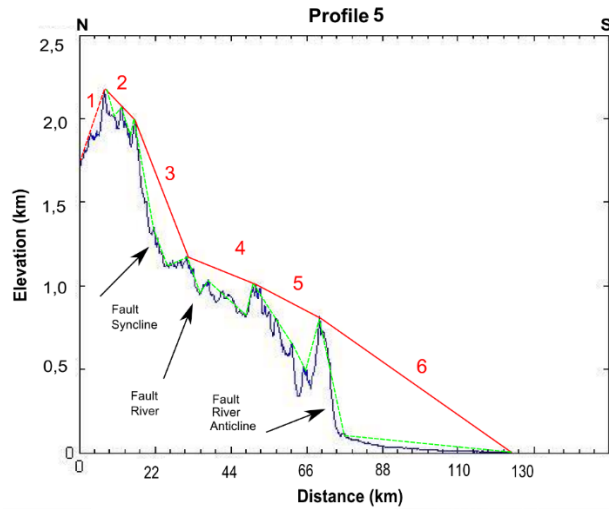
	X	Y	Z (m)	Slope (°)
1	55.6000	28.1000	1165.1692	-0.17
2	55.6293	27.7774	280.8723	0.40
3	55.6574	27.4683	1018.6689	-1.15
4	55.6721	27.3064	1409.4911	1.94
5	55.6935	27.0715	454.1298	3.00
Min. slope : -1.15° Max. slope : 3.00° Mean slope : 0.50°				



	X	Y	Z (m)	Slope (°)
1	55.9000	28.2000	857.7554	-5.98
2	55.9092	28.0992	2052.4483	1.47
3	55.9398	27.7621	1346.5803	0.15
4	55.9496	27.6546	1283.1782	1.13
5	55.9723	27.4048	675.6757	1.15
6	55.9920	27.1877	248.9633	1.17
Min. slope : -5.98° Max. slope : 1.47° Mean slope : 0.38°				

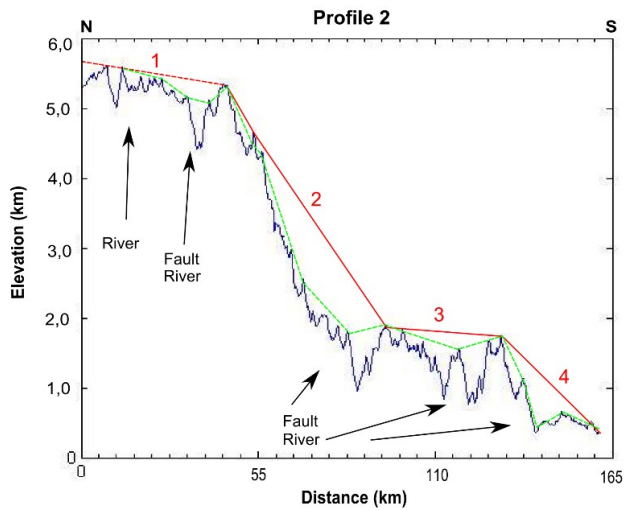


	X	Y	Z (m)	Slope (°)
1	56.5000	28.2000	1066.0723	-1.82
2	56.5134	28.0662	596.3545	0.21
3	56.5359	27.8406	1491.9992	0.44
4	56.5564	27.6355	1295.3508	1.36
Min. slope : -1.82° Max. slope : 1.36° Mean slope : 0.84°				

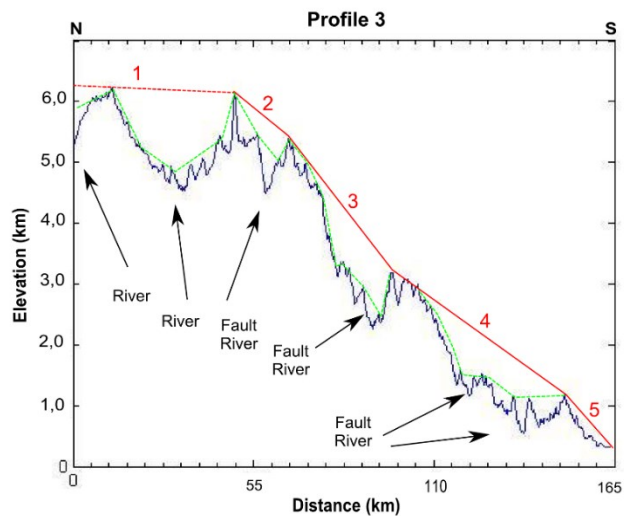


	X	Y	Z (m)	Slope (°)
1	56.7000	28.2000	1689.8026	-3.69
2	55.7085	28.1357	2167.6285	1.12
3	55.7129	27.0578	1991.6750	3.11
4	55.7251	27.9244	1157.1283	0.46
5	55.7419	27.7390	983.5096	0.65
6	55.7555	27.5894	786.6818	0.79
				Min. slope : -3.69°
				Max. slope : 3.11°
				Mean slope : 0.76°

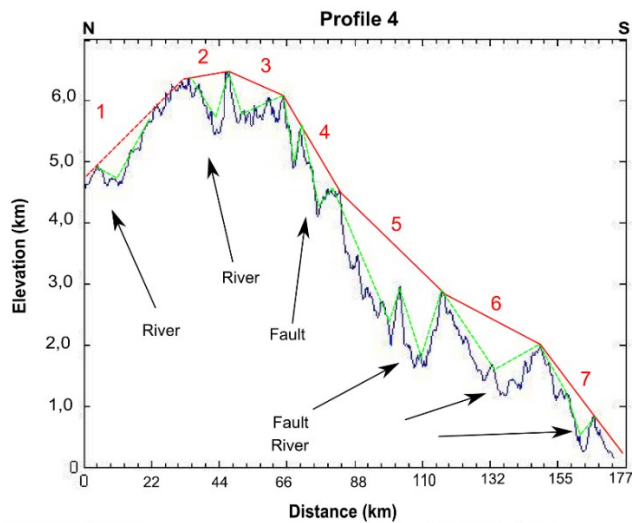
**Figure 6-3. The Zagros, regional slope for the extra profiles as well as table of coordinates and  $\alpha$ -values of the segments. Dashed line: crest of orogen. See also Fig. 3-13 for the location of profiles.**



X	Y	Z (m)	Slope (°)	
1	85.8000	28.2000	5663.6488	0.41
2	85.7722	27.8110	5341.0539	3.88
3	85.7410	27.3747	1907.6494	0.30
4	85.7187	27.0621	1712.0416	2.58
Min. slope : 0.30° Max. slope : 3.88° Mean slope : 1.87°				

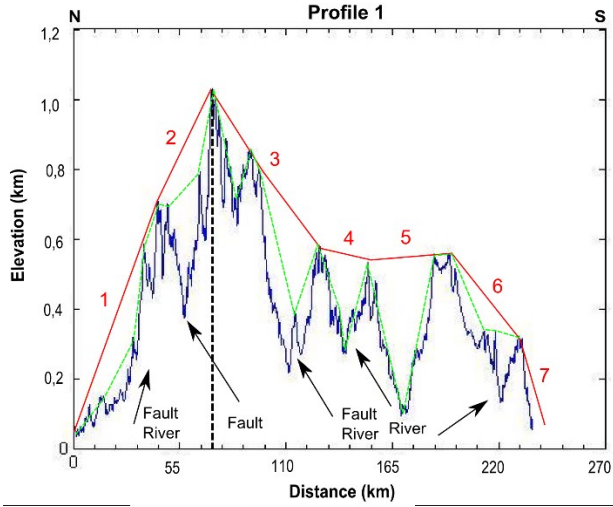


X	Y	Z (m)	Slope (°)	
1	86.3000	28.1000	6247.7238	0.17
2	86.2700	28.0011	6091.9851	2.43
3	86.2598	27.6796	5374.4936	3.98
4	86.2408	27.5367	3188.7819	2.15
5	86.2084	26.8176	1174.7600	3.53
Min. slope : 0.17° Max. slope : 3.98° Mean slope : 2.05°				

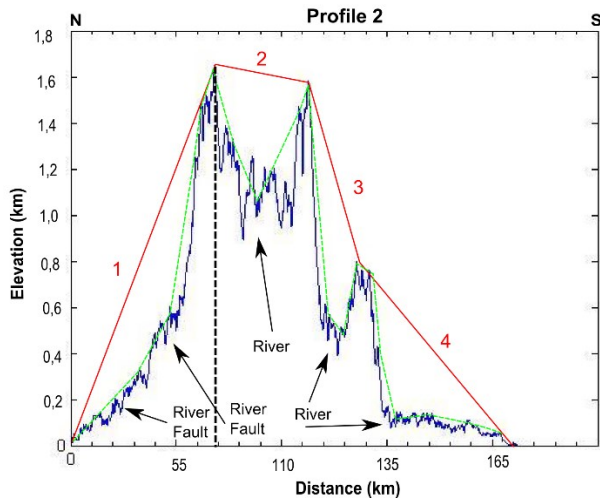


X	Y	Z (m)	Slope (°)	
1	86.8000	28.000	4700.0136	-2.77
2	86.7802	27.7227	6368.9276	-0.43
3	86.7726	27.6160	6469.6983	1.26
4	86.7623	27.4715	6072.7177	4.83
5	86.7517	27.2339	4523.2161	2.81
6	86.7323	27.0523	2866.7506	1.57
7	86.7038	26.6532	837.3542	3.79
Min. slope : -2.77° Max. slope : 4.83° Mean slope : 1.41°				

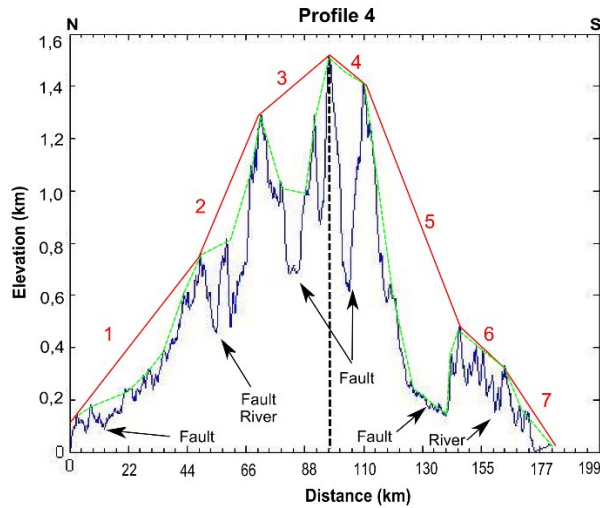
**Figure 6-4. The Himalayas**, regional slope for the extra profiles, as well as table of coordinates and  $\alpha$ -values of the segments. Dashed line: crest of orogen. See also Fig. 3-15 for the location of profiles.



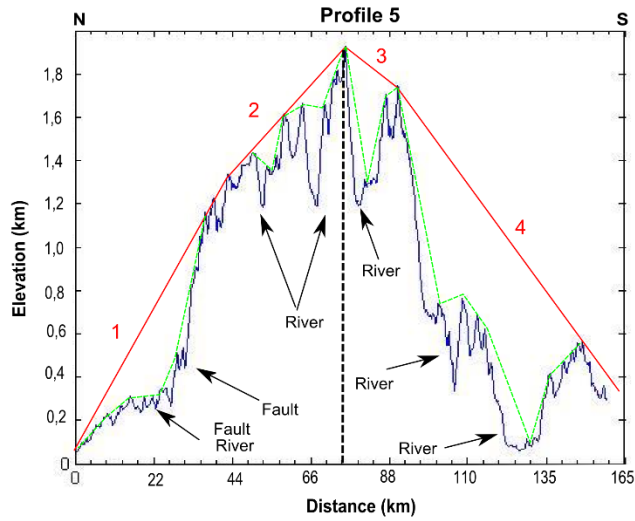
	X	Y	Z (m)	Slope (°)
1	13.4000	43.6500	40.8513	0.85
2	13.1061	43.3470	700.2116	0.66
3	13.9167	43.1516	1027.6561	0.46
4	12.5397	42.7628	570.4441	0.10
5	12.3732	42.5911	526.3797	-0.03
6	12.0916	42.3007	555.0075	0.36
7	11.8374	42.0386	312.4165	2.33
Min. slope : -0.03° Max. slope : 2.33° Mean slope : 0.78°				



	X	Y	Z (m)	Slope (°)
1	13.7500	43.3000	1.5404	1.24
2	13.2514	42.7853	1645.6465	0.08
3	12.9259	42.4493	1572.6752	1.74
4	12.7556	42.2736	785.4413	0.53
Min. slope : 0.08° Max. slope : 1.74° Mean slope : 0.80°				



	X	Y	Z (m)	Slope (°)
1	14.2500	42.4500	39.2092	0.82
2	13.9289	42.1235	752.1837	1.33
3	13.7821	42.9741	1277.8085	0.49
4	13.6133	42.8025	1503.0063	0.42
5	13.5273	41.7151	1405.8835	1.47
6	13.2924	41.4762	477.8022	0.54
7	13.1826	41.3645	318.0798	0.96
Min. slope : 0.42° Max. slope : 1.47° Mean slope : 1.01°				



	X	Y	Z (m)	Slope (°)
1	14.5500	42.2000	65.3600	1.67
2	14.2781	41.9137	1323.1869	1.01
3	14.0675	41.6921	1910.5471	0.67
4	13.6428	41.2450	562.4181	1.28
		Min. slope :		0.67°
		Max. slope :		1.67°
		Mean slope :		1.27°

Figure 6-5. The Apennines, regional slope for the extra profiles as well as table of coordinates and  $\alpha$ -values of the segments. Dashed line: crest of orogen. See also Fig. 3-17 for the location of profiles.

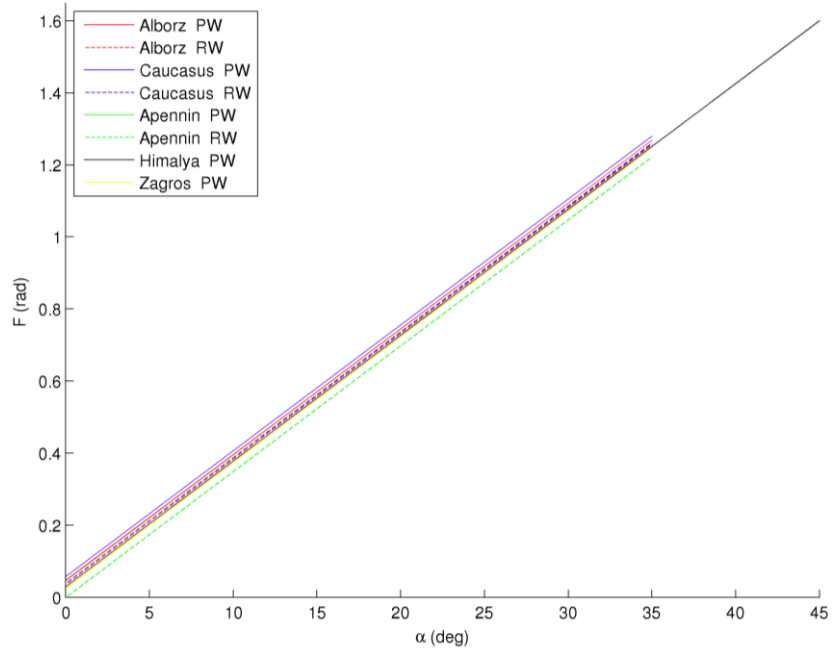


Figure 6-6. F-values of all of the orogens based on local slopes

## **Selbständigkeitserklärung**

Ich erkläre, dass ich die vorliegende Arbeit selbständig und unter Verwendung der angegebenen Hilfsmittel, persönlichen Mitteilungen und Quellen angefertigt habe.

Ort, Datum

Unterschrift des Verfassers/der Verfasserin



